2007

# A preliminary study in the area of blast resistance of civil infrastructure components with polyurea coatings

Lynne Starek
*Lehigh University*

Starek, Lynne

# A Preliminary Study in the Area of Blast Resistance of Civil Infrastructure Components with Polyurea Coatings

September 2007

# A Preliminary Study in the Area of Blast Resistance of Civil Infrastructure Components with Polyurea Coatings

by

Lynne Starek

A Thesis

Presented to the Graduate and Research Committee

of Lehigh University

in Candidacy for the Degree of

Master of Science

in

Structural Engineering

Lehigh University

September 2007

This thesis is accepted and approved in partial fulfillment of the requirements for the Master of Science.

7/31/2007

Date

Dr. Clay Naito, Thesis Advisor

Dr. Stephen Pessiki, Department Chairperson

# Acknowledgements

First, I would like to thank my incredible family for their constant love and support throughout the research and writing process of a Master's Thesis. Throughout my life they have provided me with inspiration and encouragement that has helped me to get where I am today and for which I will be forever grateful.

Next, the experimental phases of my research would not have been possible without the remarkable staff of ATLSS. I would especially like to thank John Hoffner and Carl Bowman for giving me so much of their valuable time to readily answer my endless amounts of questions and to lend a helping hand.

I would also like to thank Air Products for giving me the chance to work on such a meaningful and exciting project. Mark Connor and his co-workers helped me to make a smooth transition into the world of polymers by providing me with all of the information I could possible need about polyurea.

I would like to thank Lehigh University and the Department of Civil Engineering for funding my graduate school and research experience.

Finally I would like to thank my research advisor, Dr. Naito, for his guidance throughout my research experience.

# Table of Contents

List of Tables ..... viii

List of Figures ..... x

List of Equations ..... xix

Abstract ..... 1

1 Introduction ..... 2

1.1 General ..... 2

1.2 Blast Threat ..... 2

1.3 Introduction to Polymers and Polyurea ..... 5

1.4 Research Objectives ..... 6

1.5 Scope of Thesis ..... 7

1.6 Notation ..... 8

2 Polyurea Properties ..... 10

2.1 General ..... 10

2.2 Chemical Materials of Polyurea ..... 10

2.3 Polymerization ..... 12

2.4 Polyurea Structure ..... 13

2.5 Mechanical Properties of Polymers and Polyurea ..... 14

2.6 Air Products' Polyurea of Interest ..... 17

2.6.1 Hand Batching ..... 18

2.6.2 Air Products' Coating Techniques ..... 22

2.6.3 Mechanical Properties of Air Products' Polyurea of Interest ..... 25

3 Blast Resistance of Wall Systems Coated with Polyurea ..... 47

3.1 General ..... 47

3.2 Literature Review of Blast Tests Conducted on Wall Systems ..... 47

3.3 Air Products Blast Test Setup and Instrumentation ..... 48

3.3.1 Wall System ..... 48

3.3.2 Polyurea Material Properties ..... 50

3.3.3 Instrumentation ..... 50

3.4 Blast Test Results and Analysis ..... 54

3.5 Conclusions from Blast Tests on Polyurea Coated CMU Walls ..... 63

4 Static Center-Point Loading Tests on CMU Beams ..... 64

4.1 General ..... 64

4.2 Test Matrix ..... 64

4.3 Testing Setup ..... 67

4.4 Test Procedure ..... 68

4.5 Instrumentation ..... 69

4.6 Expected Results ..... 70

4.7 Plain Concrete Results ..... 74

4.7.1 Modifications to Load versus Displacement Curve ..... 74

4.7.2 Fracture Energy of Plain CMU Specimens ..... 78

4.8 Results of CMU Specimens Coated with Spray-on Polyurea ..... 79

4.8.1 Polyurea Strain ..... 86

4.9 Conclusions ..... 92

5 Static Center-Point Loading Tests on Concrete Beams ..... 94

5.1 General ..... 94

5.2 Test Matrix ..... 94

5.3 Testing ..... 96

5.3.1 Testing Goals and Expected Results ..... 99

5.3.2 Instrumentation ..... 101

5.4 Results of Static Concrete Beams Tests ..... 108

5.4.1 Plain Concrete Beam Results ..... 109

5.4.2 Polyurea Coated Concrete Beam Results ..... 110

5.5 Conclusions about Static Concrete Beam Tests ..... 138

6 Dynamic Testing of Polyurea Coated Concrete Beams ..... 141

6.1 General ..... 141

6.2 Test Matrix ..... 141

6.3 Testing ..... 143

6.3.1 Instrumentation ..... 144

6.3.2 Test Procedure ..... 148

6.3.3 Expected Results ..... 149

6.4 Results ..... 155

6.4.1 Energies into the System ..... 158

6.4.2 Strain Data ..... 185

6.5 Conclusions from Dynamic Testing ..... 201

7 Conclusions ..... 204

References ..... 208

Vita ..... 212

# List of Tables

Table 2-1: Mechanical Properties of Polyurea at Different Strain Rates ..... 30

Table 2-2: Summary of Polyurea Properties from Literature ..... 33

Table 2-3: True Stress and Strain Values of P-1000 Polyurea for Comparison ..... 36

Table 2-4: Average Data Values for Batch 4 Polyurea ..... 38

Table 2-5: Dynamic Physical Properties of Polyurea Batch 4 ..... 41

Table 2-6: Spray-on Polyurea Properties ..... 43

Table 3-1: Estimated and Actual Pressure and Impulse Values ..... 59

Table 4-1: Test Matrix for CMU Tests ..... 66

Table 4-2: Estimated Loads for Coated and Uncoated Specimens ..... 71

Table 4-3: Summary of Plain CMU Test Results ..... 77

Table 4-4 : Fracture Energies and Needed Values ..... 79

Table 4-5: Results of Coated and Uncoated CMU Tests ..... 83

Table 4-6: Fracture Energies for Coated and Uncoated CMU Specimens ..... 84

Table 5-1: Test Matrix for Static Concrete Beam Center-Point Loading Tests ..... 96

Table 5-2: Expected Results for Coated and Uncoated Beams ..... 101

Table 5-3: Summary of Test Results for Plain Concrete Beams ..... 110

Table 5-4: Fracture Energies for Uncoated Concrete Beams ..... 110

Table 5-5: Peak Loads and Moduli of Rupture for Coated Systems ..... 116

Table 5-6: Stiffness Values for Static Beam Tests ..... 117

Table 5-7: Adjusted Stiffness Values ..... 119

Table 5-8: Fracture Energies for Coated and Uncoated Concrete Systems ..... 120

Table 5-9: Center Strain Values at Peak Load ..... 123

Table 6-1: Test Matrix for Dynamic Series ..... 143

Table 6-2: Summary of Dynamic Testing Outcomes ..... 156

Table 6-3: Strain Rates and Maximum Strains of Dynamic Beam Tests ..... 185

# List of Figures

Figure 1-1: Types of Blast Loading (Naito&Wheaton, 2006) ..... 4

Figure 1-2: Definition of Impulse ..... 4

Figure 2-1: MDI Formula (Primeaux II, 2004) ..... 11

Figure 2-2: Formation of a Urea Linkage (Wang, 1989) ..... 12

Figure 2-3: Structure of Polymer (Kaufman, 1968) ..... 14

Figure 2-4: Melting Point of Polyurea and Other Polymers (Primeaux II, 2004) ..... 16

Figure 2-5: Comparison of Electric Mix to Hand Mix Batches ..... 21

Figure 2-6: Forms in Place for Polyurea Pour ..... 24

Figure 2-7: Specimens after Pouring of Polyurea ..... 24

Figure 2-8: Definition of Regions and Mechanical Properties for Polyurea ..... 27

Figure 2-9: Stress-Strain Curves for a Loading Rate of 2 in/min ..... 28

Figure 2-10: Average Stress-Strain Curves for Polyurea made by Air Products ..... 30

Figure 2-11: Zoomed View on Second Modulus for Three Strain Rates ..... 31

Figure 2-12: True Stress vs. True Strain for Air Product's Polyurea ..... 35

Figure 2-13: Average Stress-Strain Curve for Batch 4 Polyurea ..... 38

Figure 2-14: Dynamic and Static Stress-Strain Curve for Polyurea Batch 4 ..... 40

Figure 2-15: Bi-Linear Fit to Dynamic Stress-Strain Curve ..... 41

Figure 2-16: Engineering Stress-Strain Profile of Spray-on Polyureas ..... 43

Figure 2-17: Comparison between Polyurea Plaque and Spray-on Polyurea ..... 44

Figure 3-1: Side View of Wall and Features ..... 49

Figure 3-2: CMU Wall System for Blast Test ..... 49

Figure 3-3: Reflected Pressure Gauge Locations along Steel Column ..... 51

Figure 3-4: East Side View of Blast Test Set-up and Instrumentation Blast Loading and Predictions ..... 51

Figure 3-5: Plot to Determine Positive Shock Wave Parameters (U.S. Army Corp of Engineers, 1998) ..... 53

Figure 3-6: Predicted Reflected Pressure Curve ..... 54

Figure 3-7: End Results of East and West Wall ..... 55

Figure 3-8: East and West Wall Fracture Mapping ..... 56

Figure 3-9: Reflected Pressure and Deflection of Wall vs. Time ..... 58

Figure 3-10: Predicted Demand and Actual Demand ..... 59

Figure 3-11: Acceleration versus Time for the East Wall ..... 60

Figure 3-12: Acceleration versus Time for the West Wall ..... 61

Figure 3-13: Interior Pressures and Reflected Pressure vs. Time ..... 62

Figure 4-1: CMU Type 1 with Cinder Based Aggregate ..... 65

Figure 4-2: CMU Type 2 with Harder Aggregate ..... 65

Figure 4-3: Test Specimen Location within full CMU ..... 65

Figure 4-4: Photograph of Test Specimen ..... 66

Figure 4-5: Dimensioned Test Set-up for Static CMU Tests ..... 67

Figure 4-6: Actual Loading Fixture for Static CMU Tests ..... 68

Figure 4-7: Strain Gauge Locations for Static CMU Tests ..... 69

Figure 4-8: Loading Begins ..... 72

Figure 4-9: Cracking Occurs ..... 72

Figure 4-10: Displacement Continues as Crack Opens ..... 73

Figure 4-11: End of Test Due to Maximum Displacement ..... 73

Figure 4-12: Modifications to Load Displacement Curve ..... 75

Figure 4-13: Load versus Displacement Curves for Plain CMU ..... 76

Figure 4-14: Definition of $W_o$ ..... 79

Figure 4-15: Load versus Displacement Curves for Polyurea 70-5 ..... 80

Figure 4-16: Load versus Displacement Curves for Polyurea 70-1 ..... 81

Figure 4-17: Load versus Displacement Curves for Type 1 CMU ..... 81

Figure 4-18: Load Displacement Curves for Type 2 CMU ..... 82

Figure 4-19: Center Strain versus Displacement ..... 87

Figure 4-20: Strain 0.625" from the Center versus Displacement ..... 88

Figure 4-21: Strain 1.25" from Center versus Displacement ..... 89

Figure 4-22: Possible Delamination ..... 90

Figure 4-23: Load Values at Which Strains are plotted ..... 91

Figure 4-24: Strain along Distance of Beam for Load 1 ..... 91

Figure 4-25: Strain along Distance of Beam for Load 2 ..... 92

Figure 5-1: Concrete Beam Specimens ..... 94

Figure 5-2: Cross-sections of Concrete Beams with 5.5" Debonded Polyurea Region ..... 95

Figure 5-3: Static Test Set-Up for Concrete Beams ..... 97

Figure 5-4: Photograph of Static Test Set-Up ..... 98

Figure 5-5: String Potentiometer ..... 102

Figure 5-6: Load Cell ..... 103

Figure 5-7: Linear Voltage Differential Transducers ..... 104

Figure 5-8: Dimensions for LVDT Rotation Calculation ..... 104

Figure 5-9: Comparison of Center Displacement for Lasers and String Pot ..... 106

Figure 5-10: Comparison of Rotation Recorded with LVDTs and Lasers ..... 107

Figure 5-11: Strain Gauge Configuration ..... 108

Figure 5-12: Load versus Displacement for Plain Concrete ..... 109

Figure 5-13: Cracking Occurs ..... 111

Figure 5-14: Rotation and Displacement of Beam at End of Test ..... 112

Figure 5-15: Rebound ..... 112

Figure 5-16: Permanent Deformation of Polyurea ..... 113

Figure 5-17: Load versus Displacement for Bonded Polyurea ..... 114

Figure 5-18: Load versus Displacement for 5.5 inch Debonded Polyurea ..... 115

Figure 5-19: Initial Load versus Displacement Curves for Static Beam Tests..... 117

Figure 5-20: Adjusted Load versus Displacement for Accurate Stiffness..... 118

Figure 5-21: Full Load-Displacement Curves for Coated Specimens..... 121

Figure 5-22: Loads and Displacements at which Strains were Evaluated..... 122

Figure 5-23: Strain along Beam for Loads of Test 2..... 124

Figure 5-24: Strain along Beam for Loads of Test 3..... 126

Figure 5-25: Bottom Crack Edge Bearing into Polyurea..... 127

Figure 5-26: Strain along Beam at Max Load..... 128

Figure 5-27: Strain along Beam at Minimum Load after Cracking..... 129

Figure 5-28: Strain along Beam at Second Peak Load..... 129

Figure 5-29: Moment versus Rotation for Test 1 with Original Debonded Length . 131

Figure 5-30: Moment versus Rotation for Test 2 with Original Debonded Length 131

Figure 5-31: Moment versus Rotation with Increased Debonded Length for Test 1 133

Figure 5-32: Moment versus Rotation with Increased Debonded Length for Test 2 133

Figure 5-33: Moment versus Rotation for Test 4 with Original Debonded Length . 134

Figure 5-34: Moment versus Rotation for Test 3 with Original Debonded Length . 135

Figure 5-35: Load versus Center Strain with Different Debonded Lengths..... 136

Figure 5-36: Moment versus Rotation for Test 3 with Increasing Debonded Length
..... 137

Figure 5-37: Loads at which Debonded Length Increased..... 137

Figure 5-38: Center Strain Gauge Profiles and Point at Which Debonded Lengths Change ..... 138

Figure 6-1: Beam in Place for Dynamic Testing ..... 144

Figure 6-2: Laser Locations ..... 145

Figure 6-3: Typical Strain Gauge Layout for Dynamic Testing ..... 146

Figure 6-4: Strain Gauge Layout for Tests 12 and 13 ..... 146

Figure 6-5: Strain Gauge Layout for Test 14 ..... 146

Figure 6-6: Instrumentation for Drop Weight Tests ..... 147

Figure 6-7: Drop Weight Machine ..... 148

Figure 6-8: Hinge Model ..... 150

Figure 6-9: Load Deflection Curve for Rotational Model ..... 152

Figure 6-10: Energy States ..... 153

Figure 6-11: Predicted Drop Height versus Maximum Displacement ..... 155

Figure 6-12: Actual Results of Drop Height versus Maximum Displacement compared to Expected Results ..... 157

Figure 6-13: Full Tup Accelerations for 30 inch Drop Heights ..... 159

Figure 6-14: Initial Region of Tup Acceleration versus Time Plot for 30 inch Drop Height ..... 160

Figure 6-15: Tup Acceleration of a Coated Specimen and an Uncoated Specimen Tested at a 6 inch Drop Height ..... 161

Figure 6-16: Overall Behavior of Tup Acceleration and Displacement of a Coated and Uncoated Specimen from a 6" Drop Height ..... 162

Figure 6-17: Beam's Midspan Acceleration for Coated and Uncoated Specimen Tested at Drop Height of 6 inches ..... 163

Figure 6-18: Tup Acceleration of Tests with High Drop Heights ..... 165

Figure 6-19: Fracture Surface of Coated Specimen tested at Drop Height of 30 inches ..... 166

Figure 6-20: Beam's Midspan Acceleration ..... 167

Figure 6-21: Tup and Midspan of Beam Accelerations for Test 9 ..... 168

Figure 6-22: Tup Acceleration for 6 inch Drop Height on Plain Concrete Type 1 .. 169

Figure 6-23: Tup Acceleration for 6 inch Drop Height on Plain Concrete Type 2 .. 170

Figure 6-24: Beam's Midspan Accelerations for Type 1 Concrete Plain Specimens Tested at 6 inches ..... 171

Figure 6-25: Beam's Midspan Acceleration for Type 2 Concrete Plain Specimens with Drop Height of 6 inches ..... 172

Figure 6-26: Tup Acceleration for Specimens Tested at a 6 inch Drop Height and Coated with Polyurea Batch 7 ..... 173

Figure 6-27: Beam's Midspan Acceleration for Specimens Coated with Polyurea Batch 7 Tested at 6 inches ..... 174

Figure 6-28: Fracture Surface of Test 12 with Presence of Stress Concentration .... 174

Figure 6-29: Tup Acceleration for Specimens Tested at 6 inch Drop Height and Coated with Polyurea Batch 8 ..... 175

Figure 6-30: Beam's Midspan Acceleration for Specimens Coated with Polyurea Batch 7 Tested at 6 inches ..... 176

Figure 6-31: Tup Acceleration for Tests with 6" Drop that Fractured ..... 177

Figure 6-32: Partial Fracture of Test 11 ..... 178

Figure 6-33: Mispan Accelerations for Coated Specimens that Fractured from a 6 inch Drop ..... 178

Figure 6-34: Tup Acceleration for Plain Concrete at a Drop Height of 4 inches ..... 180

Figure 6-35: Midspan Accelerations for Uncoated Specimens Tested at a 4 inch Drop Height ..... 181

Figure 6-36: Tup Acceleration for Tests with 4 inch Drop Heights and Polyurea Coating ..... 182

Figure 6-37: Midspan Acceleration for Tests with 4 inch Drop Heights and Polyurea Coating ..... 183

Figure 6-38: Displacements of Specimens that Fractured ..... 186

Figure 6-39: Displacements of Specimens that Did not Fracture ..... 187

Figure 6-40: Rotations of Interest for Tests that Fractured ..... 188

Figure 6-41: Rotations of Interest for 6 inch Drops without Full Fracture ..... 189

Figure 6-42: Rotations of Interest for 4 inch Drops without Full Fracture ..... 189

Figure 6-43: Strain along Length of Beam at Rotation of 0.25° ..... 191

Figure 6-44: Strain along Beam for Test 14 Rotations ..... 192

Figure 6-45: Strain along Beam at a Rotation of 0.5° ..... 193

Figure 6-46: Strain along Beam at 1° Rotation ..... 194

Figure 6-47: Zoomed View of Strain along Beam at Rotation of 3° ..... 195

Figure 6-48: Strain along Beam during Loading and Rebound at Rotation of 1.5°.. 196

Figure 6-49: Center Strain ..... 197

Figure 6-50: Strain 1" From Center ..... 198

Figure 6-51: Moment versus Rotation using Original Debonded Length for Test 7 199

Figure 6-52: Moment versus Rotation with Adjusted Debonded Length for Test 7 200

Figure 6-53: Moment versus Rotation with Original Debonded Length for Test 20 200

Figure 6-54: Moment versus Rotation with Adjusted Debonded Length for Test 20

..... 201

# List of Equations

Equation 3-1: Scaled Horizontal Distance from Charge [m/kg$^{0.333}$] ..... 52

Equation 4-1: Modulus of Rupture [psi] ..... 77

Equation 4-2: Concrete Compressive Strength Multiplier ..... 77

Equation 4-3: Fracture Energy [lb-in] ..... 78

Equation 5-1: Elastic Modulus of Concrete [psi] ..... 100

Equation 5-2: Rotation of Beam using LVDTS [degrees] ..... 103

Equation 5-3: Rotation of Beam using Lasers [degrees] ..... 105

Equation 6-1: Crack Opening [in] ..... 150

Equation 6-2: Beam Displacement from Rotation [in.] ..... 151

Equation 6-3: Generalized Inertial Load of the Beam [lb] (Banthia et al., 1987) .... 184

# Abstract

The research of this thesis includes material testing of polyurea, investigations of full scale blast tests conducted on concrete masonry unit (CMU) walls coated with polyurea, and center-point loading tests conducted on CMU and concrete retrofitted specimens at static rates and dynamic rates. The correlation and conclusions drawn from the different testing phases helped to identify important aspects of polyurea as a retrofit option. The results indicate that many factors influence the behavior of polyurea and polyurea coated systems including chemical make-up and structure, method of batching, the thickness of the polyurea coating and the presence of flaws within the polyurea thickness, and temperature and rate at which the polyurea is tested. The effects of the initial debonded length of polyurea were also researched and it was discovered that a length of at least 0.875 inches is needed to ensure a bond between polyurea and concrete if fully bonded. With an adequate polyurea retrofit an increase in peak load and modulus of rupture is achieved. It allows the system to continue displacing and taking load after complete cracking of the concrete occurs. This ability allows an increase of over 100% to be achieved by the retrofitted specimens in comparison to the non retrofitted systems. Dynamic testing also indicated an increase in energy absorbing ability since at certain rates were not able to fracture the polyurea of a coated beam but were able to completely fracture plain concrete specimens. As a blast retrofitting option, with its energy absorbing ability and its flexibility, a successful polyurea batch is able to retain fragmentation and allow interior pressures to stay below levels that would cause human discomfort or have lasting physical affects on a human.

# 1 Introduction

## 1.1 General

This thesis presents research on the effectiveness of polyurea coatings for blast resistant structural elements. The initial stage of the research consisted of batching polyurea, defining the mechanical characteristics of the polyurea, and comparing the polyurea properties to literature data. In addition to the analysis of results and data from a blast test conducted on a polyurea-coated concrete masonry wall (CMU), the main experimental phase of the research included evaluation of CMU polyurea-coated beams under center-point loading at static rates, concrete polyurea-coated beams under center-point loading at static rates, and concrete beams with polyurea coatings under center-point loading at dynamic rates. This chapter discusses the threat of blast from a structural stand-point, gives an introduction to polymers and polyurea, and explains how polyurea could be used to enhance blast resistance. In addition, the scope and objectives of this research are also presented.

## 1.2 Blast Threat

There are many different concerns when considering the design of a structure which include natural hazards such as winds, floods, and earthquakes. These natural hazards have been charted for many years and statistical data has been developed in order to predict the occurrence of severe weather events in an area. A threat, which is manmade, however, is not as predictable. Where, when, and to what degree that terrorist attacks occur is difficult to define during the design process (FEMA, 2006).

The threat of blast is a growing concern in the field of structural engineering. The Bureau of Alcohol, Tobacco, Firearms, and Explosives (ATF) recorded 220 successful and intentional bombing incidents in the year 2003, killing 5, injuring 19, and causing $506,912 in damage (Explosive, 2003).

The severity of a blast threat for a structure is defined by the make-up of the bomb, its size, the distance between the explosive and the structure, and the orientation and location at which the structure is hit by the pressure wave. Figure 1-1 shows the four types of loading due to blast. The first is primary fragments, which includes the debris from the actual explosive and its casing. The debris that is picked up and projected along the path of the blast is referred to as secondary fragments. Primary and secondary fragments result in large amounts of causalities, but do not significantly contribute to structural damage. When the explosion occurs, a pressure wave, or over-pressure, radiates out from the location of detonation. As the radial distance from the detonation site increases, the over-pressure decreases. The fourth and final loading type due to blast is responsible for the majority of structural damage. The reflective pressure occurs when the over-pressure blast load is reflected off the structure or target. The reflective pressure is maximized by decreasing the stand-off distance, or distance from the explosive to the target, and if the over-pressure hits the target orthogonally (Naito&Wheaton, 2006).

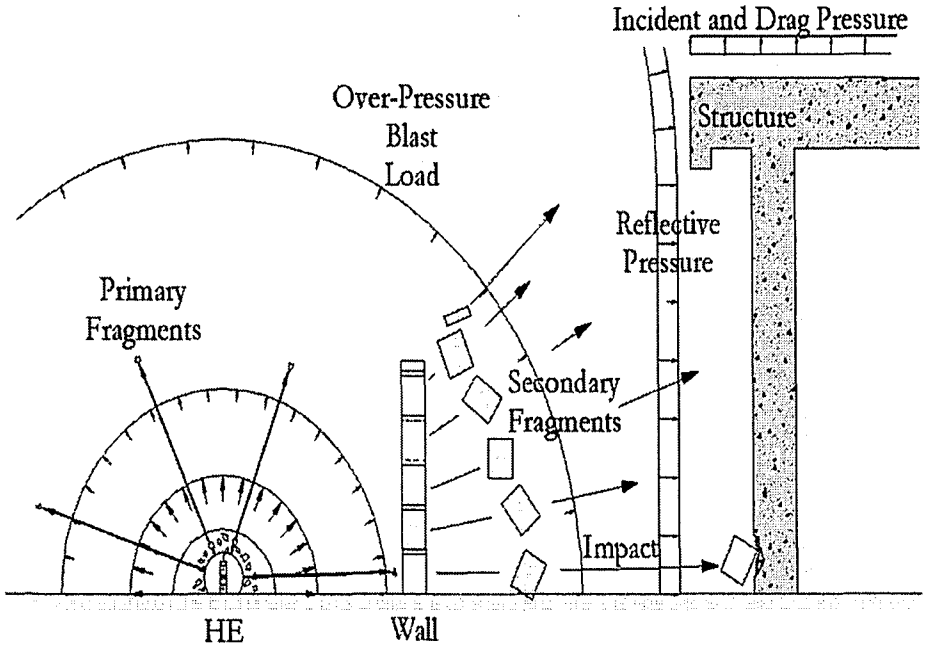


Figure 1-1: Types of Blast Loading (Naito&Wheaton, 2006)

The reflective pressure is assumed to rise to its maximum value instantaneously and then dissipates to atmospheric pressure over a few milliseconds. The area underneath the pressure-time curve defines the impulse of the blast as shown in Figure 1-2.

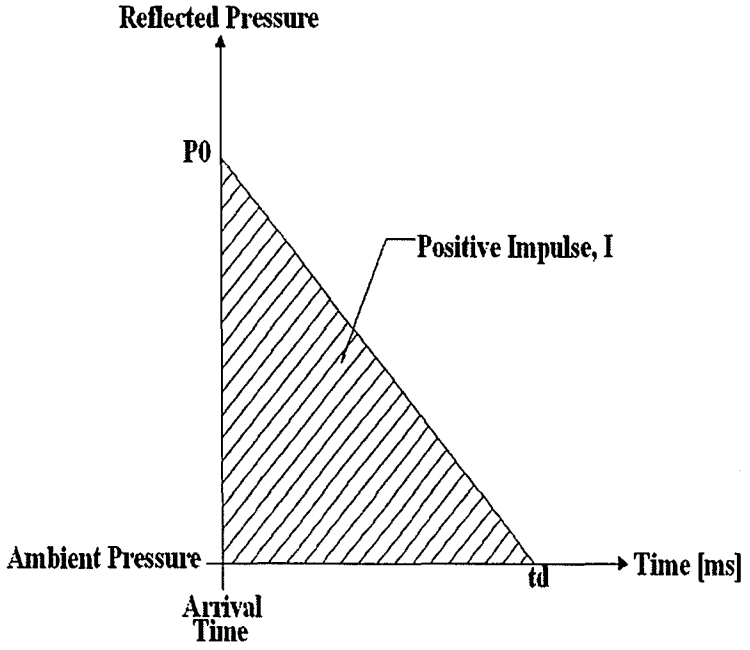


Figure 1-2: Definition of Impulse

Besides building collapse, occupant causalities are caused by fragmentation of the wall structure. Coating this material with polyurea could help to absorb some of the shock decreasing the chance of collapse as well as to act as a catch device for the fragments (Lane, Craig, & Babcock, 2001).

## 1.3 Introduction to Polymers and Polyurea

In polymer science, the word polymer refers to covalently bonded molecules made up of the repetition of simple and small chemical units (Clegg & Collyer, 1993; Moore, 1963). The earth is abundant with many natural polymers which can be found in various vegetable or animal sources. These sources range from animal horns to secretion of insects to fossilized tree resin. The use of these natural polymers not only increased over time, but drastically changed. There is evidence that the human population began to use these natural polymers as early as the fifteenth century for the purpose of artwork. Three hundred years later, the first polymer industry was developed to produce combs. It wasn't until the 1900's that these natural polymers were combined with other chemicals, resulting in the production of new substances such as vulcanized rubber (Introduction, 2005).

Polyurea is a category of polymers. The definition of a polyurea coating or elastomer is given by the Polyurea Development Association (PDA), whose objective is to disseminate information about polyurea; information such as a clear definition of polyurea products. They also are responsible for establishing protocol and standards for polyurea applications. The PDA defines a polyurea coating or elastomer as the result of a chemical reaction between a resin blend component and an isocyanate

component. A more detailed explanation of the chemical make-up and stoichiometry of polyurea will be given in Chapter 2.

Today's common applications of polyurea include linings for such things as Waste Water Treatment components, tanks, pipes, sewers, truck-beds, and aquarium linings. It is used as a coating for flooring, parking decks, bridges, and roofs. Polyurea can also be used for water or fuel containment and storage and has been used as joint fill and caulk in addition to being used in architectural design and decorative design (PDA, 2006).

## 1.4 Research Objectives

Polyurea coatings, as a blast retrofit option for structural components, has become of great interest to researchers in the field of structural engineering. There has been numerous full scale blast tests conducted on masonry walls coated with the material, of which a list of sources is given in Chapter 3. However, in addition to analyzing a full scale blast test on a structural system coated with polyurea, the research presented attempts to define mechanical properties of the polyurea determined from material testing along with tests conducted on individual coated structural elements at both static and dynamic rates. An understanding of the material itself at different strain rates as a structural material is needed along with an understanding of how it interacts with other structural materials through bond and how it affects the properties of the combined system to absorb energy before fracture. This is researched in order to help in the analysis and design of a structural system with a polyurea coating under blast load.

The objectives of this research are to:

- Develop an understanding of the mechanical properties of polyurea at different strain rates through a literature review and through experimental evaluation of the material
- Experimentally evaluate the performance of non coated and polyurea coated masonry and concrete beams under three-point loading in order to define bond strength and the combined systems ability to absorb energy
- Evaluate the recorded data and results of a full scale blast test conducted on a polyurea coated masonry wall system
- Suggest ways to adjust the design of a polyurea coated masonry wall based on the experimental results as well as the blast test results

## 1.5 Scope of Thesis

The remainder of the thesis consists of six chapters. Chapter 2 presents a detailed explanation on the chemistry and structure of polyurea and summarizes the results of the mechanical testing conducted on different polyureas used throughout the research. A comparison of the polyureas found in literature reviews to the experimental results is also provided. Chapter 3 presents the full-scale blast tests conducted on two polyurea-coated masonry walls. Chapter 4 then presents the experimental results from center-point loading tests conducted on small scale beams cut from a polyurea-coated masonry unit produced from the blast test and the results are used to understand the outcome of the full-scale blast tests. The experimental program is continued on larger scale beams made of concrete at static rates, which is presented in Chapter 5. In

Chapter 6 the concrete beams are tested under center-point loading at dynamic rates.

In Chapter 7, the researched is summarized and conclusions are derived.

## 1.6 Notation

The following notation is used within the thesis for consistency.

| | | |
|---|---|---|
| $A$ | = | cross-sectional area |
| $A_{lig}$ | = | projection of fracture zone on a plane perpendicular to beam axis |
| $b$ | = | width of specimen |
| $c$ | = | neutral axis depth |
| $d$ | = | depth of specimen |
| $E_c$ | = | concrete elastic modulus |
| $f'_c$ | = | concrete compressive strength |
| $g$ | = | gravity |
| $G_F$ | = | fracture energy |
| $h$ | = | hangover length |
| $I_g$ | = | gross moment of inertia |
| $i_r$ | = | reflected impulse |
| $l$ | = | specimen span length |
| $L$ | = | specimen span length |
| $M$ | = | ultimate moment |
| $m$ | = | Weight of beam between supports plus the weight of loading device not attached to machine following the beam until failure ($m_1+m_{2)}$ |
| $m_1$ | = | Weight of beam between supports |
| $m_2$ | = | Weight of loading device not attached to machine, following the beam until failure |
| $m_{total}$ | = | Mass of tup and 1/3 of concrete beam length |
| n.a. | = | Not applicable |
| $P$ | = | Ultimate applied load |
| $P_i(t)$ | = | Generalized inertial load |
| $P_r$ | = | Maximum reflected pressure |
| $R$ | = | Radial distance to point of interest (Chapter 3) |
| $R$ | = | Modulus of rupture (Chapter 4 and Chapter 5) |

| | | |
|---|---|---|
| $t_A$ | = | Time at which pressure rises instantaneously to maximum pressure |
| $t_o$ | = | Length of time needed for pressure to dissipate from maximum value to atmospheric pressure |
| $\ddot{u}_o(t)$ | = | Midspan acceleration |
| $v_{combined}$ | = | Velocity at which 1/3 of the concrete beam length and tup move at together |
| $W_o$ | = | Area under load-displacement curve |
| $w_c$ | = | Unit weight of concrete |
| $\Delta$ | = | System displacement |
| $\delta_o$ | = | Deformation at failure |
| $\theta$ | = | Angle of rotation |
| $\rho$ | = | Mass density of beam material |

# 2 Polyurea Properties

## 2.1 General

Essential in understanding how polyurea functions as a retrofit option, is a basic knowledge of the chemical materials that react together to form the polyurea, as well as the chemical structure that is taken by the polyurea once this reaction occurs. This chapter outlines these concepts as well as the batching techniques used to make polyurea. In addition the affect of these different elements and procedures on the mechanical properties of the material is presented. Different coating methods that could be used when implementing polyurea as a blast retrofit are presented. The polyureas used in testing throughout the duration of this project were batched at both Air Products and Lehigh University. The mechanical properties at static rates for both types of polyurea are presented and compared to each other as well as compared to polyureas from literature, some of which were also used as a structural retrofitting option. The performance of these same polyureas at dynamic load rates is also presented.

## 2.2 Chemical Materials of Polyurea

Polyurea is a category of polymers. It consists of an isocyanate component and a resin blend (PDA, 2006). An isocyanate is a group of atoms containing nitrogen, carbon, and oxygen arranged as R–N=C=O. The R represents a free radical, which has unstable valences (Kaufman, 1968 & Randall&Lee, 2002). Polyurea can also be made using a polyisocyanate component, meaning there is more than one isocyanate in the group of atoms (Primeaux II, 2004). A diisocyanate is most commonly used in the formulation of polyurea (Morton-Jones & Ellis, 1986). The isocyanate, in

polyurea, can either have aromatic or aliphatic characteristics (PDA, 2006). This defines how the isocyanate is bonded together. Aromaticity refers to a chemical component that joins atoms together using covalent bonds. The covalently bonded atoms produce a molecular structure comprising of at least one planar ring. Aliphatic compounds are any organic compounds which do not form this ring (Encyclopedia Britannica, 2007). There are many different isocyanate components available for use in polyurea. One could use a monomer, polymer, or any grouping of isocyanates. It could also be a quasi-prepolymer or a prepolymer (PDA, 2006). All of the polyurea coatings that were used in the research being presented were made with an aromatic diisocyante, MDI (diphenyl methane diisocyanate), whose formula is shown in Figure 2-1. MDI is an aromatic isocyanate component.

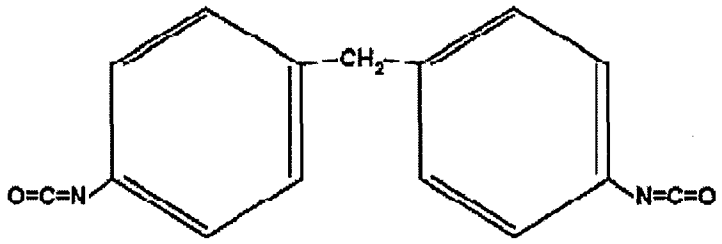


Figure 2-1: MDI Formula (Primeaux II, 2004)

The resin blend, or polyol, largely determines the properties of the polymer. The polyol of polyurea needs to contain an amine-terminated chain extender. An amine is an organic compound of which nitrogen is the vital atom (Randall&Lee, 2002). The presence of hydroxyls is a way of determining whether the resin blend is amine-terminated or not, since an amine-terminated resin will not have hydroxyls present (PDA, 2006). This is one of the major differences between polyurea versus

polyurethane, which contains the extra oxygen atom in its chain, making it more flexible. The primary amine used most often in polyureas is $NH_2$ (Wang, 1989). The use of $NH_2$ results in stronger bonds than polyurethane because there is the ability for more hydrogen bonding to occur. This leads to increased interchain attractions and higher strength (Rosthauser, 2006). The basic reaction to form a urea linkage is:

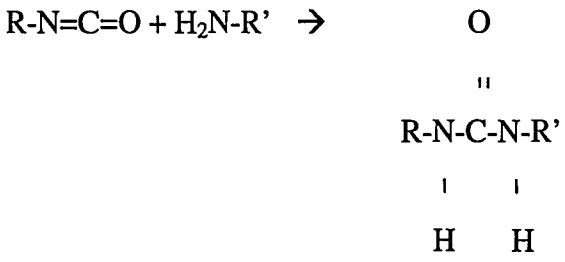


Figure 2-2: Formation of a Urea Linkage (Wang, 1989)

## 2.3 Polymerization

The polymerization of polyurea uses an addition mechanism. There are three basic steps. The first step is the initiation phase, where the double bonds in the isocyanate begin to break due to an input of energy into the system. This is usually carried through by the free radicals (R'), which have unstable valences. Their instability promotes the breaking of double bonds, allowing the isocyanates to bond with the other isocyanates as seen in Figure 2-2. The second phase is propagation or growth phase, during which the isocyanates are continually bonding together to form a chain since there is always an unsatisfied valence at the end of the chain. The third process is the termination phase, which can occur in at least two ways. The first is that two chains bond together. This would mean that they both connect at their unsatisfied

valence end, and produce a chain without unsatisfied valences. The other option is that a lone free radical bonds with the unsatisfied valence end of the chain (Wang, 1989; Kaufman, 1968). Polyureas use low molecular weight aromatic diamines, as a secondary amine. Without the secondary aromatic diamine, the primary amines would react instantaneously with the isocyanate. If the reaction occurs too quickly a non-equilibrium phase structure can result. The secondary aromatic diamine slows the reaction down (Wang, 1989).

## 2.4 Polyurea Structure

The structure of polyurea is considered crystalline; however, it is not the same type of chemical crystal structure one might typically think of, such as salt. Crystalline refers to the fact that the atoms are arranged in some type of order (Kaufman, 1968). The process of polymerization presents the idea that a polymer is made up of many chains that are each created and terminated differently and therefore can have different lengths. These chains are then distributed differently throughout the polymer (Moore, 1963).

Polyurea consists of hard segments and soft segments. The hard segments are usually the part of the polyurea that is crystalline in structure. This is the area where the chains lay parallel to each other for a significant distance due to hydrogen bonding, producing a strong interchain force (Kaufman, 1968; Randall& Lee, 2002; Moore, 1963). The hard segment regions are highlighted in Figure 2-3 (Kaufman, 1968). The hard segments create physical crosslinks across the soft segment regions, which are less polar and soft (Wang, 1989; Randall&Lee, 2002). In the soft segment region, which is referred to as the amorphous region, the chains are curved around each other

and twisted together as is also seen in Figure 2-3. Chains can pass through both the crystalline regions and the amorphous region (Kaufman, 1968). When the polymerization is occurring and the polymer hardens, the location of these regions is extremely important, because the amorphous region gives the polymer its elastic qualities whereas the hard segment regions allow the polymer to regain its original shape if the chains are stretched and, therefore, has an impact on the polymers toughness (Randall&Lee, 2002).

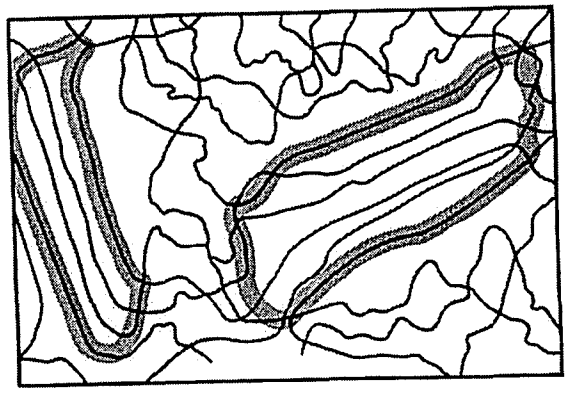

Figure 2-3: Structure of Polymer (Kaufman, 1968)

## 2.5 Mechanical Properties of Polymers and Polyurea

The structure of a polymer plays an important role in its physical properties such as elasticity and tensile strength as was just stated. A polyurea will react to an applied load or stress in three different stages. The first stage occurs due to the fact that the bonds, between links in the chain, begin to stretch. This causes a rapid response with a high modulus, but the response is reversible. If load is continually applied after the stretching of bonds occurs, the chains in the amorphous softer regions of the polymer begin to straighten out and reorient. This is elastic behavior that is reversible and, in this stage, the polymer can stretch a few hundred percent its original length. The

polymer has a low modulus during this phase. The final phase is one of viscous flow, and occurs when chains are able to slip past one another. This is irreversible. Depending on strain rate, the degree to which each of these stages will occur varies (Moore, 1963). This means that the properties of a polymer are dependent on strain rate.

There are two temperatures, which are specific to individual polymers that will give insight on the different physical properties. The first is the melting point of the mixture, which is the temperature at which no more crystal regions exist in the polymer. This is an indication of chain flexibility. The higher the melting point, the less flexible and more tough the material is. Polyurea has a high melting point due to the NH groups that allow hydrogen bonding, which means the interaction forces between chains in the crystal regions are much stronger (Moore, 1963). The melting point depends on the specific polyurea being examined as well as the number of chain atoms in a repeating unit and therefore there is no "typical" value for the melting point of polyurea. However, as can be seen in the graphical representation shown in Figure 2-4, the polyurea polymer tends to have a higher melting point than other common polymers, such as polyurethane.

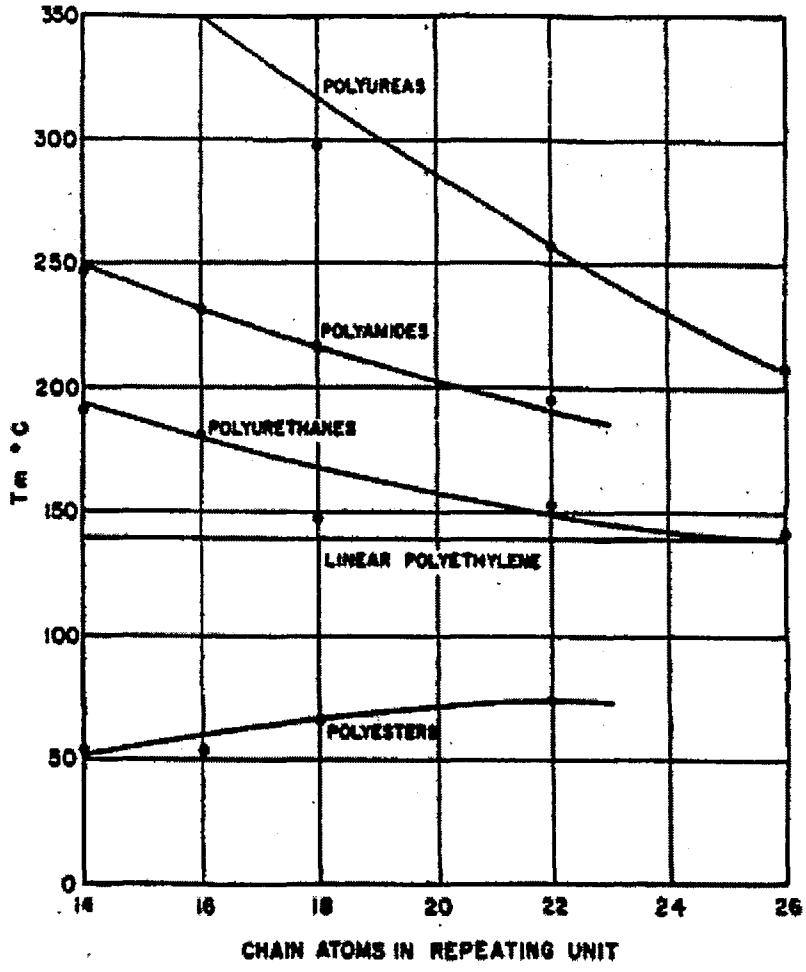


Figure 2-4: Melting Point of Polyurea and Other Polymers (Primeaux II, 2004)

The glass transition temperature is the temperature at which the properties of a polymer change from hard and brittle to soft and flexible. This temperature is more dependent on the amorphous region and the intermolecular forces between links in the chain, and therefore differs from polyurea to polyurea depending on its make-up. Below the glass transition temperature, the chains in the amorphous region are set in place. When the transition temperature is reached, the chains in the amorphous region are able to move together. This allows the curved chains to begin to straighten and reorient themselves, which makes the polymer more flexible and also tougher due

to the increased hydrogen bonding between chains. When the glass transition temperature is exceeded a significant amount of movement occurs, making the polyurea much stiffer.

The ability for polyurea to stiffen at the glass transition point is what makes it desirable for blast resistant applications. Polymers can reach the glass transition temperature by means of any energy input into the material. At rapid load rates typically associated with blast events significant energy is imparted to the polyurea which causes the material to achieve the glass transition temperature quickly. Thus under rapid loading the material acts as a stiff membrane while at slow rates the material performs in a flexible manner. The glass transition temperature is also affected by the crystalline regions; because if a larger amount of cross-linking is present the movement of the amorphous regions will be restricted, increasing the glass transition temperature (Moore, 1963).

## 2.6 Air Products' Polyurea of Interest

The polyurea examined by Air Products is like all polyureas in that it combines an isocyanate component and a polyol as discussed previously in this chapter. The isocyanate used by Air Products is a polymeric methylenediphenyldiisocyanate or MDI. The MDI is supplied by DOW Products and has a trade name of Modified MDI Isonate 143L. It is liquid at room temperature and has a low viscosity. The use of this MDI allows for more flexibility, since it has a reversible part in its formation which provides an additional isocyanate function (Dow, 2001). The amine or polyol used is produced by Air Products and is called VERSALINK P-1000 Oligomeric Diamine (VERSALINK), which is also liquid at room temperature. It has a high

viscosity, which requires it to be heated in order to lower its viscosity and allow it to be mixed with the MDI. The polyurea can be used for cast prototypes, elastomers, coatings, adhesives, sealants, and spray systems (VERSALINK).

### 2.6.1 Hand Batching

The Air Products' polyurea of interest was made at both the Air Products facilities as well as the ATLSS facilities at Lehigh University. The same batching procedure was used at both locations with varying pre-heating temperatures applied to the Versalink polyol. The following procedure was used for batching of the polyurea.

1. Store or pre-heat the P-1000 (A temperature of 158°F was used at Air Products, whereas a lower temperature of 130°F was used at Lehigh University to increase the working time. The initial temperature of the polyol controls the viscosity and pot-life of the P-1000. Higher temperatures increase the rate of reaction with the isocyanate, decreasing pot-life and viscosity).
2. Weigh the desired amount of P-1000 under a ventilation hood. This is important because P-1000 is a mild respiratory tract irritant. To make one 11-in. x 11.5-in. x 1/8-in.plaque with a volume of 15.8 $in^3$, 400 grams is used.
3. Weigh the amount of Isonate 143L that would result in a 4:1 ratio of P-1000 to Isonate 143L under a ventilation hood. Isonate is a moderate respiratory irritant which could cause sensitization by inhalation.
4. Add the weighed P-1000 to the Isonate 143L under ventilation hood.

5. Hand mix under ventilation hood until the liquid is of consistent color (no separation of color is seen). This is typically conducted with a paint stirrer over a 60 to 90 second period. Drill attached paint mixers have been used but tend to introduce small air bubble voids.

6. Put the mixture into the degassing chamber for approximately 2.5 minutes at a pressure of about 25 mmHg to allow a large amount of the air bubbles to rise out of the mixture. Using a higher pressure would increase the amount of air removed from the mixture.

7. If any containers have remnants of only the Isonate 143L, spray the container with neutralizing solution, which is made up of water, hand soap, and ammonium hydroxide, in the amount of a 1:1 ratio of neutralizing solution to Isonate 143L and allow to harden overnight. Any left over P-1000 or polyurea mixture will harden on its own overnight.

8. Before closing the Isonate 143L drum, apply a nitrogen blanket to the liquid by inserting the nitrogen hose opening into the drum for about a minute.

9. Cure the polyurea mixture at 158°F for 16 hours or at room temperature for two weeks.

If a polyurea plaque is being made, two 12 inch x 12 inch pieces of glass and a U shaped metal separator are coated first with acetone and then with Ease Release 405 from Smooth-On Inc. before preheating them along with the P-1000. After the polyurea mixture comes out of the degassing chamber, use the two pieces of glass, with the metal separator between them, to sandwich the polyurea by clipping the

bottom edges together before slowly pouring the polyurea down one side of the glass. Pouring down the side is done to reduce reentry of air into the mixture. Once a sufficient amount of polyurea has been poured down the glass, the two glass pieces are squeezed tightly together and then clipped on three of the four sides, leaving the top open to the air.

#### 2.6.1.1 Mixing Methods

Several different batching techniques were tested at the ATLSS facility before the above procedure was decided upon. One of the factors that was interchanged is the use of an electric mixing technique versus hand mixing. The polyurea plaque that resulted from this mixing technique did not enhance the physical properties of the polyurea. Tests following ASTM D-5279, which uses the process of dynamic mechanical analysis to compare relative properties of polymers such as the effects of processing and the cure of the mixture, as well as providing thermal properties, were conducted by the Polymer Science department at Lehigh University. Dynamic mechanical analysis (DMA) tests a rectangular specimen in a thermal chamber under torsional oscillations at a variation of temperatures. The tests allow the determination of elastic or storage modulus (G'), the loss or viscous modulus of the material (G"), and the damping coefficient or tan delta. When this data is plotted over a range of temperature it helps to identify the transition regions for the plastic. Figure 2-5, which plots the storage modulus, loss modulus, and tan delta of the hand mixed and mechanical mixed batches versus temperature, shows that there is little to no difference in the transition regions of the batches. The storage modulus is a good indication of hard segment content in the mix and it can be seen that the hand mixed

and mechanical mixed batches are very similar in that respect. The glass transition temperature, which is also a good indication of physical properties, in addition to hard segment content, is determined as the temperature at which the peak of the tan delta curve is achieved. The graph of Figure 2-5 shows that peaks of the tan delta curves are similar. Because the polyurea properties of the electric mixed batch were similar to those of the hand mixed batch, the hand mixed method was chosen since the electric mixing introduced a greater density of small air bubbles, which could be sources of stress concentrations when tensile loads are applied.

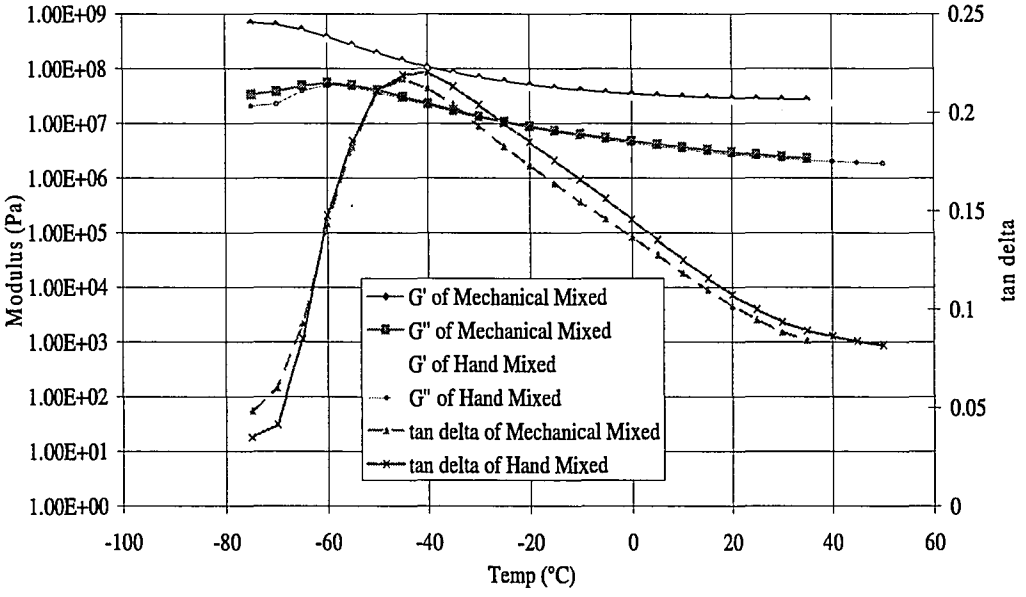


Figure 2-5: Comparison of Electric Mix to Hand Mix Batches

### 2.6.1.2 Preheated Temperature

Another variable of the batching process that was tested was the temperature at which the VERSALINK P-1000 was preheated and stored at. The recommended temperature of 158°F did not allow for a long enough cure time to produce a polyurea plaque as well as coat three concrete beam specimens. The temperature was lowered

to 100°F, but this temperature was too low to allow the chemical reaction needed for hardening to occur. When raised to 130°F, an adequate amount of working time, roughly 12 minutes, was achieved and this temperature still allowed the polyurea mixture to harden after curing.

### 2.6.2 Air Products' Coating Techniques

It is the hope that the polyurea of interest, produced by Air Products and also made at the ATLSS facility at Lehigh University, will put its mechanical properties to use in order to provide protection for structures and the people that inhabit them against blast loads. In order to do this, the components of a structure, or in the case of this research, individual specimens, must be coated with the polyurea in some way. There are different methods being investigated by Air Products at this time.

The first technique is a spray-on technique. This technique uses a different variation of the polyurea discussed in this chapter; one that is capable of being sprayed through a hose. The physical properties of this polyurea will be discussed in Chapter 3. The spraying apparatus has the capability of mixing and degassing the polyurea as it is in the process of being sprayed onto the components in need of retrofit. Once the components have been sprayed, the polyurea will begin to harden and requires a certain amount of time to reach full strength at air temperature. The amount of cure time depends on the polyurea used.

A second technique is to pre-fabricate panels of polyurea in a similar manner as was described to make polyurea plaques. The panels would be bonded to the component

in need of retrofitting using a thin coat of uncured polyurea, mixed up on-site and applied immediately.

Another method being considered is applying the uncured polyurea, mixed on-site, by paint roller. This would produce a thin coat of the polyurea, but layers could be used to achieve the required thickness. Again, an ambient temperature cure time would be needed.

The final technique, which was implemented in this research, is applicable for components not yet in place. A form is attached to the specimen, into which the polyurea is poured. Concrete beams tested for this research were coated in this manner, using wooden forms and a foam gap filler to prevent leakage outside of the beam as seen in Figure 2-6 and Figure 2-7. It is recommended that a new method of form sealant be used to prevent any inclusions on the edge of the beam. The form can be removed after an hour and if the size of the component or specimen allows it, the polyurea can be cured in a furnace at 158°F or again, the polyurea must be allowed to air dry for a certain amount of time to reach full strength.

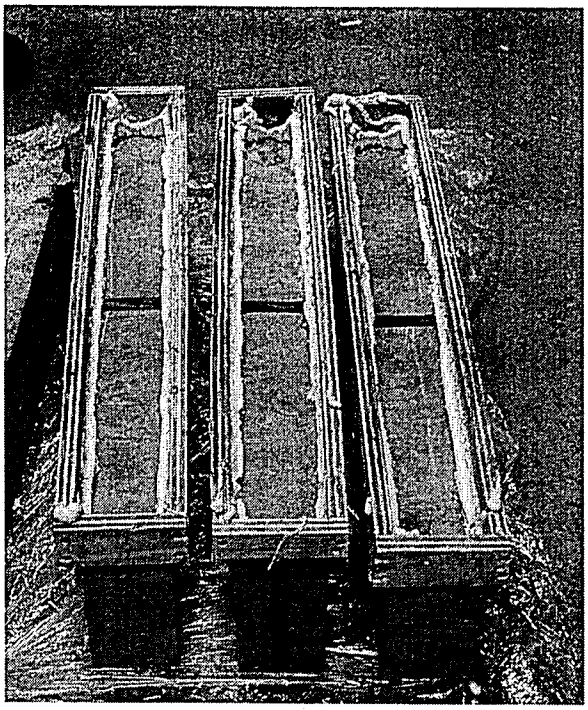

Figure 2-6: Forms in Place for Polyurea Pour

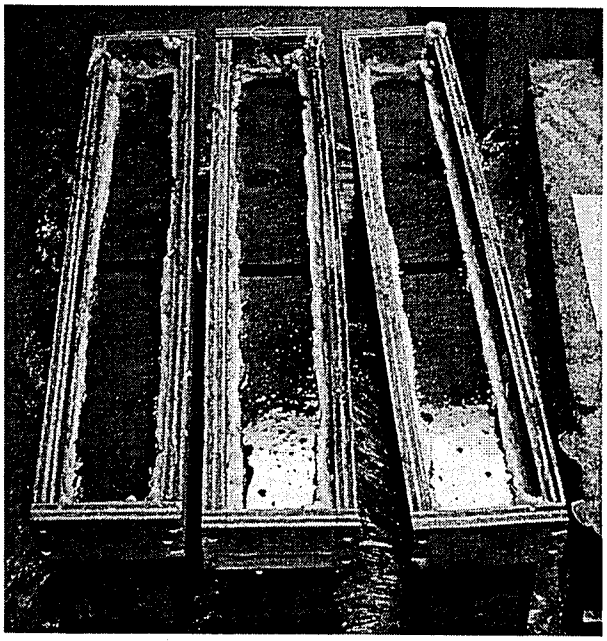

Figure 2-7: Specimens after Pouring of Polyurea

### 2.6.3 Mechanical Properties of Air Products' Polyurea of Interest

The most important mechanical properties needed to understand the use of polyurea for blast retrofitting are its tensile properties. ASTM D-412, which outlines tensile tests for rubbers and polymers, was used to obtain these characteristics.

The ASTM requires the test be conducted on a dumbbell shaped specimen. There are different dies that are acceptable for the test. Die C was used for all results presented, which has an overall length of 4.5 inches, a tab width of 1 inch and a gauge width of 0.250 inches. The thickness of the coupon must range between 0.05 inches and 0.13 inches according to ASTM D-412. The coupons were cut from the polyurea plaques with a hand press.

The specimens were then placed in the testing machine grips symmetrically, in order to distribute tension evenly throughout the cross section. Air Product testing lab measured elongation with an extensometer and the force was recorded for every specified elongation of the section. The tests done at Lehigh University also measured force for every specified elongation of the section, but the head travel of the machine was used, to measure displacement, rather than using an extensometer. This resulted in a larger strain value than the extensometer would produce, due to the fact that the elongation of the coupon tabs would be included in the head travel. The force and elongation at rupture was recorded at both Air Products and Lehigh University.

### 2.6.3.1 Polyurea Batched and Tested at Air Products

Air Products conducted ASTM D-412 tensile testing on batches of polyurea that were fabricated at their facilities. Three different loading rates were used: 2, 10, and 40 in/min. The general stress-strain behavior is seen for all tests done at static rates. This behavior is defined in Figure 2-8. E1 represents the elastic modulus. E2 is the second modulus of the material and E3 the third modulus. The tensile behavior follows the three stages of behavior described in Section 2.5, which as was stated, is a function of the polymer structure. The first modulus is generally the greatest and ends at point 1, which is the yield stress and yield strain of the material. This is calculated as the point of intersection of a line of best fit with a slope equal to E1 with the line of best fit with slope E2. The first region is followed by an almost flat region where there is a significant amount of deformation of the polyurea without a large increase in load. At the end of the test, there is a strain hardening effect, where the load again begins to increase and therefore the slope increases. At the end of the third region, the ultimate stress and strain is reached, which is point 3 of Figure 2-8. This is determined as the point at which failure of the polyurea coupon occurs.

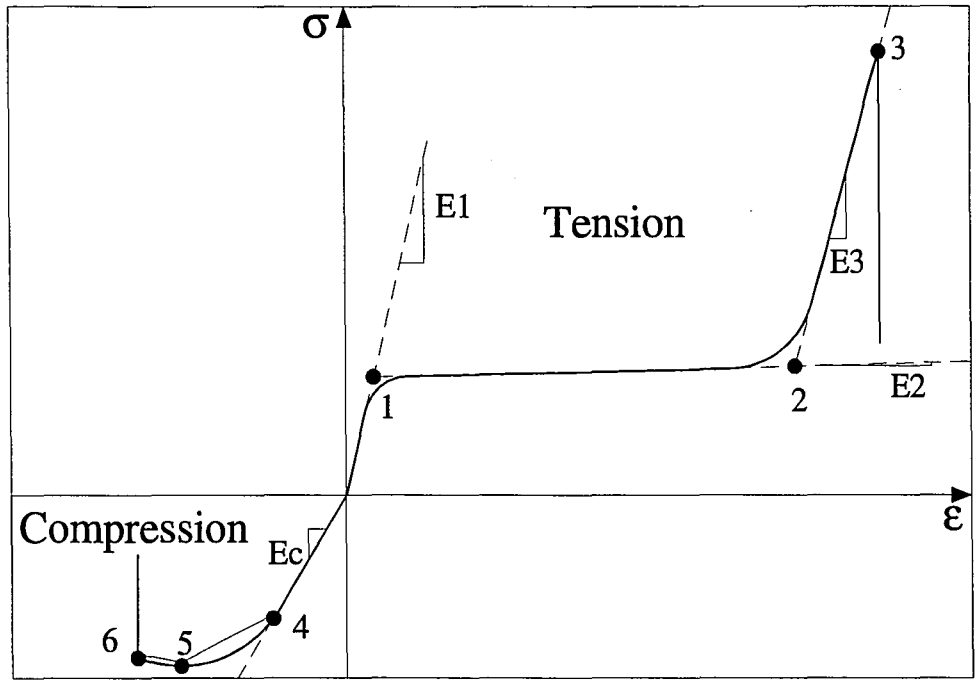


Figure 2-8: Definition of Regions and Mechanical Properties for Polyurea

For each loading rate, Air Products conducted multiple tests and the stress-strain curves were plotted together for each of the strain rates. Figure 2-9 shows the multiple curves for a strain rate of 2 in/min. From these multiple plots, an average curve was calculated, as shown in bold in Figure 2-9.

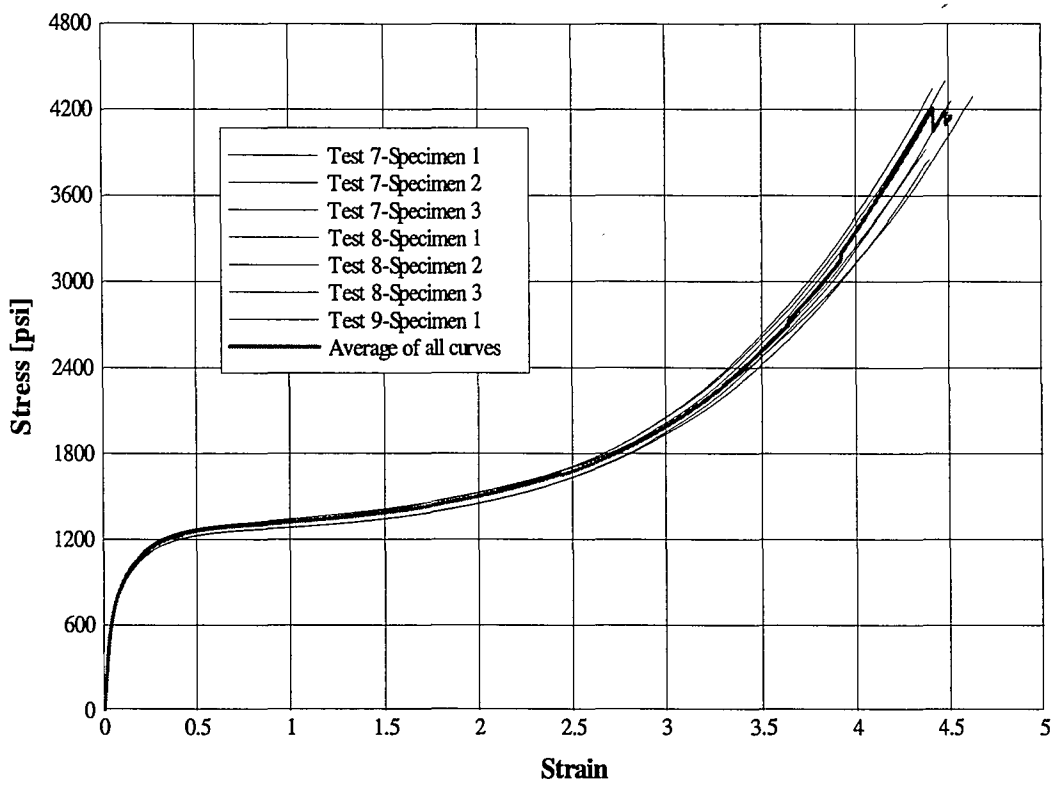


Figure 2-9: Stress-Strain Curves for a Loading Rate of 2 in/min

All tests were conducted by Air Products without direct observation by Lehigh participants. Consequently, unusual data sets were discarded and not incorporated into the averages. The average curve of Figure 2-9 follows the general smooth trend of the seven individual tests until almost near ultimate strength. The reason for the jaggedness in the average curve is that the seven tests reach failure at different stress and strain values. This causes a misrepresentation of the average curve since some of the curves do not continue while others do, but all are taken into account in the average. In order to correct this problem, the peak stresses and strains of the seven tests were manually averaged together and the resulting pair of values was used as the ultimate elongation and strength of the average curve. The next step was to fill in the gap between the last point of smoothness of the averaged curve and the calculated

ultimate stress-strain point. Different stress values, falling within the range of the last point of smoothness and the ultimate capacity, were chosen, starting with 3,200 psi (for this example). The corresponding strain values from all seven of the tests, if the test had not reached failure yet, were averaged together. This step resulted in the strains used for the average curve, but another step was taken to generate the stresses to assure a smooth averaged trend. Three different slopes were fitted to each of the seven datasets between 3,200 psi (for this example) and the individual curves' ultimate stress. These slopes and line equations were used to determine the average stresses, by inputting the average strains previously determined into these equations and averaging the resulting stresses from the different curves at a given strain value. These points then represent the average curve data. This process was followed for all three strain rates, and at least three curves were used to generate the average curves, which are presented in Figure 2-10.

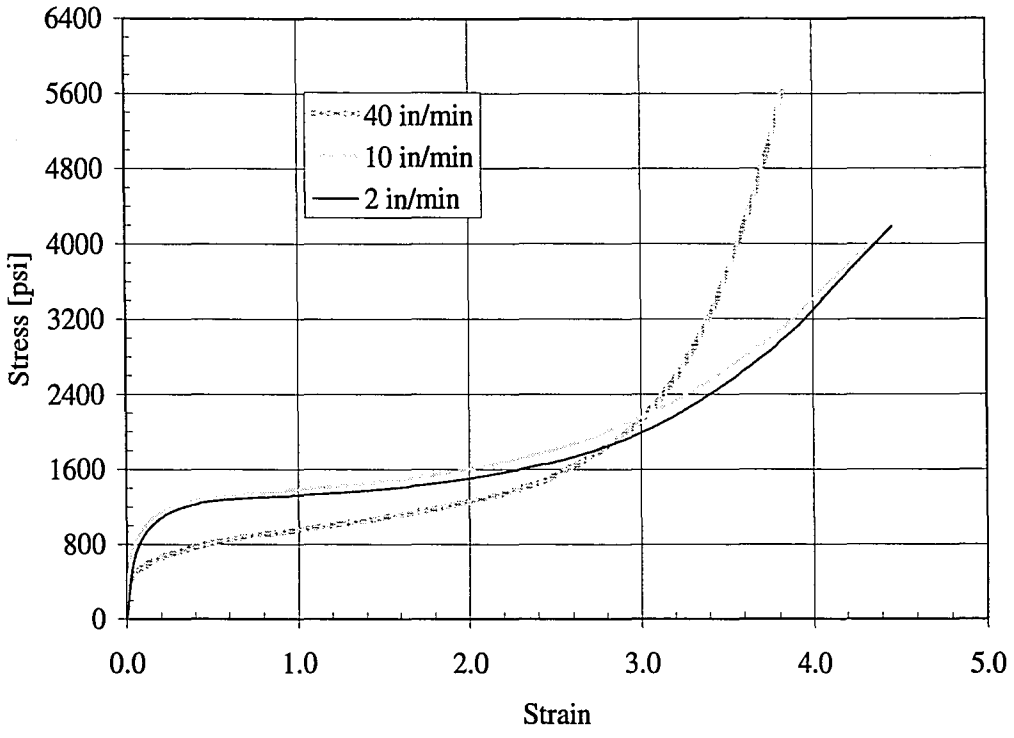


Figure 2-10: Average Stress-Strain Curves for Polyurea made by Air Products

While these strain rates are all static, there is clearly an affect on the response of the polyurea material. The differences can be described numerically by determining the important values defined in Figure 2-8. These values are given for all three strain rates in Table 2-1.

| Loading Rate | E1 [psi] | E2 [psi] | E3 [psi] | E100% [psi] | E300% [psi] | Yield Strain | Yield Stress [psi] | Ult. Strain | Ult. Stress [psi] |
|---|---|---|---|---|---|---|---|---|---|
| | | | | | | | | | |
| **2 in/min** | 18447 | 142 | 1792 | 1315 | 664 | 0.065 | 1202 | 4.460 | 4182 |
| | | | | | | | | | |
| **10 in/min** | 74029 | 187 | 1519 | 1375 | 717 | 0.016 | 1207 | 4.365 | 4043 |
| | | | | | | | | | |
| **40 in/min** | 104412 | 276 | 4917 | 950 | 710 | 0.006 | 674 | 3.825 | 5639 |

Table 2-1: Mechanical Properties of Polyurea at Different Strain Rates

The general trend observed by each of the three moduli is that as strain rate increases, the moduli increase, meaning the polyurea becomes stiffer or the hard segment areas become more active. This trend can be seen in Figure 2-11, which presents a closer look at the second modulus of all three strain rates.

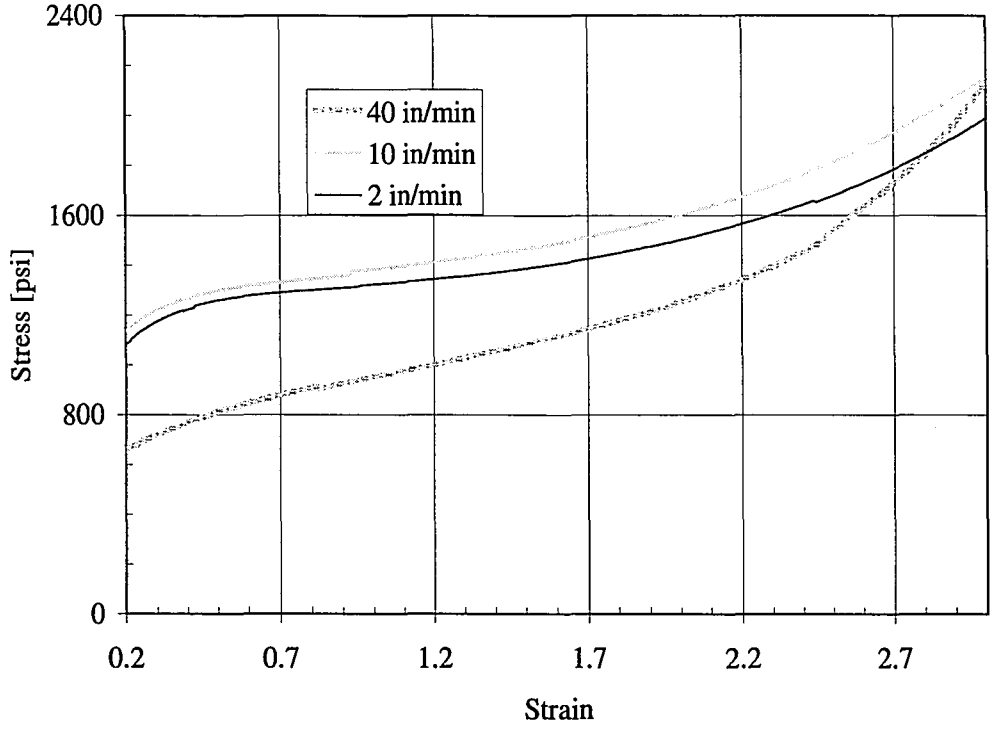


Figure 2-11: Zoomed View on Second Modulus for Three Strain Rates

There is only one data set that does not follow this trend, which is the value of E3 at a strain rate of 10 in/min. This could be due to the manual averaging that was previously described, that was applied only to this region. The yield strain decreased in value for increasing strain rate. There was almost no effect on yield strength between 2 in/min and 10 in/min, but the yield strength did decrease by almost 50% when the polyurea was tested at a rate of 40 in/min. These two trends indicate that as the strain rate increases, there is less of an elastic or first phase experienced by the

polyurea. The ultimate strain is seen to decrease with increasing strain rate and the ultimate stress, although similar at 2 in/min and 10 in/min, begins to increase with increasing loading rate. This strengthens the notion that the polyurea is becoming stiffer since overall; it is elongating less and breaking at a higher load. Also given in Table 2-1 , are the values of E100% and E300%. These values represent the slope between the origin and the data point having a strain of 100% and a strain of 300% and are used for comparison to other polyurea mixtures found in literature, some used for retrofitting in blast. There is a decrease in the E100% value when loading at a rate of 40 in/min, which again indicates that the elastic or first phase is shortened at higher loading rates. An effect on E300% is not seen between tests, meaning that as the rate of the test increases, the stress at which 300% elongation is achieved remains similar.

As a general observation the third stiffening region occurs at lower strains with increased strain rate. The increase is not linear at the load rates examined. For example a 5x increase in rate from 2 to 10 in/sec resulted in only a marginal change in response while the 4x increase from 10 to 40 in/min resulted in a significant change. This may indicate the presence of a threshold rate needed to alter the material characteristics. As discussed previously this threshold may relate to the energy input and glass transition temperature of the material. Additional research is needed to identify the source and level of this change.

#### 2.6.3.2 Comparison of Air Product's Batch and Testing Result to Literature

As was stated, the different values obtained by the testing of Air Products' polyurea can be compared to data of different polyureas found in literature, some of which

were also used as a blast retrofit. Information about the specific polyurea and stress-strain related values from different sources are summarized in Table 2-2.

| Source | Polylurea Information | Loading Rate | Modulus of Elasticity | Secant Modulus (E100%) | Secant Modulus (E300%) | Yield Stress | Elongation Capacity | Tensile Strength |
|---|---|---|---|---|---|---|---|---|
| (Davidson, 2005) | Pure, spray-on, off the shelf polyurea (True Strain, Stress) | 2 in/sec | 34,000 psi | X | X | 1,700 psi | 90% | 2,000 psi |
| (Rosthauser,1996) | $C_4$-Ether-Based Polymer with 20% trans, trans-4,4'-diisocyanatodicyclohexyl methane. | X | 19,500 psi | 1,765 psi | 4,396 psi | X | 312% | 4,410 psi |
| (Rosthauser,1996) | $C_4$-Ether-Based Polymer with 97% trans, trans-4,4'-diisocyanatodicyclohexyl methane. | X | 19,500 psi | 1,539 psi | 3,181 psi | X | 382% | 4,412 psi |
| (Rosthauser,1996) | $C_3$-Ether-Based Polymer with 20% trans, trans-4,4'-diisocyanatodicyclohexyl methane. | X | 19,500 psi | 1,427 psi | 2,646 psi | X | 459% | 4,522 psi |
| (Rosthauser,1996) | $C_3$-Ether-Based Polymer with 97% trans, trans-4,4'-diisocyanatodicyclohexyl methane. | X | 19,500 psi | 1,406 psi | 2,640 psi | X | 370% | 3294 psi |
| (Resin,1997) | PERMAX-700&700HP are made of two parts and 100% solids. It is an elastomeric coating. | X | X | X | X | X | 200-250% | 2,039 psi |
| (Knox) | Pure polyurea, spray-on liner | 33 in/sec | 34,000 psi | X | X | X | 89% | 2,011 psi |
| (Wang, 1989) | Not available | X | 34,000 psi | X | Ranges from 22,000 to 26,100 psi depending on make-up | X | Ranges from 53.6%-94.4% depending on make-up | Ranges from 1,840 to 2,040 psi depending on make-up |
| (Roshdy, 2005) | General values for polyureas | slow rate | X | 700-1,000 psi | 1,200-1,400 psi | X | 200-800%, typically more than 400% | 2,000-8,000 psi |

Table 2-2: Summary of Polyurea Properties from Literature

Looking at the data provided in Table 2-2, it must be noted that Davidson's data is reported in true stress and true strain and will be compared with Air Product's P-1000 polyurea later. Due to the fact that Wang and Knox present similar data to that of

Davidson's values, for initial modulus, tensile strength, and elongation capacity, it may be concluded that they are also reporting values of true stress and true strain.

The above data specifies an initial Modulus of Elasticity (E1) of 19,500 psi by Rosthauser, who does not supply a load rate. In comparison to Air Products' P-1000 polyurea, Rosthauser's modulus is similar to a modulus at a rate of 2 in/min, which is equal to 18,447 psi. Therefore, the load rate of Rosthauser may be close to 2 in/min. The average literary value for a secant modulus at 100% strain is 1,397 psi which is comparable to the E100% value for P1000 at a loading rate of 2 in/sec and 10 in/sec. At slow rates, P-1000 polyurea will reach 100% strain at the same stress value as other polyureas. The similarity between initial modulus and E100% values indicate that the elastic or initial phase of the P-1000 polyurea is comparable to most polyureas. However, P-1000 polyurea has an E300% secant modulus of about 700 psi at slow loading rates. This value is significantly lower than the E300% values stated in different literature sources. Therefore, Air Products' polyurea of interest reaches 300% strain at a lower stress than other polyureas. This could indicate that the P-1000 polyurea has a longer second phase or a lower second modulus then other polyureas.

The elongation capacities, stated in previous literature, range from 200% to 800% at a static rate. P-1000 polyurea has a value of 446% at a loading rate of 2 in/sec. This it is near the average of other materials used. Therefore the lower second modulus or longer second phase does not increase its overall elongation capacity. The average ultimate strength of polyurea found through literature is 4,097 psi (excluding Wang's, Davidson's, and Knox's values). At the lowest loading rate of 2 in/sec, P1000 is able

to achieve an ultimate strength of 4,182 psi and the value continues to increase as rate increases. P-1000 polyurea can therefore withstand an equal or greater total force than other polyureas, depending on load rate.

The average stress-strain curves of P1000 were converted to true stress and true strain values in order to compare the values to the remaining literary sources. The plots are shown in Figure 2-12 and the important values are summarized in Table 2-3.

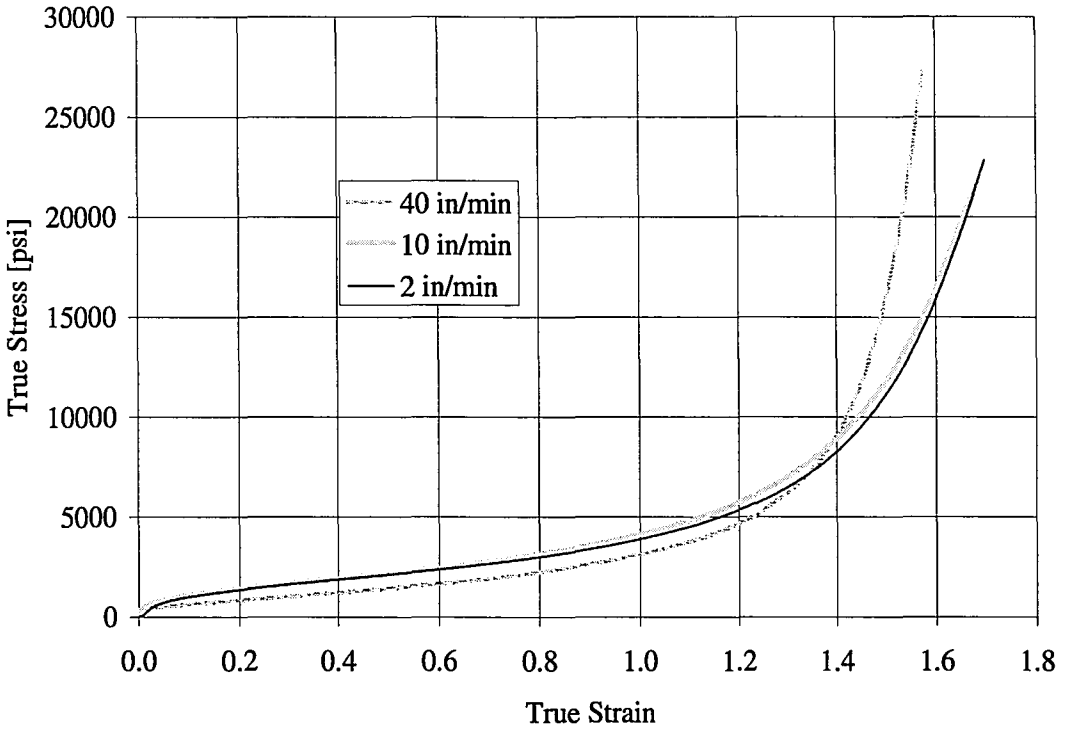


Figure 2-12: True Stress vs. True Strain for Air Product's Polyurea

| Loading Rate | E1 [psi] | Yield Strain | Yield Stress [psi] | Ult. Strain | Ult. Stress [psi] |
|---|---|---|---|---|---|
| | | | | | |
| **2 in/min** | 18474 | 0.033 | 567 | 1.697 | 22837 |
| | | | | | |
| **10 in/min** | 74642 | 0.008 | 443 | 1.680 | 21688 |
| | | | | | |
| **40 in/min** | 104856 | 0.006 | 398 | 1.574 | 27209 |

Table 2-3: True Stress and Strain Values of P-1000 Polyurea for Comparison

The value for the elastic modulus or E1, given in true stress and true strain, is listed as 34,000 psi by Davidson, Wang, and Knox. However, Davidson conducted his tests at a strain rate of 2 in/min, whereas Knox's tests were done at 33 in/min. As was seen by Air Products' tests, the initial modulus is expected to increase as strain rate increases. An explanation for this could be that the polyureas tested by Davidson and Knox could have had a completely different chemical make-up. The given value of 34,000 psi would fall in between a strain rate of 2 in/min and 10 in/min for Air Product's polyurea. This means that Air Products' polyurea is initially more flexible with less hard segments than Davidson's polyurea. Looking at yield stress, Davidson lists a much higher value of 1,700 psi compared to the Air Products' value of 567 psi. This is also an indication that Davidson's polyurea has a larger hard segment content that would allow the polyurea to continue taking load without a large amount of deformation in the beginning of the test, allowing the first region to control for longer. Since Knox's tests were conducted at 33 in/min, it seems that Air Products' P-1000 polyurea contains more hard segments than this polyurea. Wang gives a range for maximum elongation of 53 to 94% and Knox's and Davidson's maximum elongation are at the higher end of this range. However, Air Products' polyurea has a higher elongation capacity than their stated values, even at a rate of 40 in/min. The

polyurea is capable of elongating to about 150% its original length; again, supporting the idea that Air Products' polyurea is more flexible than Davidson's. The higher elongation capacity probably results from a larger second region, and based on the ultimate strength being an order of magnitude higher than Davidson's, Wang's, and Knox's, it seems that it has more strain hardening capability in phase three as well. Therefore, even though the elastic region is smaller, it has the ability to elongate more and take a higher amount of load due to its capabilities in the other two regions.

#### 2.6.3.3 Static Properties of Polyurea Batched at Lehigh University

The batching process used at Lehigh University, in the ATLSS facilities, was similar to those followed at Air Products. A few parts of the process were modified due to either limitation of the facilities, such as the amount of pressure generated in the degassing chamber, or to meet the needs of the polyurea use, such as the storage temperature of the Versalink P-1000 to acquire a longer pot life. The ingredients were the same as Air Products'. The polyurea made at ATLSS is the polyurea that was used as a coating for two out of the three testing phases conducted for this research that will be discussed later. This polyurea was batched and tested at Lehigh University. The static tension tests were carried out at a rate of 4 in/min following the guidelines of ASTM D-412. The elongation was measured from the head displacement, not an extensometer on the specimen as it was done at Air Products. An average stress-strain curve of Batch 4 out of eight batches is shown in Figure 2-13 along with the data provided by Air Products previously presented. Values of interest for Batch 4 are presented in Table 2-4.

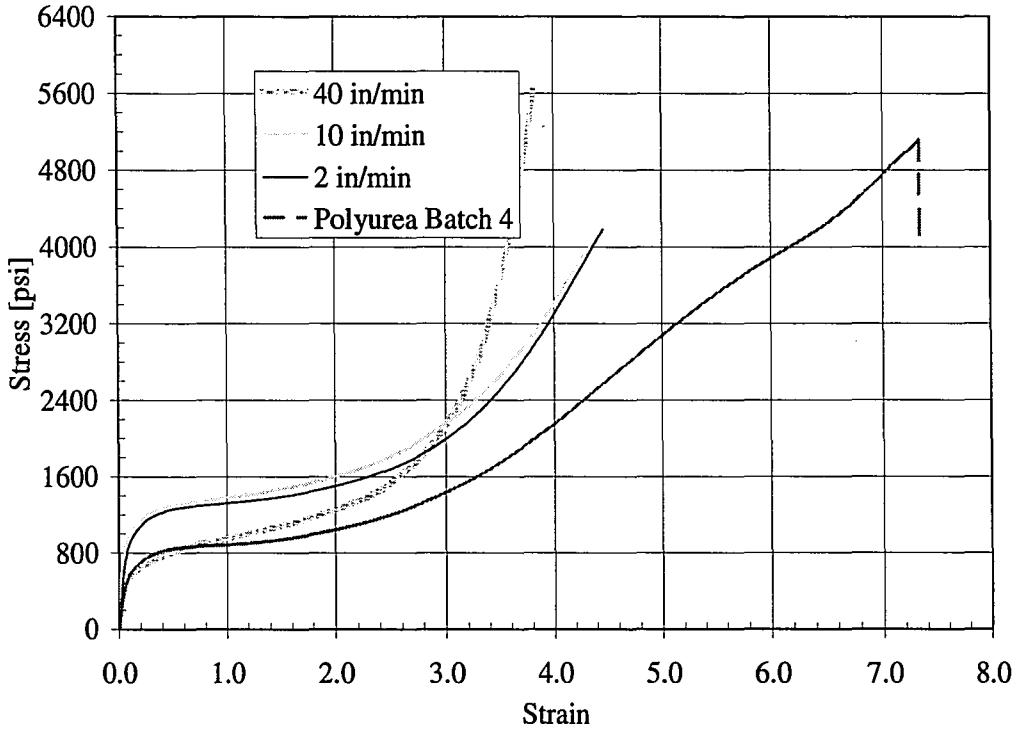


Figure 2-13: Average Stress-Strain Curve for Batch 4 Polyurea

| Loading Rate | E1 [psi] | E2 [psi] | E3 [psi] | E100% [psi] | E300% [psi] | Yield Strain | Yield Stress [psi] | Ult. Strain | Ult. Stress [psi] |
|---|---|---|---|---|---|---|---|---|---|
| 4 in/min | 8890 | 79 | 853 | 888 | 450 | 0.09 | 816 | 7.3 | 5121 |
| 250 1/sec | 10200 | 677 | - | 2480 | - | 0.18 | 1860 | 1.8 | 2940 |

Table 2-4: Average Data Values for Batch 4 Polyurea

It would be expected that the data from this test, conducted at a rate of 4 in/min would fall between the data sets conducted at 2 in/min and 10 in/min by Air Products. However, the data indicates a much more flexible polymer. All three moduli are on average 49% lower than those of Air Products' polyurea that was tested at 2 in/min, meaning in all three regions, the ATLSS's polyurea is less stiff. The E100% and E300% values are 32% lower than that of the Air Products' polyurea values at 2

in/min. This means that these specified elongations occur at a much lower stress value than those of the Air Product's polyurea, again indicating a less stiff polymer. This difference in stiffness allows the ATLSS's polyurea to stretch 59% more than the Air Products' polyurea and withstand a load that is 22% higher than that of the Air Products' batch. The difference in stiffness may be contributed to, not only the actual chemical make-up and structure of the polyurea, but by the presence of a higher quantity of air bubbles than is seen at Air Products. The presence of air bubbles could lower the overall stiffness of the entire coupon by reducing the cross-sectional area of the material.

#### 2.6.3.4 Dynamic Properties of Polyurea Batched at Lehigh University

Dynamic tensile tests, using the same grips and general testing procedure of ASTM D- 412, were used to test Polyurea Batch 4 made at Lehigh University. A more thorough description of testing procedures and results can be found in the Master's Thesis of Ken O'Kelly Lynch at Lehigh University. The tests were conducted at a range of strain rates, but a rate of 250 /sec is of interest, as it is the average strain rate seen by the polyurea in the dynamic test series of this research. Compared to the static rate of 0.03/sec, the rate is increased by 249.97/sec during dynamic testing. The stress-strain curve of the Batch 4 Polyurea is shown in Figure 2-14 along with the static stress-strain curve of Batch 4 for comparison.

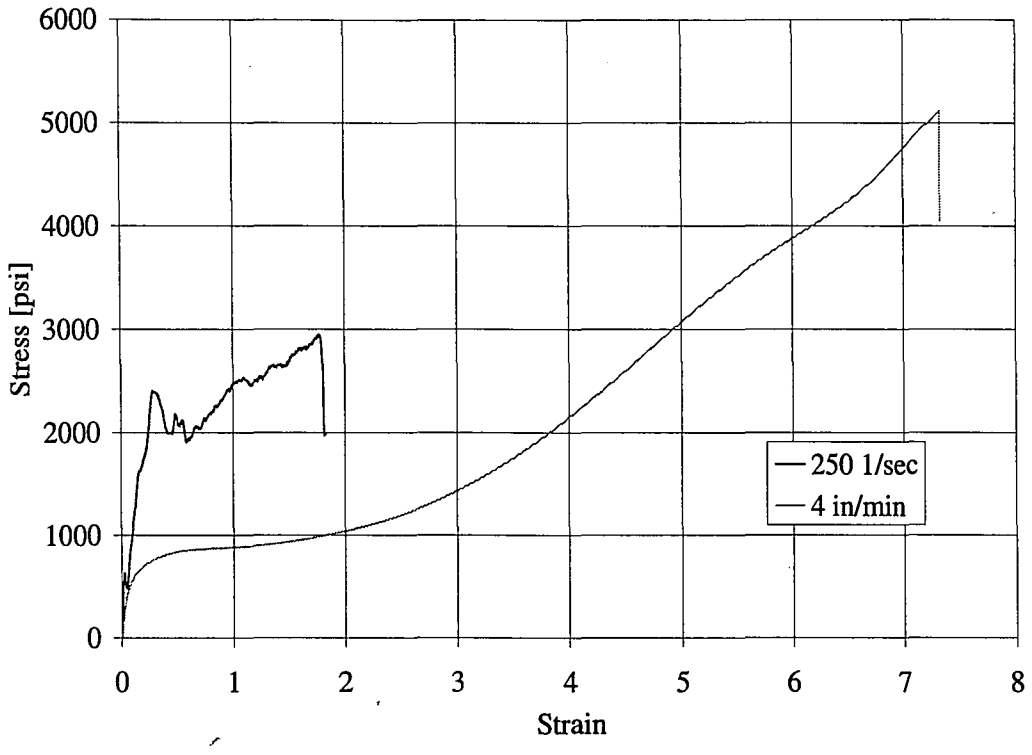


Figure 2-14: Dynamic and Static Stress-Strain Curve for Polyurea Batch 4

The dynamic data is not as smooth as the static rate data, due to vibrations of the test set-up, instrumentation, and specimen. However, two distinct regions can be seen. An approximate bi-linear fit was correlated to the data as shown in Figure 2-15. From this fit, a comparison between static and dynamic properties can be compared looking at the important values of Figure 2-15.

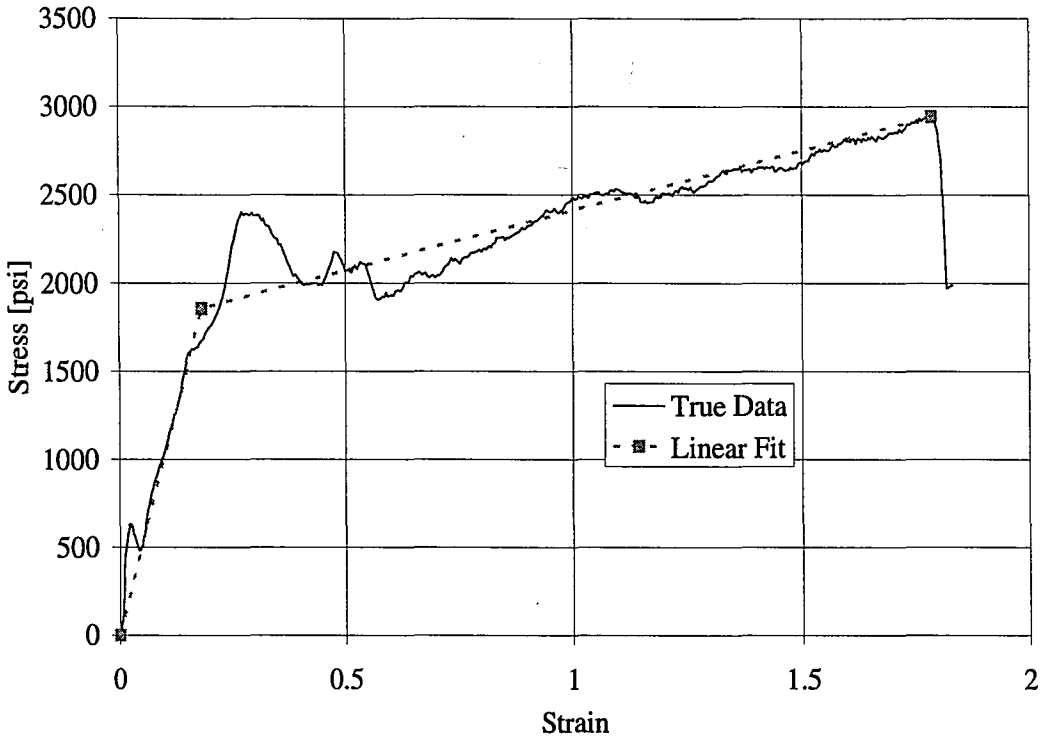


Figure 2-15: Bi-Linear Fit to Dynamic Stress-Strain Curve

| Loading Rate | E1 [psi] | E2 [psi] | E3 [psi] | E100% [psi] | E300% [psi] | Yield Strain | Yield Stress [psi] | Ult. Strain | Ult. Stress [psi] |
|---|---|---|---|---|---|---|---|---|---|
| 4 in/min | 8890 | 79 | 853 | 888 | 450 | 0.09 | 816 | 7 | 5121 |
| 250 1/sec | 10200 | 677 | - | 2480 | - | 0.18 | 1860 | 1.8 | 2940 |

Table 2-5: Dynamic Physical Properties of Polyurea Batch 4

The initial modulus stays almost exactly the same at dynamic rates as it does at static rates, with only a 14.7% increase. However, the second modulus, which is the last modulus seen by the dynamic test specimen, has increased by 757%. This means that the polyurea has become stiffer in the second phase or that the second phase is extremely short when tested at high rates and that this region is actually the third region. There is a much stronger relationship between the static rate third modulus and the dynamic rate "second modulus", with only a decrease of 26%. This could

indicate that the dynamic response of polyurea is defined only by the first and third stage of behavior. The strain at which yield occurs is larger for the dynamic tests and yield also occurs at a higher stress, as well. This indicates that the first phase is longer at dynamic rates than at static rates, but may not necessarily be an elastic region and therefore not true yield. The ultimate strain has decreased by 74.3% at dynamic rates as compared to the ultimate strain reached at static rates. This also supports the conclusion that the polyurea has become stiffer in the second region. A stiffer polyurea would fracture earlier and at a lower stress value, which is true of the dynamic rate, which has an ultimate stress that is 42.6% lower than the same polyurea at static rates.

#### 2.6.3.5 Spray-on Polyurea Produced and Tested at Air Products

Air Products uses the spray-on coating technique described earlier in this chapter in Section 2.6.2. The make-up and properties of the spray-on coatings have to be different than the mixtures that have been previously examined due to the fact that it must be viscous enough to be sprayed through a hose apparatus. Therefore, the ingredients of the spray-on polyureas are not P-1000 and Isonate 143L. The stress-strain curves of the two different spray-on mixes made at Air Products are shown in Figure 2-16 and the properties of the mixtures are described in Table 2-6.

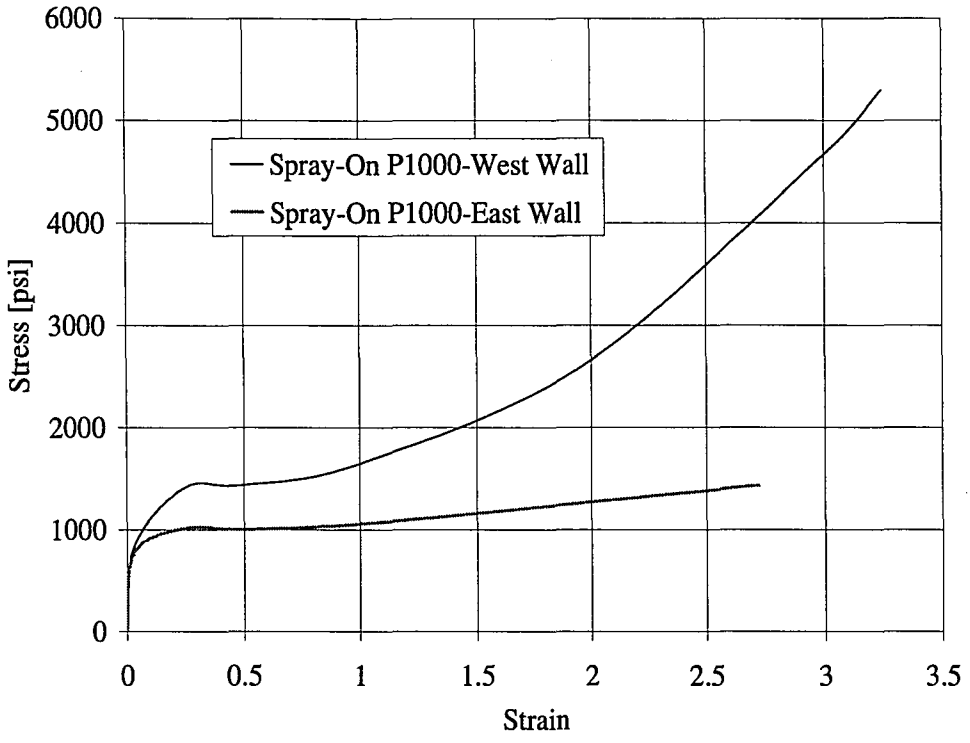


Figure 2-16: Engineering Stress-Strain Profile of Spray-on Polyureas

| Polyurea | Wall | Modulus of Elasticity [psi] | Yield Strength [psi] | Ultimate Strength [psi] | Maximum Elongation [%] |
|---|---|---|---|---|---|
| 70-1 | East | 25800 | 776 | 1,400 | 272 |
| 70-5 | West | 27840 | 841 | 5,300 | 323 |

Table 2-6: Spray-on Polyurea Properties

A comparison can be made between the spray-on polyurea properties and the plaques made and tested at Air Products, for which a visual is shown in Figure 2-17. The testing rate for the spray-on mixture is 4 in/min, which is between 2 in/min and 10 in/min, but closer to 2 in/min. The initial modulus of the spray-on mixtures is higher than the initial modulus of the polyurea plaque discussed previously tested at 2 in/min. For the Polyurea 70-1, the modulus is 39.9% greater and for Polyurea 70-5,

it is 50.9% greater. This is expected, since the loading rate is higher. Also expected, is that the initial modulus of the spray-on systems is less than that of the plaque's tested at 10 in/min, by an average of 63.8%. As can be seen from Figure 2-17, Polyurea 70-1 is considerably less stiff than the plaques made at Air Products after the yield point is passed, whereas Polyurea 70-5 is stiffer than these plaques. Also the elastic range is shorter, due to lower yield strength than the plaques tested at 10 in/min and 2 in/min. The ultimate elongation is less for both Polyurea 70-5 and Polyurea 70-1 than that achieved by the plaque tested at both rates by at least 100% elongation. The stiffer Polyurea 70-5 achieves a higher ultimate strength, which is greater than that of the plaque tested at 2 in/min by 26.7%. The less stiff Polyurea 70-1 has an ultimate strength that is 66.5% less than the ultimate strength of the plaque tested at 2 in/min.

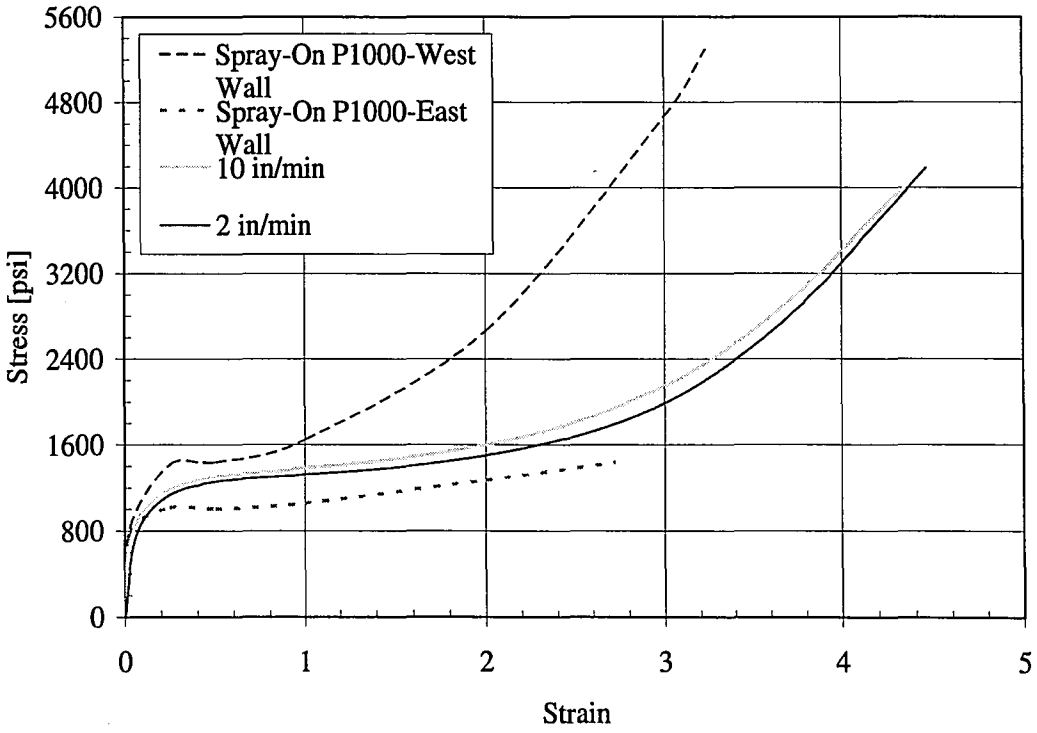


Figure 2-17: Comparison between Polyurea Plaque and Spray-on Polyurea

#### 2.6.3.6 Conclusions about Mechanical Properties of Air Products' Polyurea of Interest

It is clear that there are many factors that influence a polyurea's physical properties and that no two polyureas are guaranteed to have the same or similar properties, unless batched and cured at the same facilities with the same ingredients. The physical properties depend on not only the ingredients used, but the polymer structure including the length of the chains present and their orientation in regards to other chains, the mixing and curing process of the polyurea, the presence of air bubbles, and also the rate at which the polyurea is tested at.

Looking solely at the two different spray-on polyureas, which were mixed and applied in the same manner but were different in their components or ratios of components, a major difference in stiffness and ultimate capacity was seen. When the same components and ratios of components were used differences still occurred. Looking at the Air Products' polyurea that was made with the same ingredients and a similar process as was used at Lehigh University; there were still differences in their physical properties. The polyurea produced at Lehigh University was much more flexible than that produced at Air Products, which allowed for a larger elongation capacity. The Lehigh University polyurea also achieved a higher ultimate strength. Therefore, the differences must be due to the physical structure which the polymer took when cured in addition to the presence of more air bubbles or flaws in the Lehigh University batch.

Literature seems to present two different types of polyureas. The first had a similar initial region to that of the polyurea batched at Air Products. However, the Air

Products' polyurea was less stiff in the second region, but still had more strain-hardening ability that allowed it to achieve a higher ultimate strength at about the same ultimate elongation.

The second polyurea presented in literature, such as the polyureas of Davidson and Wang, seemed to be much stiffer during the initial phase than that of the polyurea produced by Air Products. The decrease in stiffness also allowed the Air Products' polyurea to achieve a higher ultimate elongation. However, the Air Products' polyurea also achieved a higher ultimate strength, meaning it may have had better strain-hardening capabilities.

The effect of strain rate was seen even at static rates. When the rate of loading was increased statically, all three moduli increased, meaning the polyurea acted more stiff. This is probably why the ultimate strain decreased and the ultimate strength increased. The effect of the initial region decreased as the yield point was reached earlier. This could be why there were only two regions seen during the dynamic test. The initial, elastic region may not have occurred. The second region seen in the dynamic test was much stiffer and the polyurea broke at an earlier elongation, but also a lower load.

# 3 Blast Resistance of Wall Systems Coated with Polyurea

## 3.1 General

This chapter provides a literature review of previous blast tests conducted on both plain concrete masonry unit (CMU) walls as well as polymer coated wall systems. The literature review is used as a comparison to the full-scale blast test that Air Products carried out on polyurea coated CMU walls. An evaluation of the blast test results was conducted to examine the performance of the two CMU walls, each coated with a different spray-on polyurea. A summary of the testing set-up and results are provided and discussed. Video, pressure, and acceleration measurements were used to determine the performance of the coated CMU walls from a structural and a human safety stand-point. The data was also used to provide possible reasons for the outcome of the blast tests.

## 3.2 Literature Review of Blast Tests Conducted on Wall Systems

In the past few years there have been many successful and unsuccessful full-scale blast tests conducted and analyzed on CMU walls coated with polyurea. The different tests look at different bonding methods, different polyurea chemical constituents, and different degrees of blast loading. For more information on these tests please refer to the following papers:

Broekaert, M. (2003). "Polyurea spray applied systems for concrete protection." *4th European Congress on Construction Chemicals*, Nürnberg, Germany.

Davidson, J.S., Fisher, J.W., Hammons, M.I., Porter, J.r., and Dinan R.J. (2005). "Failure mechanisms of polymer-reinforced concrete masonry walls subjected to blast." *J. Struct. Engrg.*, 131(8), 1194-1205.

Davidson, J.S., Porter, J.R., Dinan, R.J., Hammons, M.I., and Connell, J.D. (2004). "Explosive testing of polymer retrofit masonry walls." *J. Perform. Constr. Facil.*, 18(2), 100-106.

Knox, K.J., Hammons, M.I., Lewis, T.T., and Porter, J.R. (2000). *Polymer materials for structural retrofit*, Report, Force Protection Branch, Air Expeditionary Forces Technology Division, Air Force Research Laboratory, Tyndall AFB, Florida.

## 3.3 Air Products Blast Test Setup and Instrumentation

A blast test was conducted by Air Products in a remote desert of New Mexico to assess the suitability of a spray-on polyurea blend for enhancing the blast resistance of a masonry block wall. One test was conducted on two masonry walls using 220 pounds of TNT detonated from a stand-off distance of 32 feet from the center of the two walls.

### 3.3.1 Wall System

The CMU walls measured 128-in. tall. The west wall was 100 inches in width and the east wall was 98.75 inches wide. The two walls were installed in a reaction structure consisting of two separate rooms made of concrete and detailed to be undamaged during the test. A steel column separated the two CMU walls at the center of the front face of the reaction structure. This can be seen in the photograph

of the exterior wall system shown in Figure 3-2. The CMU walls, which were 17 blocks high, were a half block taller than the ceiling and extended a block and a half below the floor. There was an eight to twelve inch interior curb that rose behind the CMU wall from the floor. These details are shown in Figure 3-1.

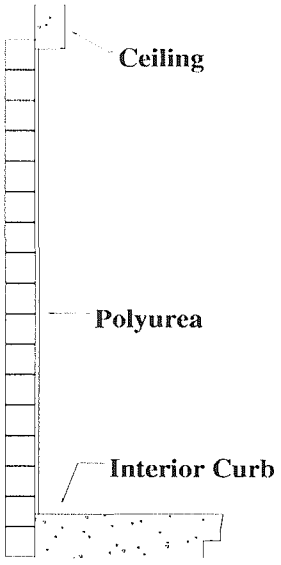


Figure 3-1: Side View of Wall and Features

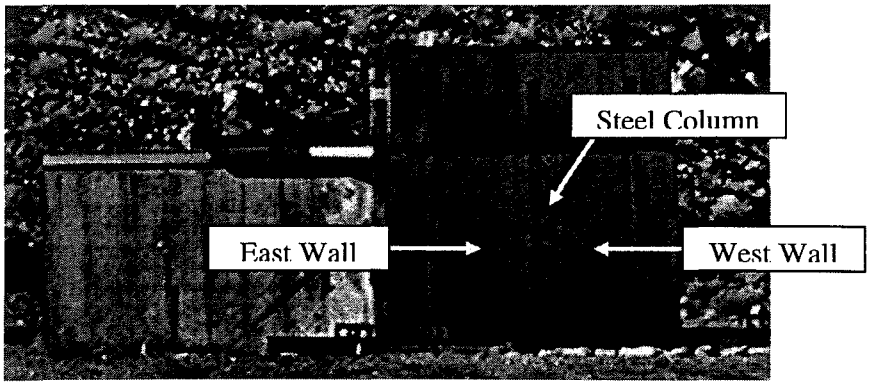


Figure 3-2: CMU Wall System for Blast Test

### 3.3.2 Polyurea Material Properties

Spray-on polyurea formulas were used to coat the interior side of the CMU walls. The polyurea thickness for both walls was nominally 3/8 inches and was marked with a one foot by one foot grid to help track displacements and movement from the video. The wall was detailed to have gaps between the vertical faces of the test structure. This was done to ensure a one-way action of the wall.

The east wall and west wall were coated with spray-on polyurea mixtures with different physical properties. The physical properties of the materials differed in that the west wall spray-on material had a higher modulus, higher strength, and a higher maximum elongation than that of the east wall polyurea. This was determined from static tensile tests, following procedures of ASTM D-412 described in Chapter 2, conducted at a rate of 4 in/min. The stress-strain curves of the two materials are shown in Figure 2-16 and the properties of the materials are summarized in Table 2-6.

### 3.3.3 Instrumentation

To assess the performance of the walls, a series of measurements were taken. This includes:

- Displacement at the center of each wall
- Acceleration of each wall using two accelerometers per wall, located along the horizontal center
- Reflected pressure measured with five pressure gauges located on the exterior of the center steel column between walls (Shown in Figure 3-3 )
- Interior pressure using pressure gauges located at the rear of the rooms

- Incident pressure using pressure gauges located at set distances from the sides and back of the explosion

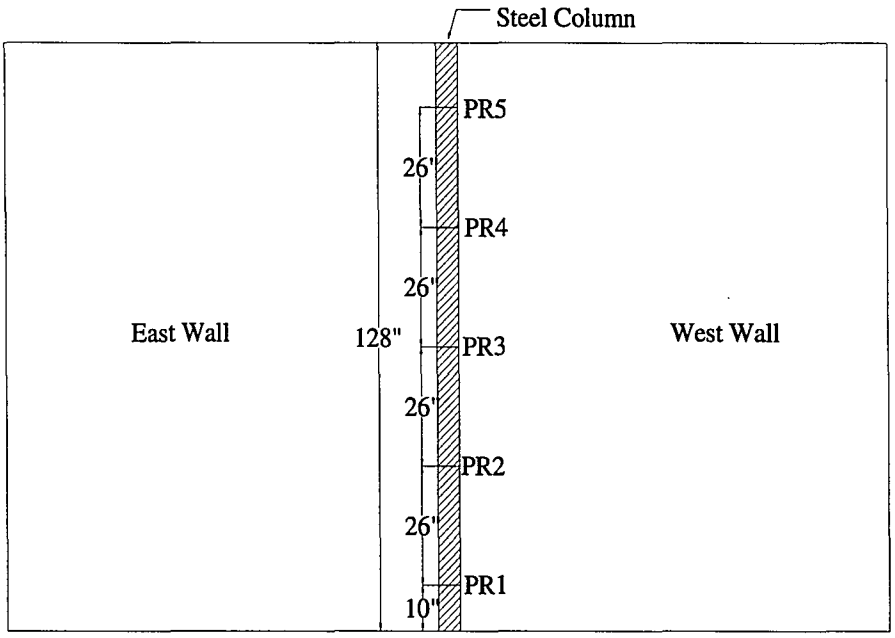


Figure 3-3: Reflected Pressure Gauge Locations along Steel Column

Another view of the test set-up is shown in Figure 3-4. This picture is taken from the east side of the building and the instrumentation and testing devices are labeled.

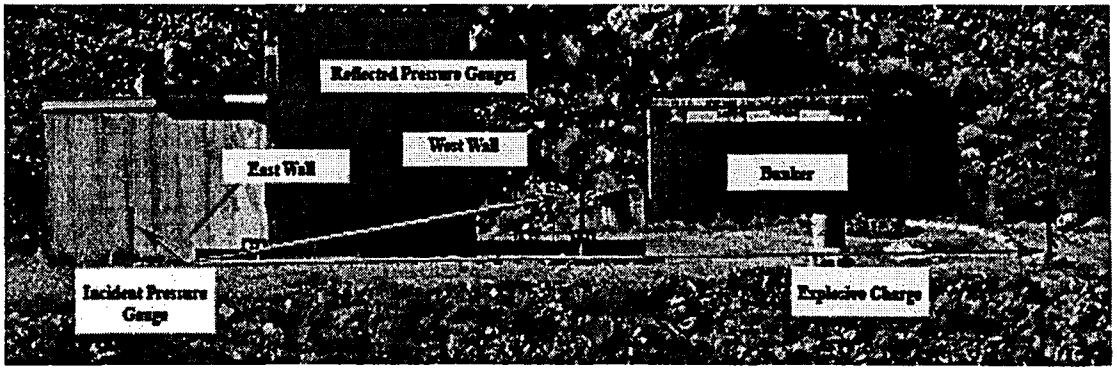


Figure 3-4: East Side View of Blast Test Set-up and Instrumentation Blast Loading and Predictions

The blast loading was the resultant of 220 pounds of TNT located 32 feet from the steel column located in between the two rooms. This information can be used to estimate the positive portion of the reflected pressure versus time curve, or the demand on the wall system. Reflected pressure occurs when the over pressure wave comes in contact with the structure and reflects. The intensity of the reflected pressure depends on the distance from the explosive charge to the structure as well as the angle at which the over pressure wave comes in contact with the wall. The reflected pressure is what causes most of the structural damage of infrastructure experiencing blast loading.

The first step in predicting the reflected pressure curve is to calculate Z, the scaled horizontal distance from the charge using Equation 3-1 (U.S. Army Corp of Engineers, 1998).

$$Z = \frac{R}{W^{1/3}}$$

where:

$R$ = radial distance to point of interest [m]

$W$ = Weight of TNT [kg]

Equation 3-1: Scaled Horizontal Distance from Charge [$m/kg^{0.333}$]

Next, knowing the value of Z, a plot such as the one shown in Figure 3-5 is used to determine the reflected maximum pressure ($P_r$), the reflected impulse ($i_r$), the time at which the pressure rises instantaneously to the maximum pressure ($t_A$), and the length of time until the pressure dissipates back to atmospheric pressure ($t_o$). These values can be used to plot points an approximate pressure-time curve shown in Figure 3-6 (U.S. Army Corp of Engineers, 1998).

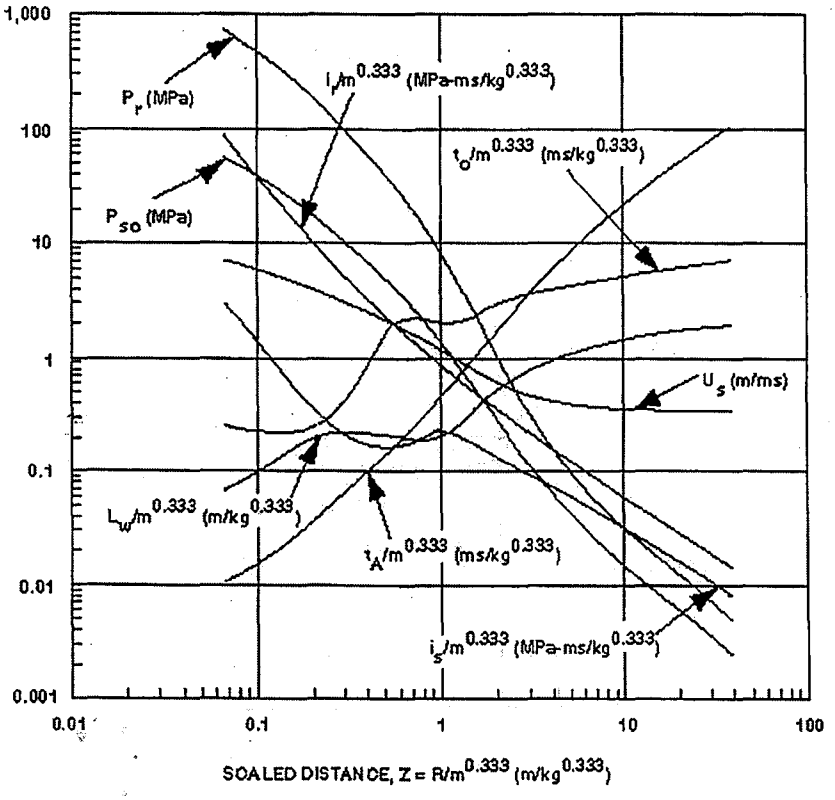


Figure 3-5: Plot to Determine Positive Shock Wave Parameters (U.S. Army Corp of Engineers, 1998)

An equivalent triangular pressure demand curve can be constructed using the reflected impulse value and the maximum reflected pressure found from Figure 3-5 and solving for time duration knowing that the impulse is equal to the area underneath the pressure-time curve. This equivalent pressure demand is also shown in Figure 3-6.

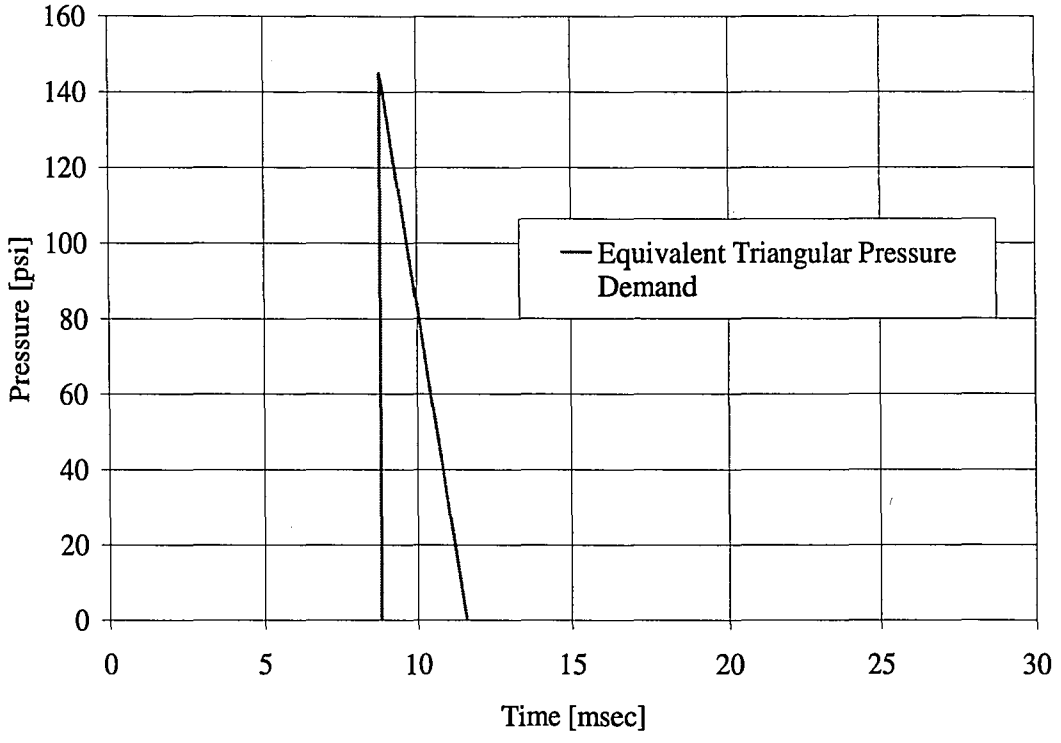


Figure 3-6: Predicted Reflected Pressure Curve

## 3.4 Blast Test Results and Analysis

The two walls experienced similar initial behavior during the blast test. Each wall experienced two-way action, with the maximum displacement occurring at the center of the wall. However, the two walls had very different end results as can be seen in Figure 3-7.

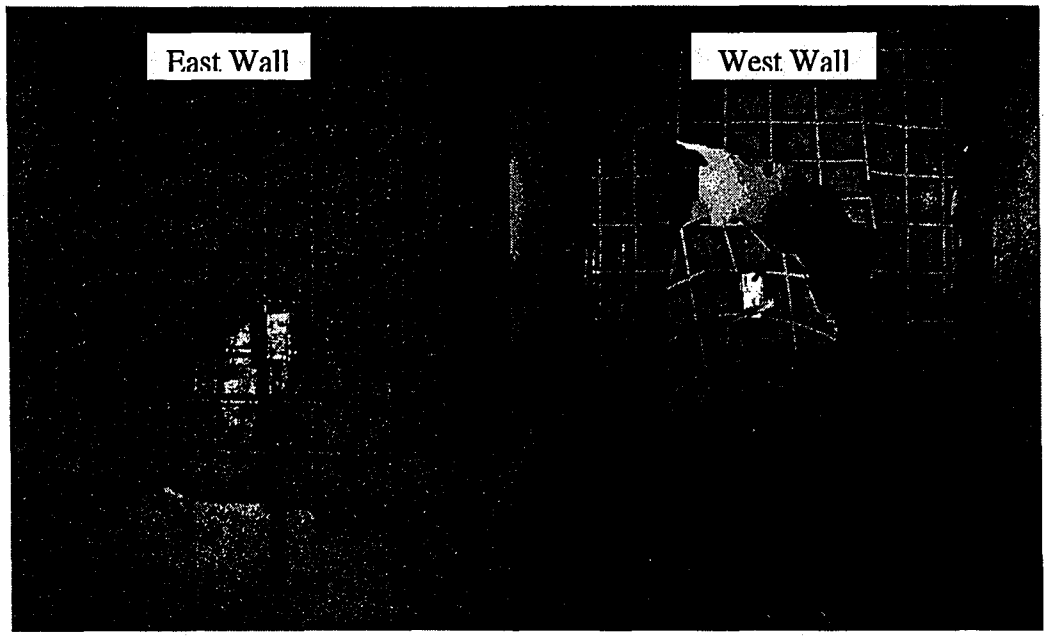


Figure 3-7: End Results of East and West Wall

The east wall developed a fracture about one foot above the interior curb of the wall which propagates outward from the center width of the wall. Due to the quality of the blast video, it is difficult to pinpoint the time of fracture for the east wall. The first visual of the fracture appears at 49.78 msecs, it could be that the crack may not become visible, in the video, until rebound of the wall occurs and appears only then due to the reflected fireball through the crack as seen in Figure 3-2. It is possible that the east wall fracture occurred at a similar time as the first west wall fracture. This will be discussed later in the chapter. The east room had only some dust debris enter the interior.

The west wall developed its initial fracture at the same location as the east wall; however other cracks also developed and began to propagate until all of the fractures connected together causing the center of the wall to blow out along with considerable debris at high velocities.

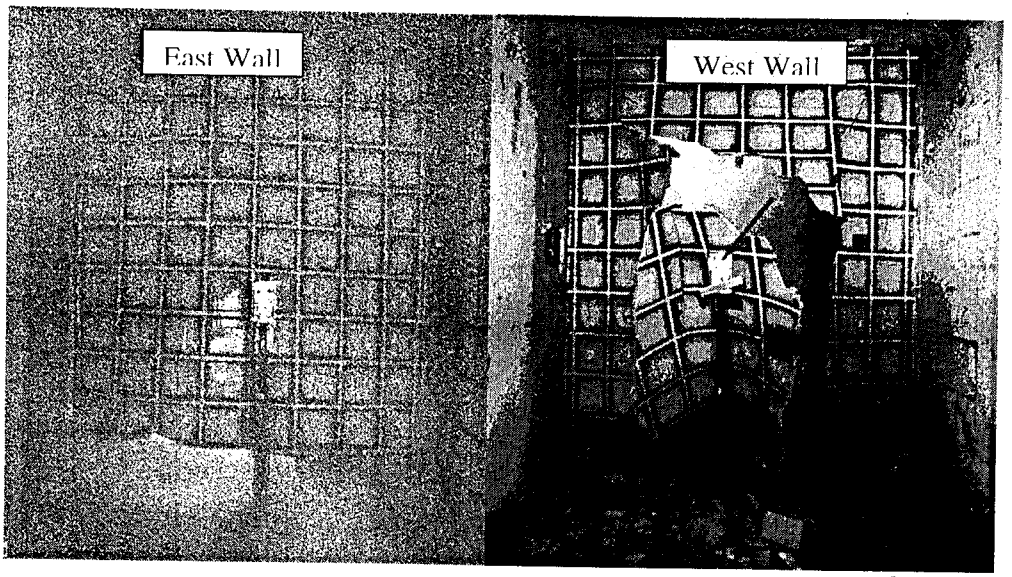


Figure 3-7: End Results of East and West Wall

The east wall developed a fracture about one foot above the interior curb of the wall which propagates outward from the center width of the wall. Due to the quality of the blast video, it is difficult to pinpoint the time of fracture for the east wall. The first visual of the fracture appears at 49.78 msecs, it could be that the crack may not become visible, in the video, until rebound of the wall occurs and appears only then due to the reflected fireball through the crack as seen in Figure 3-2. It is possible that the east wall fracture occurred at a similar time as the first west wall fracture. This will be discussed later in the chapter. The east room had only some dust debris enter the interior.

The west wall developed its initial fracture at the same location as the east wall; however other cracks also developed and began to propagate until all of the fractures connected together causing the center of the wall to blow out along with considerable debris at high velocities.

Figure 3-8 presents a sketch of the east and west wall fracture locations, how they propagated, and the time of the fracture relative to the trigger of the explosion. These fracture mappings were prepared using the videos of the blast test. It is possible to see the occurrence of a fracture by going from frame to frame, having a difference in time of one msec, and zooming in on a specific area of the wall.

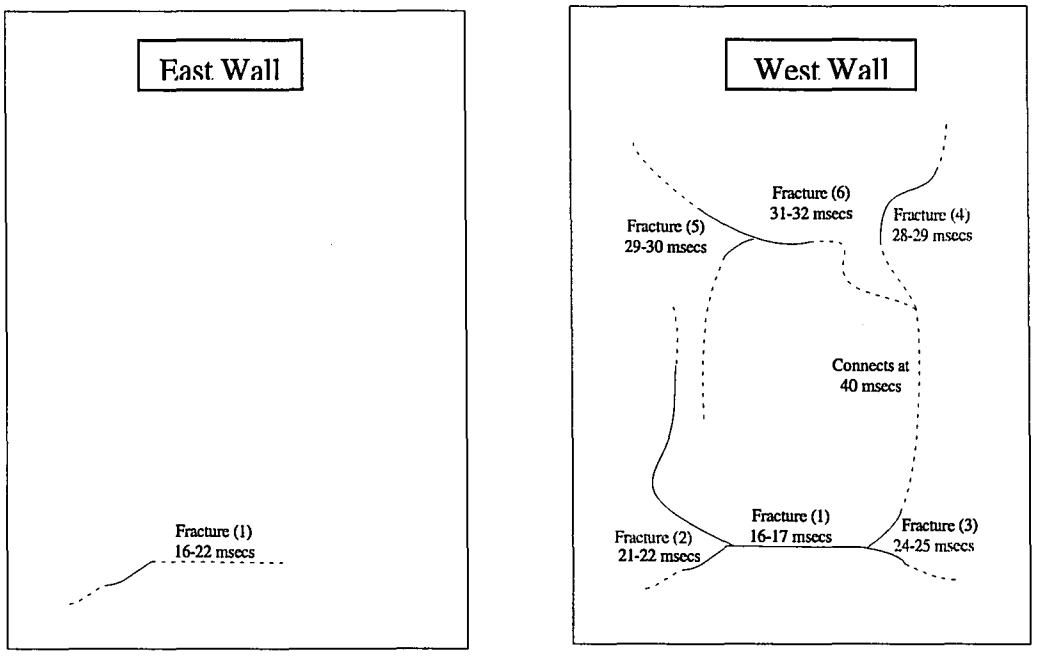


Figure 3-8: East and West Wall Fracture Mapping

The demand on the wall system is described by the reflected pressure data. As can be seen in Figure 3-9, the reflected pressures, which are measured at five different heights along the center of the two walls as seen in Figure 3-3, show no value until the pressure wave reaches the wall, at which point there is an instantaneous rise to the maximum pressure value, followed by a short time period where the pressure diminishes back to atmospheric pressure. At this point the pressure begins its negative pressure phase, causing a suction action on the wall, until the pressure again

returns to atmospheric pressure. The slight difference in peak pressure and time of the instantaneous rise for the five gauges is due to the location of each gauge relative to the charge. The lag time will increase as the distance increases and the pressure will decrease as the distance and angle from the charge is increased.

One aspect of the wall system reaction is its displacement. Looking at the displacement versus time graphed with reflected pressure versus time, shown in Figure 3-9, it is apparent that the wall displacements begin at the time of the instantaneous maximum reflected pressure. Also, after the initial fracture in the west wall, and even as more west wall fractures occur and propagate, the west wall and east wall have very similar deflections with time. It is only when tearing out of the west wall occurs that the deflections begin to differ. It can be seen that eventually the east wall begins to rebound. Due to the similarities in deflection, it seems that fractures in the polyurea do not effect the deflection of the polyurea coated walls until the free vibration response of the wall occurs.

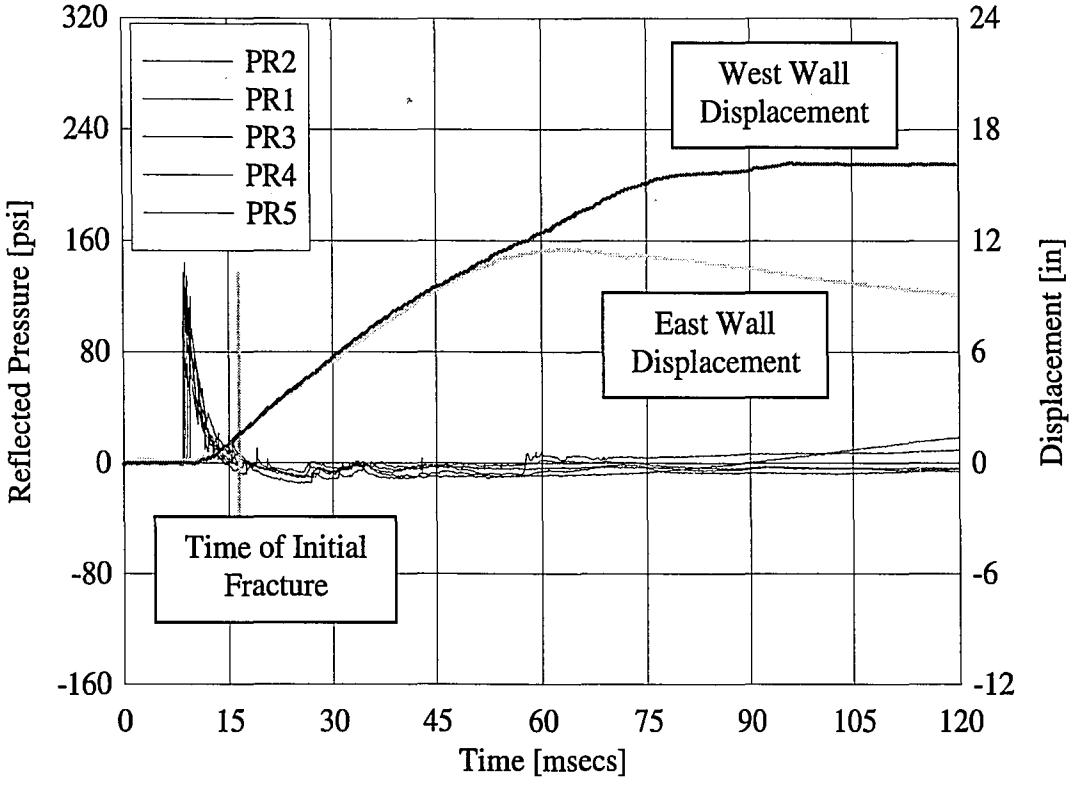


Figure 3-9: Reflected Pressure and Deflection of Wall vs. Time

The reflected pressure estimate made in Figure 3-6 can now be compared with the actual reflected pressure seen by the wall. The estimation is graphed with an actual pressure-time curve from the center reflected pressure gauge, PR3 in Figure 3-10.

Table 3-1 provides the predicted and actual maximum pressure and impulse values. It can be seen that the estimate of the positive demand region is accurate and therefore the blast demand behaved as it was expected to.

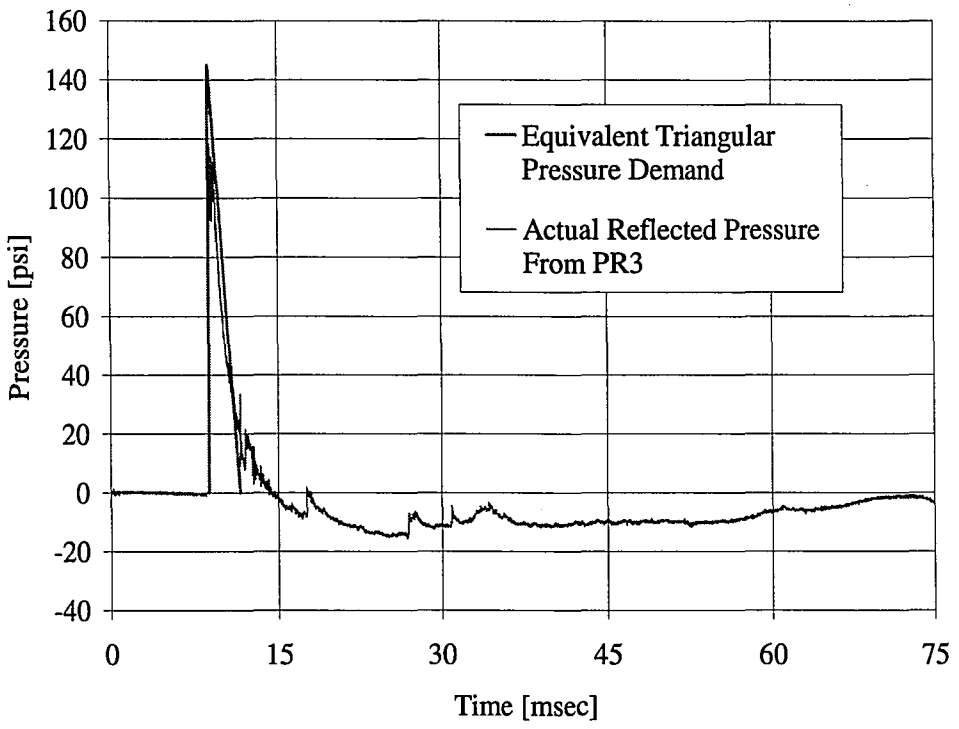


Figure 3-10: Predicted Demand and Actual Demand

| | Pmax [psi] | Imax [psi msec] |
|---|---|---|
| **Actual** | 144 | 198 |
| **Predicted** | 145 | 202 |

Table 3-1: Estimated and Actual Pressure and Impulse Values

Besides the displacement of the wall, the reaction of the wall system is also described by the acceleration data recorded. As can be seen in the graphs of acceleration versus time for the east and west wall shown in Figure 3-11 and Figure 3-12, an expected trend is seen. Again, there is no acceleration of the wall until the pressure wave comes in contact with the wall, at which point the acceleration rises to its maximum value instantaneously and begins to decrease back to zero. However, looking at the west wall acceleration data of Figure 3-12, there is a large excitation after the last

major fracture occurs at the bottom of the wall and before fractures begin to occur near the top of the wall height. The fact that the wall had not started fracturing in the top section before this acceleration increase is seen means that the acceleration is not due to the wall caving in. This excitation is not seen in the east wall, which is shown in Figure 3-11. This additional excitation, which has a maximum value of about 500 g's, could be due to a hit sustained by the west wall. The hit could be a result of primary or secondary fragments from the blast and may have led to the fracturing at the top of the wall and the propagation of previously formed fractures at the bottom of the wall, helping to fail the wall completely. It is possible that, if this hit did not occur, then the west wall polyurea may have also been successful at containing the blast.

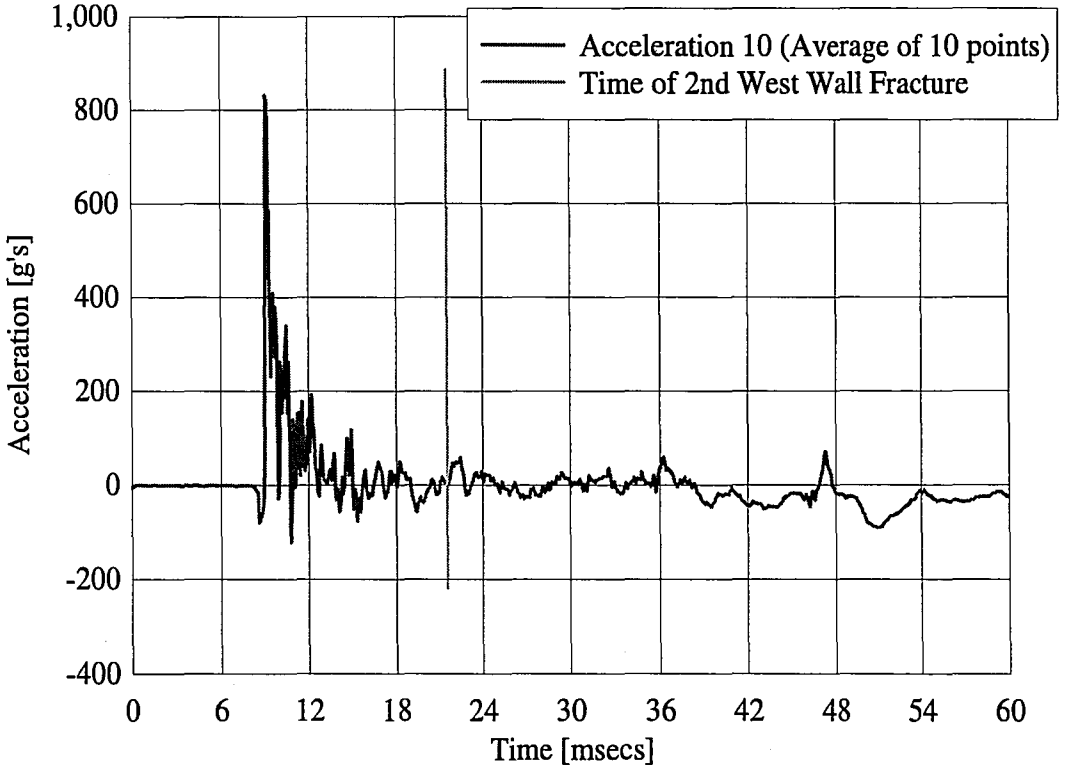


Figure 3-11: Acceleration versus Time for the East Wall

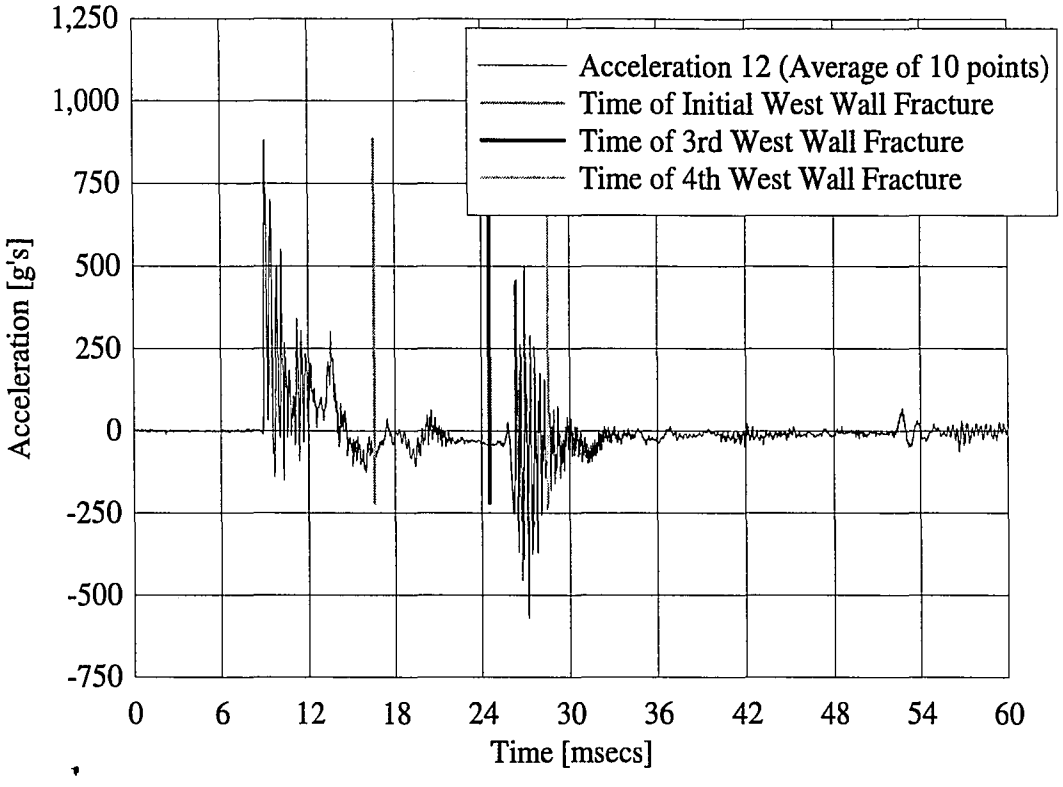


Figure 3-12: Acceleration versus Time for the West Wall

From a human safety point of view, the resistance of the wall system to the blast load also includes the ability to keep the interior pressures at a comfortable level as well as its ability to contain debris from entering the room.

Looking at the interior pressure versus time for both the west (Gauge 8) and east room (Gauge 6) shown in Figure 3-13, it can be seen that both rooms see an increase in interior pressure when the reflected pressure reaches its maximum value. It can be seen that the west room sees a much larger interior pressure value (Gauge 8) then that of the east room, especially when the wall starts to open into the room, at this point there is a sharp increase of the interior west room pressure to a maximum value of about 7 psi. Examining the east room interior pressure curve (Gauge 6), it can be seen that there is a sharp increase in pressure at the time of initial fracturing of the

west wall as is highlighted. This is the largest increase in interior pressure over time that occurs in the east room. This helps to validate the assumption that the east wall fracture may have occurred close to the same time as the initial west wall fracture.

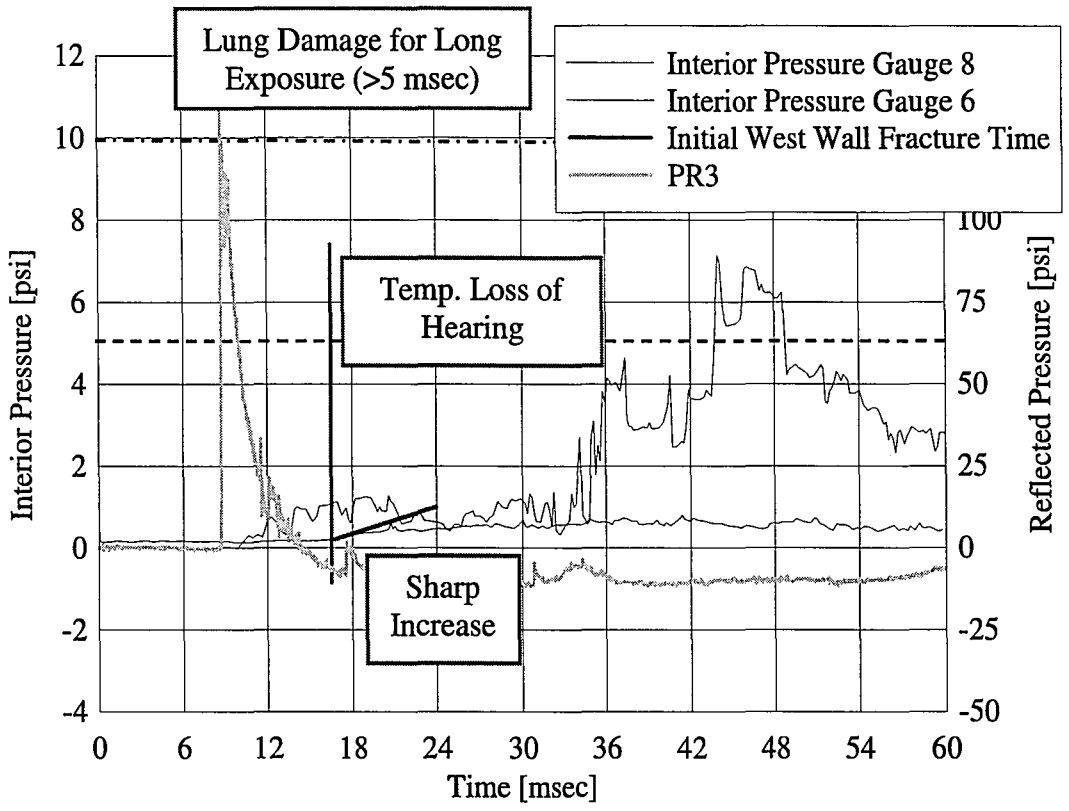


Figure 3-13: Interior Pressures and Reflected Pressure vs. Time

Interior pressures can become dangerous to occupants. Injury to the lungs occurs at an interior pressure of 30 to 40 psi for a short duration of about 5 msec. For longer duration changes in interior pressure, lung damage can occur at 10 psi. Ear drums are ruptured at an interior pressure of about 15 psi and temporary loss of hearing or discomfort will occur at 5 psi. The interior pressures of the east room can therefore be deemed safe, since the pressure increase would not have incurred damage or discomfort to the occupants. Even the interior pressure in the west room would not be enough to incur permanent injuries, only slight ear discomfort or temporary

hearing loss would occur. Nevertheless, the secondary fragments generated by the failure of the West wall would have resulted in significant loss of life and is not an acceptable level of damage.

## 3.5 Conclusions from Blast Tests on Polyurea Coated CMU Walls

Based on the lack of fragments entering the east room and the interior pressures staying at acceptable human safety levels, it can be concluded that the polyurea coating on the east wall was a success, even with a fracture occurring. Although the interior pressures within the west room were acceptable, the amount of fragmentation that occurred is not acceptable performance. However, it is thought that an additional impact may have resulted in the complete failure of the wall. The results of the blast test lead to the need for further material characterization before an understanding of how and why the polyurea coating works in achieving a blast resistant system for CMU walls. The difference in physical properties of the polyurea wall coatings at static rates do not support the outcome of the blast tests, since the weaker and less elastic polyurea was more successful. While their properties may vary at higher loading rates the difference in performance makes it difficult to predict which polyurea mixtures will be successful at blast mitigation without further testing. The fractures seen in both walls are a concern and therefore bond strength and interaction between materials needs to be studied in order to recommend an attachment scheme for polyurea on CMU walls in the future.

# 4 Static Center-Point Loading Tests on CMU Beams

## 4.1 General

This chapter presents the static flexural capacity of CMU blocks coated with spray-on polyurea. To asses the strength, a simply supported setup was developed using center-point loading. The test procedure mimics that of ASTM C-293 Standard Test Method for Flexural Strength of Concrete (Using Simple Beam with Center-Point Loading). The tests are conducted on small size beams cut from CMU pieces fabricated from the same material as the blast wall retrofit as described in Chapter 3. The CMU blocks' front faces were coated with the spray-on polyurea mixes used on the east and west wall of the blast test. Both plain and coated specimens were tested and the results are presented. The effect of the polyurea coating is examined by looking at changes in the modulus of rupture, load-displacement curves, fracture energies, and strain values along the length of the polyurea. The results are used to help formulate hypotheses regarding the outcomes of the two walls tested under blast.

## 4.2 Test Matrix

The static test specimens described in this chapter were cut from CMU blocks that were present at the blast test site and coated with the same spray-on polyurea materials described in Figure 2-16 and Table 2-6. There were two types of CMU blocks used in the construction of the blast wall. One consisted of a cinder-based aggregate (CMU Type 1) and the other used a harder aggregate (CMU Type 2). Photographs of the two block surfaces are shown in Figure 4-1 and Figure 4-2.

Figure 4-1: CMU Type 1 with Cinder Based Aggregate

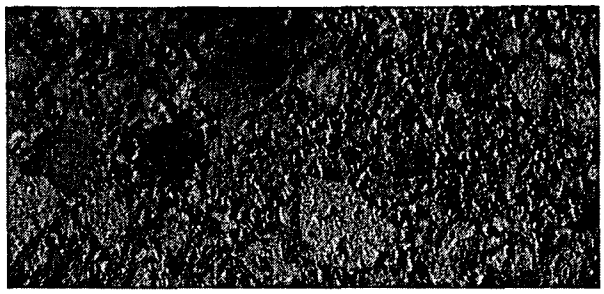

Figure 4-2: CMU Type 2 with Harder Aggregate

Two CMU samples of each type were taken from the blast testing site, one coated with the west wall spray-on polyurea (70-5) and the other coated with the east wall spray-on polyurea (70-1).

The dimensions of the test specimens vary due to the sawing technique used. The CMU specimens measure approximately 6 inches x 1.325 inches x 1.25 inches. Figure 4-3 illustrates how the samples were proportioned from the main CMU block.

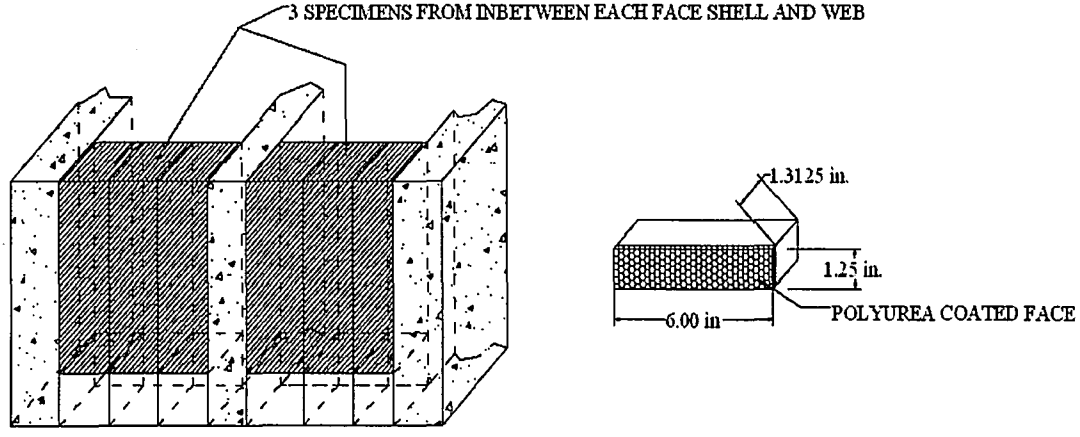


Figure 4-3: Test Specimen Location within full CMU

Twelve samples were fabricated for each polyurea type. Six samples were from CMU Type 1 and six from CMU Type 2. The samples consisted of both coated

specimens and uncoated specimens. The uncoated specimens would serve as a comparison and would help to define the strengths of the CMU Types. The first round of six tests was used to help understand what steps needed to be taken in order to improve the test set-up and instrumentation in order to achieve the best results. The remaining six tests are presented throughout the chapter. The test matrix is given in Table 4-1. It must be noted that the specimen for Test 5 is of smaller scale than the rest of the tests. This is due to the fact that there was not a substantial enough area on the original block where a coating free specimen could be cut. A photograph of a coated test specimen is shown in Figure 4-4.

| Test ID | Rate | Polyurea Batch | Poly Thickness [in] | CMU Type | L [in] | b [in] | d [in] | weight [lb] |
|---|---|---|---|---|---|---|---|---|
| 1 | Static | 70-5 | 0.375 | 1 | 3.625 | 1.125 | 1.25 | 0.661 |
| 2 | Static | 70-5 | 0.375 | 2 | 3 | 1.25 | 1.25 | 0.495 |
| 3 | Static | 70-1 | 0.375 | 1 | 3.875 | 1.1875 | 1.3125 | 0.689 |
| 4 | Static | 70-1 | 0.375 | 2 | 4.125 | 1.125 | 1.375 | 0.732 |
| 5 | Static | n.a. | n.a. | 1 | 2.875 | 1.125 | 0.9375 | 0.361 |
| 6 | Static | n.a. | n.a. | 2 | 3.75 | 1.125 | 1.25 | 0.61 |

Table 4-1: Test Matrix for CMU Tests

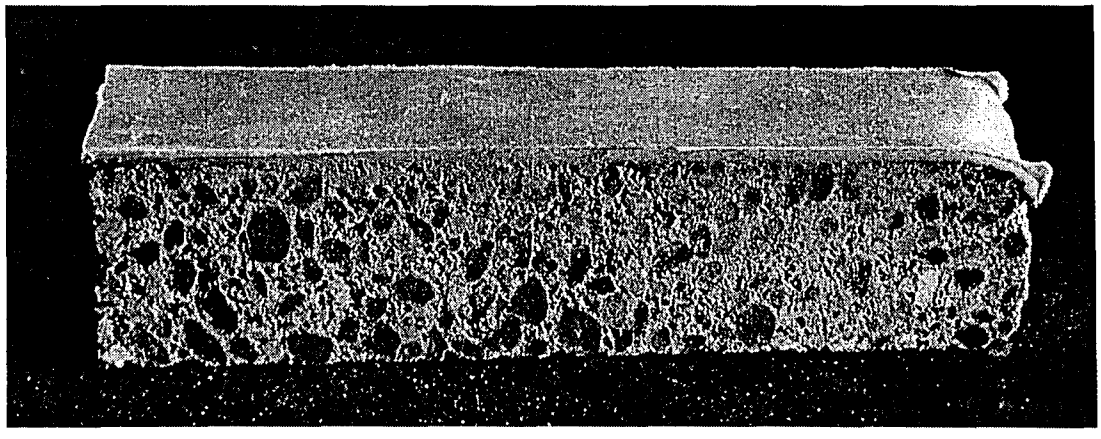

Figure 4-4: Photograph of Test Specimen

## 4.3 Testing Setup

A variation on ASTM C-293 is used to determine the flexural strength and deformation of the coated polyurea blocks. The tests are conducted with a Baldwin Universal Testing Machine. ASTM C-293: Standard Test Method for Flexural Strength of Concrete (Using Simple Beam with Center-Point Loading) applies a center-point load to a simply supported concrete block to determine the modulus of rupture of concrete. This ASTM was used as a guideline in order to determine the flexural strength of the combined masonry/polyurea system as well as to determine a fracture energy using the resulting load-displacement curve. These tests serve as a comparison to non-retrofitted masonry units. The test set-up is shown in Figure 4-5 and Figure 4-6.

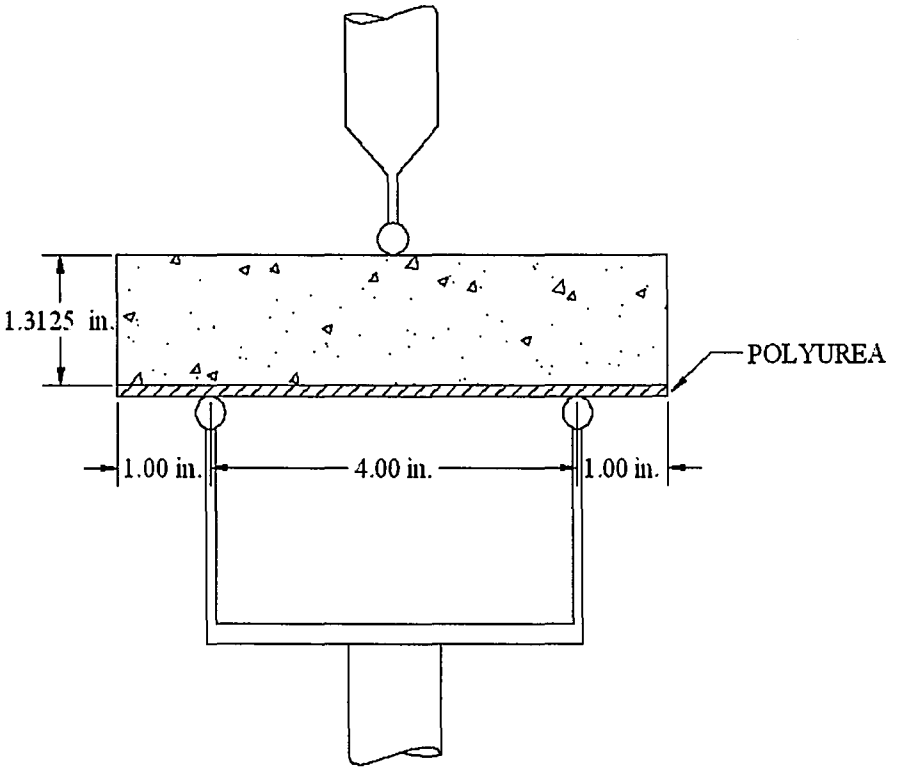


Figure 4-5: Dimensioned Test Set-up for Static CMU Tests

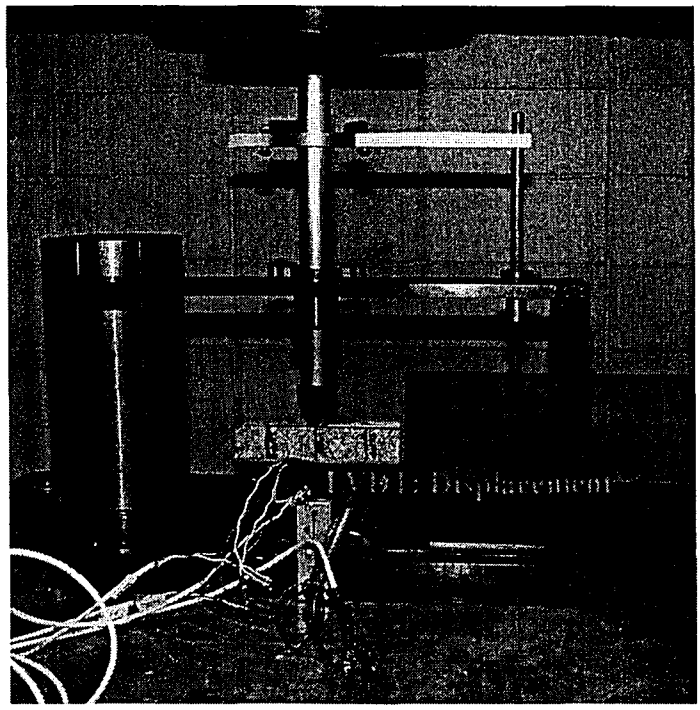

Figure 4-6: Actual Loading Fixture for Static CMU Tests

The ASTM C-293 requires that the dimensions of the test specimen be within 2% of having a 3:1 aspect ratio (assuming that there is a 1 inch overhang after each support). The dimensions of the test specimens met this requirement.

## 4.4 Test Procedure

The load was applied at midspan and perpendicular to the top surface of the test specimen, with no eccentricity. The width of the loading head was greater than that of the specimen to ensure a uniform line load and was applied across the entire midspan width of the test specimen. Simple supports were located 1 inch from each end of the test specimen and were parallel to the applied line load. The loading rate, before cracking of the concrete occurred, was on average 10 lb/sec. After cracking of concrete, for the polyurea coated specimens, the loading rate decreased to 0.34 lb/sec on average. For the plain specimens, failure was considered cracking through the

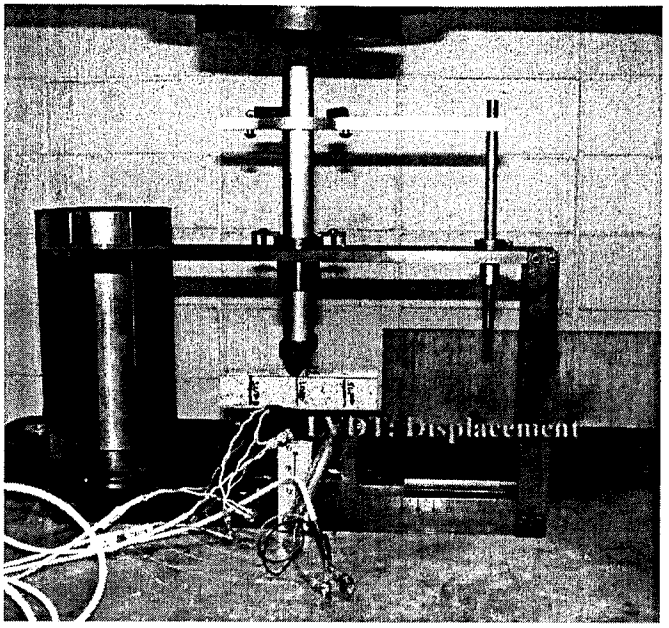


Figure 4-6: Actual Loading Fixture for Static CMU Tests

The ASTM C-293 requires that the dimensions of the test specimen be within 2% of having a 3:1 aspect ratio (assuming that there is a 1 inch overhang after each support). The dimensions of the test specimens met this requirement.

## 4.4 Test Procedure

The load was applied at midspan and perpendicular to the top surface of the test specimen, with no eccentricity. The width of the loading head was greater than that of the specimen to ensure a uniform line load and was applied across the entire midspan width of the test specimen. Simple supports were located 1 inch from each end of the test specimen and were parallel to the applied line load. The loading rate, before cracking of the concrete occurred, was on average 10 lb/sec. After cracking of concrete, for the polyurea coated specimens, the loading rate decreased to 0.34 lb/sec on average. For the plain specimens, failure was considered cracking through the

height of the specimen, when the specimen had a complete loss of load capacity. The test was ended for the polyurea coated system when the first of two events occurred. Either the maximum deflection for the test setup, of 2 inches, was reached, or crushing of the concrete at the crack tip occurred.

## 4.5 Instrumentation

The load was recorded using a linear voltage differential transducer (LVDT) which is able to read the movement of a needle that is part of the Baldwin testing machine. The needle rotates within a marked dial which is calibrated to show the load applied on the specimen in the machine.

The displacement is measured with an LVDT connected at the midspan. The LVDT has a displacement range of 2 inches. It is illustrated in Figure 4-6. The strain in the outer most fiber of polyurea was recorded by applying three high elongation strain gauges to the bottom surface in the pattern shown in Figure 4-7.

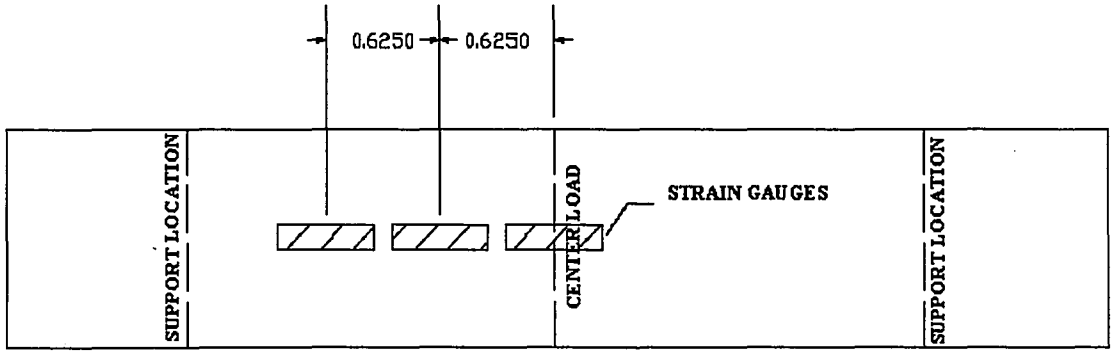


Figure 4-7: Strain Gauge Locations for Static CMU Tests

## 4.6 Expected Results

In order to make some predictions as to the test results, the compressive strength of the CMU Types was needed. To determine the compressive strength, a test following ASTM C-109 on 1 inch cubes was conducted. The cubes were tested in compression until crushing occurred. The maximum load was then divided by the cross-sectional area of the cube to determine the strength. The compressive strength of the cinder based aggregate CMU was 6,500 psi and the compressive strength of the harder aggregate CMU was 2,500 psi. Once the compressive strengths were determined, the modulus of rupture (R) is calculated as $7.5\sqrt{(f'_c)}$, where $f'_c$ is the compressive strength of the concrete. Then the ultimate moment can be calculated using the formula: $R(I_g)/c$, where $I_g$ is the gross moment of inertia of the cross section, and c is the neutral axis depth. For a simply supported beam, the moment at the center is equal to PL/4. Using this formula, the ultimate expected load, P, and the ultimate expected moment, M, is determined. For the polyurea coated specimen, the polyurea width was transformed into an equivalent width of concrete by multiplying its actual width by a ratio of the polyurea elastic modulus and the elastic modulus of the concrete. This transformed section was used to calculate the $I_g$ and c of the section. Therefore the expected results for the polyurea coated systems are different than those of the plain specimens. The results are summarized in Table 4-2.

| Test ID | CMU Type | Polyurea Batch | $f'_c$ from cube test [psi] | Calculated R [psi] | c [in] | Ig [in4] | M [lb-in] | P [lb] |
|---|---|---|---|---|---|---|---|---|
| 1 | 1 | 70-5 | 6500 | 605 | 0.987 | 0.198 | 122 | 134 |
| 2 | 2 | 70-5 | 2500 | 375 | 0.986 | 0.221 | 84 | 112 |
| 3 | 1 | 70-1 | 6500 | 605 | 1.019 | 0.240 | 142 | 147 |
| 4 | 2 | 70-1 | 2500 | 375 | 1.050 | 0.261 | 93 | 90 |
| 5 | 1 | n.a. | 6500 | 605 | 0.625 | 0.077 | 75 | 104 |
| 6 | 2 | n.a. | 2500 | 375 | 0.999 | 0.183 | 69 | 73 |

Table 4-2: Estimated Loads for Coated and Uncoated Specimens

## Results

Figure 4-8 through Figure 4-11 shows the failure modes of a CMU polyurea coated specimen under the static center-point load. Loading was increased until concrete fracture was reached. At this point a crack would progress to the compression zone and the load would drop to a lower value. As the load again began to increase the tip of the fracture became a center of rotation and the system began to deflect downward as the crack continued to increase in width. The test ended either when the concrete began to bear at the point of rotation or the maximum displacement was reached. Fracture of the polyurea was not achieved through static testing due to the limited deformation.

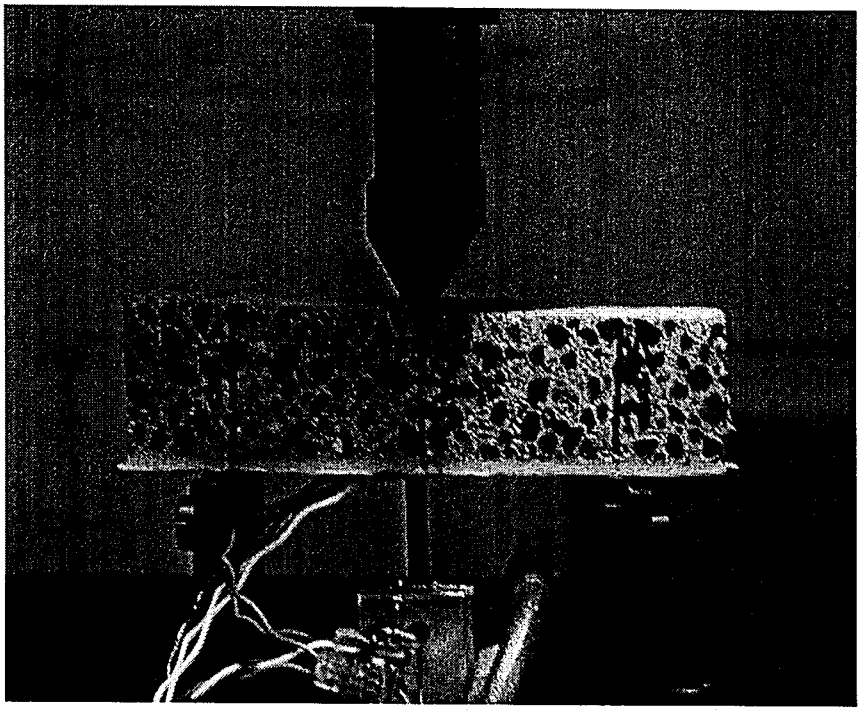

Figure 4-8: Loading Begins

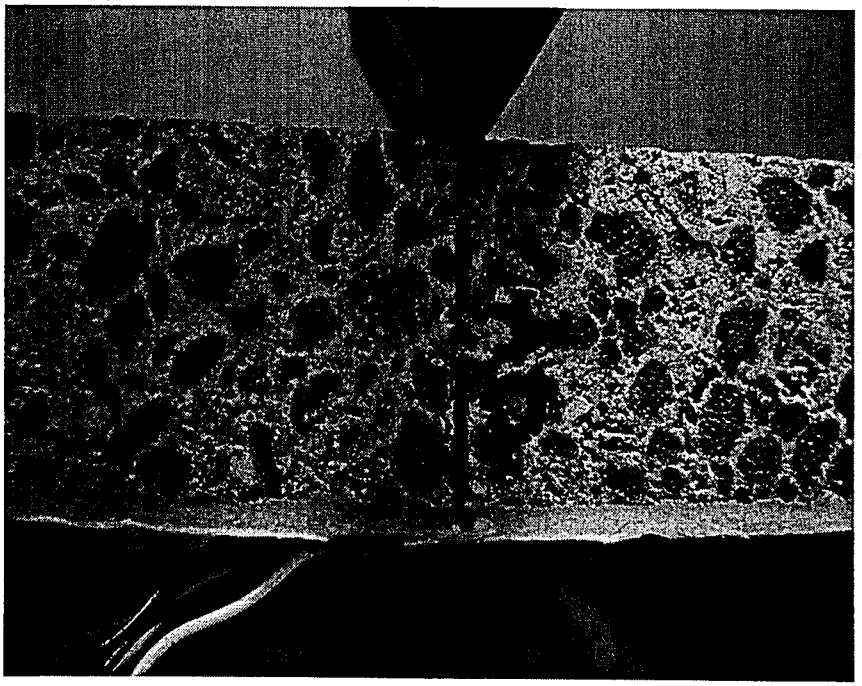

Figure 4-9: Cracking Occurs

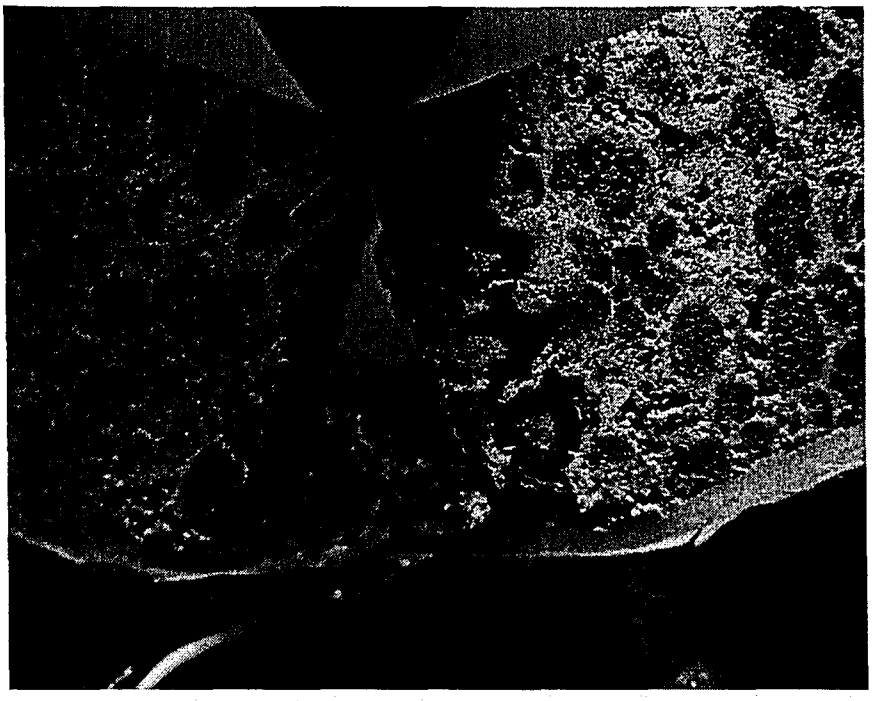

Figure 4-10: Displacement Continues as Crack Opens

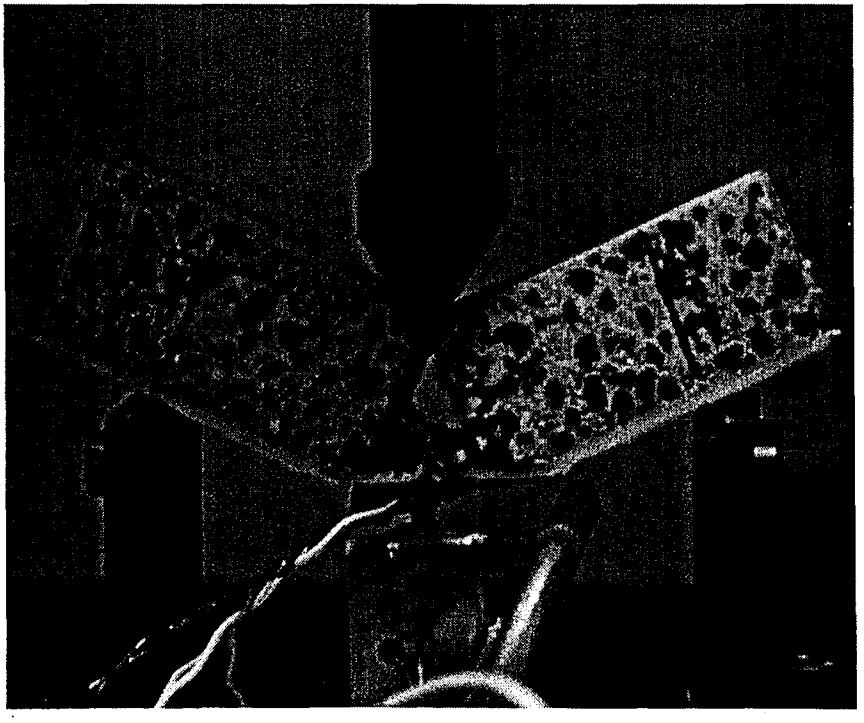

Figure 4-11: End of Test Due to Maximum Displacement

## 4.7 Plain Concrete Results

The plain concrete specimens serve as the basis for comparison for the coated specimens and allow for the rough calculation of the strength of the concrete. The test of the plain specimens saw an increase in load until the modulus of rupture was reached, at which point the specimen broke into two pieces and fell into the center.

### 4.7.1 Modifications to Load versus Displacement Curve

Due to local crushing of concrete at the point of contact of the load head with the concrete and the rate at which the test reached failure, the original load and displacement data required some modifications to quantify the fracture energy. Figure 4-12 shows the original load versus displacement curve for CMU Type 1. The effect of localized crushing of concrete can be seen as a soft slope at the beginning of the test before reaching a steady higher value. A plateau can also be seen after the maximum load is reached. There is a large gap between data points along this plateau from one side to the next. This plateau and gap in data points is due to the testing fixture. When the concrete specimen cracks completely, there is a rapid increase in deflection that occurs faster than the recording rate.

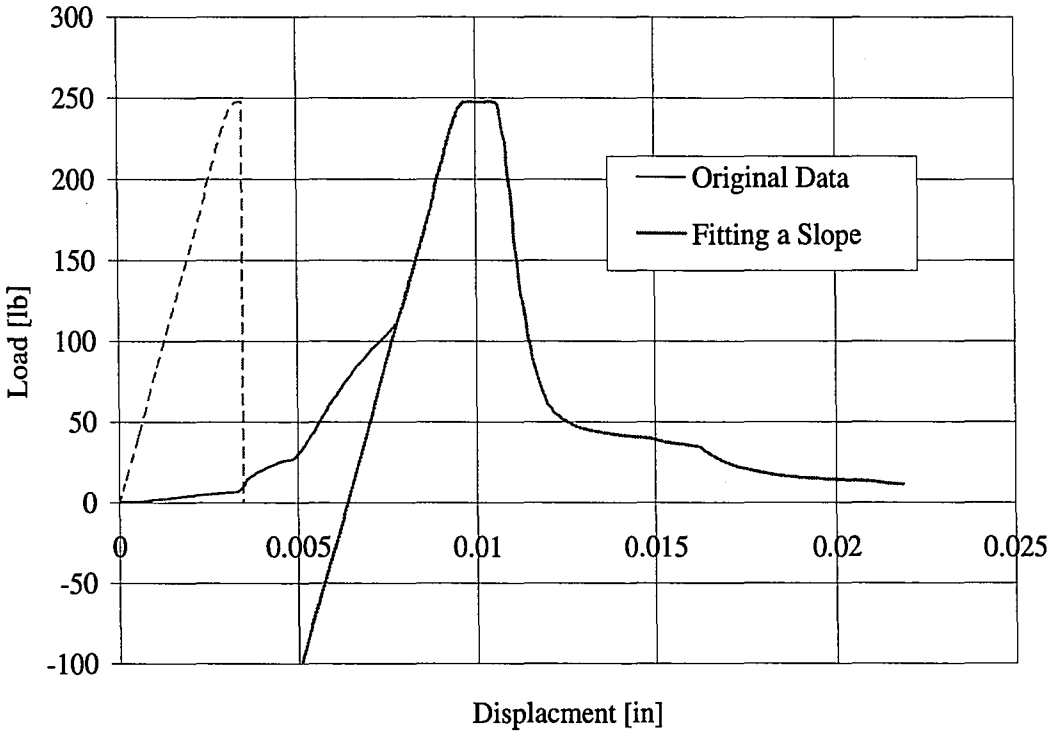


Figure 4-12: Modifications to Load Displacement Curve

A line was fit to the upper portion of the data. The slope fit to the data had a correlation factor of 0.999 for this CMU Type. The equation of the line was then used to determine a load value for the displacements prior to the data used for generating the line equation, as is shown in Figure 4-12. The next step was to shift the data back to the origin. This was done by determining at which displacement the newly generated data had approximately zero loads. This pair of values was then used as the starting point of the test and the displacement value was subtracted from itself and all following displacements. The final step was done to eliminate the plateau seen. The test was ended at its maximum load by having the load return to zero at the same displacement seen at maximum load. The modified curve can be seen in Figure 4-12. A comparison of the modified load versus displacement curve

for both types of CMU is shown in Figure 4-13. The maximum load for CMU Type 1 is 247.5 pounds and the maximum load for CMU Type 2 is 280 pounds.

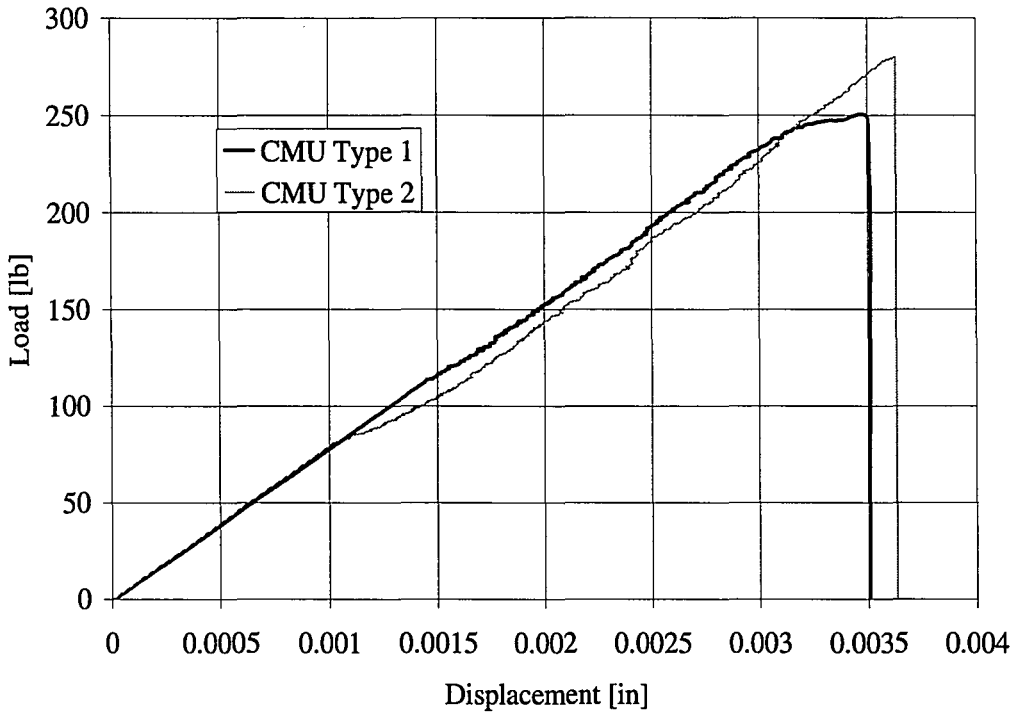


Figure 4-13: Load versus Displacement Curves for Plain CMU

The maximum load can be used to calculate the rupture stress of each CMU type and from this, an approximation on the multiplier to determine the strength of the concrete can be made. According to ASTM C-293 the modulus of rupture can be calculated with Equation 4-1.

$$R = 3PL/2bd^2$$

where:

$R$ = modulus of rupture

$P$ = maximum applied load [lb]

$L$ = specimen span length [in]

$b$ = average width of specimen [in]

$d$ = average specimen depth [in]

Equation 4-1: Modulus of Rupture [psi]

Using the maximum load and individual beam dimensions for each CMU type, the modulus of rupture was calculated and recorded in Table 4-3. As was stated earlier, for concrete, an approximate modulus of rupture can be calculated using the compressive strength of the material, using the formula $7.5\sqrt{(f'_c)}$, where $f'_c$ is the compressive strength of the concrete. The multiplier for the two CMU Types was back calculated using Equation 4-2. The results of the plain specimen tests are given in Table 4-3.

$$multiplier = \left( \frac{R}{\sqrt{f'_c}} \right)$$

where:

$R$ = modulus of rupture [psi]

$f'_c$ = concrete compressive strength [psi]

Equation 4-2: Concrete Compressive Strength Multiplier

| Test ID | Rate | Polyurea Batch | CMU Type | Max. Load [lb] | Modulus of Rupture [psi] | Concrete Compressive Strength [psi] | Multiplier |
|---|---|---|---|---|---|---|---|
| 5 | Static | n.a. | 1 | 248 | 1080 | 6,500 | 13.4 |
| 6 | Static | n.a. | 2 | 280 | 896 | 2,500 | 17.9 |

Table 4-3: Summary of Plain CMU Test Results

The multipliers for each CMU are greater than the ACI 318 recognized value of 7.5. The measured values are presented in Table 4-3. Also, it should be noted that CMU Type 2, with the harder aggregate has a lower compressive strength than that of the cinder based aggregate, CMU Type 1.

### 4.7.2 Fracture Energy of Plain CMU Specimens

Due to the outcome of the full-scale blast tests, where both the east and west coated CMU walls were fractured during the duration of the test, another important point of comparison for plain specimens to coated specimens is fracture energy, $G_F$. Also, this is an important comparison between the two different coatings since the west wall was seen to fracture much more severely than the east wall. According to standard techniques (50-FMC, 1985), the fracture energy, $G_F$, can be computed according to Equation 4-3.

$$G_F = \frac{(W_o + mg\delta_o)}{A_{lig}}$$

where:

$W_o$ = area under load - displacement curve (Figure 4 - 14) [lb - in]

$m = m_1 + m_2$

$m_1$ = weight of beam between supports $[\text{lb} * \frac{\text{s}^2}{\text{in}}]$

$m_2$ = weight of loading device not attached to machine, following the beam until failure $[\text{lb} * \frac{\text{s}^2}{\text{in}}]$

$g$ = gravity $[\text{in/s}^2]$

$\delta_o$ = deformation at failure [in]

$A_{lig}$ = projection of fracture zone on a plane perpendicular to beam axis $[\text{in}^2]$

Equation 4-3: Fracture Energy [lb-in]

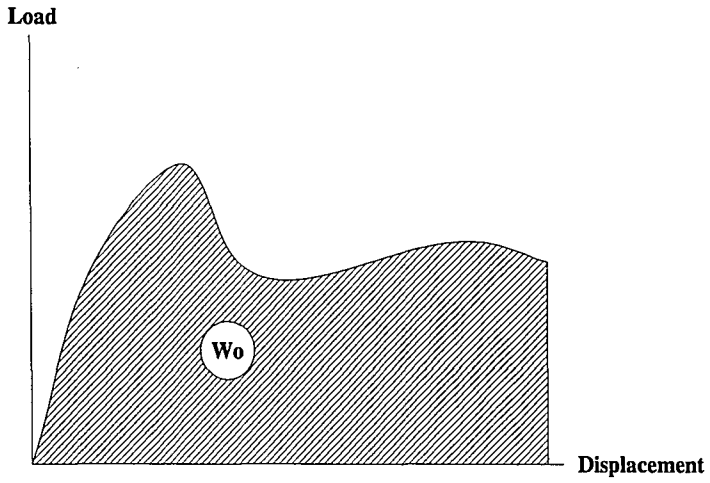


Figure 4-14: Definition of $W_o$

The fracture energy values, along with the values used for calculating these energies, are presented in Table 4-4 for Test 5 and 6.

| Test ID | Polyurea Batch | CMU Type | $W_o$ [lb-in] | $m_1$ [lbf] | $m_2$ [lbf] | m [lbf] | $\delta_o$ [in] | $A_{lig}$ [$in^2$] | $G_F$ [lb-in] |
|---|---|---|---|---|---|---|---|---|---|
| 5 | n.a. | 1 | 0.469 | 2.510E-05 | 0 | 2.510E-05 | 0.0035 | 1.055 | 0.445 |
| 6 | n.a. | 2 | 0.491 | 7.708E-05 | 0 | 7.708E-05 | 0.0036 | 1.406 | 0.349 |

Table 4-4 : Fracture Energies and Needed Values

## 4.8 Results of CMU Specimens Coated with Spray-on Polyurea

Referring to the test matrix of Table 4-1, Test 1 through Test 4 were conducted on polyurea coated specimens. All combinations of CMU Type and Polyurea Batch were tested once. Data processing techniques similar to the ones used for the plain specimens, described in Section 4.7.1, were used for the coated specimens as well. The adjusted load-displacement curves for Polyurea Batch 70-5 are shown in Figure 4-15 and the load-displacement curves for Polyurea Batch 70-1 are shown in Figure 4-16. The same data is presented, separating the tests by CMU Type rather than

Polyurea Batch along with the plain specimen load displacement results in Figure 4-17 and Figure 4-18.

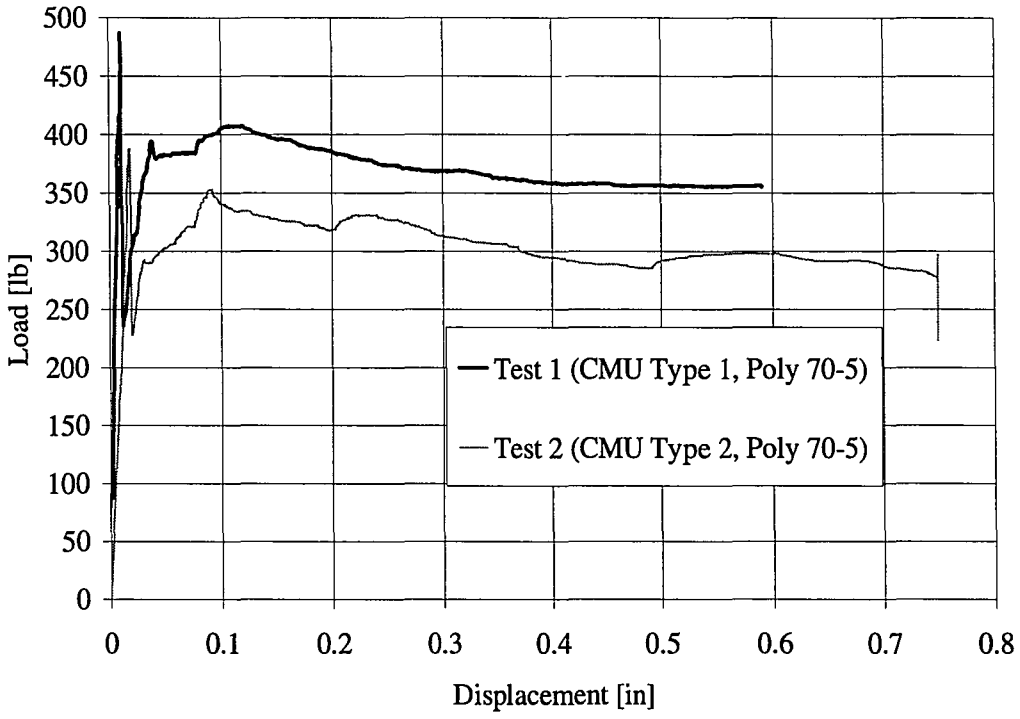


Figure 4-15: Load versus Displacement Curves for Polyurea 70-5

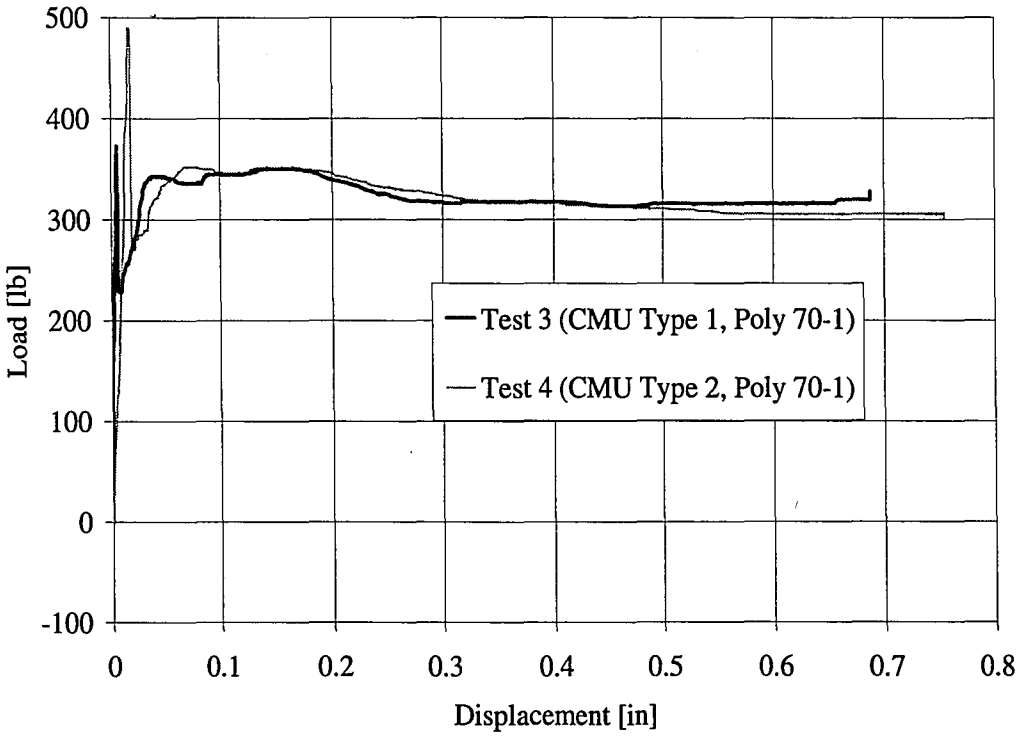


Figure 4-16: Load versus Displacement Curves for Polyurea 70-1

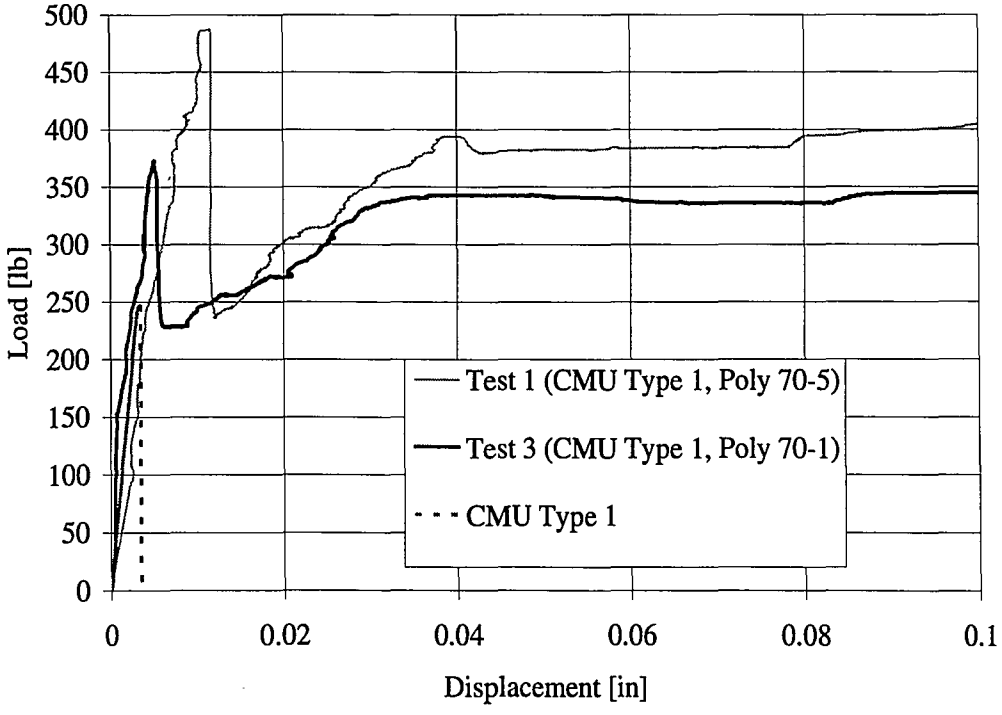


Figure 4-17: Load versus Displacement Curves for Type 1 CMU

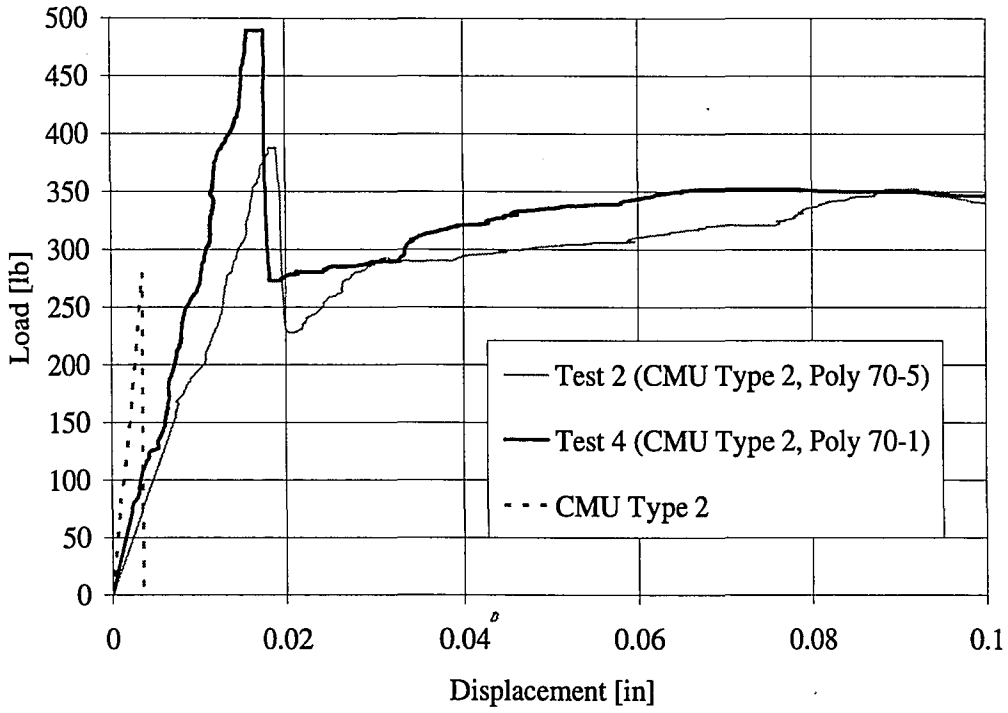


Figure 4-18: Load Displacement Curves for Type 2 CMU

Looking only at these figures, a general trend does not present itself, except that the maximum loads of the polyurea coated systems are at least 40% higher than the maximum loads of the plain specimens. Besides that the CMU Type that achieves the highest load is different from one Polyurea Batch to the other. The Polyurea Batch is different for the specimens able to achieve the higher loads for the different CMU Types as well. However, properties like fracture energy and modulus of rupture depend on the size of the specimens, which varies from test to test. As can be seen by the results of the plain specimens, even though the CMU Type 2 was able to achieve a higher maximum load, it had the lower modulus of rupture, lower compressive strength, and lower fracture energy due to the size of the specimens tested. The important aspect of the figures presented is the behavior after the maximum load is achieved, since this behavior is purely the polyurea coating. Looking at the west wall

polyurea (70-5), it can be seen that the behavior of the polyurea is very similar after the cracking of concrete occurs; only differing in the load values, which could be due to an inconsistency in the polyurea mix. The load drops to a certain value at which point it begins to increase again and after reaching a second maximum load, decreases slightly as the majority of the displacement occurs. This is true of the east wall polyurea (70-1). In order to more clearly understand the effects of the polyurea coatings and the difference between the two, the numerical results are presented in Table 4-5.

| Test ID | Rate | Polyurea Batch | CMU Type | Max. Load [lb] | Stiffness [lb/in] | Max. Displacement at Test End [in] | Modulus of Rupture [psi] | % Increase in Modulus of Rupture |
|---|---|---|---|---|---|---|---|---|
| 1 | Static | 70-5 | 1 | 487 | 41700 | 0.592 | 2200 | 103 |
| 2 | Static | 70-5 | 2 | 388 | 21000 | 0.75 | 1300 | 45 |
| 3 | Static | 70-1 | 1 | 373 | 61400 | 0.687 | 1530 | 42 |
| 4 | Static | 70-1 | 2 | 489 | 32200 | 0.754 | 2030 | 126 |
| 5 | Static | n.a. | 1 | 248 | 78800 | 0.0035 | 1080 | 0 |
| 6 | Static | n.a. | 2 | 280 | 79900 | 0.0036 | 896 | 0 |

Table 4-5: Results of Coated and Uncoated CMU Tests

The stiffness values reported for the coated systems are all lower than that of the plain specimens. Coating both CMU Types with polyurea lowers the initial stiffness of the specimens, but it is seen that the stiffness values for CMU Type 1 and 2 coated with Polyurea Batch 70-5 are lower than CMU Type 1 and 2 coated with Polyurea Batch 70-1. Therefore it can be concluded that Polyurea Batch 70-5 is less stiff than Polyurea Batch 70-1, and therefore it allows for a higher maximum elongation at the end of the test for both CMU Types.

Table 4-5 does not seem to present a trend in modulus of rupture. However, each test has a different combination of CMU Type and Polyurea batch and it can be seen that

the maximum load and modulus of rupture are dependent on both materials. Therefore, the data would be expected to differ in all cases. The fracture energies of the different systems could provide more insight as to the performance of the different polyurea batches.

The energies of the coated system were calculated in the same way that the fracture energies were calculated for the uncoated specimens (Equation 4-3). It must be noted that the calculated energies are not truly "fracture" energies for the coated systems, since failure was never reached. Instead the values represent the amount of energy absorbed by the CMU/Polyurea system at a certain displacement. Two different points of displacement were used for comparison and the results are summarized in Table 4-6.

| Test ID | Polyurea Batch | CMU Type | $W_o$ at Peak Load [lb-in] | $W_o$ at end of Test 1 [lb-in] | m [lbf] | δo at Peak Load [in] | δo at end of Test 1 [in] | Alig [$in^2$] | $G_F$ at Peak Load [lb-in] | GF at end of Test 1 [lb-in] |
|---|---|---|---|---|---|---|---|---|---|---|
| 1 | 70-5 | 1 | 3.27 | 217.73 | 9.37E-05 | 0.01 | 0.59 | 1.41 | 2.33 | 154.84 |
| 2 | 70-5 | 2 | 3.73 | 180.66 | 9.46E-05 | 0.02 | 0.59 | 1.56 | 2.39 | 115.64 |
| 3 | 70-1 | 1 | 1.19 | 191.17 | 1.10E-04 | 0.01 | 0.59 | 1.56 | 0.76 | 122.67 |
| 4 | 70-1 | 2 | 3.61 | 191.23 | 1.20E-04 | 0.02 | 0.59 | 1.55 | 2.33 | 123.64 |
| 5 | n.a. | 1 | 0.47 | 0.47 | 2.51E-05 | 0.004 | 0.004 | 1.05 | 0.44 | 0.44 |
| 6 | n.a. | 2 | 0.49 | 0.49 | 7.71E-05 | 0.004 | 0.004 | 1.41 | 0.35 | 0.35 |

Table 4-6: Fracture Energies for Coated and Uncoated CMU Specimens

The first displacement corresponds to the peak load achieved by each system, or the load when cracking of the concrete occurred. For the uncoated specimens, this was the maximum displacement of the system. At this point of the test all of the coated specimens are seen to have absorbed more energy than that of the uncoated specimens. On average the absorbed energy of the coated systems is 400% greater

than that of the non retrofitted specimens. CMU Type 2 has the higher fracture energies than that of CMU Type 1 for both polyurea batches. Since this is opposite then the results of the plain specimens, it indicates that the bond between the polyurea coatings and the harder aggregate CMU, CMU Type 2, is better than the bond to CMU Type 1.

The next displacement used for comparison is the ultimate displacement of Test 1. This is a displacement that all four coated specimens were able to achieve and therefore would be a good point of comparison between tests. The energy values for a coated system at this displacement are, on average, 32600% than the total fracture energy of the uncoated specimen having the same CMU Type. Therefore the increase in fracture energy of a coated system versus an uncoated system is almost solely due to the polyurea's ability to continue absorbing energy after cracking of the concrete occurs. The energy values, at this displacement value, indicate that Polyurea 70-5 does not have a consistent physical structure throughout. The Test 1 specimen is able to absorb 34% more energy than the specimen of Test 2. It can be concluded that this is not due to the differing CMU Types since the energy absorbed in Test 4 is only 0.7% greater than that of the energy absorbed in Test 3 and these tests are done on the two different CMU types with the same polyurea coating (70-1). For Polyurea 70-5, the hard to soft segment ratio may differ throughout the supply of polyurea or more air may be introduced into the system at certain points during the spray application. Both of these factors mean that, at different points along the wall or CMU block, the polyurea could have had different physical properties.

### 4.8.1 Polyurea Strain

As was stated in the Instrumentation section of this chapter, each polyurea coated specimen had three strain gauges located along the polyurea surface, centered along the width. One gauge was located at the center of the specimen, the second was located 0.625 inches from center, and the final gauge was 1.25 inches from the center of the specimen length.

Figure 4-19 presents the recorded center strain versus the center displacement of the section. Data from these gauges are lost early on in the testing phase due to the range of the gauge versus the high strain values achieved by the polyurea. The gauge is active for at least concrete cracking, the drop in load, followed by another rise in load for all tests. As can be seen, Test 1 and Test 3 show similar behavior and strain values as well as do Test 2 and Test 4. This indicates that the post-cracking response is controlled by the CMU Type rather than the Polyurea Batch. This is understandable of the center gauge up until cracking of the concrete occurs. An explanation for why the strain values may be similar for the same CMU Type after cracking of the beam could be due to how the crack forms and where. The aggregate within the concrete could play a role in this. If the crack propagates off-center, then the gauged location is not actually within the cracked region and will therefore show a much smaller strain than a gauge within the crack-opening region of polyurea.

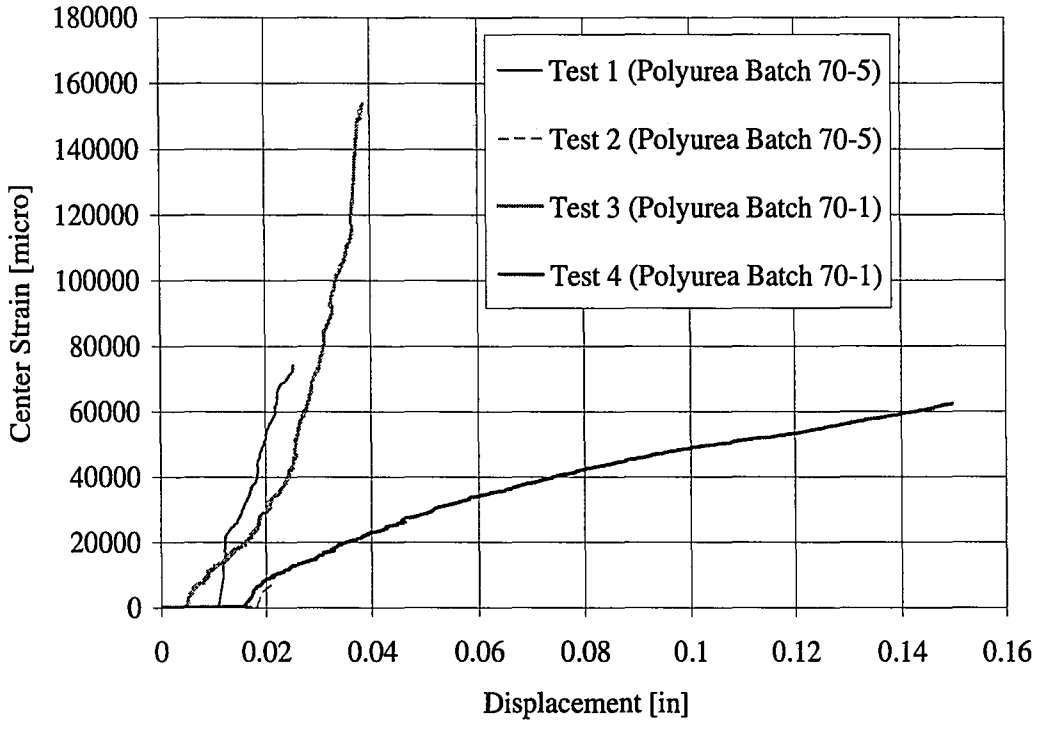


Figure 4-19: Center Strain versus Displacement

Figure 4-20 shows the same plot for the gauge located 0.625 inches from the center of the span length. In this plot, Test 3 and Test 4, whose specimens are both coated with Polyurea 70-1, are clustered together with similar slopes and do not diverge until later in the test. Again Tests 1 and 3, which both have the CMU with the cinder based aggregate, are also clustered together and don't diverge in strain pattern. The plot further supports that what is being seen in the strain gauges is more a property of crack location and opening rather than polyurea type. Test 2 sees much lower strain at this location than any of the other tests. This could mean a difference in location from the actual crack location or it could again justify that the 70-5 polyurea is not consistent in its chemical make-up and therefore physical properties.

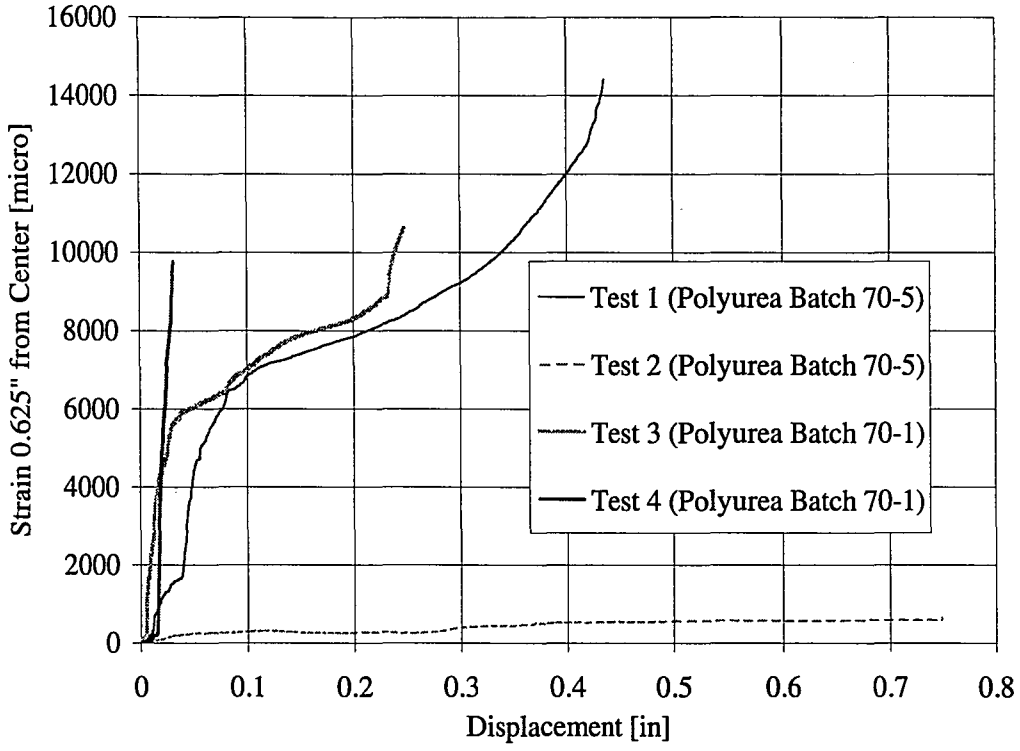


Figure 4-20: Strain 0.625" from the Center versus Displacement

Figure 4-21 depicts the strain at 1.25 inches from the center of the specimen length. It can be seen that all the strains start at a negative value, Test 3 and Test 4 increase to positive values as the test progresses, while Test 1 and Test 2 continue to become more negative for a larger range of the displacement before finally starting to increase with a positive slope. Since these gauges are located much closer to the supports than the others, and are further away from the influence of the crack opening, the negative values could be due to the supports pushing into the polyurea. This would cause it to deform in compression slightly. It seems that polyurea 70-5 is more susceptible to the inward force of the supports due to its larger negative values. Figure 4-21 also indicates that polyurea 70-1 does behave similarly regardless of CMU Type when looking at the behavior far enough away from the crack location.

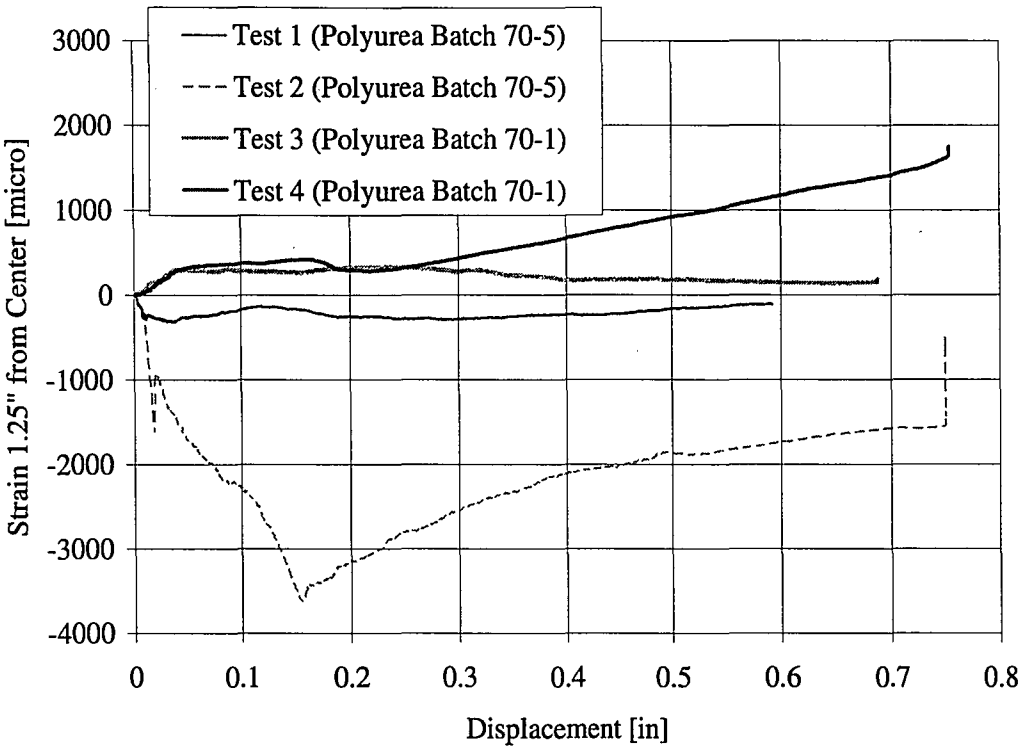


Figure 4-21: Strain 1.25" from Center versus Displacement

#### 4.8.1.1 Delamination

Due to the fact that the polyurea is completely bonded along the length of the specimen, a horizontal shear force is developed between the concrete and the polyurea as the specimen is loaded. This force would be highest near the point of loading and would decrease in value with increasing distance away from the load head. As loading increases, the friction forces will grow. When the friction force is equal to the value of the bond strength, then delamination occurs and a constant tension force and therefore constant strain should be achieved through the delaminated polyurea.

Although there are visual signs of delamination occurring as seen in

Figure 4-22, the data does not indicate its presence. For two different loads, shown in Figure 4-23 for the different tests, the strain gauge values were plotted at their distance from the center of the specimen. These plots are presented in Figure 4-24 and Figure 4-25. As can be seen from these figures, no constant strain is achieved between gauges. When the second load is reached, the center strain gauge is lost, so it is inconclusive whether, at this point, the strains between the center gauge and the gauge located 0.625 inches away from the center are of the same value.

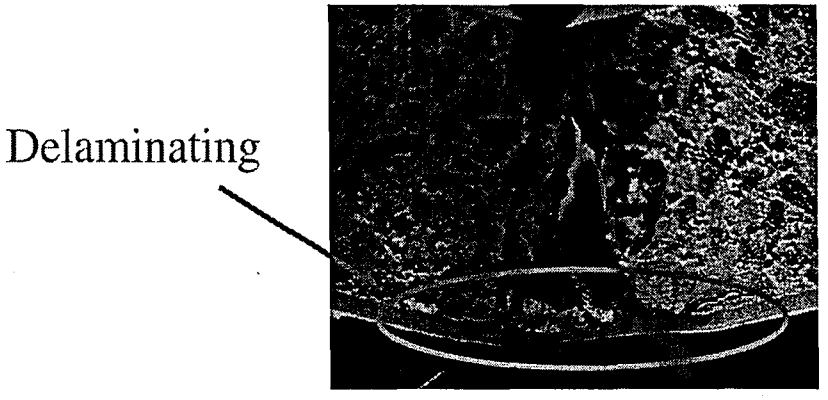


Figure 4-22: Possible Delamination

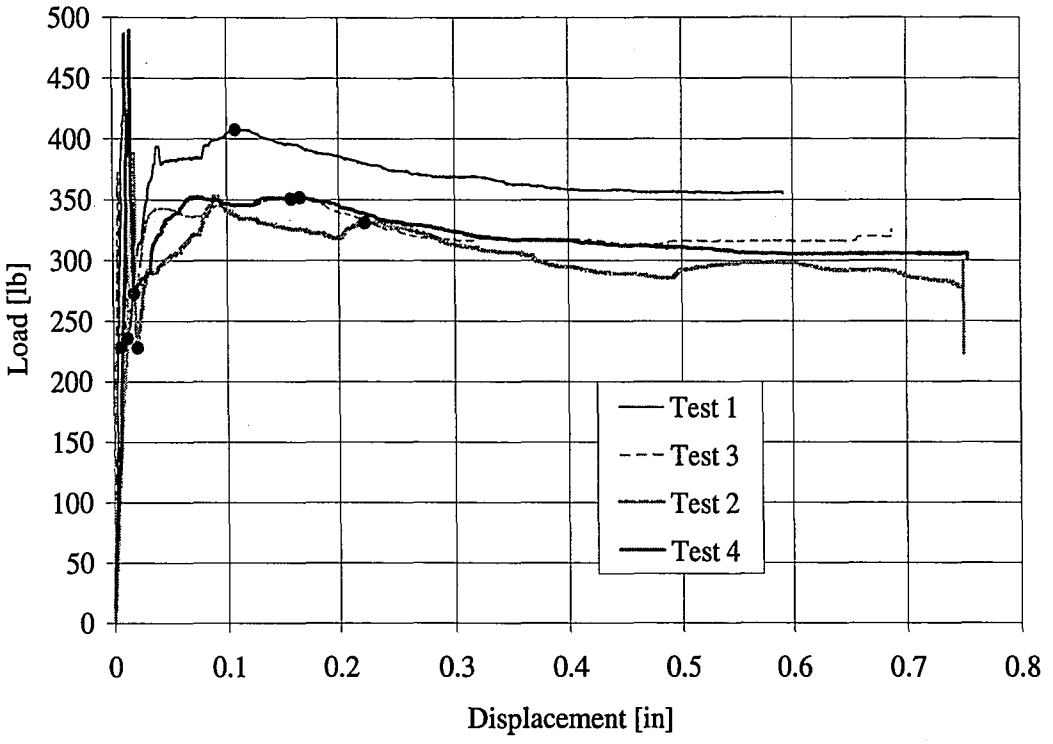


Figure 4-23: Load Values at Which Strains are plotted

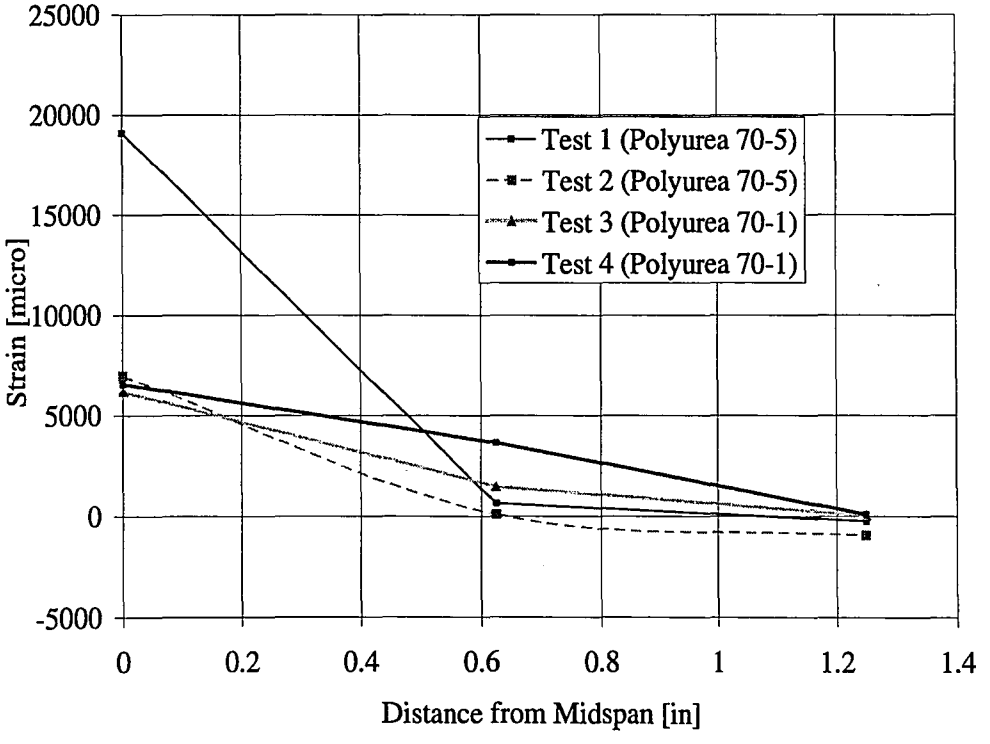


Figure 4-24: Strain along Distance of Beam for Load 1

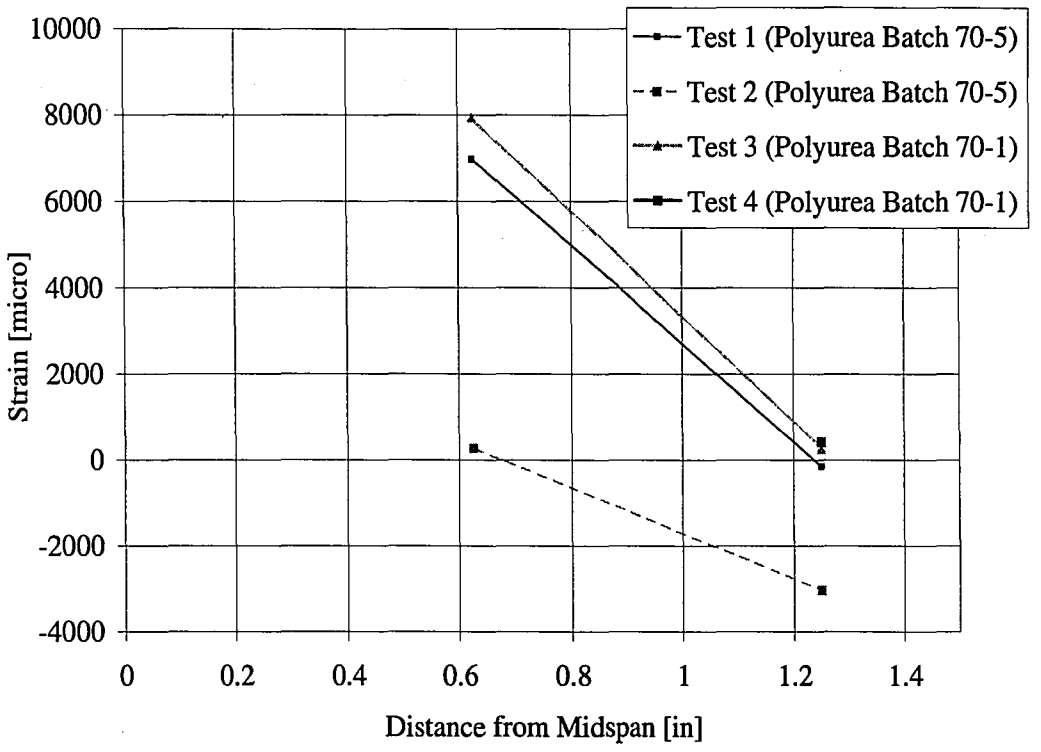


Figure 4-25: Strain along Distance of Beam for Load 2

## 4.9 Conclusions

When a specimen, undergoing center-point loading at static rates, is coated with polyurea on the underside of the beam, it will allow for an increase in modulus of rupture and an increase in the peak load that the system is able to achieve compared to an non retrofitted specimen. The polyurea also allows the system to continue deforming as well as to hold load after cracking of the concrete occurs. In addition, the ability to absorb energy is significantly increased at static rates when the specimen is retrofitted with a polyurea mix.

The initial behavior of the system, such as the modulus of rupture and peak load, rely on both the properties of the polyurea coating as well as the properties and size of the material that is being coated. Also, the energy absorbed at the point of cracking of

the concrete is also dependent on both material properties. Strains within the polyurea near the crack location are dependent on where and how the crack forms in the specimen. However, as the distance from the crack location increases, the strains are more dependent on only the polyurea properties. Due to the high poisson ratio of the material, a negative strain could be present near the support location, where a contraction of the polyurea may occur.

The visual evidence of delamination could not be supported by the strain data recorded during testing. However, this could be due to the fact that the capacity of the strain gauges is lower than the strains achieved by the polyurea at the center of the specimen. The strains between the center strain gauge and the gauge located at 0.625 inches from the center may have become constant at a point beyond the loss of the center gauge.

The performance of the center-point loading tests also gives insight on the performance of the walls that underwent the full-scale blast test performed by Air Products, which were described in Chapter 3. The west wall that was coated with Polyurea 70-5, saw fracturing at both the top and bottom of the wall. These fractures propagated until most of the wall blew in. Some of the inconsistent results between the two tests that included Polyurea 70-5 coatings, including the load displacement curves, the fracture energies at the end of Test 1, and the strains seen at the gauge located 1.25 inches from the center, may indicate that the west wall mix was not standard in its chemical properties at different locations. This inconsistency in chemical make-up may have made the mixture weaker at certain locations, allowing for fracture to occur.

# 5 Static Center-Point Loading Tests on Concrete Beams

## 5.1 General

This chapter describes the center-point static rate tests that were carried out on pre-cracked concrete beams with a polyurea coating and compares them to the center-point static rate test results of uncoated pre-cracked concrete beams. The test matrix and procedure is described. The results of these tests help to quantify load versus displacement performance of different systems, fracture energies of the different systems, and further help to define bond strength.

## 5.2 Test Matrix

The static tests were carried out on concrete beams having a compressive strength of 3,410 psi. The dimensions of the beams were 6.5 inches x 3.5 inches x 27 inches as shown in Figure 5-1. Also seen in Figure 5-1, the concrete beams were made with a pre-crack at the center, having a height of 1 inch and a width of a 1/4 inch. Due to the scale of the beam and the presence of the crack, the maximum aggregate size used was 3/8 inches.

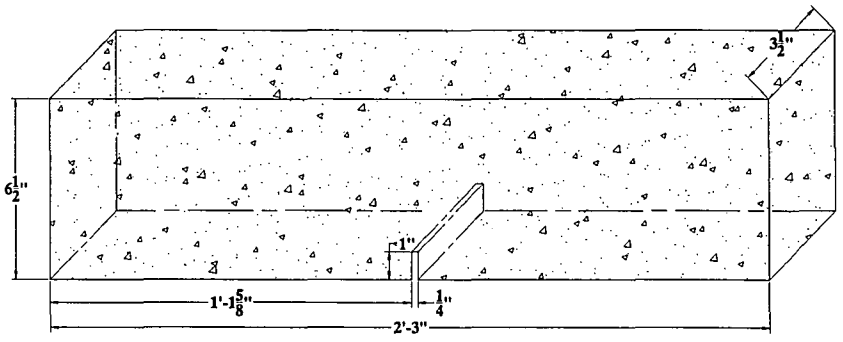


Figure 5-1: Concrete Beam Specimens

The static center-point loading tests were carried out on polyurea coated and uncoated concrete beams. The polyurea coating was made and applied at the ATLSS facilities of Lehigh University. The process of batching polyurea is described in Chapter 2, along with the typical polyurea material properties. The test matrix included two beams with a debonded length of 5.5 inches as well as two beams that were completely bonded aside from the ¼ inch width below the pre-crack. The cross-sections of a beam with a 5.5 inch debonded polyurea region are shown in Figure 5-2. The beam with a ¼ inch debonded region would contain only cross-sections one, XS1, and three, XS3. Since only three beams could be coated with polyurea at a time, as described in Chapter 2, the beams examined were coated with different polyurea batches. The test matrix is described in Table 5-1.

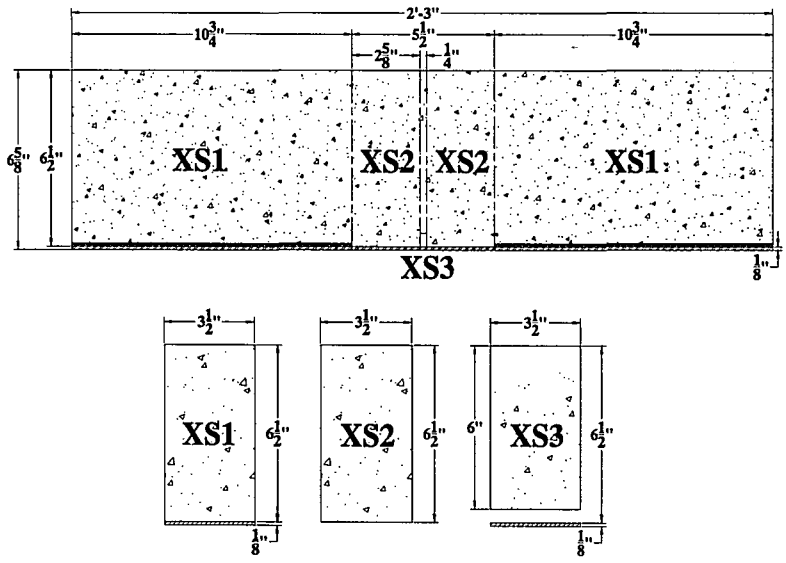


Figure 5-2: Cross-sections of Concrete Beams with 5.5" Debonded Polyurea Region

| Test ID | Height | Polyurea Batch | Concrete Type | Debond Length |
|---|---|---|---|---|
| 1 | Static | 5 | 1 | 0.25 |
| 2 | Static | 5 | 1 | 0.25 |
| 3 | Static | 4 | 1 | 5.5 |
| 4 | Static | 4 | 1 | 5.5 |
| 5 | Static | n.a. | 1 | n.a. |
| 6 | Static | n.a. | 1 | n.a. |

Table 5-1: Test Matrix for Static Concrete Beam Center-Point Loading Tests

## 5.3 Testing

The series of flexural tests were conducted using a variation on ASTM C-293, to determine the flexural strength and deformation of the concrete specimens. ASTM C-293: Standard Test Method for Flexural Strength of Concrete (Using Simple Beam with Center-Point Loading) applies a center-point load to a simply supported concrete beam to determine the modulus of rupture of concrete. This ASTM was used as a guideline in order to determine the fracture energy of the system as well as the flexural strength of the concrete/polyurea system. These tests will serve as a comparison to non-coated concrete beams. The test set-up and instrumentation used for the series of static tests is shown in the diagram of Figure 5-3 and the photograph of Figure 5-4.

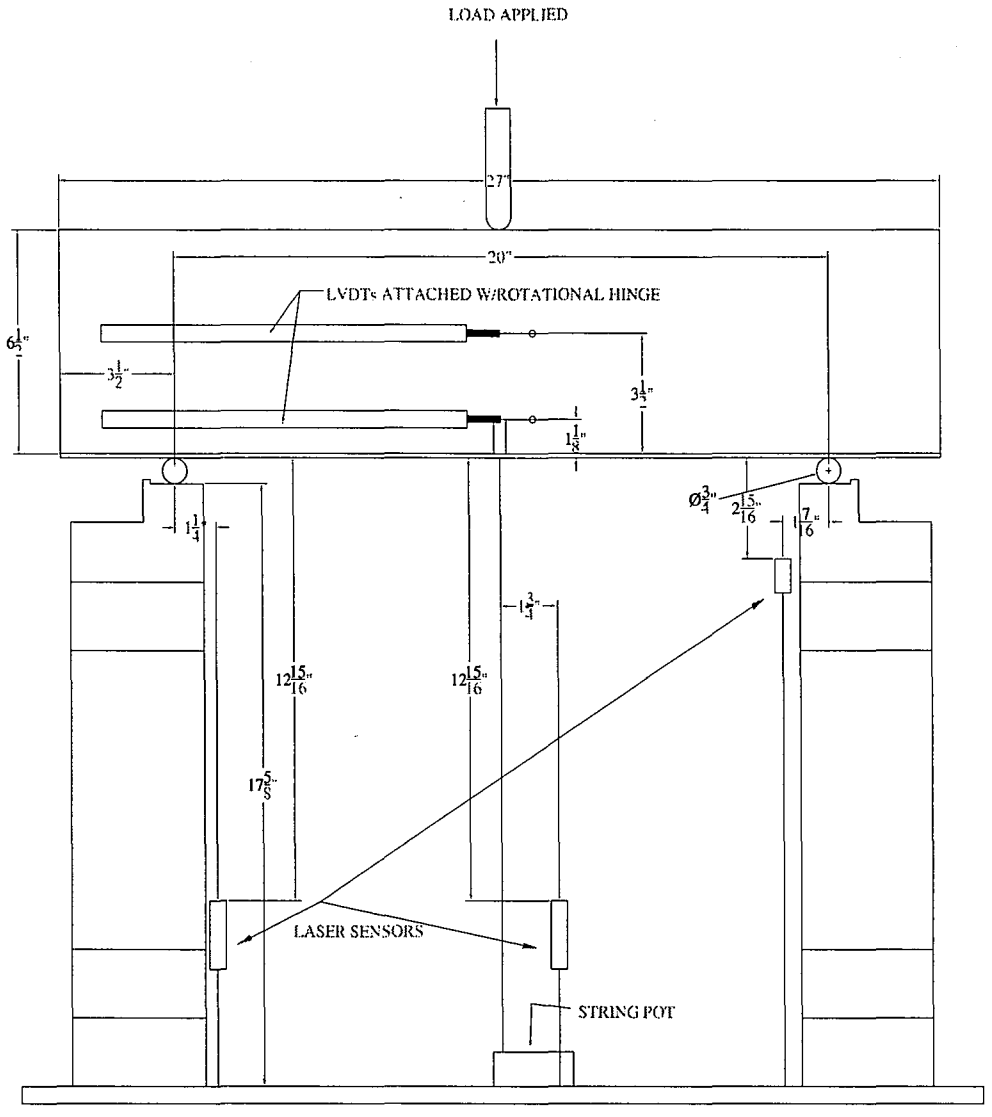


Figure 5-3: Static Test Set-Up for Concrete Beams

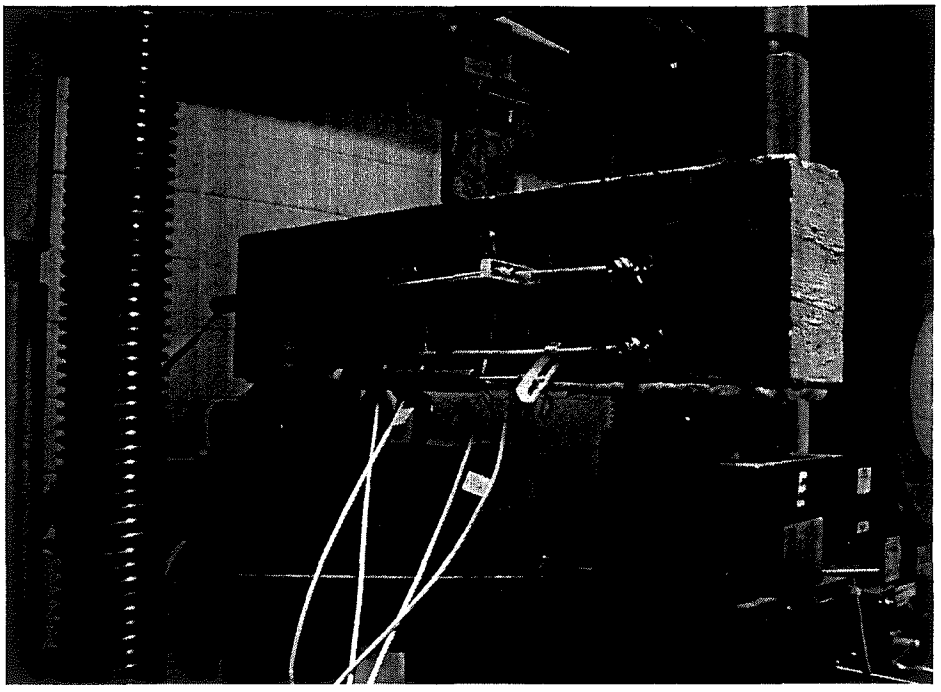

Figure 5-4: Photograph of Static Test Set-Up

For the ASTM C-293 variation, the load was applied at midspan and perpendicular to the top surface of the test specimen. The width of the loading head was greater than that of the beam to ensure a uniform line load was applied across the entire midspan width of the test specimen. Simple supports were located 3.5 inches from each end of the test specimen and were parallel to the applied line load. The beam was supported with actual rollers to create the ideal support condition.

The procedure for conducting the tests was as follows:

1. Centered the test specimen on the loading fixture support blocks.

2. Centered the loading fixture in the test machine.

3. Applied load continuously at a constant average rate of 14.3 lb/sec until cracking of the concrete occurred, then continued to apply load at an average constant rate of 0.423 lb/sec for the coated specimen.

The test was ended when the maximum range of the center laser was reached or fracture of the specimen occurred.

### 5.3.1 Testing Goals and Expected Results

The goals of the test were to determine and compare the following properties for both uncoated and coated specimens:

- The modulus of rupture of the composite system
- The maximum deflection of the system
- Strain in polyurea as cracks open in concrete
- The level of debonding and the interface bond strength

To achieve the goals of the test program a series of measurements were made. These include:

- Strain in the polyurea along the length of the specimen
- Vertical displacement of the beam at midspan
- Load applied
- Cross-sectional area of the test specimen and the polyurea coating
- Rotation and crack opening of the concrete

Concrete cylinders were made from the same batch of concrete used for the beams and were cured for the same duration as the beams. These cylinders were tested in compression following ASTM C-39 to determine the strength of the concrete at the time of the beam tests. These tests resulted in an average concrete compressive strength of 3,410 psi. Using this strength, the expected results for both an uncoated and coated beam were calculated. An approximation of the modulus of rupture was calculated as $7.5\sqrt{(f'_c)}$, where $f'_c$ is the compressive strength of the concrete. Once the modulus of rupture was determined, the ultimate moment was calculated using the formula: $R(I_g)/c$, where R is the modulus of rupture, $I_g$ is the gross moment of inertia of the cross section, and c is the neutral axis depth. A transformed cross-section was used to determine $I_g$ and c for the polyurea coated beams. The width of the polyurea was transformed to an equivalent width of concrete by multiplying it by the ratio of the elastic modulus of polyurea divided by the elastic modulus of the concrete. The elastic modulus of the polyurea was assumed to be similar to the Batch 4 polyurea tested under tension as described in Chapter 2, (properties listed in Table 2-4). To determine the elastic modulus for the concrete the ACI formula, shown in Equation 5-1, was used.

$$E_c = 33 * w_c^{1.5} * \sqrt{f'_c}$$

where:

$E_c$ = concrete elastic modulus

$w_c$ = weight of concrete [lb/ft$^3$]

$f'_c$ = concrete compressive strength [psi]

Equation 5-1: Elastic Modulus of Concrete [psi]

For a simply supported beam, the moment at the center is equal to PL/4. Using this formula and the ultimate moment previously calculated, an estimate for the ultimate load was determined. The values are presented in Table 5-2.

| Type | Polyurea Batch | $f'_c$ [psi] | Calculated R [psi] | c [in] | Ig [$in^4$] | M [lb-in] | P [lb] |
|---|---|---|---|---|---|---|---|
| Plain | n.a. | 3410 | 438 | 3.25 | 80.10 | 10794 | 2159 |
| Coated | 4 | 3410 | 438 | 3.51 | 80.12 | 10005 | 2001 |

Table 5-2: Expected Results for Coated and Uncoated Beams

### 5.3.2 Instrumentation

In order to attain the measurements needed to achieve the testing goals, an intricate instrumentation scheme was put into place. All data was recorded at a speed of 40 Hz throughout the test and stored using a Campbell scientific data logger. The center displacement of the beam is recorded using a string potentiometer (string pot) as shown in Figure 5-3 and Figure 5-5.

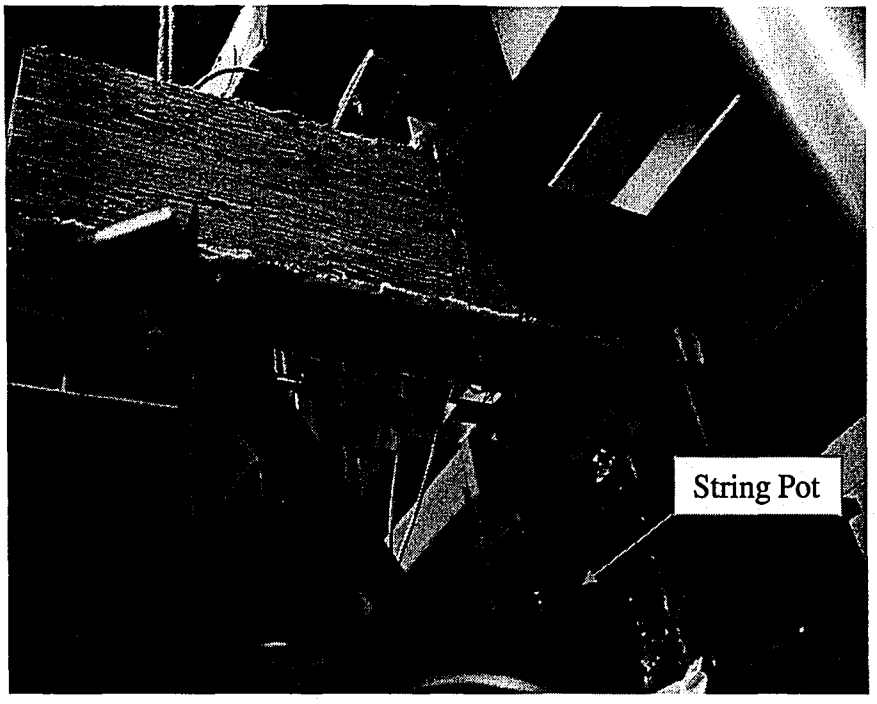


Figure 5-5: String Potentiometer

The string pot data will show some slack due to the fact that it is reading off of the loading head rather than the beam itself. When the loading head comes in contact with the beam, there will be some localized crushing of the concrete at the point it is applied. When this occurs the beam will move a small amount away from the loading head. This displacement will not be read by the string pot, but the displacement needed to reach the beam again will be recorded. The data can be corrected to take this into account by using a linear fit to data that occurs at higher loads and extending this fit to the start of the test, which would then be shifted back to zero for the start of the test.

The load is recorded by using an S-shaped load cell shown in Figure 5-6.

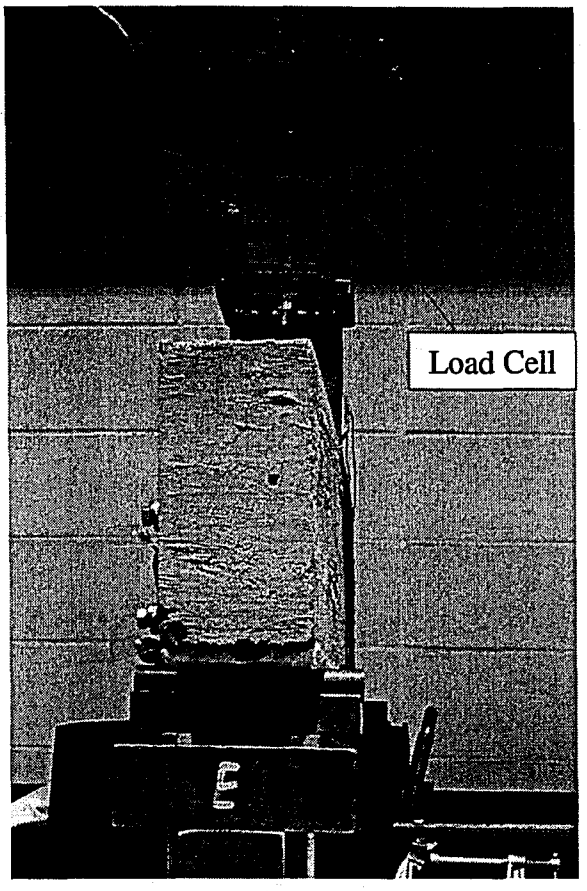


Figure 5-6: Load Cell

The rotation is calculated using the horizontal displacement data of the linear voltage differential transducers (LVDTs) shown in Figure 5-3 and Figure 5-7. The equation used to calculate the rotation is shown in Equation 5-2 and refers to the dimensioning and labeling of Figure 5-8.

$$\theta=ATAN[\{(a+b+\Delta_1)*d-(c+d+\Delta_2)*b\}/\{(c+d+\Delta_2)*d_1-(a+b+\Delta_1)*d_2\}]$$

Equation 5-2: Rotation of Beam using LVDTS [degrees]

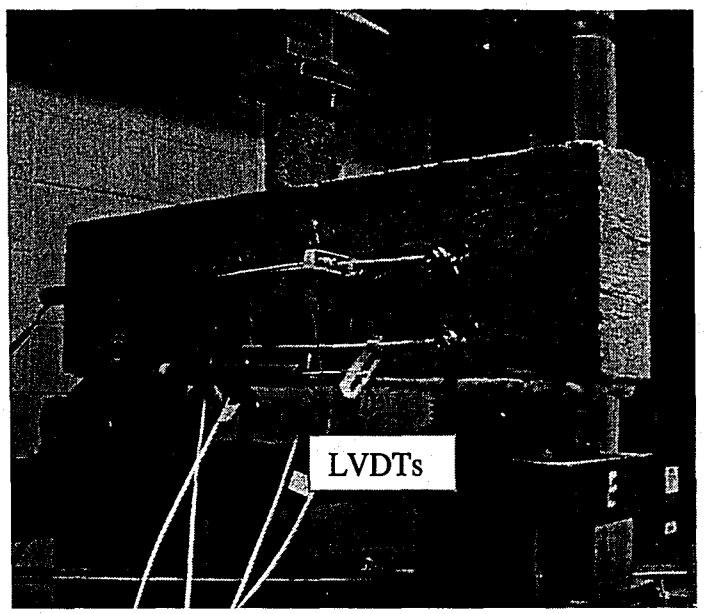


Figure 5-7: Linear Voltage Differential Transducers

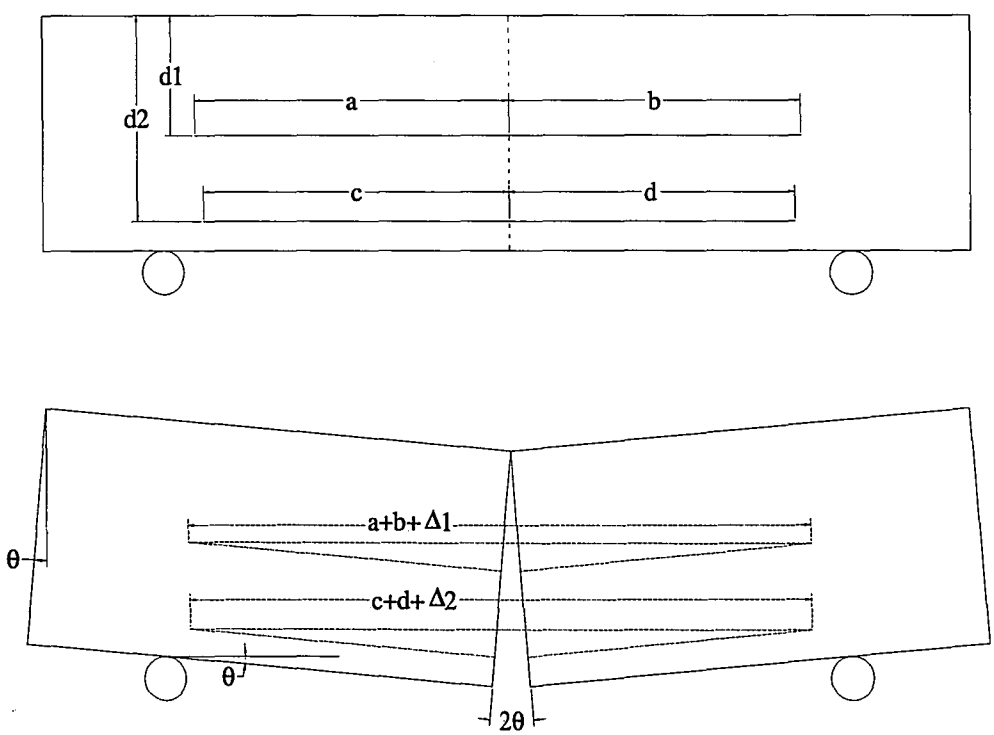


Figure 5-8: Dimensions for LVDT Rotation Calculation

As can be seen in Figure 5-3, the instrumentation also includes three laser sensors. The laser sensors are able to measure relative displacement of a rotating surface up to

30 degrees with accuracy. There is one laser sensor located a small distance from the center to get the maximum displacement of the system. There are also two laser sensors located at a fixed distance close to the supports in order to be able to calculate the rotation of each side of the beam by using Equation 5-3. Looking at Figure 5-8, theta is shown as the angle between the horizontal line drawn from the top of the support, or the beams initial position, and the new position of the bottom surface. The laser would measure the initial position of the beam as zero and then record the vertical displacement above its fixed distance from the support from this point. That is how Equation 5-3 works.

$$\theta = \text{ATAN}(\text{laser sensor read-out} / \text{fixed distance to laser})$$

Equation 5-3: Rotation of Beam using Lasers [degrees]

This will take into account unsymmetrical behavior should one side rotate more than the other when loaded. The laser sensors are used in addition to the other instrumentation to verify that the recorded data is accurate. Figure 5-9 compares the center displacement measured using the string pot and Laser 2. The two devices produce comparable measurements. As can be seen, the plots remain essentially on top of each other until the laser shows a drop in load at a given displacement earlier than the string pot device shows this. The string pot is attached to the load head and therefore, even if the displacement of the bottom of the beam had ceased for a moment, the head could have caused some local crushing at the point of rotation and therefore the string pot shows a continuation of displacement. The local crushing may also account for the fact that the string pot achieved a higher maximum elongation. Figure 5-10 shows a plot of the calculated rotations using the LVDT

data and the Laser data versus time to show its accuracy. The plots are from Test 3 data.

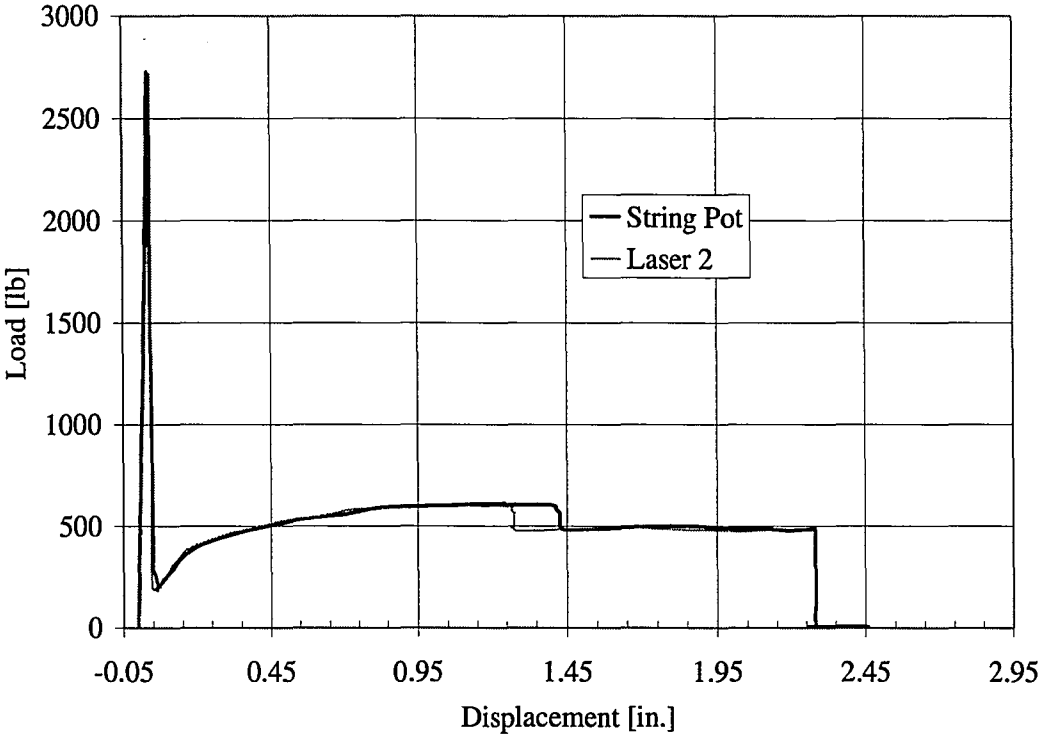


Figure 5-9: Comparison of Center Displacement for Lasers and String Pot

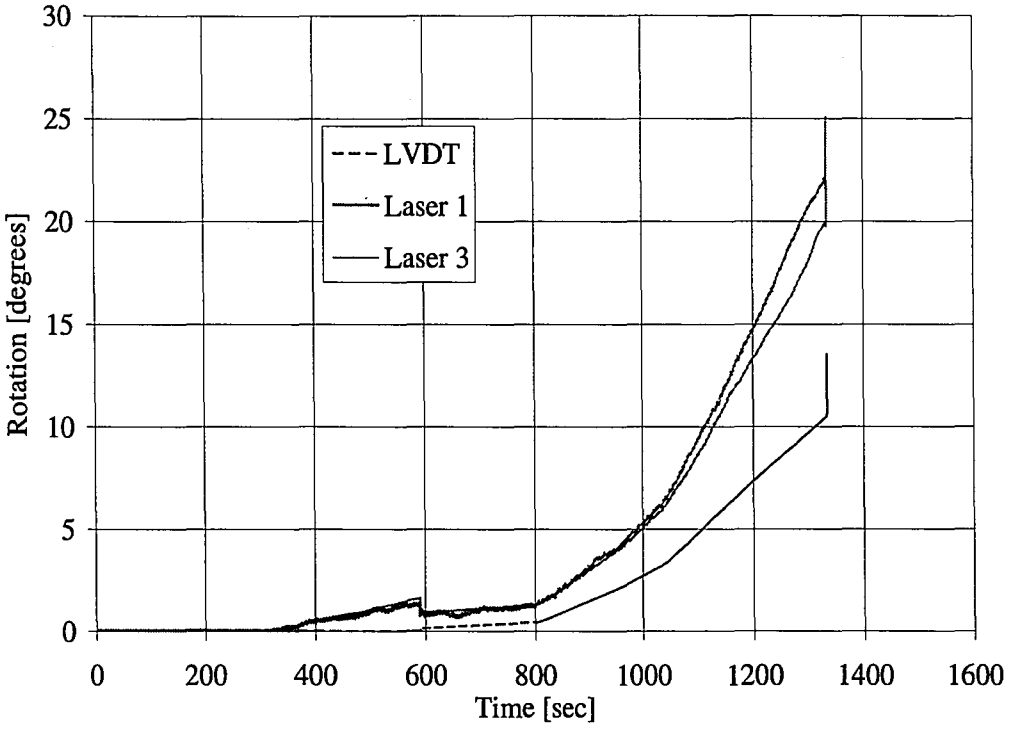


Figure 5-10: Comparison of Rotation Recorded with LVDTs and Lasers

It can be assumed that the lasers are accurate based on the center displacement comparison of Figure 5-9. This conclusion is supported by Figure 5-10, which shows that the rotation behavior recorded from the LVDTs and Lasers follow the same trend but differ slightly in value. The LVDT rotation calculation of Equation 5-2 relies on symmetric behavior of the beam, but as can be seen in Figure 5-10, Laser 1 and Laser 3 show that one side rotates more than the other near the end of the test. It is near the end of the test where the difference between the LVDT data and Laser data is the greatest.

The strain in the polyurea was recorded at five different locations along the length of the beam. The locations of the strain gauges, which were the same gauges used for

the CMU Tests described in Section 4.5, are shown in Figure 5-11. It should be noted that gauge 4 is reading lateral strain.

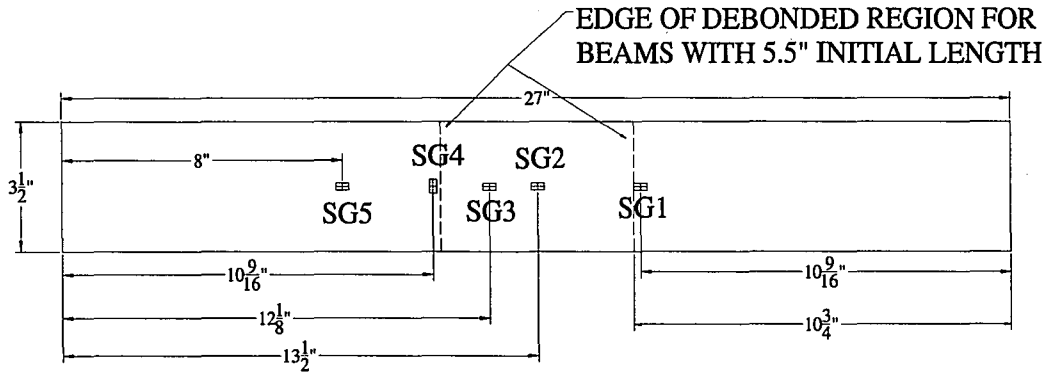


Figure 5-11: Strain Gauge Configuration

## 5.4 Results of Static Concrete Beams Tests

As seen in the test matrix, polyurea coated beams with two different debonded lengths were tested along with a set of plain concrete beams. The polyurea coating is a retrofitting option, and therefore the results are always dependent on a comparison to the behavior of plain concrete beams. Load versus displacement curves are used to examine debonding length and the fracture energy resisted by each beam (Equation 4-3). Rotations and strain gauges are also used to examine the bond strength. Strain gauges at different locations reading the same strain point to a constant strain region between the two gauges meaning, as was discussed previously, the polyurea is debonded along this length. Also, comparing the polyurea strain given by the center strain gauge to that of the expected strain from calculations using the rotation data could identify the changing debonded length of polyurea throughout the duration of the test as well.

### 5.4.1 Plain Concrete Beam Results

Test 5 and Test 6 examines uncoated concrete beams. The beams were loaded at a constant rate until failure. At initiation of the test localized crushing occurred at the point of contact between the load head and the specimen. The data was modified using the same process introduced in section 4.7.1 to minimize the effect of the localized crushing. The load versus displacement curves are presented in Figure 5-12 and results are given in number format in Table 5-3.

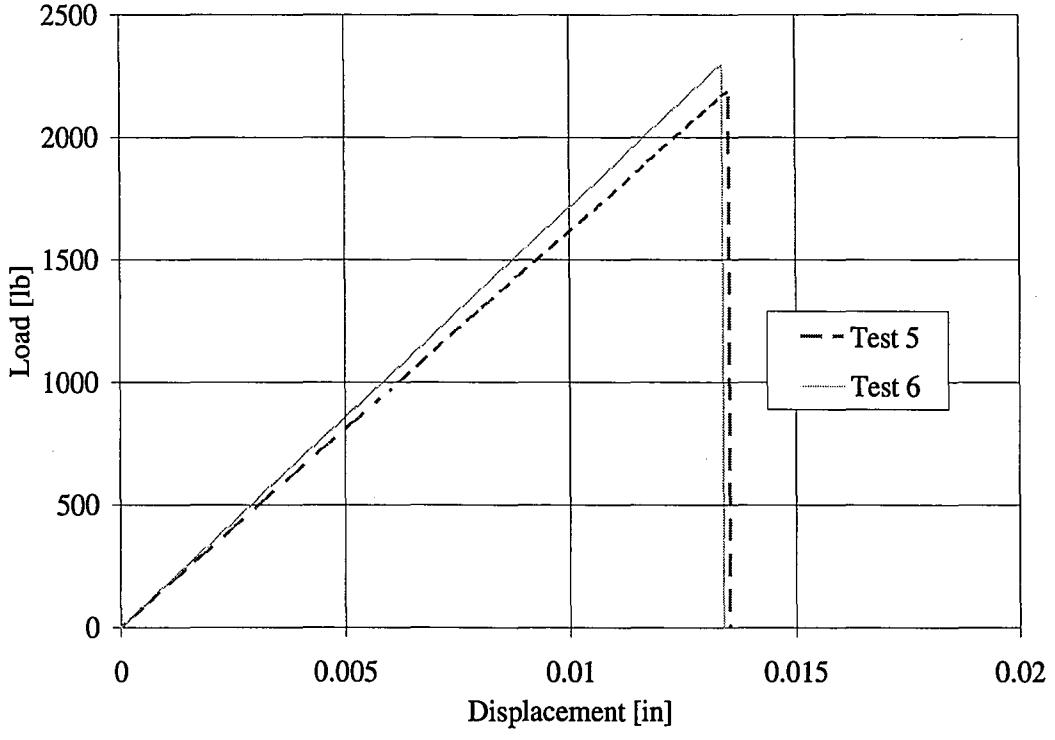


Figure 5-12: Load versus Displacement for Plain Concrete

| Test ID | Rate | Polyurea Batch | Concrete Type | Maximum Load [lb] | Modulus of Rupture [psi] | Multiplier for $(f'_c)^{0.5}$ |
|---|---|---|---|---|---|---|
| 5 | Static | n.a. | 1 | 2190 | 444 | 7.6 |
| 6 | Static | n.a. | 1 | 2300 | 467 | 8.0 |
| | | | AVG. | 2245 | 455 | 7.8 |

Table 5-3: Summary of Test Results for Plain Concrete Beams

The fracture energies for the two plain beams were calculated using Equation 4-3 and are summarized, along with the important values for the calculations, in Table 5-4.

| Test ID | Concrete Type | $W_o$ [lb-in] | $m_1$ [lbf] | $m_2$ [lbf] | m [lbf] | $\delta_o$ [in] | $A_{lig}$ [$in^2$] | $G_F$ [lb-in] |
|---|---|---|---|---|---|---|---|---|
| 5 | 1 | 14.9 | 0.553 | 0 | 0.553 | 0.014 | 22.75 | 0.783 |
| 6 | 1 | 15.4 | 0.553 | 0 | 0.553 | 0.013 | 22.75 | 0.803 |
| | | | | | | | AVG. | 0.793 |

Table 5-4: Fracture Energies for Uncoated Concrete Beams

The values of Table 5-3 and Table 5-4 will be used as base values and will be compared to the polyurea coated specimens to examine the coating's contribution to energy resistance.

### 5.4.2 Polyurea Coated Concrete Beam Results

The behavior of the coated system is similar to that of the CMU coated specimens of Chapter 4. Due to crack initiator located at midspan once the cracking load of the concrete was reached, the crack formed at a known location and progressed through the depth of the specimen as shown in Figure 5-13. As the crack opening increased, the polyurea actively resisted the opening as seen in Figure 5-14. The polyurea continues to elongate at the crack. Due to limitations in the test setup fracture was

not achieved. At the end of the test, as the load is taken off, a rebound was observed as shown in Figure 5-15. The elastic recovery was significant; however permanent elongation of the polyurea was clearly visible (Figure 5-16).

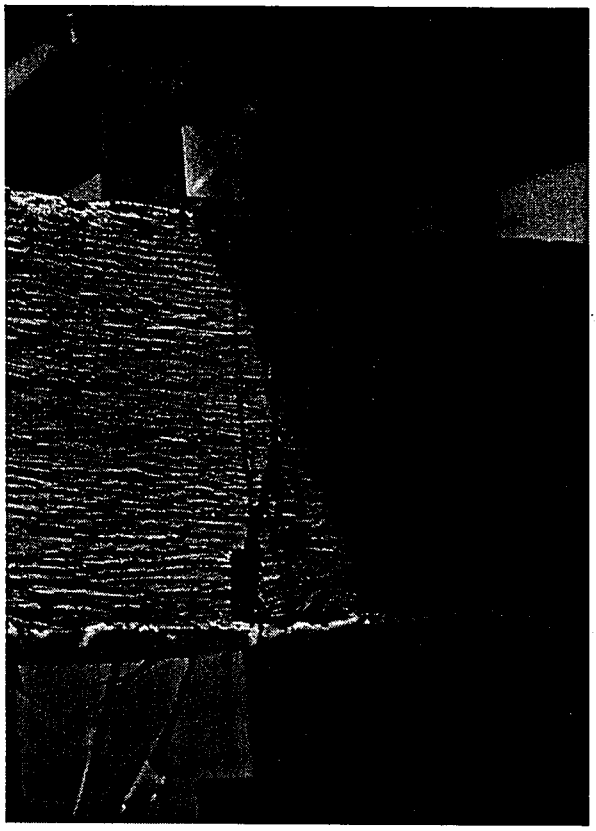

Figure 5-13: Cracking Occurs

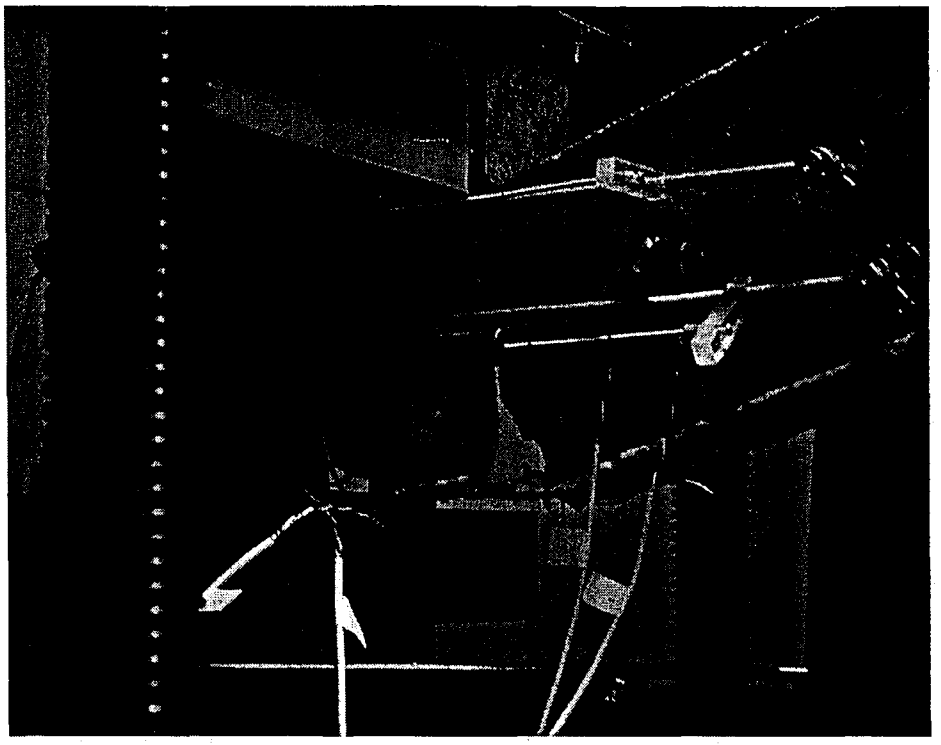

Figure 5-14: Rotation and Displacement of Beam at End of Test

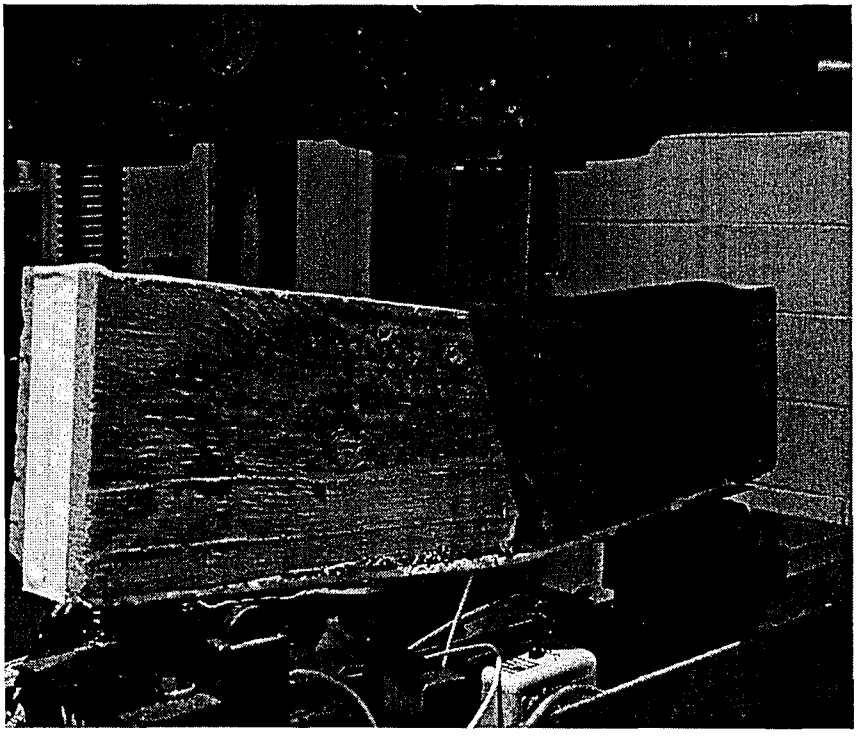

Figure 5-15: Rebound

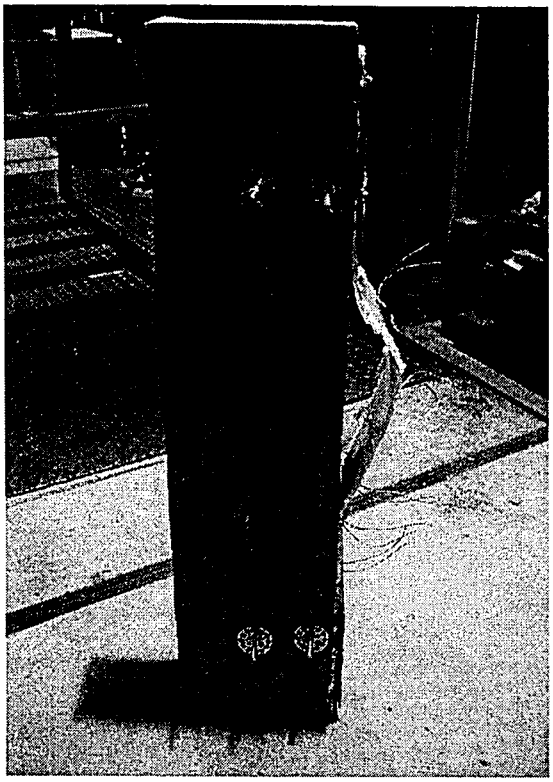

Figure 5-16: Permanent Deformation of Polyurea

#### 5.4.2.1 Modulus of Rupture and Fracture Energy of the Coated System

The load versus displacement curves for the bonded polyurea coated specimens is presented in Figure 5-18. As can be seen, a similar behavior to that of the coated CMU blocks is seen. Once the maximum load is reached, causing the concrete to crack, the load decreases to a smaller value, at which point it starts to slowly increase again before almost reaching a constant load value until the maximum displacement allowed by the test set-up is achieved.

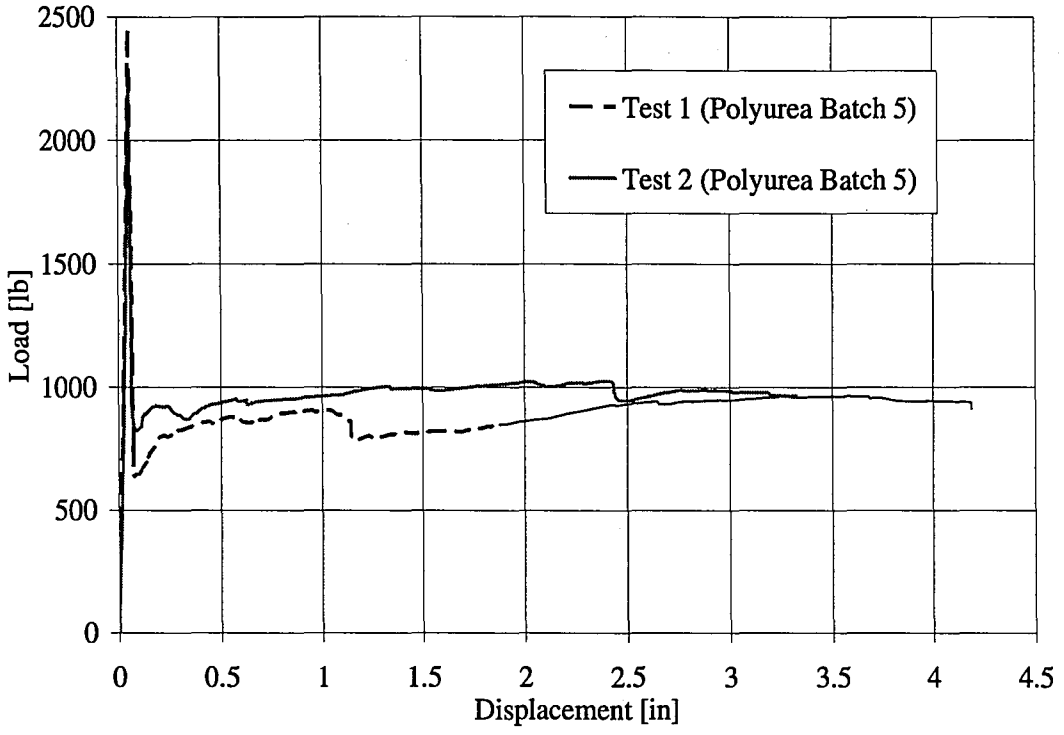


Figure 5-17: Load versus Displacement for Bonded Polyurea

In these tests, the same polyurea batch is applied to the concrete specimens and is only debonded across the ¼ inch initial crack width. The peak loads for the two specimens are similar as well as the almost constant load reached by the polyurea after concrete cracking occurs. Both tests ended due to the roller supports being pushed off the stands due to a wedging action created by the rotation of the specimen. The peak load and modulus of rupture, based on the peak load, are given in Table 5-5.

The load-displacement curves for the polyurea coated concrete blocks having a 5.5 inch debonded region are presented in Figure 5-17. In Test 3, the polyurea fractured and failure of the system was reached, whereas in Test 4, the test was ended when the roller was pushed out of the test set-up. The early fracture of the polyurea in Test 3 is due to a flaw in the polyurea at the crack location caused by the tape between the

concrete and polyurea, meant to ensure the debonded area. The tape had lifted up and was embedded within the polyurea.

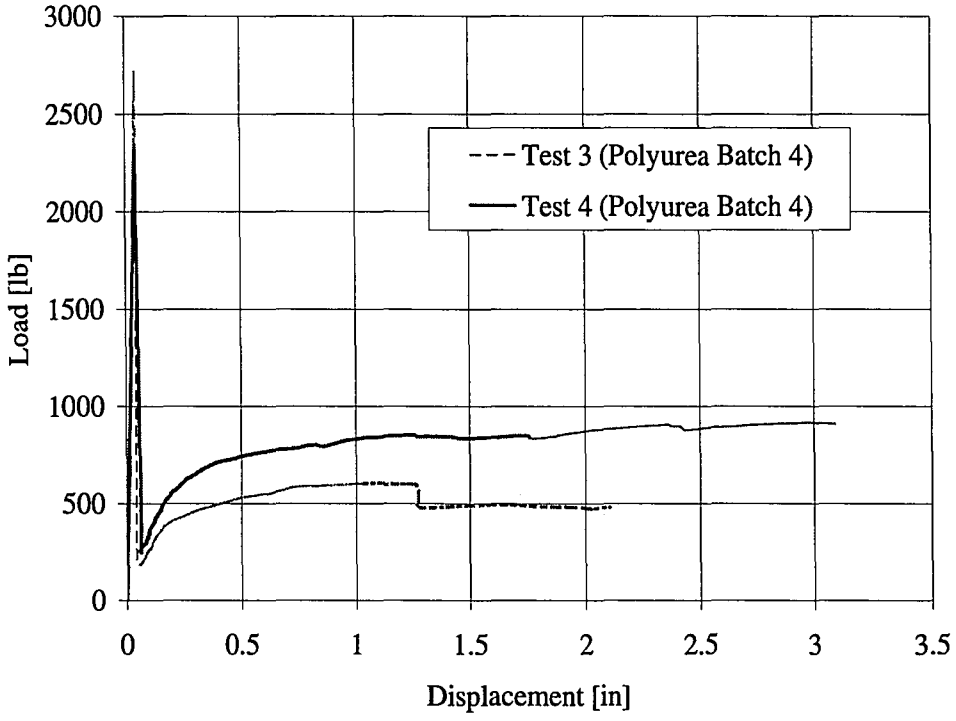


Figure 5-18: Load versus Displacement for 5.5 inch Debonded Polyurea

The two specimens plotted are coated with the same batch of polyurea, batch 4, and have the same debonded region of 5.5 inches. The concrete is also the same for both tests. As can be seen, there is a difference in peak load (defined in Table 5-5), as well as the value that the polyurea is able to achieve after cracking. The value the load drops to, immediately after cracking occurs, is similar for both tests. The drop in load seen in Test 3 occurs when tearing of the polyurea is initiated. Therefore, the difference between the two tests is due to the consistency of the polyurea batch as well as the presence of the initial flaw that did not allow the polyurea to reach its full potential in Test 3.

The same type of concrete is used for Test 1 and Test 2 as was used for Test 3 and Test 4. However the beams for Test 1 and Test 2 are coated with a different polyurea batch than Test 3 and Test 4. A comparison of peak load values and moduli of rupture can be made with the information presented in Table 5-5.

| Test ID | Rate | Polyurea Batch | Concrete Type | Maximum Load [lb] | % Increase in Max. Load | Modulus of Rupture [psi] | % Increase in Modulus of Rupture |
|---|---|---|---|---|---|---|---|
| 1 | Static | 5 | 1 | 2440 | 8.69 | 534 | 17.3 |
| 2 | Static | 5 | 1 | 2280 | 1.56 | 499 | 9.6 |
| 3 | Static | 4 | 1 | 2720 | 21.16 | 595 | 30.7 |
| 4 | Static | 4 | 1 | 2320 | 3.34 | 508 | 11.5 |

Table 5-5: Peak Loads and Moduli of Rupture for Coated Systems

According to the table, the outlier seems to be Test 3. This is the test in which the polyurea fractured. Due to the initial flaw that was present, a stress concentration was developed as loading began and therefore the polyurea reached higher values of strain and stress earlier on in the test than the other tests. Therefore the polyurea may have had a larger impact prior to and up to cracking then the other tests. Otherwise a trend between bonded and debonded polyurea and its effect on maximum load and modulus of rupture does not appear according to Table 5-5.

A plot of all six tests, shown in Figure 5-19, does present a trend. Initial stiffness values seem to depend on the length of the debonded region. However, it would not be expected that there would be a softening in stiffness from plain beams to coated beams; nor would it be expected that as the debonded region decreases in size, a decrease in stiffness of the system is seen. However, this is the trend also described

numerically in Table 5-6.

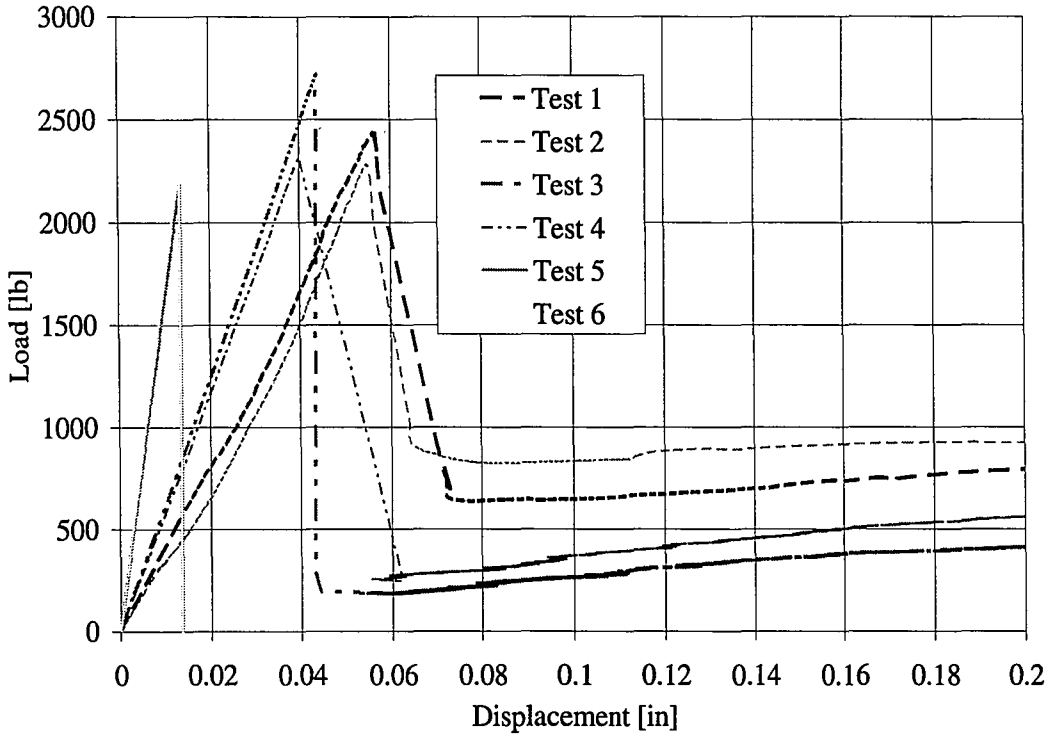


Figure 5-19: Initial Load versus Displacement Curves for Static Beam Tests

| Test # | Polyurea Batch | Polyurea Thickness [in] | Stiffness [lb/in] | Correlation Coefficient |
|---|---|---|---|---|
| 1 | 5 | 0.27 | 42000 | 0.994 |
| 2 | 5 | 0.275 | 36900 | 0.994 |
| 3 | 4 | 0.2283 | 61700 | 0.951 |
| 4 | 4 | 0.258 | 58000 | 0.946 |
| 5 | n.a. | n.a. | 162000 | 0.985 |
| 6 | n.a. | n.a. | 172000 | 0.985 |

Table 5-6: Stiffness Values for Static Beam Tests

The decrease in stiffness from a non-coated specimen shows that there is compression of the polyurea at the supports that is adding to the overall displacement of the coated systems and therefore effects the stiffness calculated. To account for this additional displacement, compression data for polyurea was needed. Following the procedures

given by ASTM D-575-91, Air Products was able to provide an average compression modulus for their polyurea of 6,260 psi for polyurea made in their labs. Using this modulus, the polyurea at the location of the support can be modeled as a spring with stiffness equal to AE/L, where A is the cross-sectional area, E is the compression modulus, and L would be the thickness of polyurea in this case. For every force value, the displacement at the supports was determined by multiplying half of the force (which would be equal to the force seen at the support) by the inverse of the stiffness. The resulting displacement was then subtracted from the recorded displacement of the system. Figure 5-20 was plotted using the adjusted force-displacement set of data and Table 5-7 presents the adjusted stiffness values.

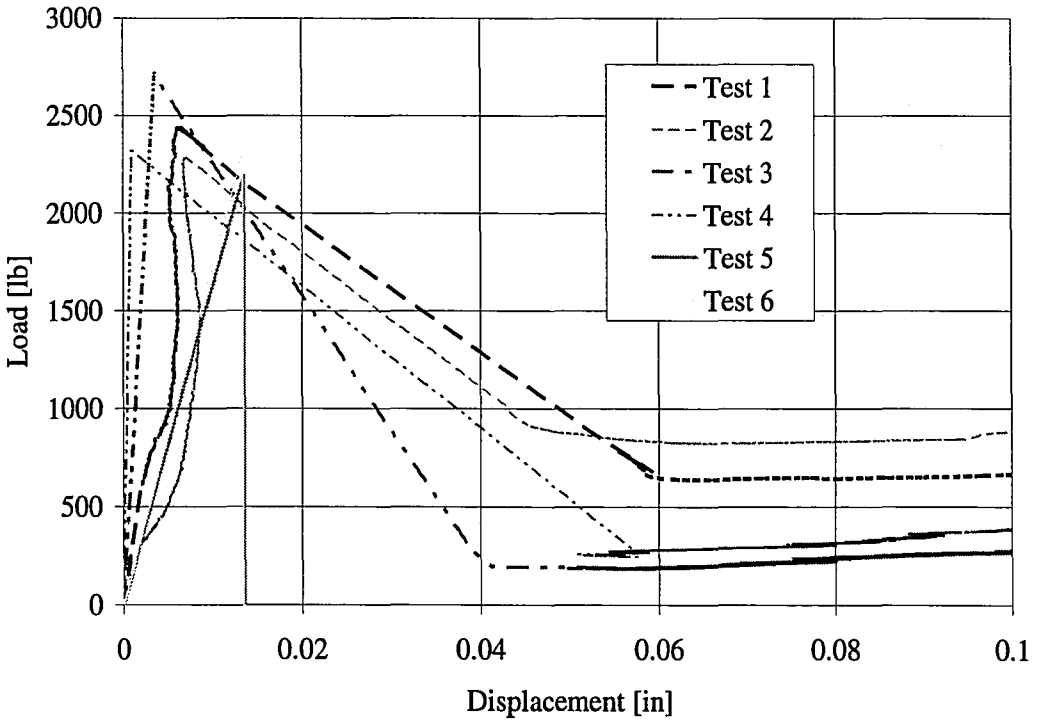


Figure 5-20: Adjusted Load versus Displacement for Accurate Stiffness

| Test # | Polyurea Batch | Polyurea Thickness [in] | Stiffness [lb/in] | Correlation Coefficient |
|---|---|---|---|---|
| 1 | 5 | 0.27 | 202000 | 0.986 |
| 2 | 5 | 0.275 | 157000 | 0.997 |
| 3 | 4 | 0.2283 | 763000 | 1 |
| 4 | 4 | 0.258 | 2440000 | 1 |
| 5 | n.a. | n.a. | 162000 | 0.985 |
| 6 | n.a. | n.a. | 172000 | 0.985 |

Table 5-7: Adjusted Stiffness Values

It is seen that the specimens with a 5.5 inch debonded region still have higher stiffness values than those beams that are coated with fully bonded polyurea. Two different polyurea batches are used, one for the fully bonded specimens and the other for the 5.5 inch debonded specimens. It could be that the polyureas differ in their compression modulus and therefore the adjusted stiffness values are still not accurate. Polyurea Batch 5 could be more compressible than has been accounted for, and therefore the systems deflections are still accounting for some displacement at the supports, making the stiffness of these specimens less than those of the 5.5 inch debonded specimens. It can be concluded that the initial stiffness is affected by the debonded length, since repeatable results and groupings of the different debonded lengths are seen in the plots of Figure 5-19 and Figure 5-20. The difference in length of bonded region may also be more of a concern when looking at fracture energies of the systems.

The fracture energies of the coated systems were calculated using Equation 4-3 and the important values and energies are presented in Table 5-8. It must be noted that the energies calculated for the coated systems are not truly "fracture" energies, except

for Test 3, due to the fact that the systems did not fail. The energies computed represent the amount of energy that has been absorbed by the system up until cracking of the concrete for each test as well as for the displacement at fracture of Test 3, which is a displacement value that all of the coated systems were able to reach.

| Test ID | Concrete Type | $W_o$ at Max Load [lb-in] | $W_o$ at End of Test 3 [lb-in] | $m_1$ [lbf] | $m_2$ [lbf] | m [lbf] | $\delta_o$ at Max Load [in] | $\delta_o$ at End of Test 3 [in] | $A_{lig}$ [$in^2$] | $G_F$ at Max Load [lb-in] | $G_F$ at End of Test 3 [lb-in] |
|---|---|---|---|---|---|---|---|---|---|---|---|
| 1 | 1 | 66.3 | 1800 | 0.553 | 0 | 0.553 | 0.0564 | 2.111 | 22.75 | 3.44 | 98.93 |
| 2 | 1 | 56.4 | 2000 | 0.553 | 0 | 0.553 | 0.0549 | 2.111 | 22.75 | 2.99 | 107.73 |
| 3 | 1 | 60.0 | 1100 | 0.553 | 0 | 0.553 | 0.0441 | 2.111 | 22.75 | 3.05 | 68.17 |
| 4 | 1 | 46.4 | 1700 | 0.553 | 0 | 0.553 | 0.0400 | 2.111 | 22.75 | 2.42 | 94.55 |
| 5 | 1 | 14.9 | 14.9 | 0.553 | 0 | 0.553 | 0.0136 | 0.0136 | 22.75 | 0.78 | 0.78 |
| 6 | 1 | 15.4 | 15.4 | 0.553 | 0 | 0.553 | 0.0134 | 0.0134 | 22.75 | 0.80 | 0.80 |

Table 5-8: Fracture Energies for Coated and Uncoated Concrete Systems

The energies of the coated systems indicate that, besides Test 3, which fractured due to an initial flaw, the polyurea coated systems absorbed a similar amount of energy at a given level of displacement. This means that the two different polyurea batches used to coat all of the test specimens are similar in make-up and behavior. The average fracture energy at maximum load for Test 1 and Test 2 is 3.22 lb-inch, which is greater than the 2.74 lb-inch average of Test 3 and Test 4, which had a debonded region of 5.5 inches. The average absorbed energy for the fully bonded specimens at the end of Test 3 was 103 lb-inch. The average energy of the 5.5 inch debonded specimens at the end of Test 3 was 81.4 lb-inch. The displacement at the end of Test 3 corresponds to a rotation of 14 degrees and a crack opening of 3.15 inches. The results indicate that debonding the polyurea lowers the energy absorption up to moderate crack openings. However, the differences are not significant and could be due to the lower fracture energies of Test 3, for which the polyurea was not able to

reach its full potential due to the presence of a flaw. The full load-displacement curves presented in Figure 5-21 also validate this conclusion. Except for Test 3, the curves are very similar. The only difference being that the load value that Test 4 drops down to, after fracture, is lower than Test 1 and Test 2, but it regains the load values of these tests soon after. This explains why its fracture energy is slightly lower. At a displacement of 2.111 inches, on average, the increase in energy absorbed between a coated system and an uncoated system is greater than 100%.

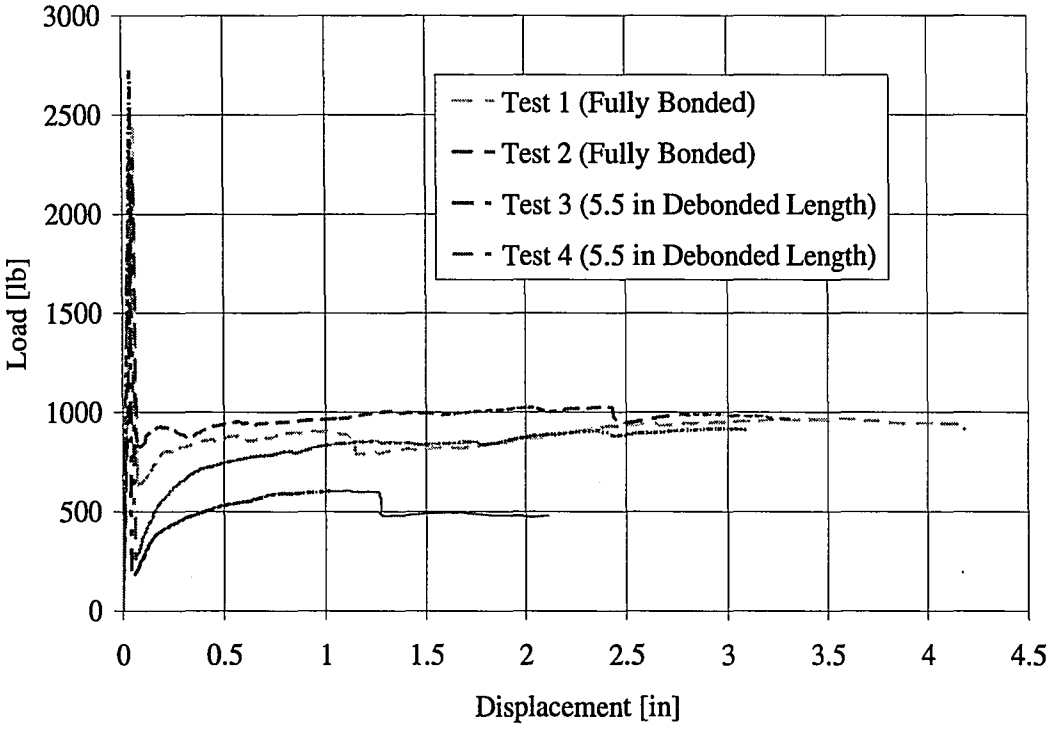


Figure 5-21: Full Load-Displacement Curves for Coated Specimens

### 5.4.2.2 Polyurea Strains

The strain history of the polyurea was examined along the length of the beam. The strain was examined at peak load, the minimum load after cracking, a point during the

initial rise in load after cracking, the second peak load, and the drop in load near the end of the test. The exact points for the different tests are shown in Figure 5-22.

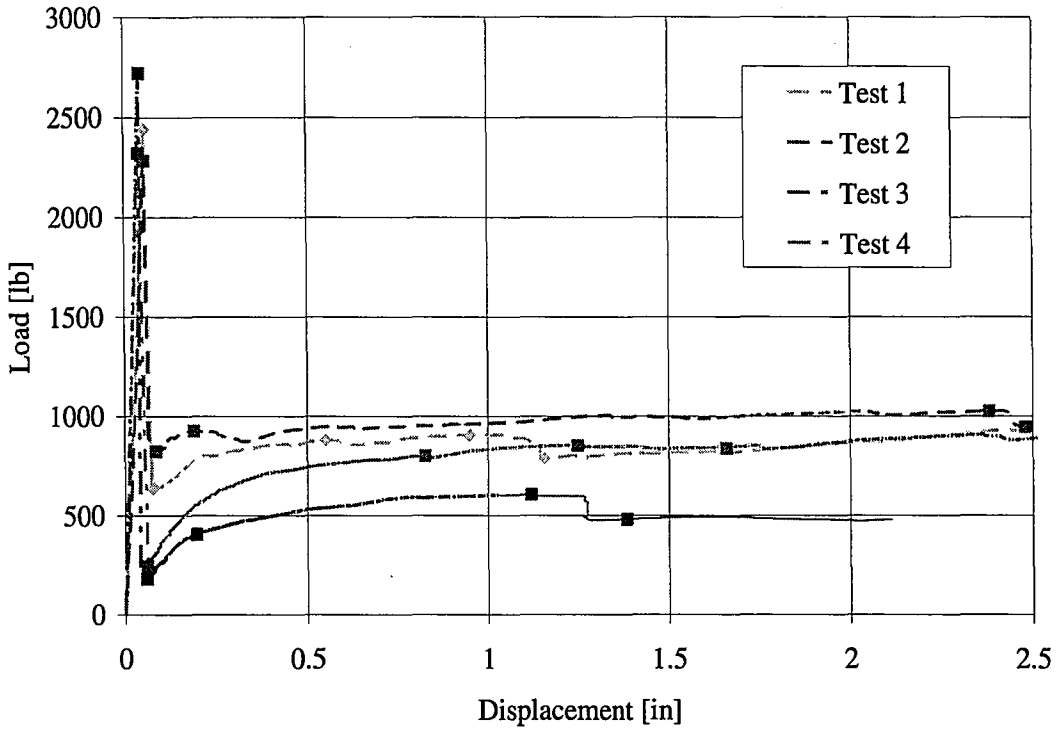


Figure 5-22: Loads and Displacements at which Strains were Evaluated

Figure 5-23 shows the strain along the length of the beam, measured from the center, at the different points of interest for Test 2. This is the typical behavior of the concrete beam specimens having a ¼ inch debonded region. The strain in the polyurea is very low at the peak load, when the concrete cracks. Table 5-9 shows the center strain gauge value for all tests at peak load. The values are large enough to conclude that it is not noise and that the polyurea is active at the point of maximum load. As can be seen, the polyurea is more active, at maximum load, for the systems that are fully bonded.

| Test ID | Center Strain at Peak Load |
|---|---|
| 1 | 510 |
| 2 | 708 |
| 3 | 212 |
| 4 | 314 |

Table 5-9: Center Strain Values at Peak Load

After cracking the center strain begins to increase throughout the test. The strain gauges away from the center do not increase until the end of the test, where only a slight increase is seen. This indicates that the polyurea in the gauged areas away from the center remain bonded throughout the length of the test. The increase in strain near the end of the test could be due a small amount of debonding near the center of the specimen, causing the strain to spread to a farther length. No constant strain value is seen between the applied strain gauges, so it can be concluded that the debonded length, during the time that the center strain gauge was active, is less than 2.75 inches, which is two times the distance to the closest gauge.

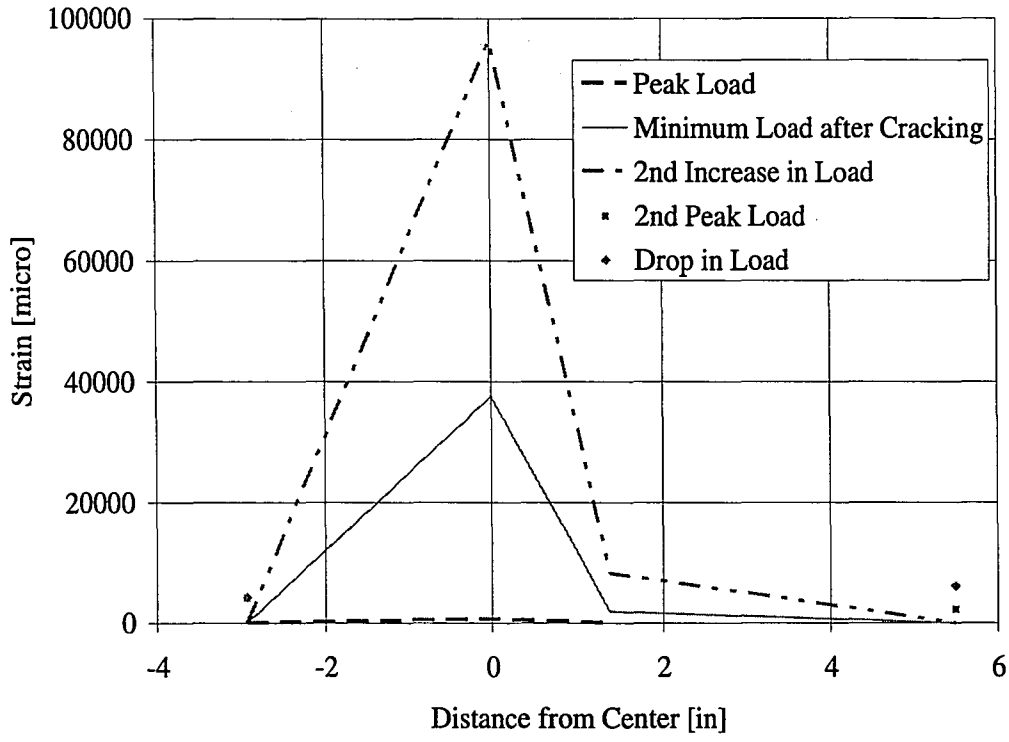


Figure 5-23: Strain along Beam for Loads of Test 2

The behavior of strain along the length of the beam for coated concrete specimens having an initial debonded polyurea length of 5.5 inches is apparently different as is seen in Figure 5-24. Again, the polyurea sees small strains at the peak load as shown in Table 5-9, but the polyurea is active. After cracking occurs, the center strain starts to rise as the load again begins to increase, but the value of strain at the center for a 5.5 inch debonded length is much lower than that of a specimen having a ¼ inch debonded length. It can also be seen that the polyurea away from the center becomes active much earlier and shares more of the overall strain. There is almost a constant strain value seen between the center gauge and the gauge located 1.375 inches from the center. One would expect that there would be a constant strain region here since both the center gauge and the gauge located at 1.375 inches from the center are located within the initial debonded region. However, the strain within the debonded

region is also influenced by the crack opening. As can be seen in Figure 5-25, as the crack opens the bottom edges of the crack bear into the polyurea, which would cause the polyurea within the crack opening to be under higher strain than the polyurea outside the crack opening, even if the polyurea outside of the crack opening is within the debonded region. Also, the debonded polyurea outside the crack opening is experiencing friction due to being pulled along the concrete surface. However, since the polyurea outside of the crack opening is still debonded, it will still see more strain than the fully bonded specimen at this same location, as is seen in Figure 5-23 and Figure 5-24. At the second peak load, there is a large increase in strain at a distance of 2.938 inches from the center for the specimens with a 5.5 inch debonded length. At this point the center gauge and the gauge located at 1.375 inches from the center have reached their capacity, but if these gauges were active it may have shown a larger constant strain region, indicating that the debonded region may have increased.

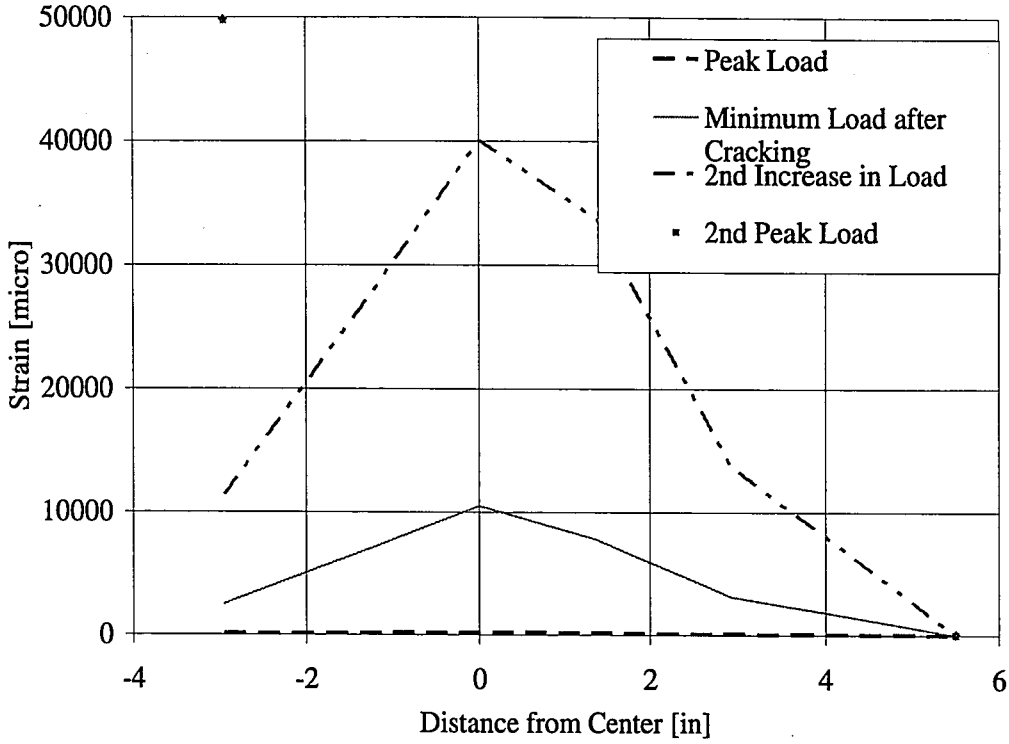


Figure 5-24: Strain along Beam for Loads of Test 3

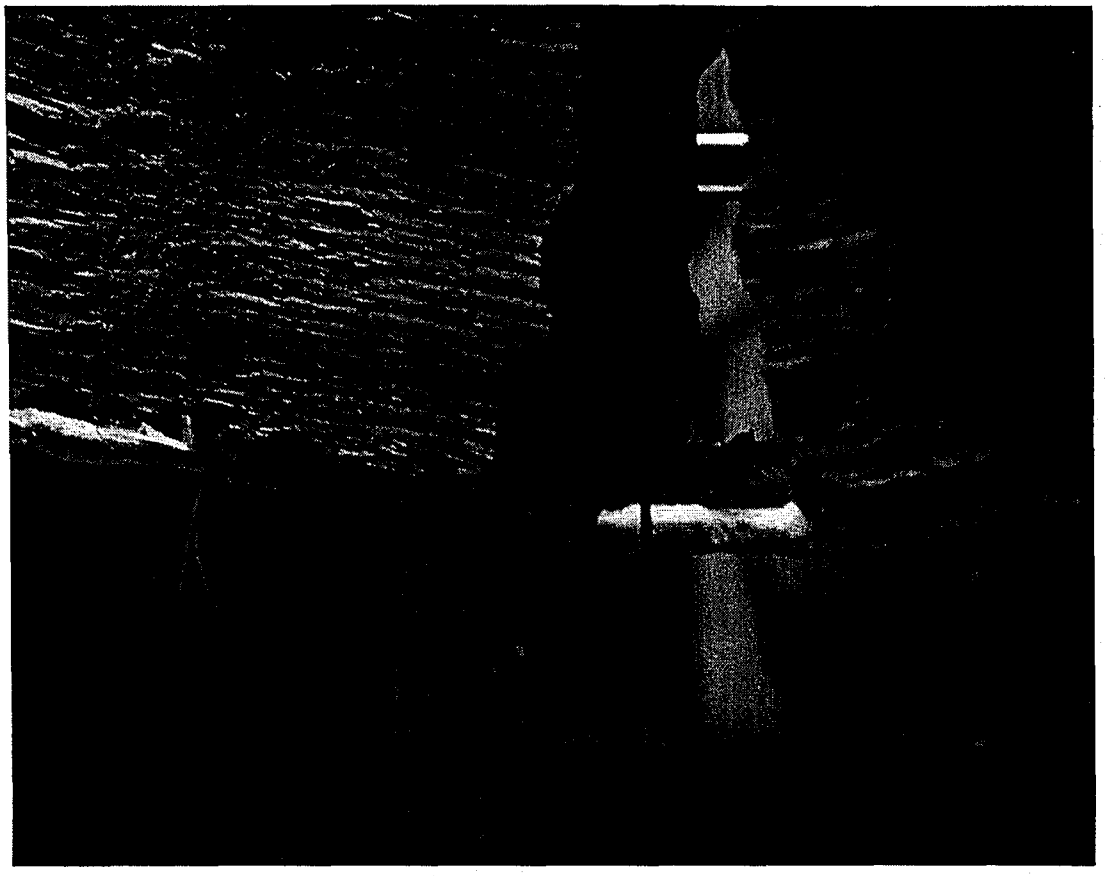

Figure 5-25: Bottom Crack Edge Bearing into Polyurea

A graph of the strains for Test 1 through Test 4, at the maximum loads of the individual tests, is shown in Figure 5-26. At this point, all center gauges are seeing strain, although small, within the polyurea. This again indicates that the polyurea is active at this point of testing. The differences in strains caused by the debonded length can be seen clearly. For Tests 1 and 2, the strain is concentrated at the center, whereas, for Tests 3 and 4 it is spread over a larger distance, decreasing the strain experienced by the polyurea at the center.

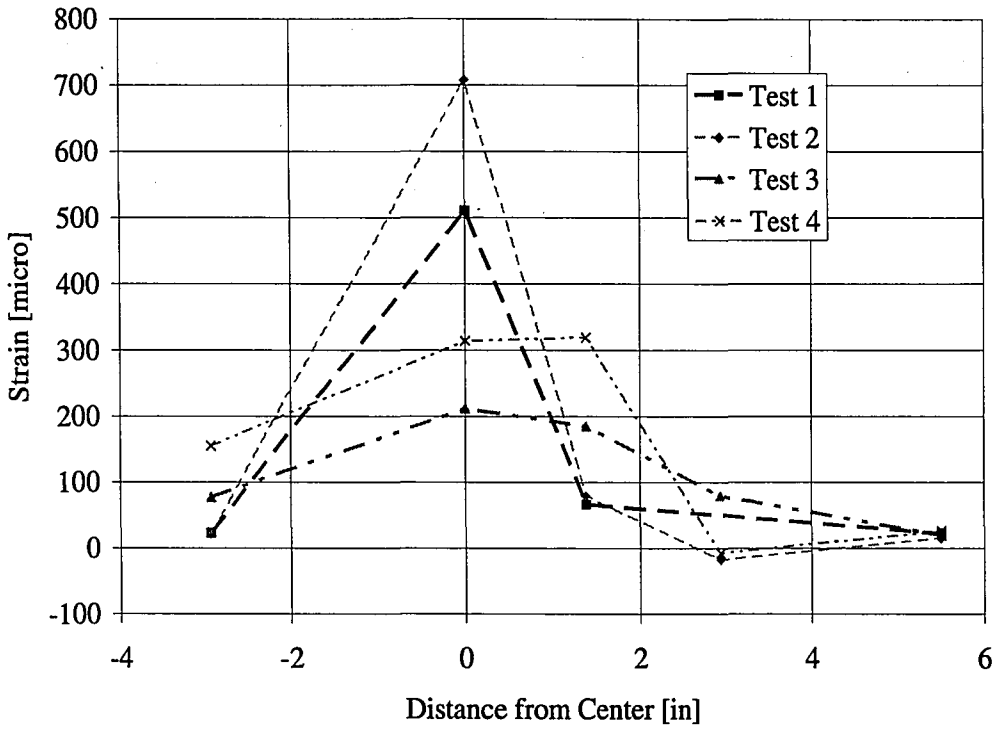


Figure 5-26: Strain along Beam at Max Load

After cracking occurs, when the minimum load is reached by the different systems, although all strains are increasing, the difference in center strain between the ¼ inch debonded specimens versus the 5.5 inch debonded specimens is growing. This can be seen in Figure 5-27. In addition, the difference in outer strain gauges is increasing, but for these gauges, the polyurea having 5.5 inch debonded regions is higher than the polyurea having ¼ inch debonded regions. This trend continues as the second maximum load is reached for all systems, as seen in Figure 5-28. At this point, the average of the outer most gauges of the specimens that are completely bonded are 99.7% less than the average of those having a 5.5 inch debonded region.

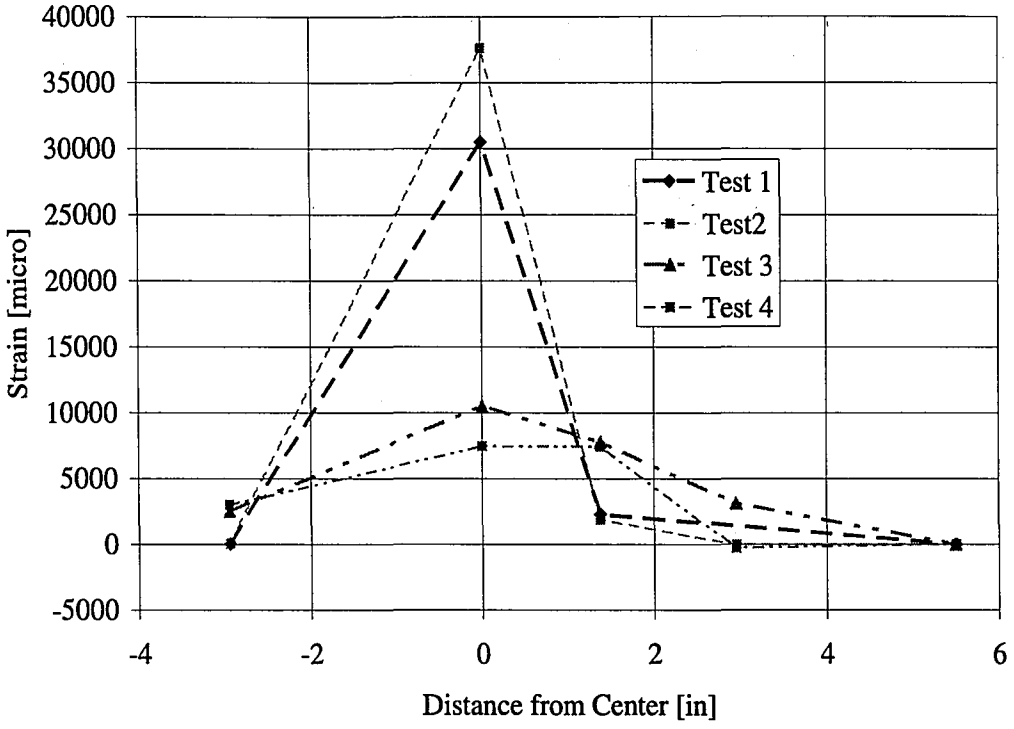


Figure 5-27: Strain along Beam at Minimum Load after Cracking

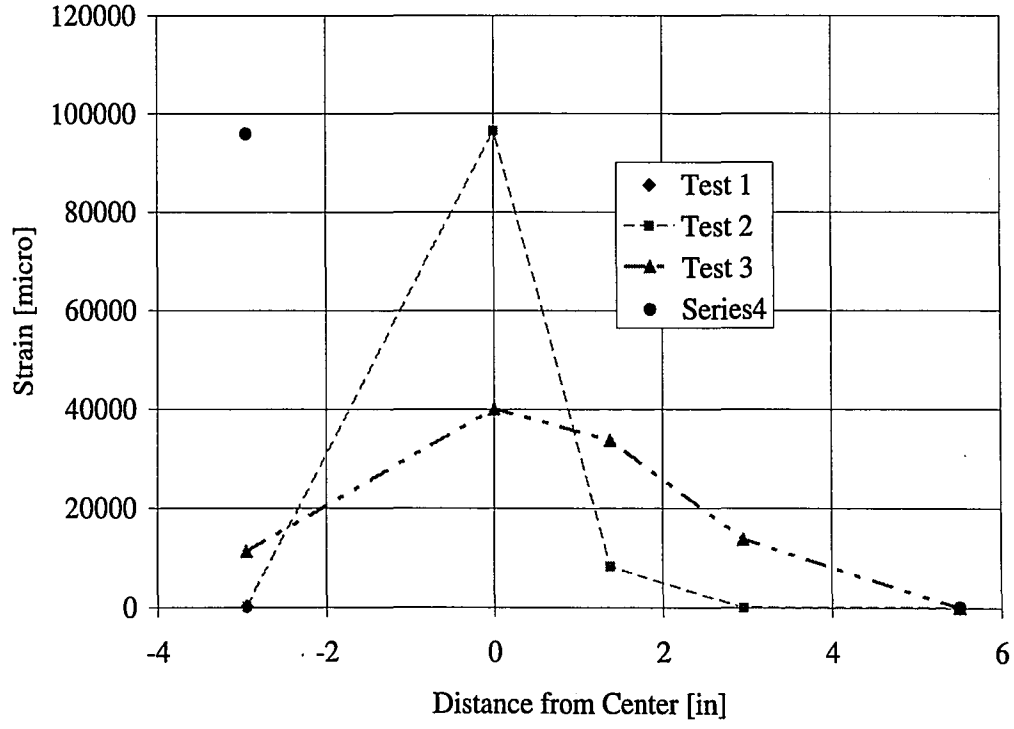


Figure 5-28: Strain along Beam at Second Peak Load

In addition to strain gauges, these tests recorded the crack opening of the systems. Using Equation 5-2 and the LVDT data, the rotation of the specimens could be calculated. This rotation was then used to calculate the strain in the polyurea at the center of the specimen by determining the length of the crack opening, or the change in length of the polyurea, and dividing this by the original debonded length. Using the calculated strain value, the stress was determined using the stress-strain relationship developed for Batch 4 polyurea in Chapter 2. The stress was multiplied by the cross-sectional area of polyurea to determine the tension force, which was then multiplied by the distance between the polyurea and the center of rotation, or the crack tip. This gives the moment. A moment was also determined from the strain gauge data. This was done for Test 1 and Test 2 and similar results were seen. The calculated moments from the LVDT data and the strain gauge data of Test 1 are compared in Figure 5-29 versus rotation. The values are compared for Test 2 in Figure 5-30.

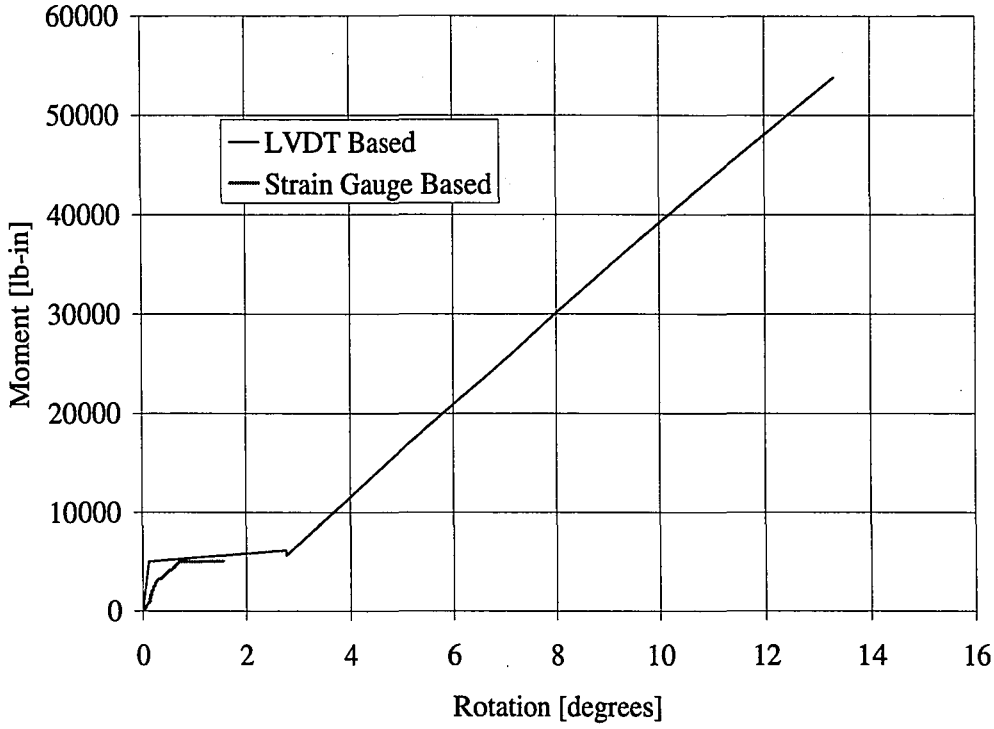


Figure 5-29: Moment versus Rotation for Test 1 with Original Debonded Length

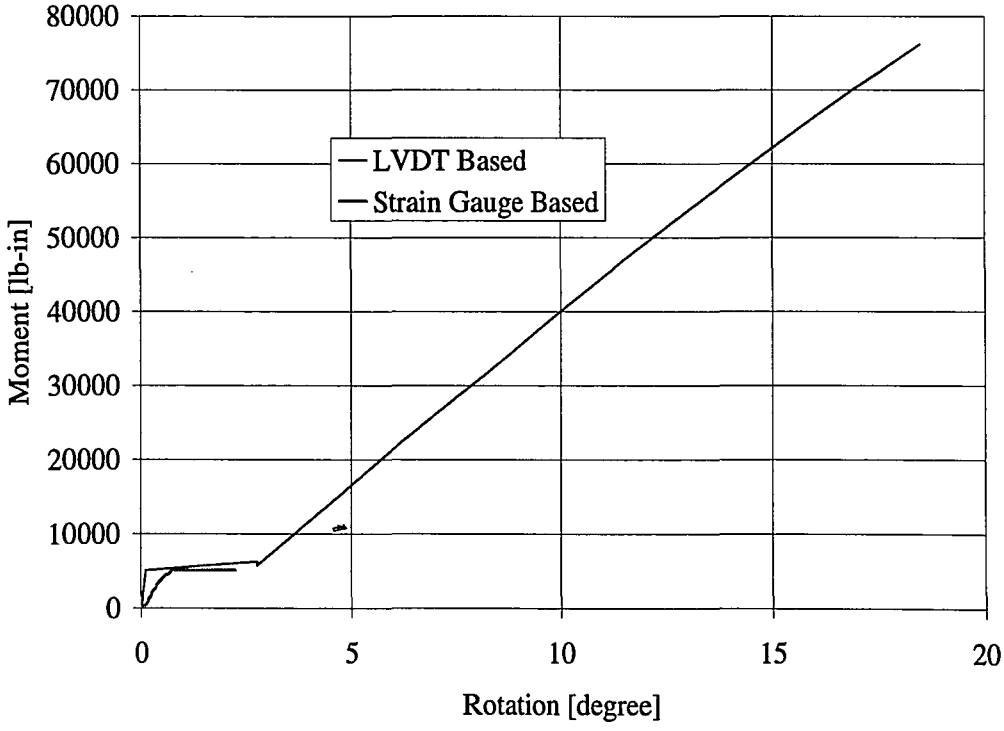


Figure 5-30: Moment versus Rotation for Test 2 with Original Debonded Length

Using a debonded length of ¼ inch for the calculation of strain from the LVDT data gives rise to moment values that are higher than the moment values produced by the strain gauge data. However, if a larger original debonded length is used in the calculation of strain, in this instance 1.8 inches, the calculated strain values align with the strain gauge values as seen in Figure 5-31. The same alignment was achieved for Test 2 using a debonded length of 2.2 inches as seen in Figure 5-32. If these debonded lengths are true, a constant strain was not seen in Figure 5-23, between strain gauges, because the closest gauge to the center was outside this debonded length. It was expected that the debonded length would change as the test progressed and not be a constant value, which may occur later on, after the center gauge was no longer in range. The gauge is lost early on in the testing of the beams. Looking at Figure 5-31, the gauge data and calculated strain seem to begin to diverge, meaning at this point the debonded length may be increasing.

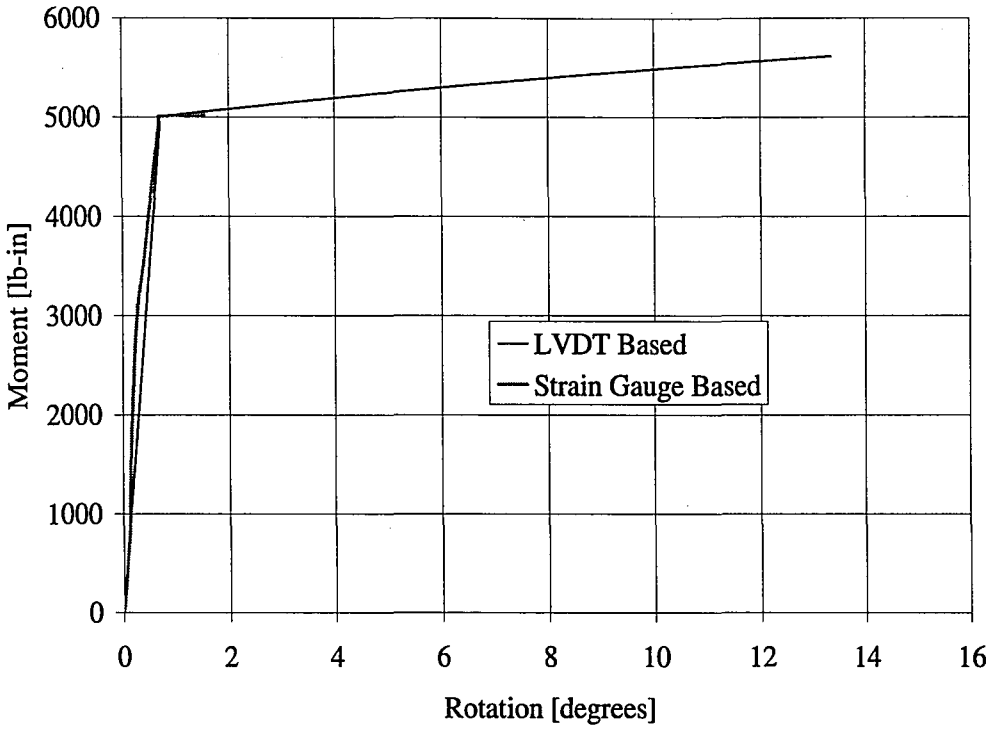


Figure 5-31: Moment versus Rotation with Increased Debonded Length for Test 1

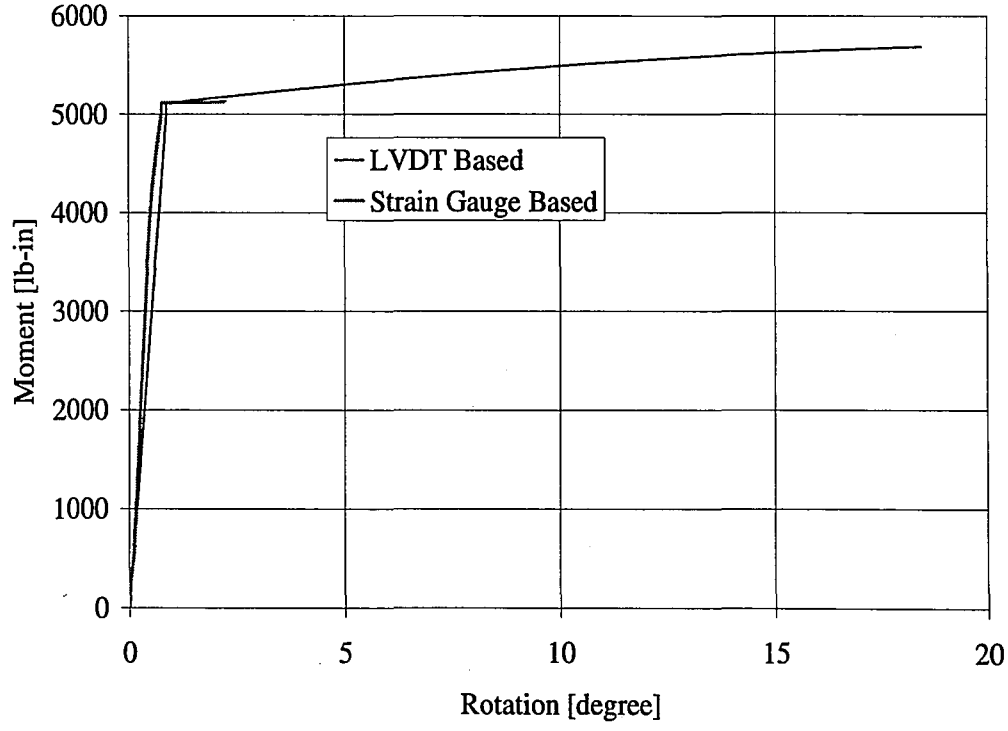


Figure 5-32: Moment versus Rotation with Increased Debonded Length for Test 2

A plot of the center strain gauge data and the calculated strain for Test 4 and Test 3, with a 5.5 inch original debonded length, is presented in Figure 5-33 and Figure 5-34. The calculated strain and the measured strain are much closer in value using the original debonded length in the calculation of strain than those seen in Figure 5-29 and Figure 5-30.

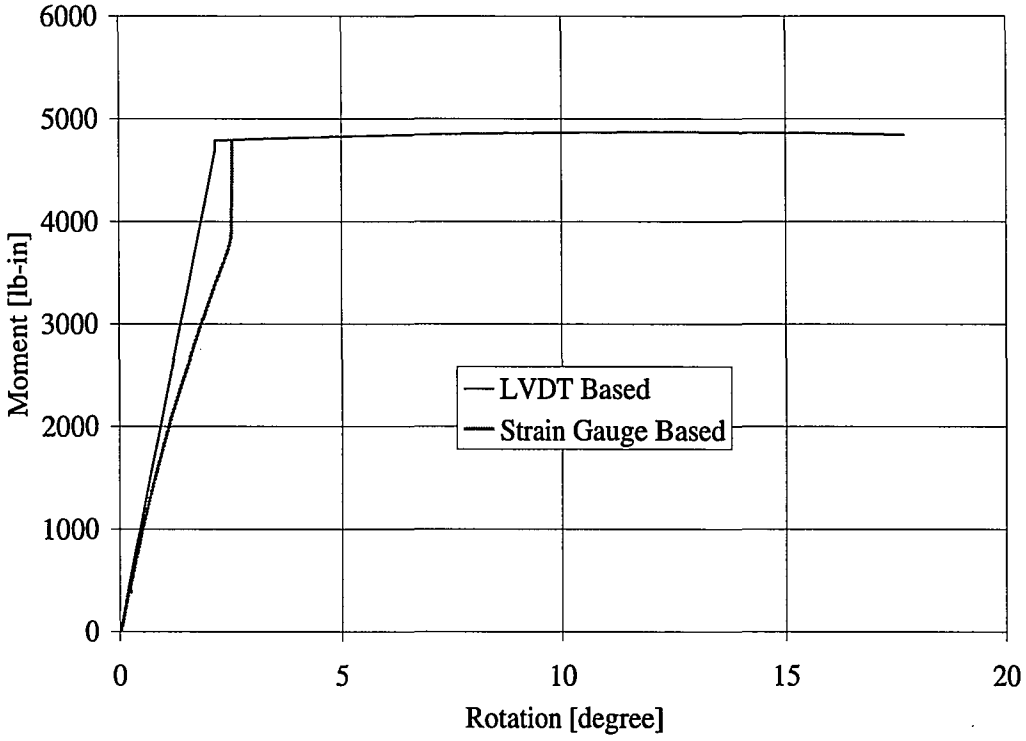


Figure 5-33: Moment versus Rotation for Test 4 with Original Debonded Length

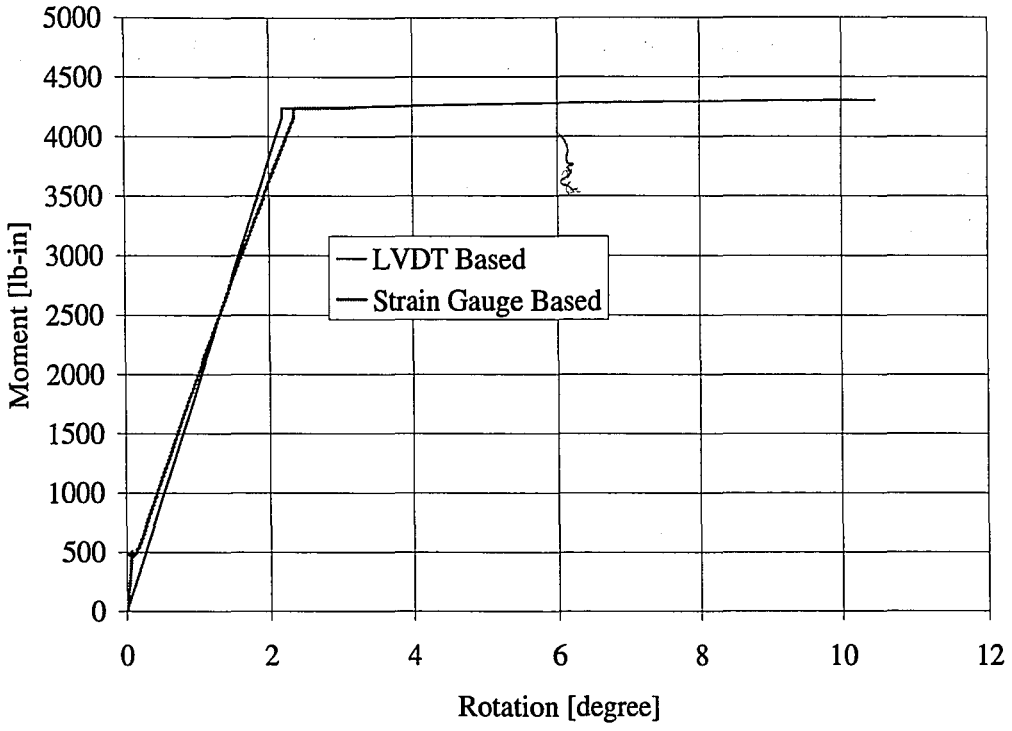


Figure 5-34: Moment versus Rotation for Test 3 with Original Debonded Length

However, changing the debonded lengths used in the calculations a few times during the loading phase of the test provides a better fit of the data sets as can be seen in Figure 5-35 and Figure 5-36. The debonded length is changed from 5.5 inches in the beginning to 6.5 inches by the end of Test 4. In Test 4, the debonded length changes from 5.5 inches to 5.8 inches. The larger increase in debonded length could be due to the fact that Test 3 started to fracture and relied on more of the polyurea length than a test that did not see any fracture of the polyurea, such as Test 4. The load and displacement values at which the debonded lengths are changed are highlighted in Figure 5-37. Figure 5-38 shows the center strain gauge profiles for the two different tests, and highlights the strain values at which point the debonded length was changed to match the strain gauge data and the rotation data. It seems that the debonded length changes when there is a change in the strain profile, except for the first change

in strain, which probably occurs at cracking and causes the strain to jump from almost zero immediately. However, the change in debonded length also occurs between changes in the strain profile as well. All of the strain values are below the initial yield strain for Polyurea Batch 4. The debonding trend is assumed to continue as testing continues.

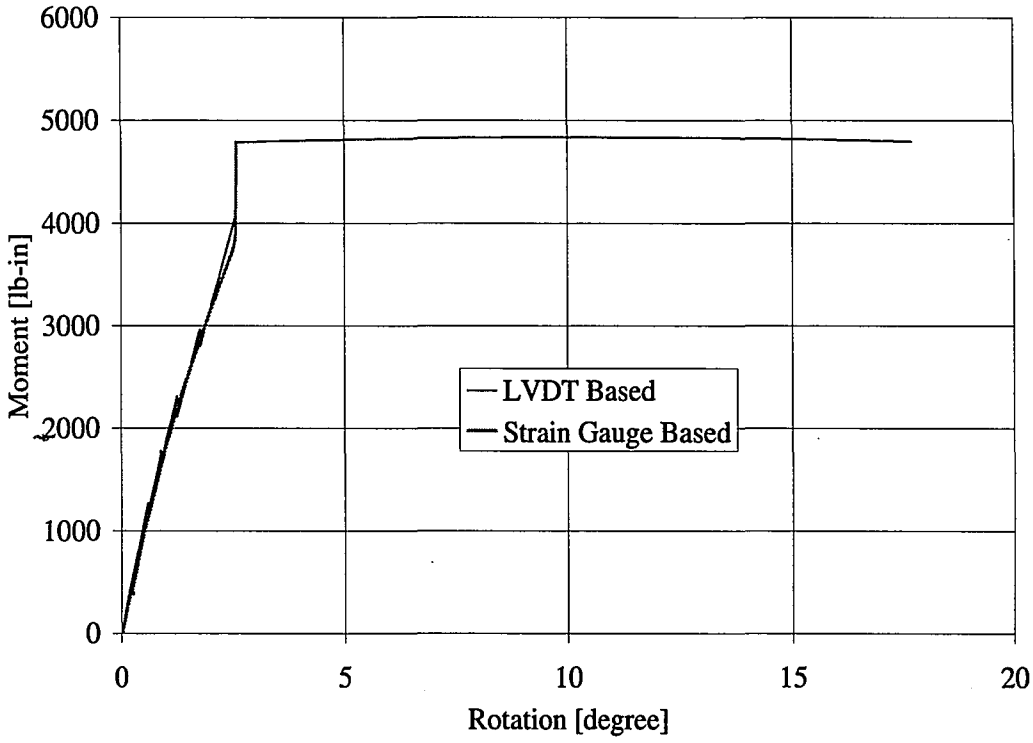


Figure 5-35: Load versus Center Strain with Different Debonded Lengths

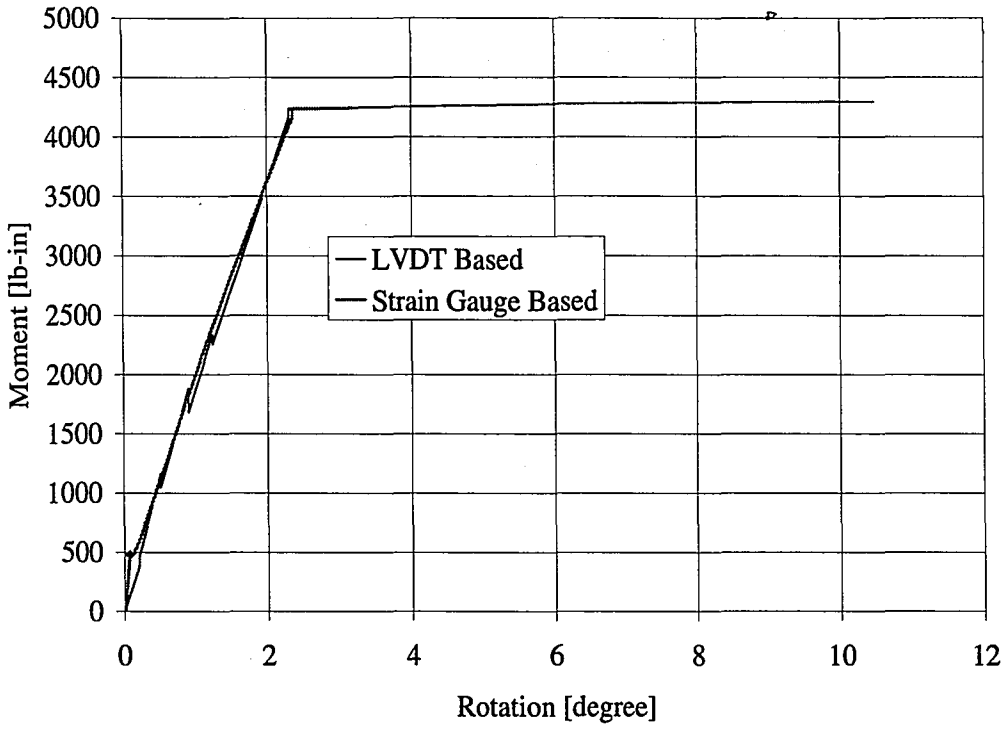


Figure 5-36: Moment versus Rotation for Test 3 with Increasing Debonded Length

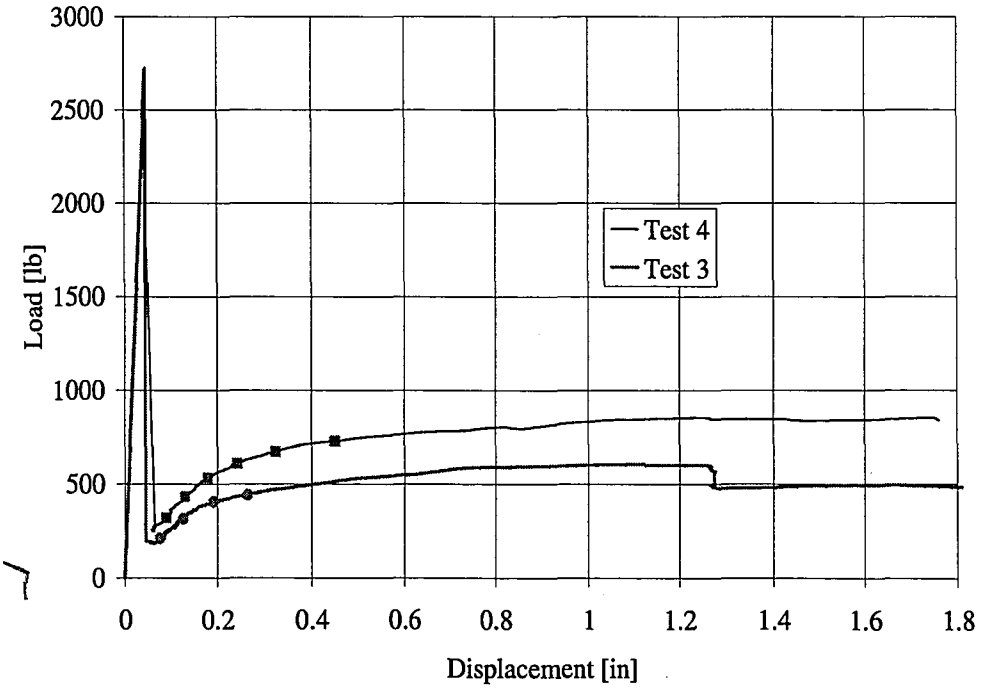


Figure 5-37: Loads at which Debonded Length Increased

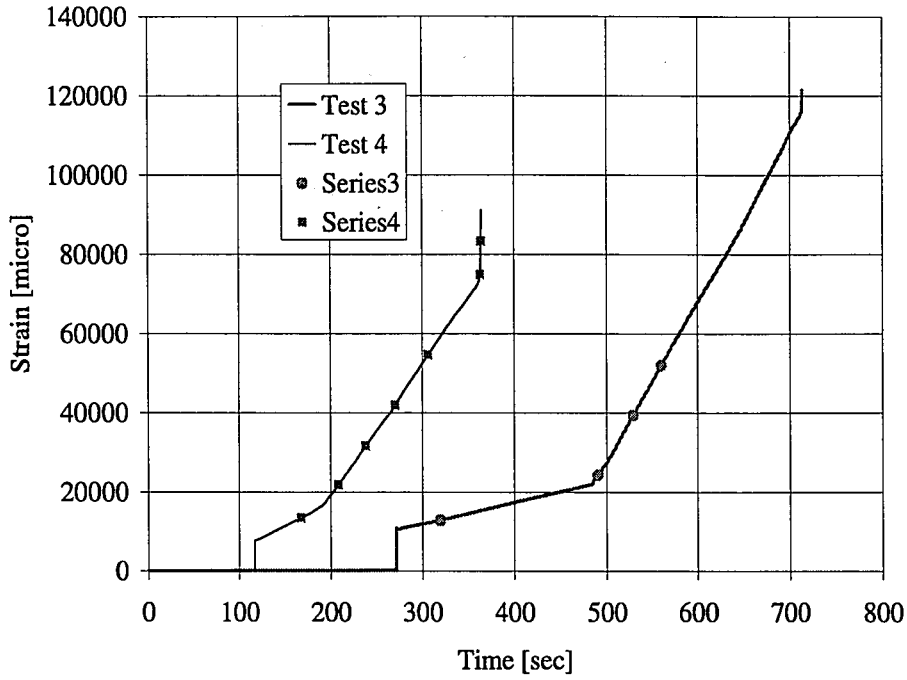


Figure 5-38: Center Strain Gauge Profiles and Point at Which Debonded Lengths Change

## 5.5 Conclusions about Static Concrete Beam Tests

Applying a polyurea coating to the underside of a concrete beam allows the system to continue displacing as well as to take more load after complete cracking of the concrete has occurred, with the crack tip becomes the center of rotation. The system is able to rebound after loading has been stopped, but permanent deformation to the polyurea is seen. The amount of permanent deformation to the polyurea increases as the initial debonded region of the polyurea increases.

The peak load at which the concrete cracks is slightly increased, by less than 10%, when the concrete beam is retrofitted with a polyurea coating. The modulus of rupture is also increased, by between 10 and 20%. The ability of the polyurea coated beam to absorb energy is significantly higher than a plain concrete beam. At cracking

of the concrete, a retrofitted beam has absorbed, on average, 275% more energy than that of a non retrofitted beam. At a displacement of 2.11 inches, which is before failure for most polyurea coated systems, the increase in absorbed energy is already 11550% larger than that of a plain concrete beam.

When a flaw in the polyurea is introduced, which creates a stress concentration; there is still an increase in peak load, modulus of rupture, and fracture energy. However, these increases are not as significant as other polyurea systems. Also, it allows the fracture of the polyurea to occur at static rates, which means it is occurring at a lower load and displacement than is typical since the other coated beams could not be brought to failure at static rates.

The length of the debonded region does play some role in the behavior of the polyurea. It was seen that increasing the debonded length causes a change in initial stiffness. After compression of the polyurea at the supports, which causes an added displacement, is accounted for, it can be shown that the initial stiffness is increased with a polyurea coating. A larger debonded length of polyurea results in lower polyurea strains at the center of the beam as compared to the strains at the center of the beam of a completely bonded system. This is achieved by activating a longer length of polyurea, which allows the strain to spread. Therefore, away from the center of the beam, the specimen with a 5.5 inch debonded length sees higher strains than a fully bonded beam does away from the center.

Aligning the calculated strain values, obtained using the crack opening data, with the strain gauge data for specimens with a 5.5 inch debonded region indicates that the initial debonded region grew over an inch in length at least. Aligning the calculated

strain values with the strain gauge data for the fully bonded specimens indicates that at least 0.875 inches on either side of the pre-crack is needed to ensure a full bond between concrete and polyurea, making the debonded length equal to 2 inches rather than only a ¼ inch.

With less of a debonded length, a good portion of polyurea remains almost entirely ineffective and inactive during the loading process of the retrofitted system and therefore, it is recommended that in order to utilize the full retrofit, that a larger initial debonded length is used, which is capable of maintaining similar increases in peak load, modulus of rupture, and fracture energy.

# 6 Dynamic Testing of Polyurea Coated Concrete Beams

## 6.1 General

This chapter describes the center-point loading dynamic tests that were conducted on polyurea coated concrete beams and plain concrete beams. The dynamic test series was conducted to determine the effect of strain rate on properties of the polyurea coated concrete beams, such as fracture energy and the bond strength. In this chapter, the results of polyurea coated concrete beams will be compared to the results from plain concrete beams tested at the same dynamic strain rates.

## 6.2 Test Matrix

The dynamic test series was carried out on beams of the same size used in the static testing of concrete beams, so that the results would be comparable. The concrete beams had a height of 6.5 inches, a width of 3.5 inches, and a length of 27 inches. They had a crack initiator at the center of the span that was ¼ inch wide and one inch high. Two concrete types were used. The first concrete, Type 1, is the same concrete used in static testing, having a compressive strength of 3,410 psi at the time when the beam tests were conducted. The second concrete, Type 2, was batched at a later time. Type 1 concrete was 4 months of age and Type 2 concrete was 1 month of age during the dynamic testing phase. The concrete was supplied by the same vendor and had the same maximum aggregate size of 3/8 inches. However, the concrete compressive strength of the Type 2 concrete is greater. The compressive strength is equal to 5,630 psi around the time the tests were completed. The lower strength in the first batch is due to a higher water/cement ratio as a result of water added prior to placement to achieve higher slump. During the second pour, no additional water was needed.

The polyurea coated beams were coated using the method described in Section 2.6.2. Since only three beams could be coated with polyurea at a time, different beams were coated with different polyurea batches that may have different mechanical properties. The average thickness of polyurea was measured and recorded for each specimen. In contrast to the static testing, only one initial debonded length was tested. All specimens that had a polyurea coating had an initial debonded length of a ¼ inch. This means that the polyurea was completely bonded except for the length that spanned the crack initiator at the center. The debonded length of a ¼ inch was chosen to ensure that failure of both the concrete and the polyurea would occur at a higher strain rate.

The beams were loaded in a drop hammer test fixture under various demands. A summary of the variables studied are presented in the test matrix of Table 6-1. Drop height, polyurea batch, the thickness of the polyurea, and concrete type for each specimen is detailed. In addition, the surface temperature of the polyurea was occasionally taken before testing in order to see if this factor would affect results.

| Test ID | Drop Height [in] | Polyurea Batch | Thickness [in] | Temp. [°F] | Concrete Type |
|---|---|---|---|---|---|
| 7 | 30 | 6 | 0.2542 | 73.2 | 1 |
| 8 | 30 | n.a. | n.a. | n.a. | 1 |
| 9 | 18 | 7 | 0.273 | not taken | 2 |
| 10 | 6 | 7 | 0.247 | not taken | 2 |
| 11 | 6 | 6 | 0.247 | not taken | 1 |
| 12 | 6 | 7 | 0.251 | 76.7 | 2 |
| 13 | 6 | 8 | 0.338 | not taken | 2 |
| 14 | 6 | 8 | 0.223 | 75.2 | 2 |
| 15 | 6 | n.a. | n.a. | n.a. | 1 |
| 16 | 6 | n.a. | n.a. | n.a. | 2 |
| 17 | 6 | n.a. | n.a. | n.a. | 2 |
| 18 | 6 | n.a. | n.a. | n.a. | 2 |
| 19 | 4 | 6 | 0.271 | not taken | 1 |
| 20 | 4 | 5 | 0.255 | 80.4 | 1 |
| 21 | 4 | n.a. | n.a. | n.a. | 1 |
| 22 | 4 | n.a. | n.a. | n.a. | 2 |
| 23 | 4 | n.a. | n.a. | n.a. | 1 |

Table 6-1: Test Matrix for Dynamic Series

## 6.3 Testing

The dynamic testing also used center-point loading and followed ASTM C293 to the extent of specimen size and the location and direction of supports and loading head. The testing set-up was similar to that of the static test set-up shown in Figure 5-3. The similarities act as controls between the two experimental modes and allow for comparisons of the results. The same support conditions and loading head that were used for static testing were used for the dynamic tests, as seen in Figure 6-1. The distance between supports had to be changed to 22 inches rather than 20 inches due to the testing equipment, which resulted in a hangover length of 2.5 inches beyond the

support. Also seen in Figure 6-1, the specimens were securely fastened with brass rods to the supports so as to minimize any vibrations between the beam and support that may skew the results. Brass rods were used because of their flexible nature, which would bend with the beam and not hinder its rotational capability. The rollers were also held in place by springs in order to counteract the wedging action that caused them to slide during static testing.

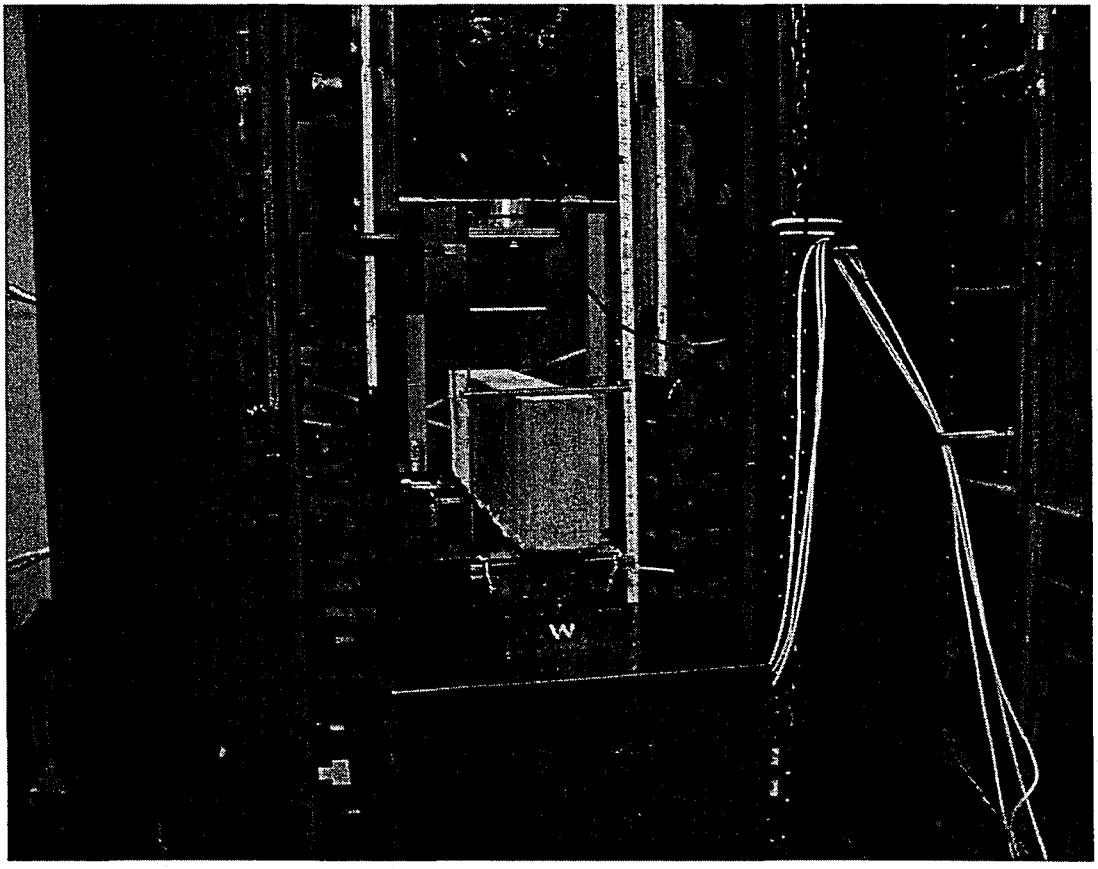


Figure 6-1: Beam in Place for Dynamic Testing

### 6.3.1 Instrumentation

As was stated in Section 5.3.2, the static test results provided confidence in the fact that the LVDTs and string pot equipment were not needed to measure rotation and displacement. With the laser sensors in place at midspan and close to the support,

they were capable of accurately capturing the motion of the beam. For the dynamic tests two lasers were used. One laser was located at midspan, or 11 inches from the support. The other laser was used to calculate rotation, and was located 5 inches from one support. Under impact loading, the behavior is assumed to be symmetric, and therefore, only one laser was used. A schematic of the location of the laser signals on the beam can be seen in Figure 6-2 and the photograph of Figure 6-6 shows the laser signal on the bottom of the beam.

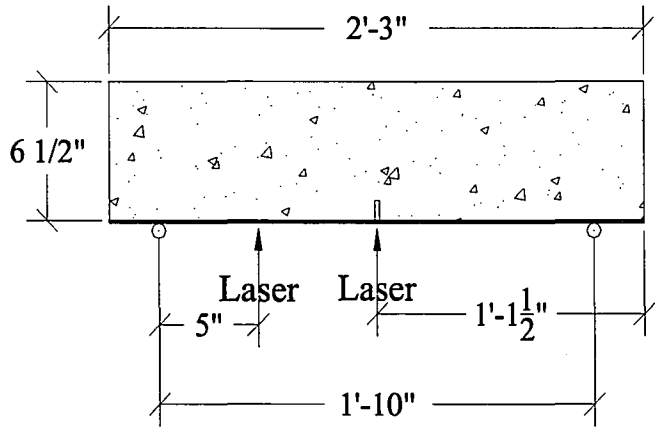


Figure 6-2: Laser Locations

Four strain gauges were located along the length of the beam. A similar strain gauge pattern to that used for the static tests was used. Figure 6-3 shows the gauge locations for the majority of the tests. Test 12 and Test 13 moved the center strain gauge 1 inch away from the center in hopes of picking up more of the strain behavior before the gauge is lost, this strain gauge pattern is seen in Figure 6-4. Test 14 had a different gauge pattern than any of the other tests. The gauges were located ½ inch, 1 inch, 2 inches, and 5.5 inches from the center of the beam as shown in Figure 6-5. This was one of the final tests conducted and the polyurea area of interest was near the center,

where most of the strain occurred, therefore the gauges were moved closer and clustered together.

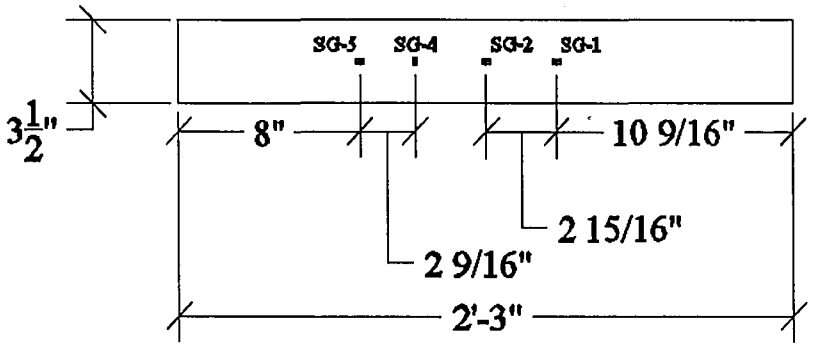


Figure 6-3: Typical Strain Gauge Layout for Dynamic Testing

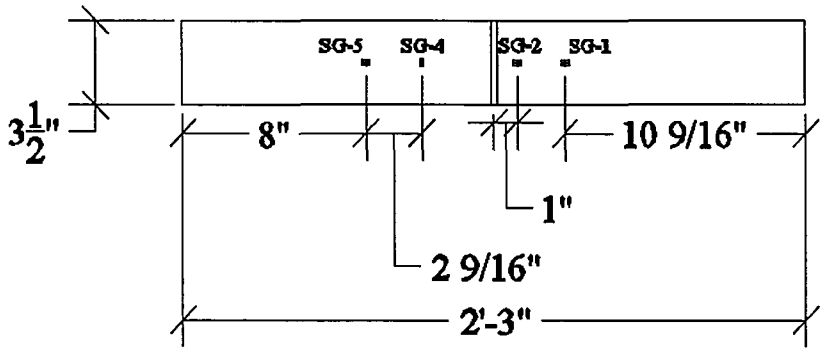


Figure 6-4: Strain Gauge Layout for Tests 12 and 13

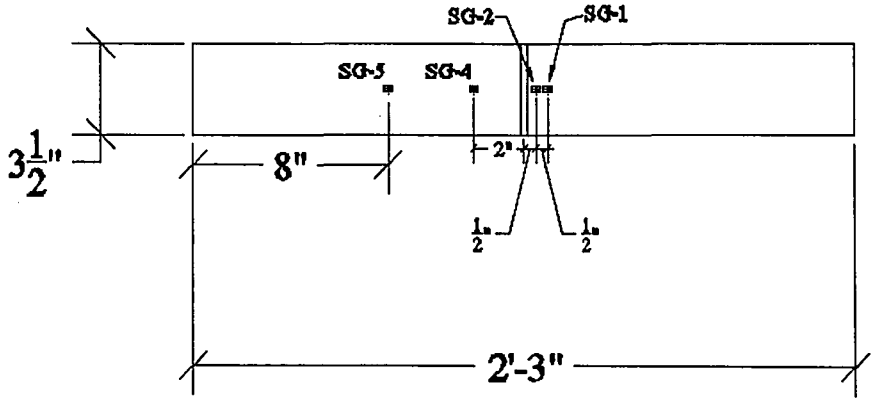


Figure 6-5: Strain Gauge Layout for Test 14

In addition to the laser sensors and the strain gauges, accelerometers were used to quantify the energy of the tup or loading head and the energy of the beam once in motion. One accelerometer was located at the center axes of the loading head. Another was attached 1.5 inches away from the center of the beam using a stiff steel angle bonded to the concrete beam. The attached accelerometer can be seen in Figure 6-6. The distance was chosen based on the fact that it was close enough to the center to be able to extrapolate the acceleration data to the midspan, but would not interfere with the crack opening and rotation of the beam.

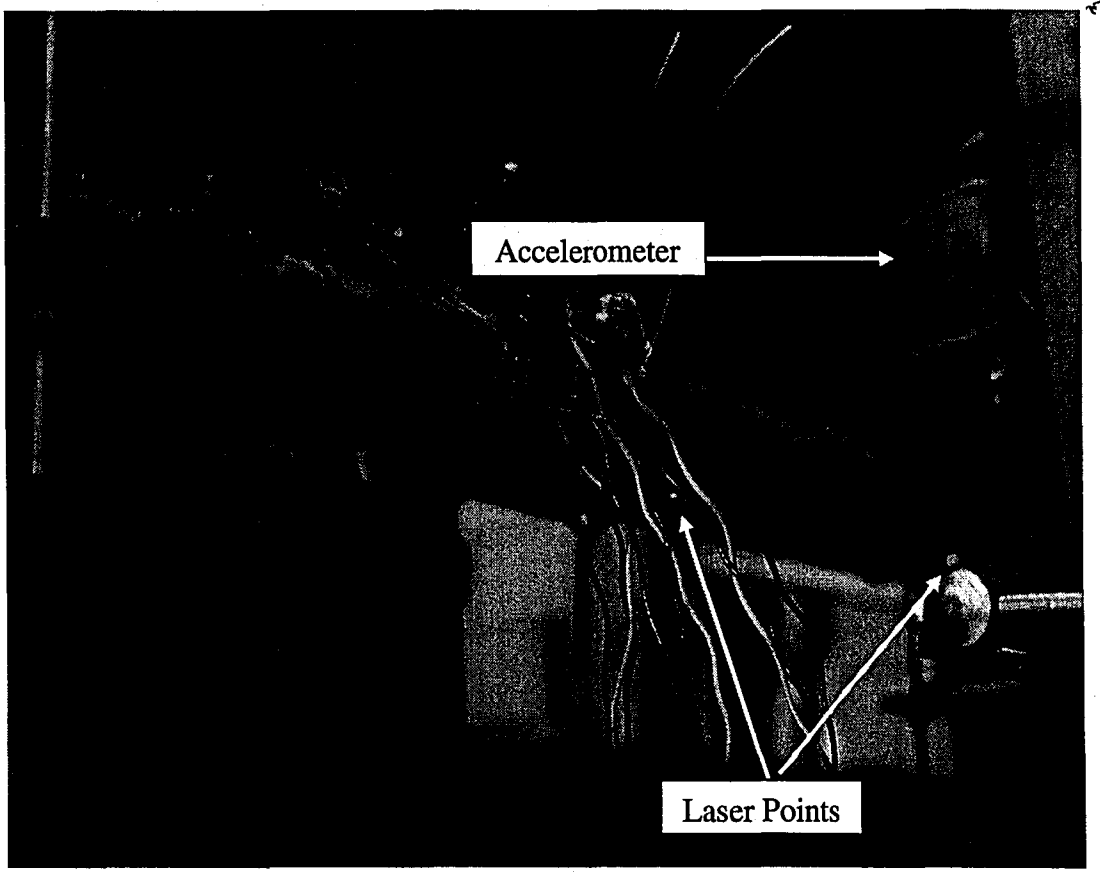


Figure 6-6: Instrumentation for Drop Weight Tests

### 6.3.2 Test Procedure

The dynamic test series was conducted in a drop weight machine, which is shown in Figure 6-7.

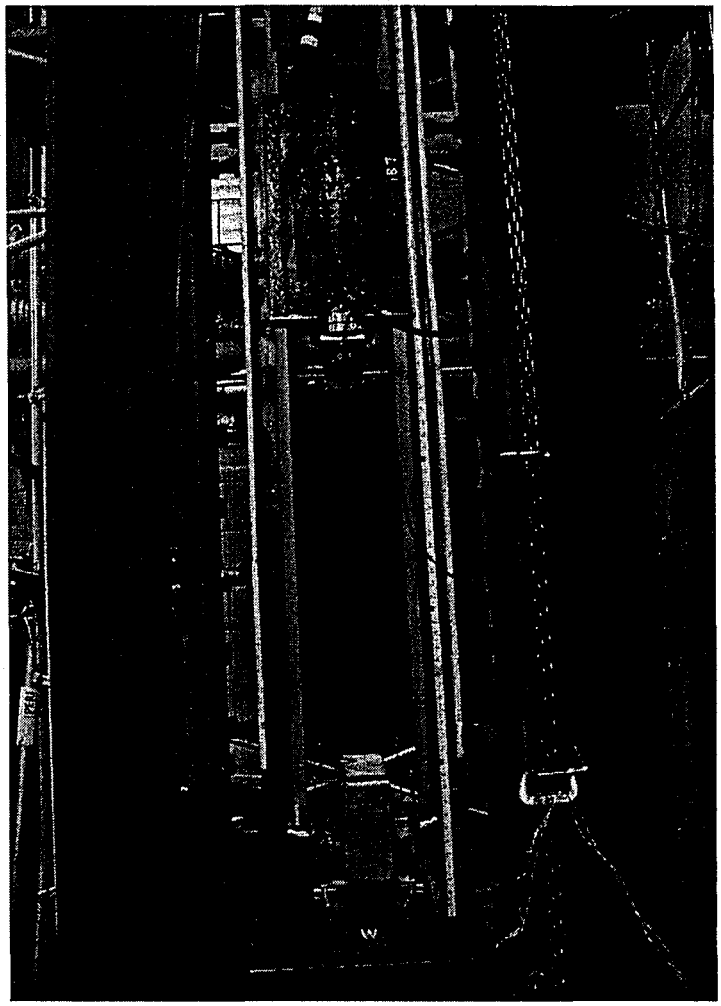

Figure 6-7: Drop Weight Machine

The drop hammer consists of a weighted loading head and low friction rail guide system. The hammer has a drop height capacity of 25 feet. The specimen is placed on large steel supports centered between the rails. The tup or impact head for the dynamic test was threaded into the drop weight. The two components made for a total of 206.55 lbs. After the beam was instrumented and installed, the bottom of the

tup was raised to the desired height above the top of the specimen. An increase in drop height allowed for different increasing strain rates to be achieved. Once the desired height was established the data recorder was initiated, recording data at a rate of 5 kHz. The weight was then released. The release of the weight caused it to travel downward toward the specimen, along the rails, under the force of gravity. The rails are coated with Teflon; therefore only minimal friction is introduced during the drop. After contact was achieved between the loading head and beam, the test was ended when the system stopped its movement. For more information on the exact design and procedure of the drop weight machine, as well as detailed information on the implementation of instrumentation, please refer to the Master's Thesis of Kenneth O'Kelly Lynch titled "Development of an Experimental Technique for Tensile Testing of a Material at High Strain Rate with Application to Polyurea" on file at Lehigh University.

### 6.3.3 Expected Results

As was seen in the static rate testing, the majority of the behavior within the polyurea took place after the concrete had cracked through completely. This will be even more prominent in the dynamic tests, since the cracking of the concrete occurs almost instantaneously with contact from the drop weight. Therefore, to predict the behavior of the system, a rotational hinge model was used that would put the polyurea in pure tension across the crack opening, as seen in Figure 6-8.

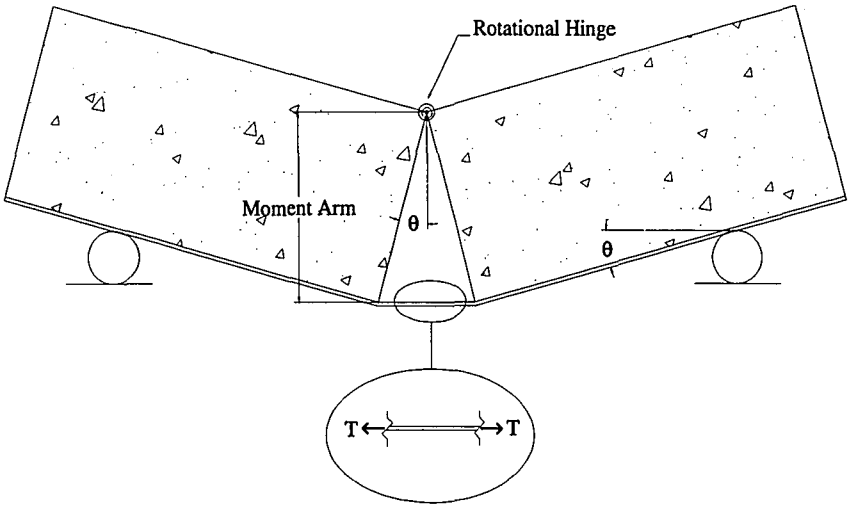


Figure 6-8: Hinge Model

For a given rotation of the beam, the length of the crack opening can be calculated using Equation 6-1, derived from the geometry of the system.

$$\text{Opening} = 2(6.5 * \sin(\theta))$$

Equation 6-1: Crack Opening [in]

Using this opening and the original debonded length (which was determined to be closer to 2 inches for the fully bonded specimens according to the results of Section 5.4.2.2) the strain in the polyurea can be calculated as the crack opening divided by the debonded length. The following debonded lengths were used in the calculations in order to construct an envelope or the actual data: ¼ inch, 1.5 inches, 2 inches, and 4 inches. The next step in the modeling process would be to determine the stress in the polyurea. Since the testing will be done at dynamic rates, the stress was determined from the dynamic stress-strain profile of Chapter 2. The stress can then

be multiplied by the average polyurea cross-section of 0.917 $in^2$ to get the tension force. The displacement of the system can be calculated using Equation 6-2.

$$\Delta = 10\tan(\theta) - \frac{(10\tan(\theta))(6.5\sin(\theta))}{10}$$

where:

$\Delta$ = displacement of system

Equation 6-2: Beam Displacement from Rotation [in.]

Once cracking has occurred the systems only form of resistance comes from the tension capacity of the polyurea, therefore the internal energy of the system, at any point, can be quantified as the area beneath the tension force versus displacement diagram at that specific displacement. The tension force versus displacement plot is presented in Figure 6-9 for all aforementioned debonded lengths. As expected a greater amount of debonded length allows for greater amount of deformation.

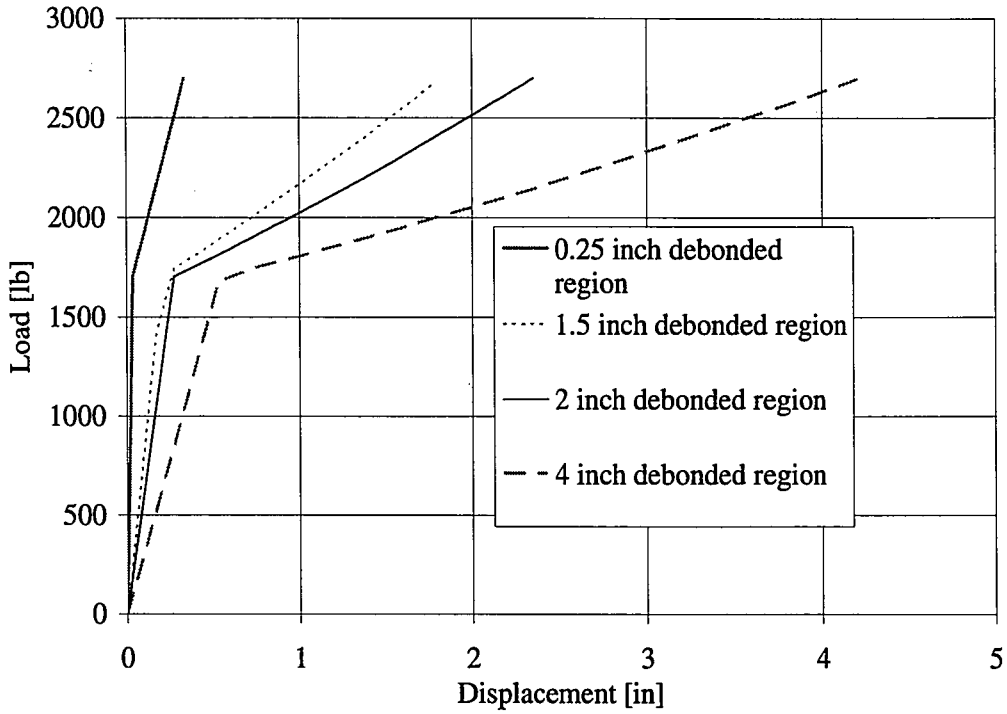


Figure 6-9: Load Deflection Curve for Rotational Model

Using the principles of conservation of momentum and conservation of energy, a drop height can be determined for a given displacement under the assumption that once contact is made between the tup and beam, they move together as one item. The diagrams of Figure 6-10 show the process of determining the drop height.

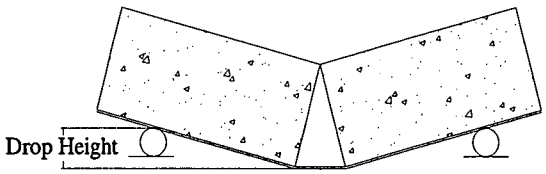


4. Final State of Beam

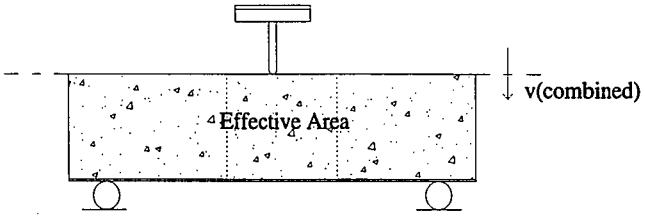


3. Tup in Contact With Beam

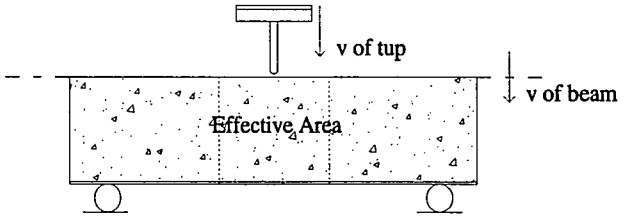


2. Tup Right Before Contact With Beam

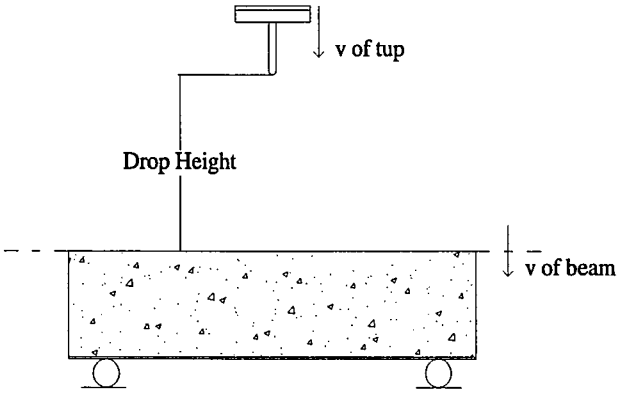


1. Tup at Initial Drop Height

Figure 6-10: Energy States

Starting with a given displacement, the internal energy of system 4 is determined as the area underneath the tension force versus displacement diagram, as stated previously. Since the system is no longer moving, the kinetic energy of system 4 is zero. However, there is still potential energy. Therefore the potential energy is set equal to the internal energy of the system. Using the conservation of energy between system 4 and system 3, which has no potential energy, but has kinetic energy with a combined mass equal to that of $\frac{1}{2}(m_{total})*(v_{(combined)})^2$, the combined velocity can be solved for. The assumption is made that the tup and beam stick together on impact and no restitution occurs in the tup. Furthermore only the inertial mass of the beam is used toward $m_{total}$, which is equal to 1/3 of the total mass of the beam. The conservation of momentum is used between system 3 and system 2 to solve for the velocity of the tup right before contact, since for system 2, the beam has no velocity, only the tup. The final step is to use the conservation of energy between system 2 and system 1, which only has potential energy equal to that of the $m_{tup}*g*$drop height, to solve for the drop height. Repeating this process for different rotations and displacements of the beam, allows for the construction of a drop height versus displacement plot of Figure 6-11 for the different debonded lengths.

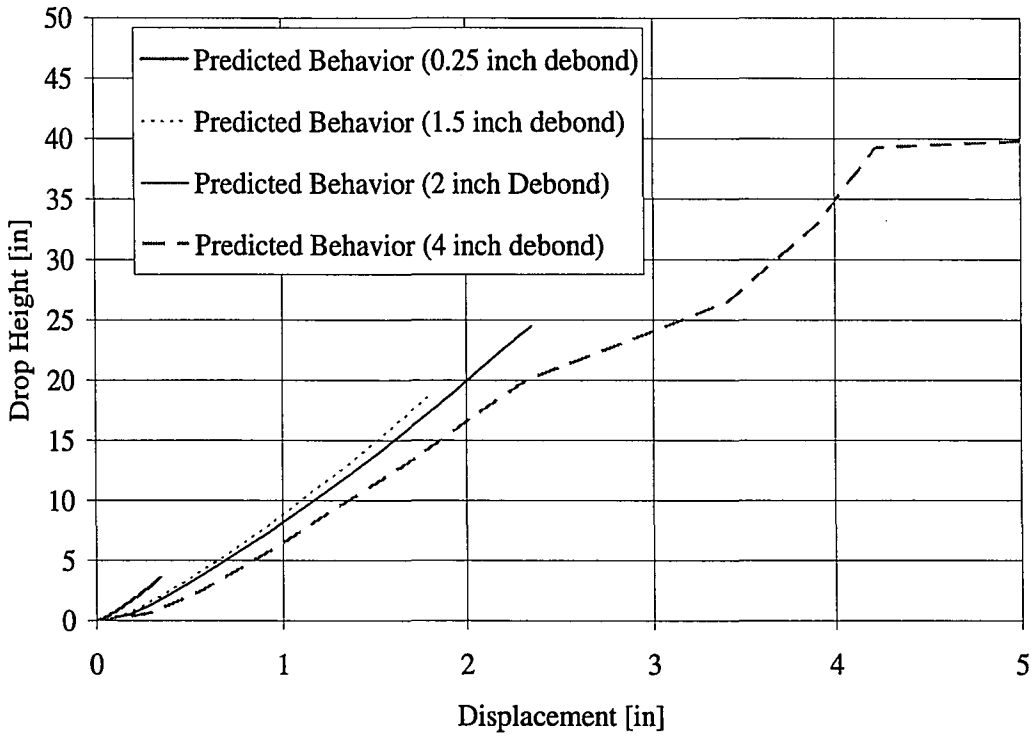


Figure 6-11: Predicted Drop Height versus Maximum Displacement

## 6.4 Results

The response of the polyurea coated beams was dependent on the drop-height of the weight and tup, as well as the presence of any discontinuities in the polyurea, through the thickness. The pre-crack in the concrete would instantly rise to the full height of the section once the drop weight came in contact with the beam for all tests. The tip of the fracture would become the center of rotation for the system. If the drop height was less than 6 inches above the coated specimen and there were no discontinuities in the coating, then the crack width increased, the beam deflected downward, and then rebounded. There were no full fractures of the polyurea. However, if there was a discontinuity within the thickness of the polyurea or if the drop height was set at 18 inches or 30 inches, cracking of the concrete occurred and the crack width increased

the system as the system deflected downward followed by fracture of the polyurea.

Table 6-2 summarizes the damage to the polyurea observed at the end of each test.

| Test ID | Drop Height [in] | Polyurea Batch | Thickness [in] | Temp. [°F] | Concrete Type | Date Tested | End of Test |
|---|---|---|---|---|---|---|---|
| 7 | 30 | 6 | 0.2542 | 73.2 | 1 | 4/18/2007 | Fracture |
| 8 | 30 | n.a. | n.a. | n.a. | 1 | 4/16/2007 | Fracture |
| 9 | 18 | 7 | 0.273 | not taken | 2 | 4/20/2007 | Fracture |
| 10 | 6 | 7 | 0.247 | not taken | 2 | 4/24/2007 | No Fracture |
| 11 | 6 | 6 | 0.247 | not taken | 1 | 4/19/2007 | Partial Fracture |
| 12 | 6 | 7 | 0.251 | 76.7 | 2 | 4/25/2007 | Fracture |
| 13 | 6 | 8 | 0.338 | not taken | 2 | 4/25/2007 | No Fracture |
| 14 | 6 | 8 | 0.223 | 75.2 | 2 | 4/25/2007 | No Fracture |
| 15 | 6 | n.a. | n.a. | n.a. | 1 | 4/19/2007 | Fracture |
| 16 | 6 | n.a. | n.a. | n.a. | 2 | 4/24/2007 | Fracture |
| 17 | 6 | n.a. | n.a. | n.a. | 2 | 4/25/2007 | Fracture |
| 18 | 6 | n.a. | n.a. | n.a. | 2 | 4/25/2007 | Fracture |
| 19 | 4 | 6 | 0.271 | not taken | 1 | 4/20/2007 | Partial Fracture |
| 20 | 4 | 5 | 0.255 | 80.4 | 1 | 4/24/2007 | No Fracture |
| 21 | 4 | n.a. | n.a. | n.a. | 1 | 4/20/2007 | Fracture |
| 22 | 4 | n.a. | n.a. | n.a. | 2 | 4/24/2007 | Fracture |
| 23 | 4 | n.a. | n.a. | n.a. | 1 | 4/25/2007 | Fracture |

Table 6-2: Summary of Dynamic Testing Outcomes

Using the maximum displacement of each test recorded by the laser located at midspan of the specimen, a plot of the actual drop height versus maximum displacement can be compared to the expected result plots of Section 6.3.3 as presented in Figure 6-12. The maximum displacement represents the peak midspan deformation achieved. Aside from the 30 in. drop height the maximum displacements were not used for specimens where fracture occurred.

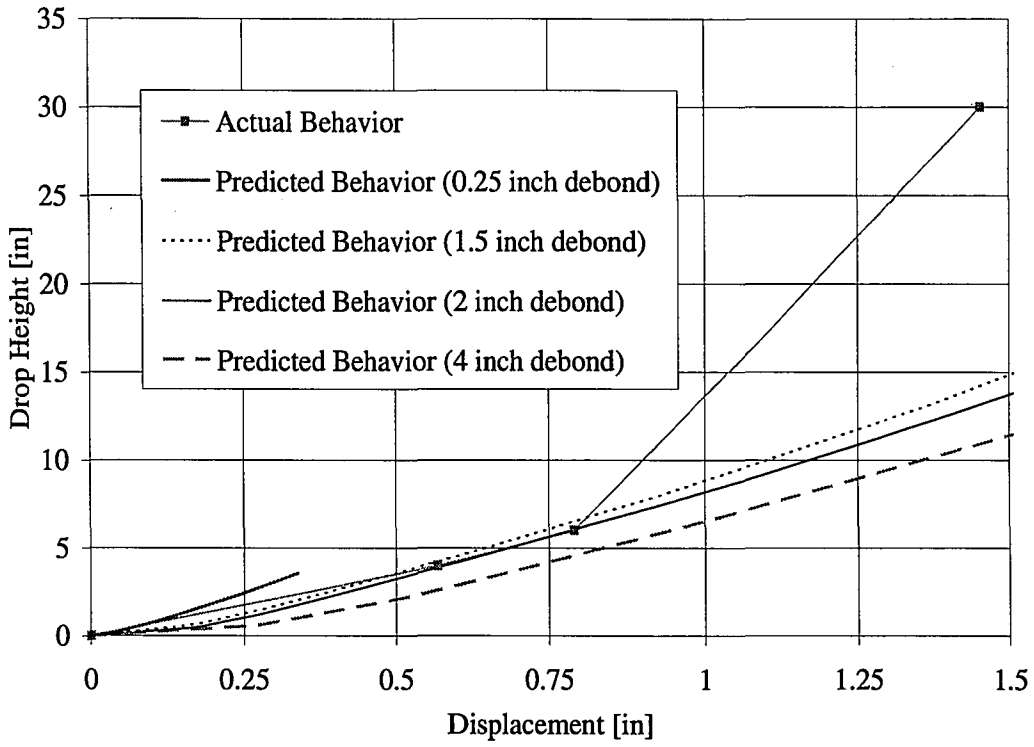


Figure 6-12: Actual Results of Drop Height versus Maximum Displacement compared to Expected Results

As can be seen from this figure, the actual drop height versus displacement curve, which is the result of a fully bonded specimen, is bounded by the debonded lengths of ¼ inch and 2 inches. The four inch and six inch drop height and displacement pairs are located almost exactly on the predicted behavior curve for a 2 inch debonded region. After this drop height however, the behavior is no longer bound by any of the predicted behavior curves. The predicted behavior is plotted until failure of the polyurea occurs using the material properties of polyurea tested at a strain rate of 250 1/sec. The 30 inch drop height may have exposed the polyurea to a higher strain rate, which would make the polyurea stiffer, and therefore the prediction using a slower strain rate would result in more displacement than the actual behavior.

### 6.4.1 Energies into the System

The loading phase is given by tup acceleration and the reaction of the system is defined by the beam acceleration. The plot of either tup or beam acceleration versus time should be similar for tests having the same drop height. The plot of Figure 6-13, which presents tup acceleration data from both a coated specimen and an uncoated specimen tested at a 30 inch drop height, shows the typical behavior of the tup acceleration for all tests. It would be expected that when the tup comes in contact with the specimen, a rapid deceleration is seen (which for the tup, would be a positive or upward movement of the acceleration), then as the beam begins to displace, the system begins to accelerate negatively if the tup and beam stay in contact with each other. Before cracking, the concrete would stiffen, again causing deceleration of the system (or positive slope of acceleration data). Once cracking occurs, there should be a high negative peak in acceleration. At this point, the behavior of a coated and uncoated specimen should deviate. The uncoated specimen, which has cracked, has reached its failure and therefore after the negative peak in acceleration due to cracking and fracture, the acceleration should return to zero. Because the test set-up required that the tup be stopped before contact with the laser sensors be made, the vibration in acceleration seen in Figure 6-13 for Test 8, which is uncoated, could be due to the tup hitting the stoppers, bouncing off of them, hitting them again, and so on until motion has stopped. For a polyurea coated beam after the acceleration due to cracking occurs, another deceleration should be seen, due to the stiffening of the polyurea. If the polyurea fractures, as is the case for Test 7, the system would have another negative acceleration once fracture has occurred and the acceleration data

would then show the tup hitting the stoppers as was the case for the uncoated specimen.

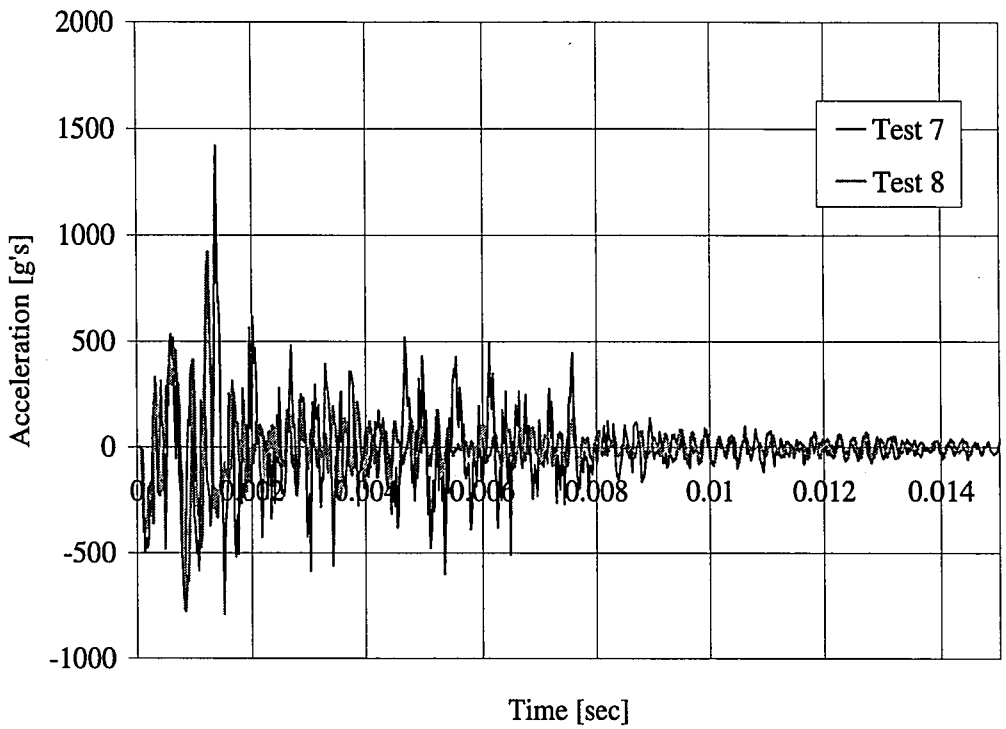


Figure 6-13: Full Tup Accelerations for 30 inch Drop Heights

A closer view of the tup accelerations for a 30 inches drop height, which is shown in Figure 6-14, with displacement of the systems on the second y-axis, shows that up until a time of about .0013 seconds, the plots and peak accelerations are similar, after which point, Test 7 has higher acceleration peaks then Test 8, which is followed by a large deceleration that is not prominent in Test 8. It can also be seen that displacement does not increase much until after the large peak in acceleration, which, if the assumptions of behavior are correct, could be the point at which contact occurs. It can be seen that Test 7 displaces at a slower rate than Test 8, which is expected since Test 7's specimen is coated with polyurea. If this is where contact occurs, this

means that all of the frequencies seen in the tup before this point are noise and vibrations of the test set-up and may not be real. The larger negative acceleration of Test 7, which follows the high acceleration peak, is not expected since the downward acceleration of a non-coated beam should be more than that of a coated system where the polyurea is resisting the motion. Test 7 is seen to resonate more than Test 8 and this could be due to the polyurea reaching different yield values, which would cause the system to behave differently. Some of the vibration, as is the case with Test 8 is due to the tup hitting the stoppers, rebounding, and so on until movement ceases, but there is noise present. It is not certain what the real acceleration data is and what is not for the tup.

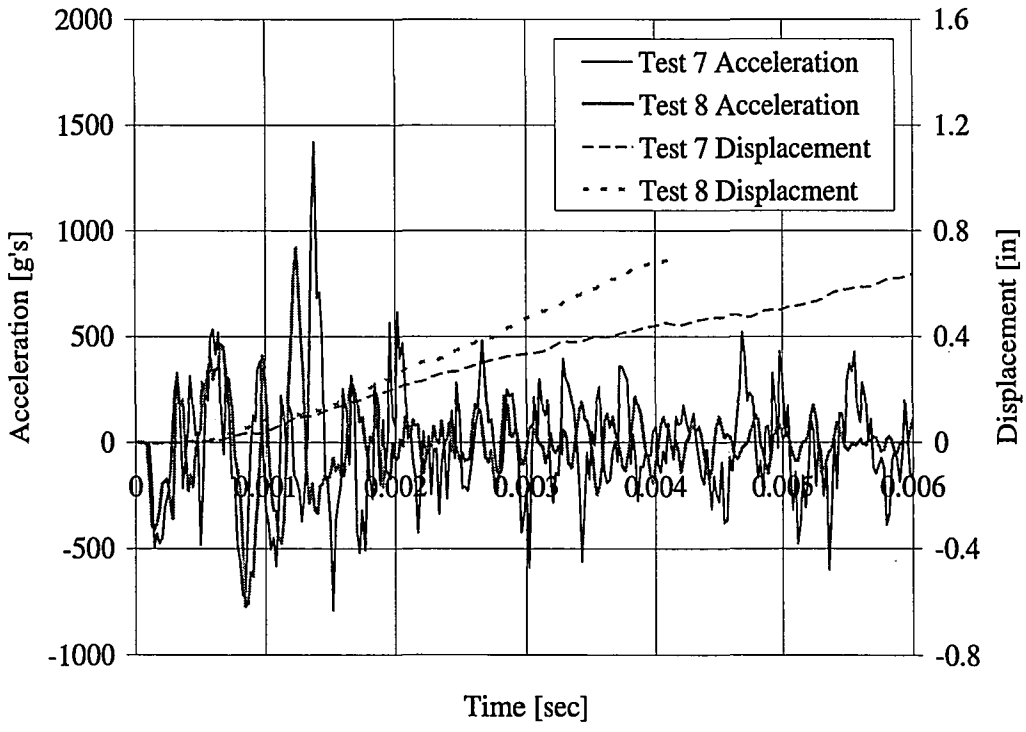


Figure 6-14: Initial Region of Tup Acceleration versus Time Plot for 30 inch Drop Height

Looking at the tup acceleration of a coated specimen from 6 inches that did not fracture, compared to the tup acceleration of an uncoated 6 inch drop height, which did fracture in Figure 6-15, the same behavior is seen, but over a longer period of time. For the coated specimen this would be expected, because you would have acceleration due to the stiffening of the polyurea, deceleration as yield is reached, and so on, and then you would have deceleration due to the rebound, and the system could begin displacing downward again, followed by another rebound, until coming to rest. The tup accelerations for the plain concrete for the 6 inch drop height do reach a steady zero balance before the coated system, since the rebound action does not occur, nor is there any polyurea coating to stiffen and yield.

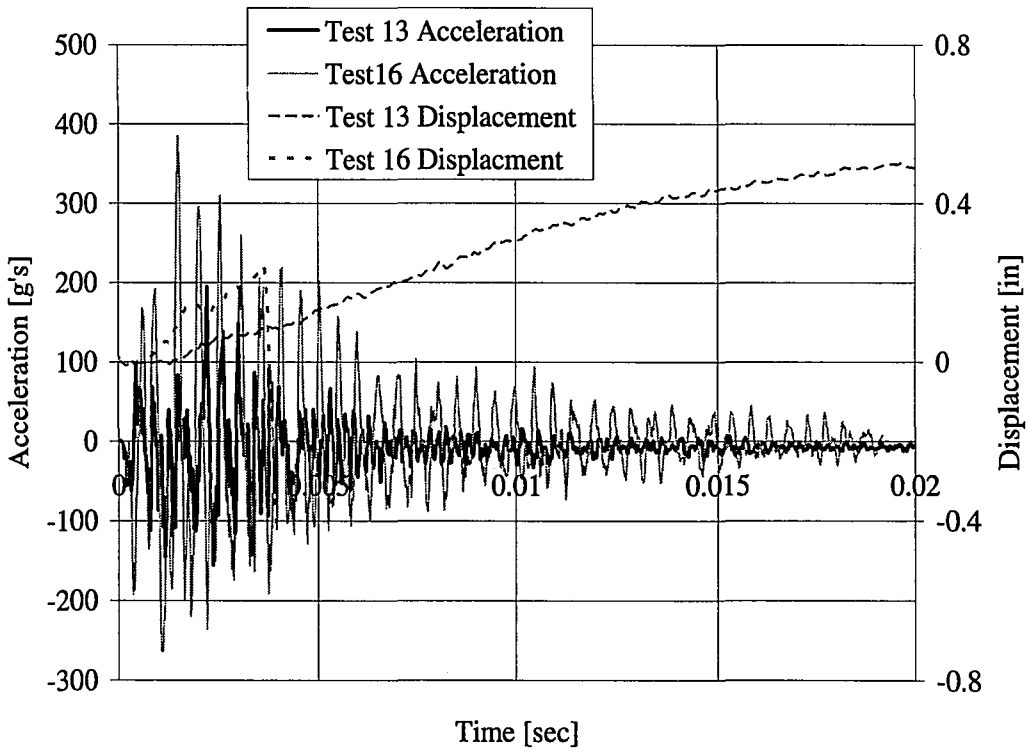


Figure 6-15: Tup Acceleration of a Coated Specimen and an Uncoated Specimen Tested at a 6 inch Drop Height

The overall behavior of the 6 inch drop heights presented, as shown in Figure 6-16, in addition with displacements of the systems, clearly shows that the coated beam rebounds, but that this occurs outside of the tup accelerations. Meaning that the system is hit, and some of the reaction occurs during the loading frequencies and some of the reaction occurs outside of the loading frequency.

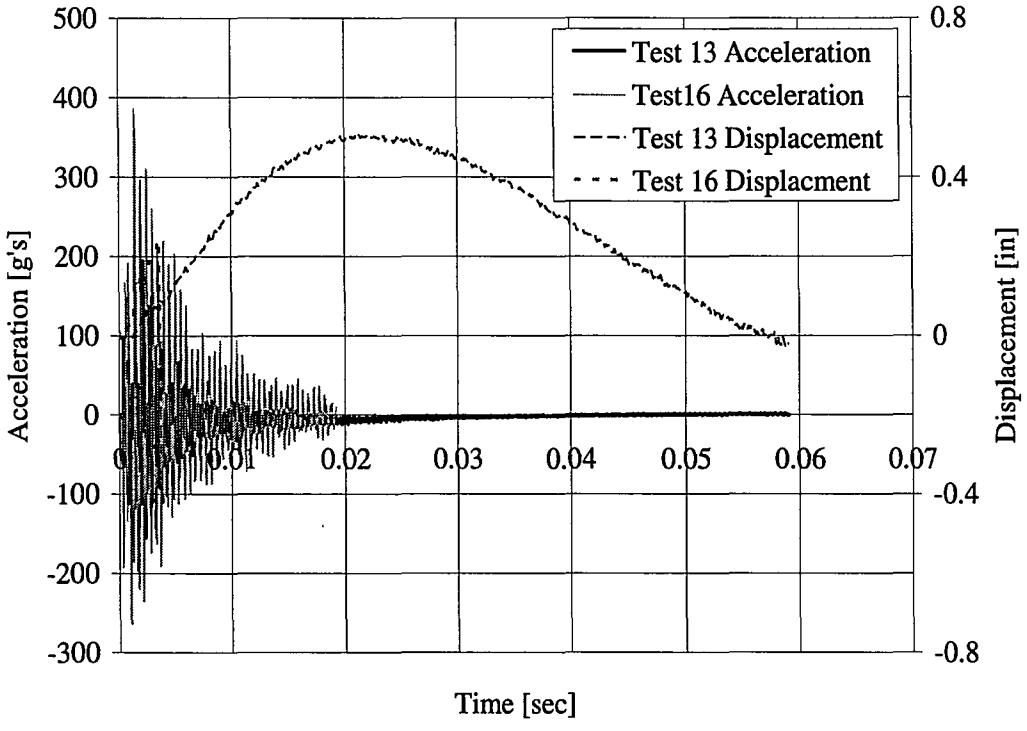


Figure 6-16: Overall Behavior of Tup Acceleration and Displacement of a Coated and Uncoated Specimen from a 6" Drop Height

Since the accelerometers on the beam are in the opposite orientation than the accelerometer located on the tup, the beam is expected to have a negative acceleration when contact is made, meaning it is accelerating downward, then as the beam stiffens, it should start to decelerate in its downward motion (giving a positive slope to the acceleration data). This is followed by cracking of the concrete, which would resume

the downward acceleration. If the system is coated, the polyurea will stiffen, and the downward acceleration will be decelerated again, then as the polyurea reaches its different yields the beam will accelerate downwards, and then decelerate its downward motion. If the beam does not fracture, as it rebounds it will accelerate upwards, which may be followed by another displacing downwards or downward acceleration, until the beam comes to rest. If the beam does fracture, it will see acceleration downward at fracture. This behavior is similar and opposite to that of the tup accelerations, however the periods may differ depending on whether the response occurs within the loading phase or outside of the loading phase.

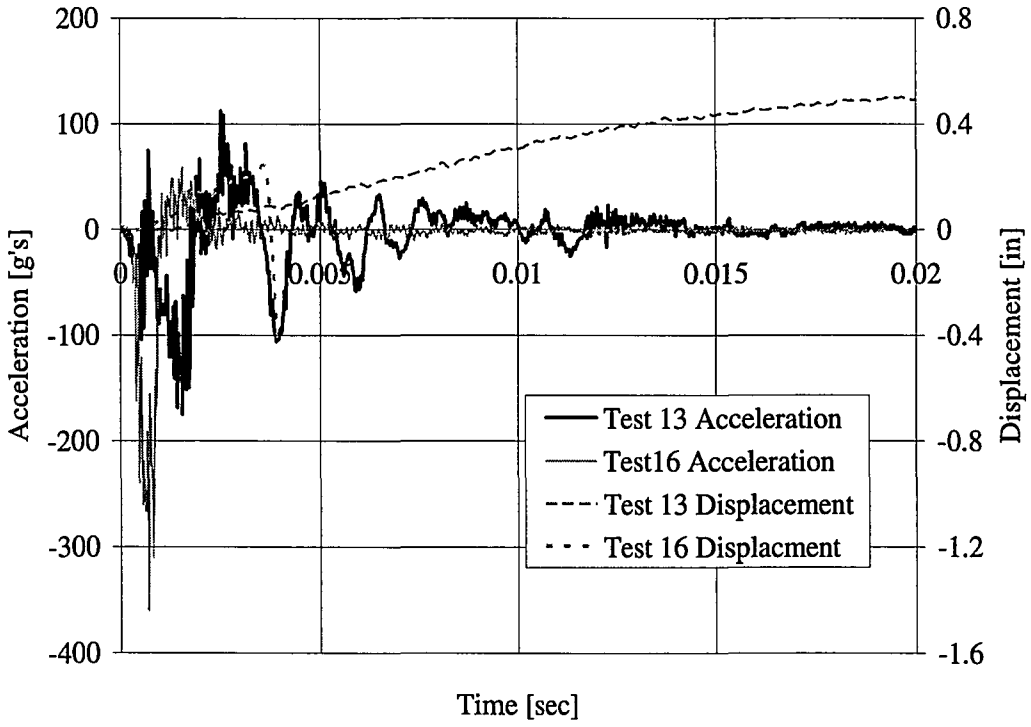


Figure 6-17: Beam's Midspan Acceleration for Coated and Uncoated Specimen Tested at Drop Height of 6 inches

As is seen in Figure 6-17, which is the beam accelerations for the same tests from 6 inches whose tup accelerations were presented, the behavior is clearer. If you look closely you can see a small negative frequency at the beginning of the acceleration data for the uncoated specimen of Test 16, which shows that it accelerates downward when hit, at which point the concrete stiffens, giving a small positive acceleration, before it fractures, which causes the large downward acceleration, before the beam comes to rest in the test set-up, returning the acceleration to zero. The coated specimen of Test 13, accelerates downward when hit, the concrete stiffens giving a positive acceleration before the concrete cracks, allowing beam to accelerate downward again. It then stiffens due to the polyurea, allowing for positive acceleration. When the polyurea yields, it accelerates downward again. The acceleration then begins upward again due to rebound, and eventually levels out to zero. Again, maximum displacement is seen outside the region of beam accelerations.

#### 6.4.1.1 Coated Systems from Higher Drop Heights

As is stated in the Test Matrix of Table 6-1, Test 7 dropped the weight and tup onto a polyurea coated system from a height of 30 inches and Test 9 dropped the weight and tup onto a polyurea coated system from a height of 18 inches. Although the concrete types and polyurea batches differ between the specimens, the tup accelerations of Figure 6-18 show the expected trend when comparing the two. A similar behavior is seen, but the peak accelerations from the 18 inch drop are less than those from the 30

inch drop. Both tests resulted in a full fracture of the polyurea. The breaks were clean and not due to large stress concentrations as is seen in Figure 6-19.

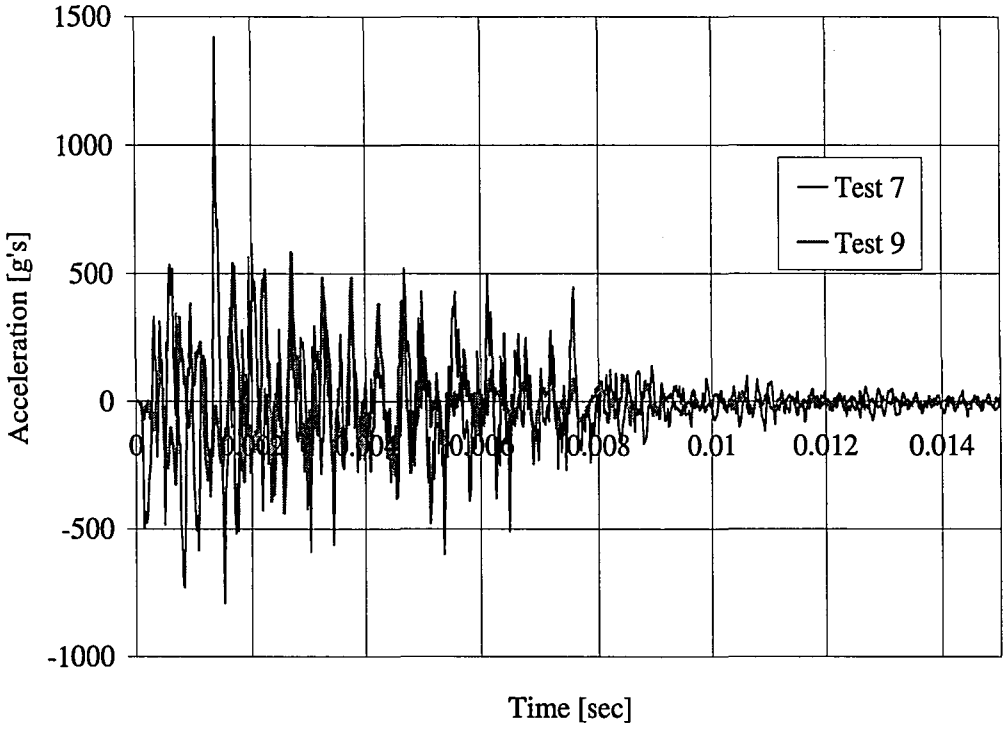


Figure 6-18: Tup Acceleration of Tests with High Drop Heights

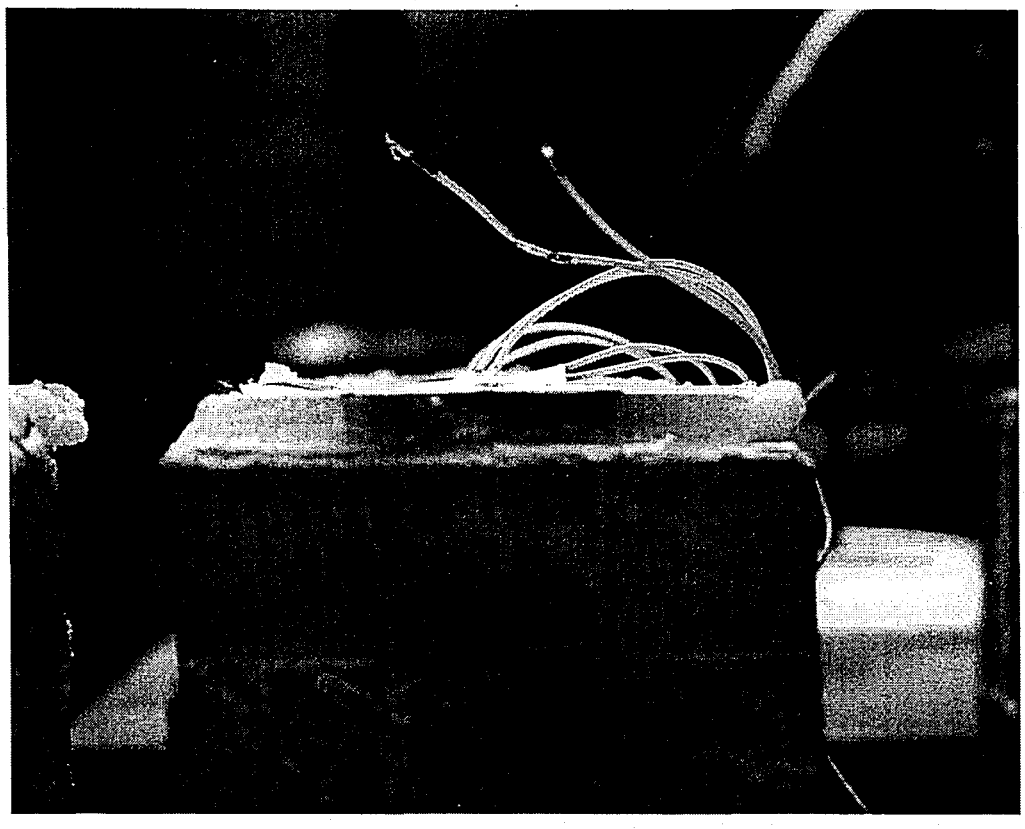

Figure 6-19: Fracture Surface of Coated Specimen tested at Drop Height of 30 inches

The acceleration of the midspan of the beam, shown in Figure 6-20, also shows the expected trend between the two tests. The rate of the downward acceleration of Test 9 is slower than that of Test 7, which has the larger drop height and would be expected to accelerate downward faster.

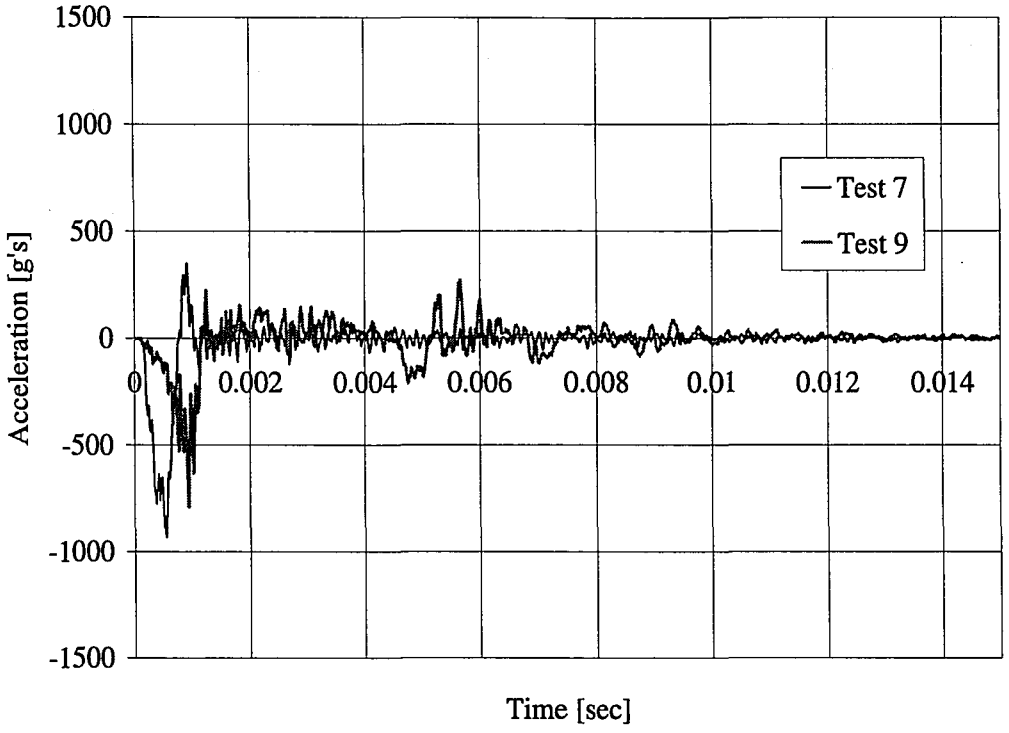


Figure 6-20: Beam's Midspan Acceleration

Figure 6-21 shows a plot of the tup and beam acceleration together. In this case the initial behavior by the tup is an upward acceleration, which correlates to the deceleration that would be expected when contact is made, which correlates to the stare of the negative acceleration of the midspan. However, the presence of noise can be seen in the tup acceleration as it jumps from negative to positive during the midspan's negative acceleration phase. Both the tup and the beam accelerations seem to damp out at about the same point in time as well.

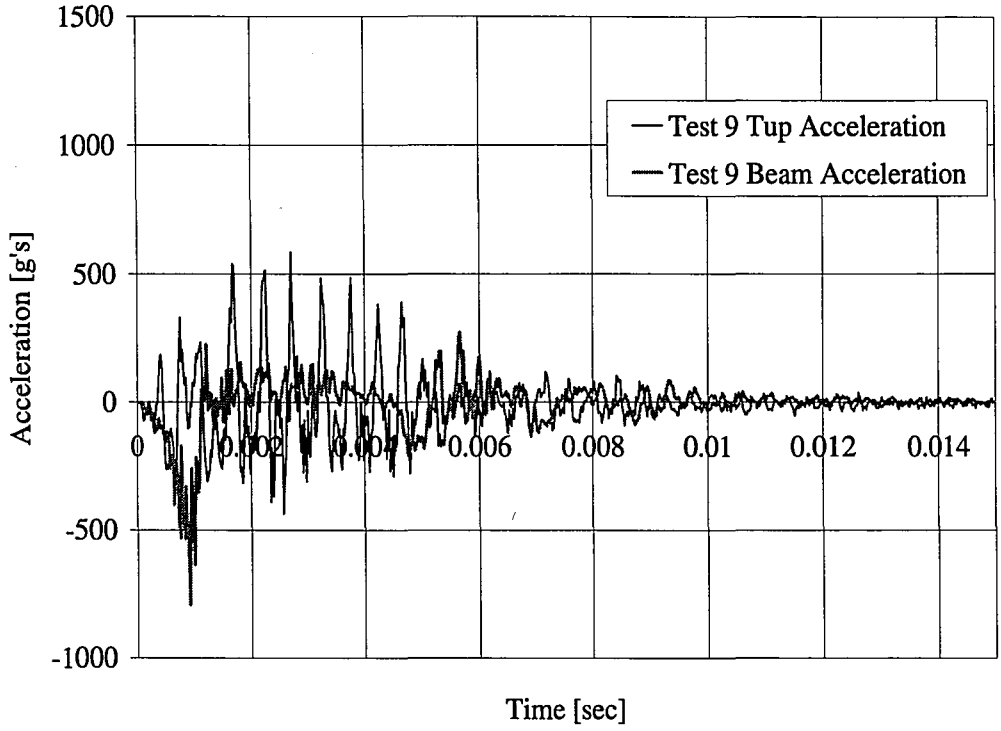


Figure 6-21: Tup and Midspan of Beam Accelerations for Test 9

### 6.4.1.2 Plain and Coated Concrete Specimens at Low Drop Heights

The plot of Figure 6-22 shows the tup acceleration of Test 15 and Test 18, which both tested plain concrete of Type 1 at a six inch drop height. As can be seen, the peak acceleration values are similar, as well as time to dissipation of acceleration. However, that same repeatability is not seen for the same tests performed on Type 2 concrete, as seen in Figure 6-23. There is a difference in the range of accelerations seen by Type 1 and Type 2 concrete. The range of accelerations for Type 1 concrete is -200 g's to about 300 g's, whereas the range of accelerations for Type 2 concrete is -300 g's to 400 g's. This could be due to the difference in strength of the two concrete types. Due to the fact that Type 2 concrete is stronger than Type 1 concrete,

it will have a higher elasticity value, meaning it is stiffer than the Type 1 concrete. Because it is stiffer, when it comes in contact with another stiff object, such as the tup, the two will have more bounce off of each other, meaning it will have a higher coefficient of restitution. A higher coefficient of restitution means that less of the kinetic energy is transformed into other forms of energy that would take away from its velocity such as material deformation. This would result in Type 2 concrete causing higher accelerations than Type 1 concrete.

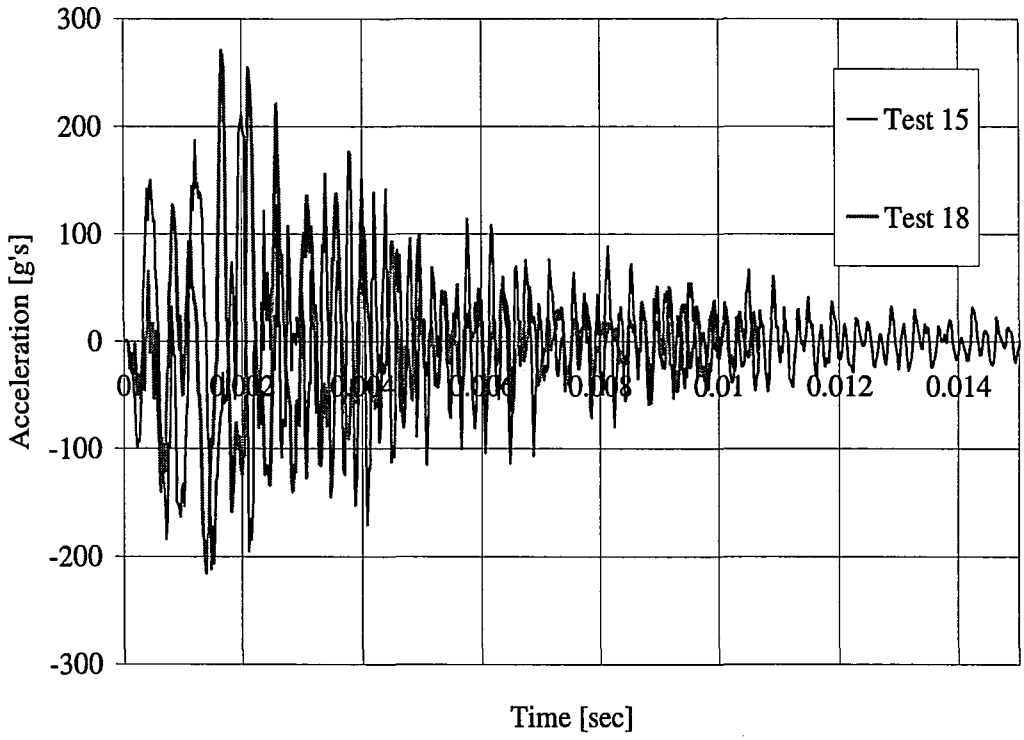


Figure 6-22: Tup Acceleration for 6 inch Drop Height on Plain Concrete Type 1

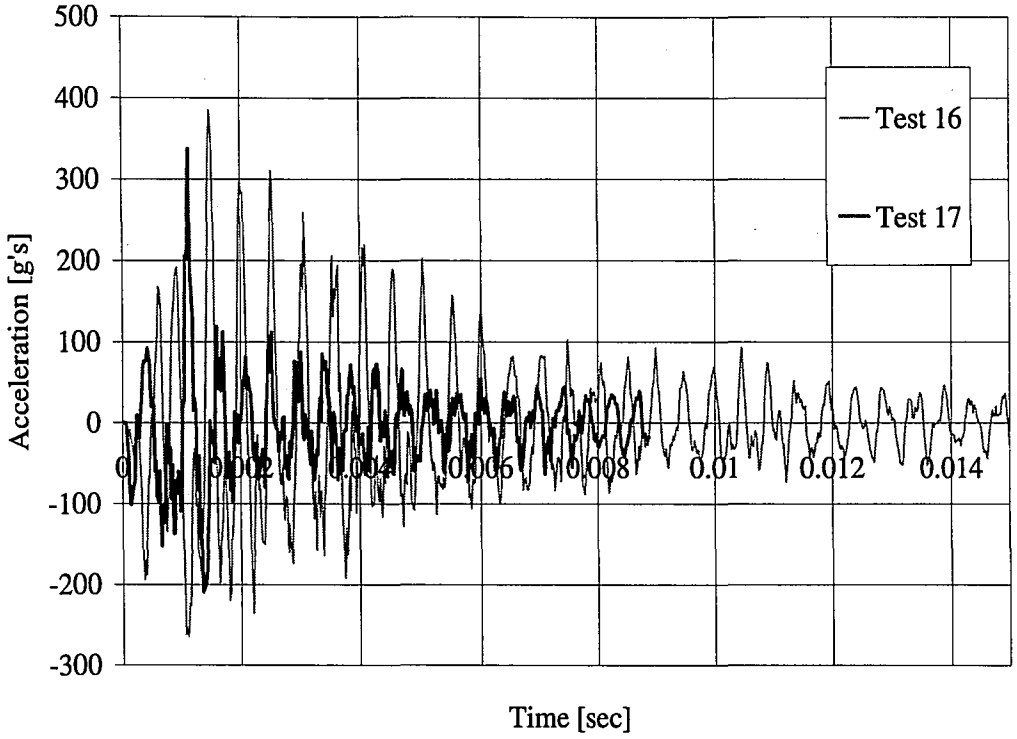


Figure 6-23: Tup Acceleration for 6 inch Drop Height on Plain Concrete Type 2

Looking at the midspan accelerations of the plain specimens of concrete Type 1, shown in Figure 6-24, extremely similar behavior is shown. The downward acceleration is followed by the upward acceleration due to stiffening of concrete. This is followed by the most negative acceleration as the concrete fractures and deflects downward, before the beam pieces come to rest at zero acceleration. Figure 6-25 shows the same midspan acceleration behavior for the 6" drops with Type 2 concrete. There is no discernable difference in the maximum beam accelerations between Type 1 and Type 2 concrete, which are between 300 and 400 g's, meaning that the kinetic energy of the hit may have been transferred more to the tup rather than the beam in the case of the Type 2 concrete or the difference in tup acceleration is due to noise.

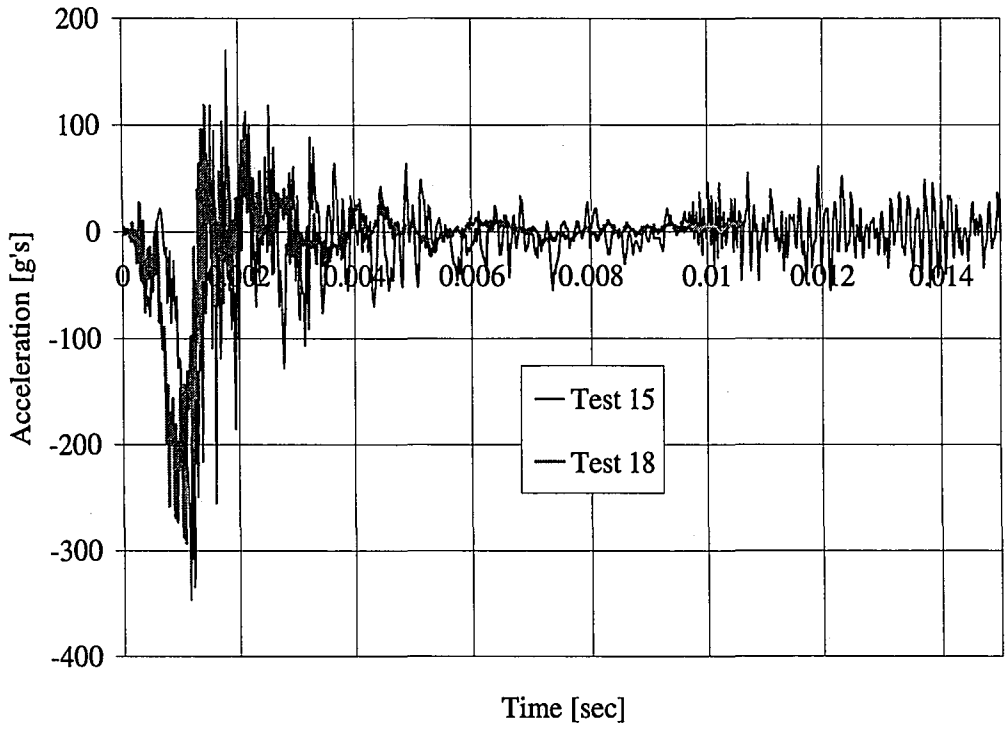


Figure 6-24: Beam's Midspan Accelerations for Type 1 Concrete Plain Specimens Tested at 6 inches

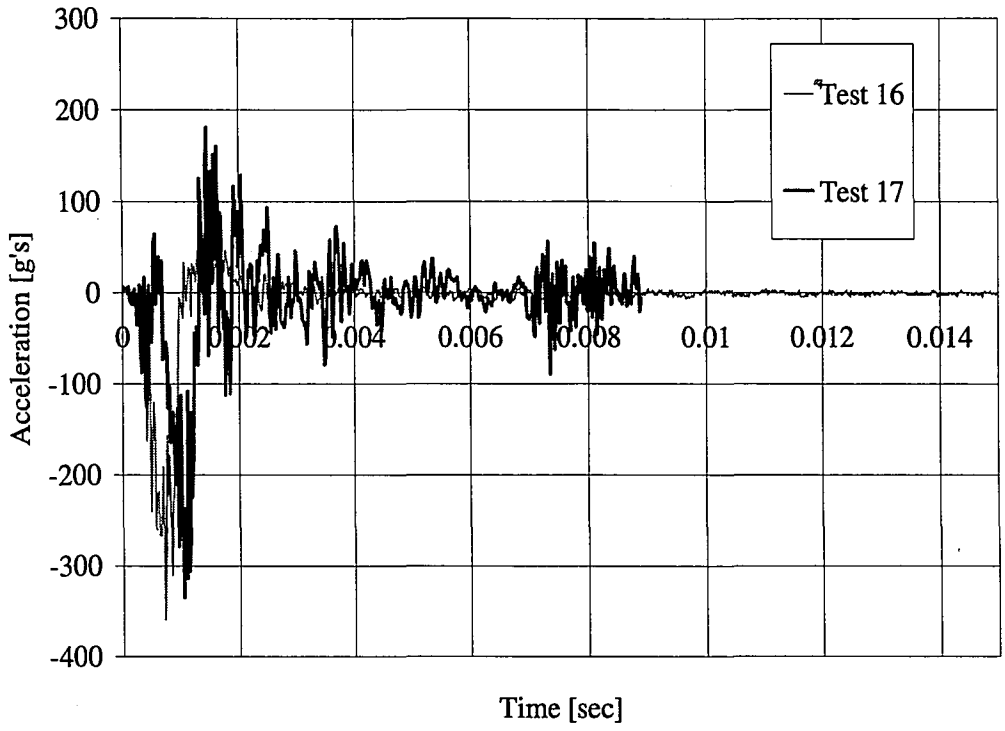


Figure 6-25: Beam's Midspan Acceleration for Type 2 Concrete Plain Specimens with Drop Height of 6 inches

The tup accelerations for systems coated with Polyurea Batch 7, with a drop height of 6 inches are shown in Figure 6-26. There is an obvious difference in peak acceleration, which could be due to the fact that Test 12 saw fracture of the coated specimen due to the presence of tape within the thickness of polyurea, which caused a stress concentration, as can be seen in Figure 6-28. The beam's midspan accelerations also support this, as seen in Figure 6-27. It shows that the fractured beam's acceleration or response is about 400 g's less than that of the not fractured beam of Test 10.

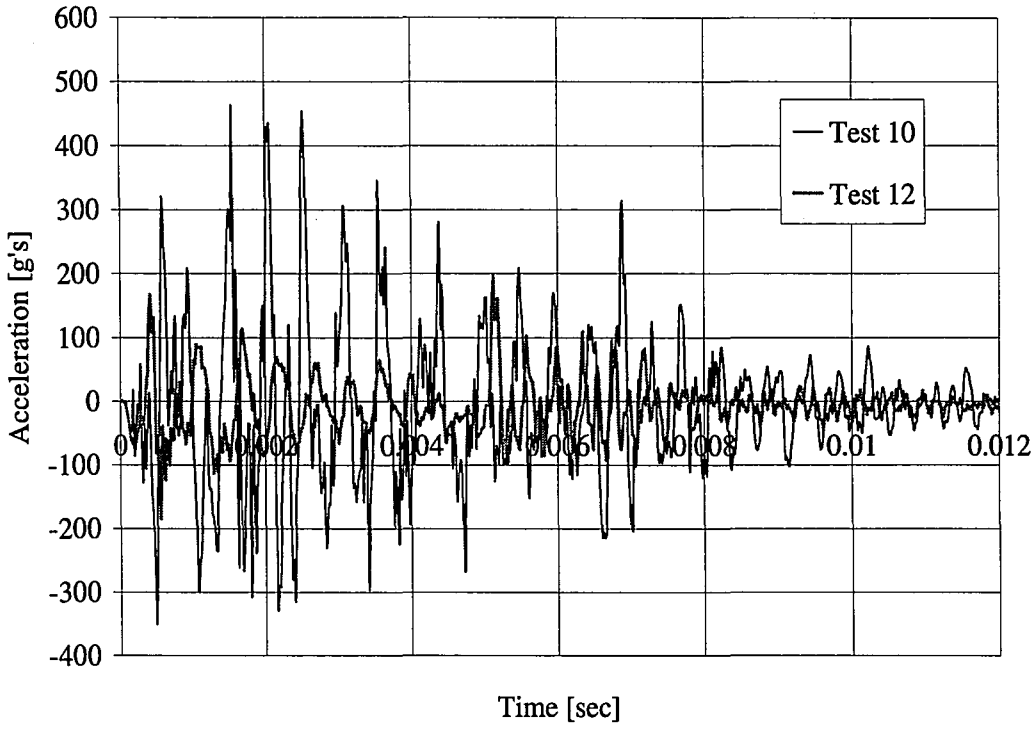


Figure 6-26: Tup Acceleration for Specimens Tested at a 6 inch Drop Height and Coated with Polyurea Batch 7

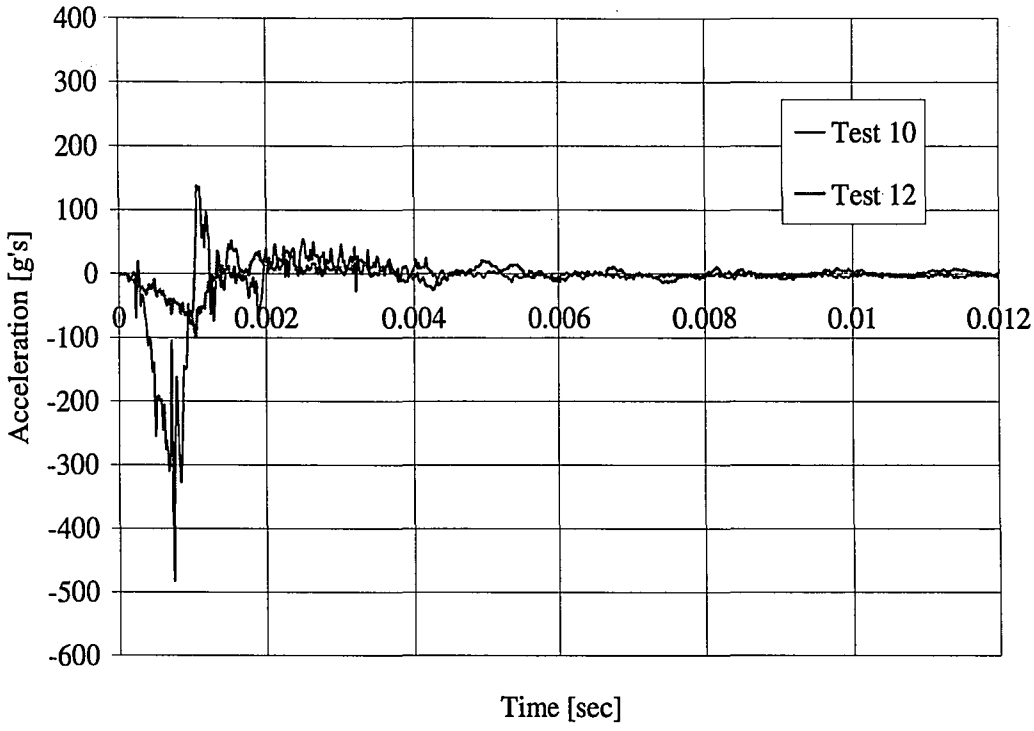


Figure 6-27: Beam's Midspan Acceleration for Specimens Coated with Polyurea Batch 7 Tested at 6 inches

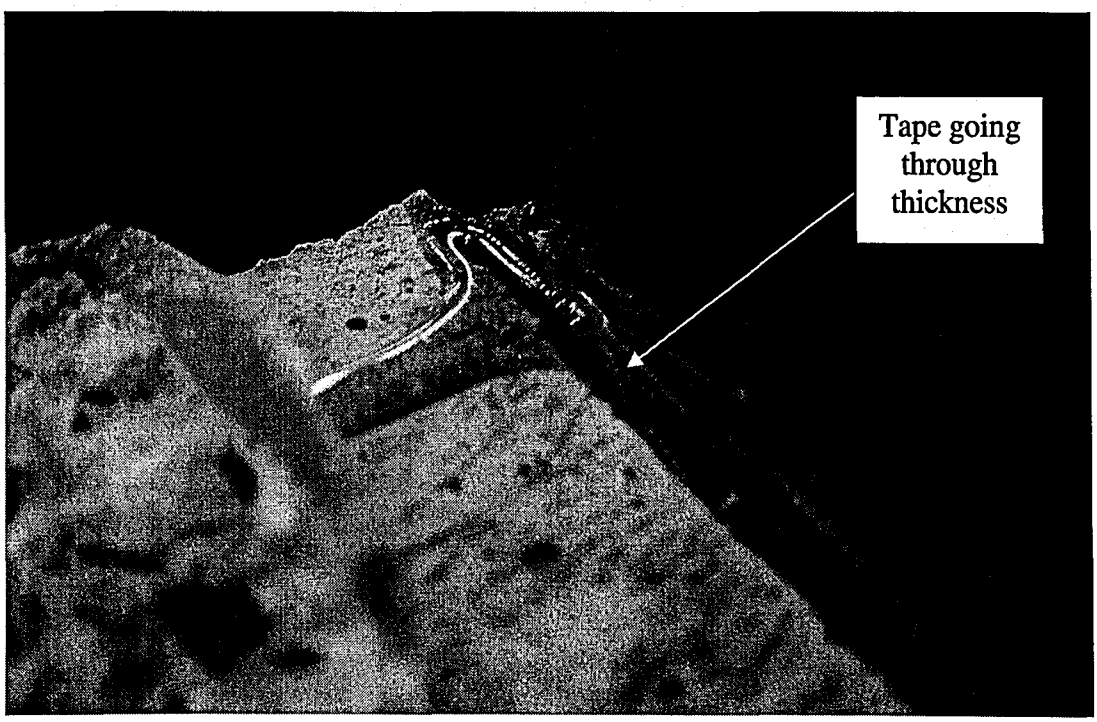


Figure 6-28: Fracture Surface of Test 12 with Presence of Stress Concentration

Test 13 and Test 14 used a 6 inch drop height on specimens having Type 2 concrete and Polyurea Batch 8. The only difference between the two specimens is the thickness of the polyurea. The specimen for Test 14 had a polyurea thickness that was 34% less than the thickness of polyurea in Test 13. The tup acceleration data is similar in the earlier part of the test, but then Test 13 sees accelerations 125 g's higher than that of Test 14. Interestingly, the midspan accelerations of the two specimens, presented in Figure 6-30, are more similar, but it seems that the maximum negative acceleration of Test 14 is roughly 150 g's higher than that of Test 13. It could be that the difference in the tup accelerations were transferred to the beams accelerations. There is a much larger secondary response for Test 13 and 14, showing how the polyurea effects the accelerations when it does not fracture.

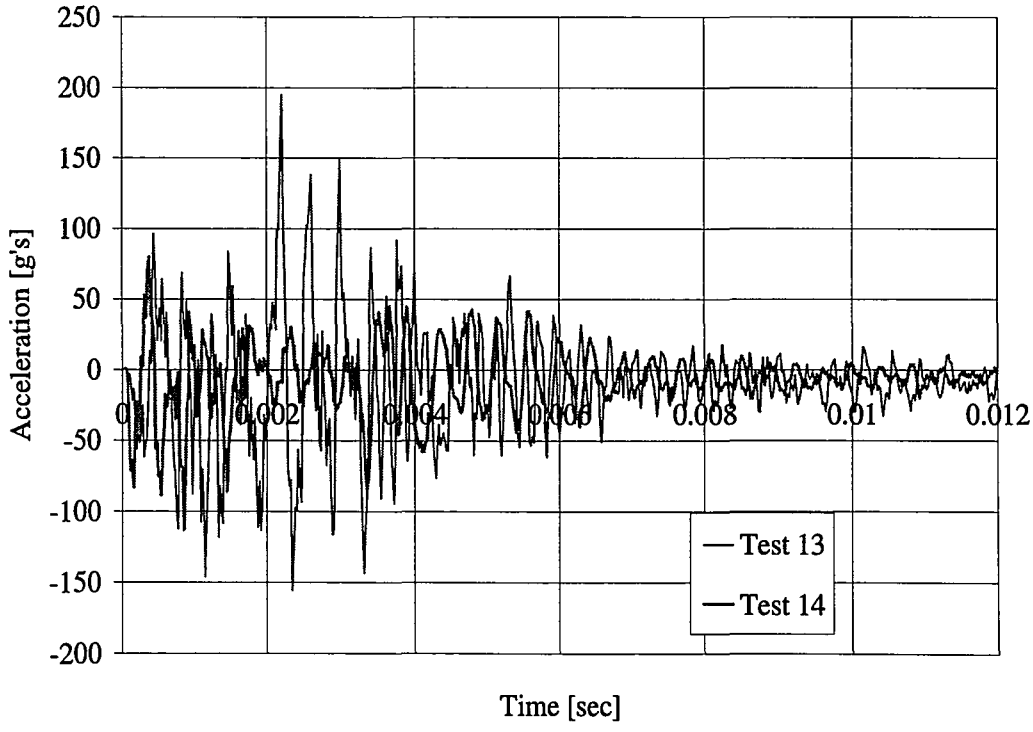


Figure 6-29: Tup Acceleration for Specimens Tested at 6 inch Drop Height and Coated with Polyurea Batch 8

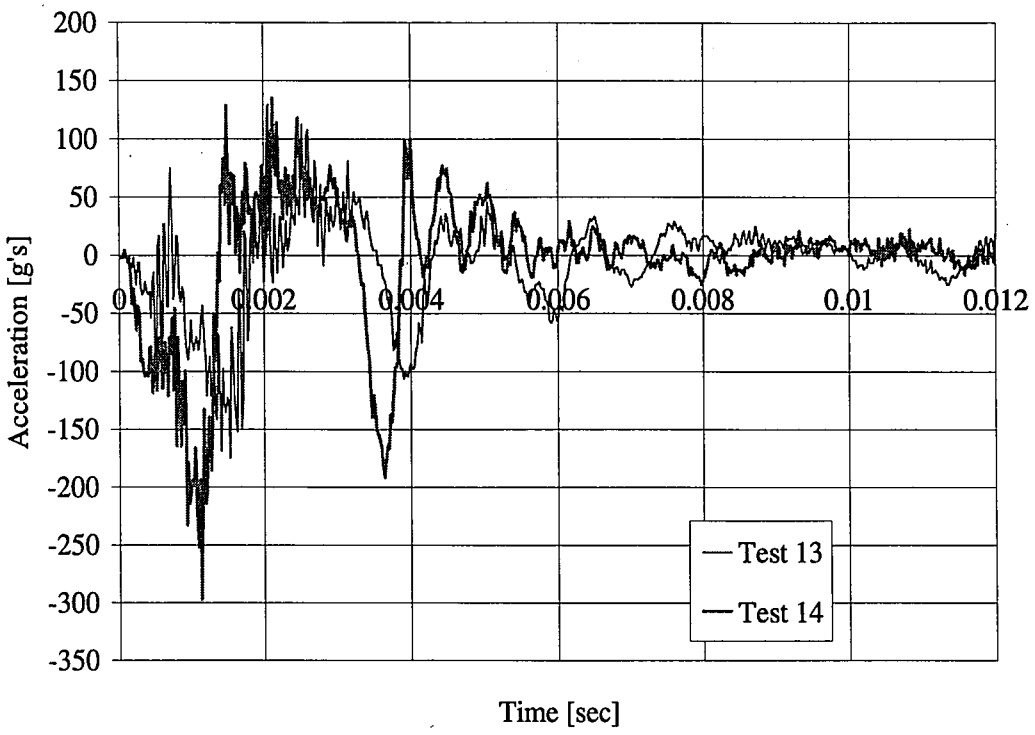


Figure 6-30: Beam's Midspan Acceleration for Specimens Coated with Polyurea Batch 7 Tested at 6 inches

Figure 6-31 shows a plot of the two tests that saw fracture of the polyurea. In Test 12, the polyurea fractured completely due to the stress concentration shown in Figure 6-28. For test 11, there was only a partial fracture or tearing of the polyurea near the edge as shown in Figure 6-32. The first three acceleration peaks are almost exact between the two tests. After these peaks, the acceleration of Test 11 increases significantly and may point to the time of tearing of the polyurea. The stress concentration or weakness in the polyurea surface of Test 11 was not as severe as that in Test 12. It may have been the presence of an air bubble in the polyurea which allowed for the partial fracture, making it harder for the fracture to occur in this polyurea compared to the fracturing of the polyurea of Test 12, where a large stress concentration was present. Figure 6-33 shows the midspan accelerations for the

beams that fractured. The partial tear resulted in extremely high midspan accelerations of 1750 g's, supporting the fact that more energy was needed to cause the partial tear rather than the full fracture seen in Test 12.

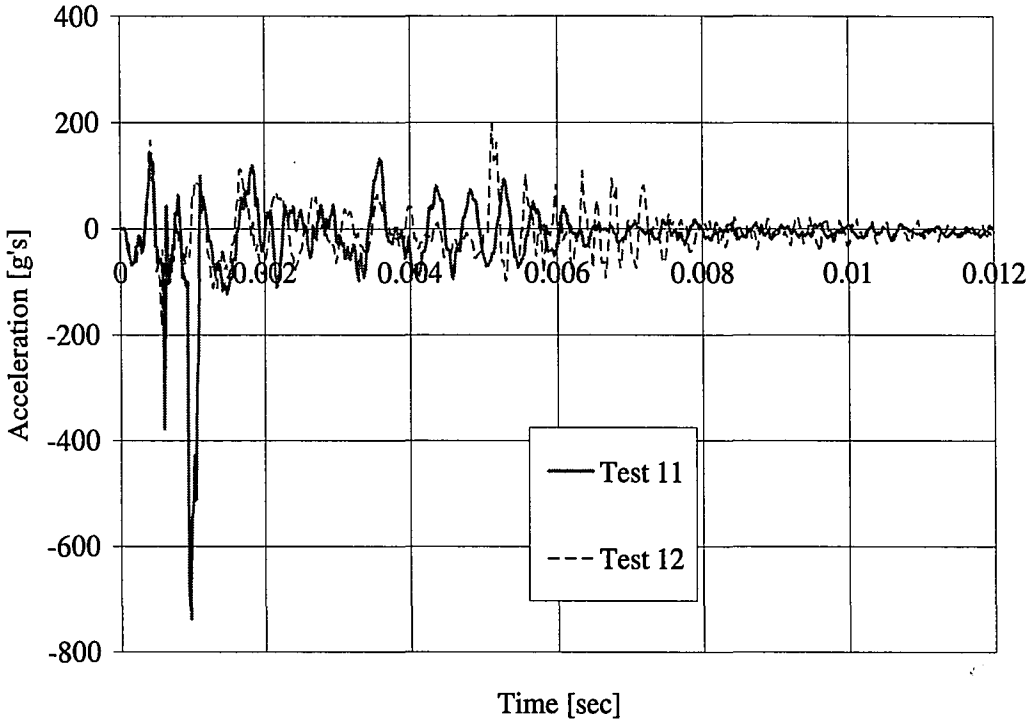


Figure 6-31: Tup Acceleration for Tests with 6" Drop that Fractured

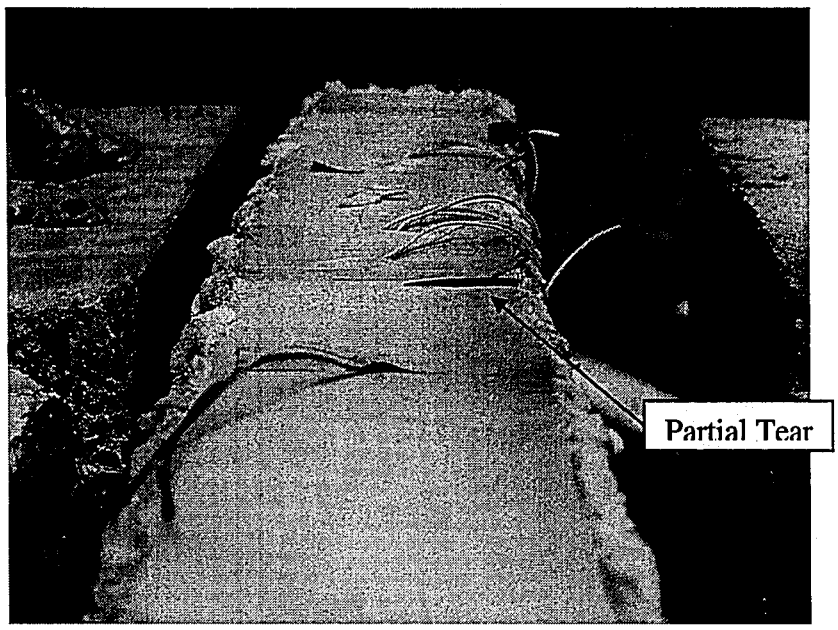


Figure 6-32: Partial Fracture of Test 11

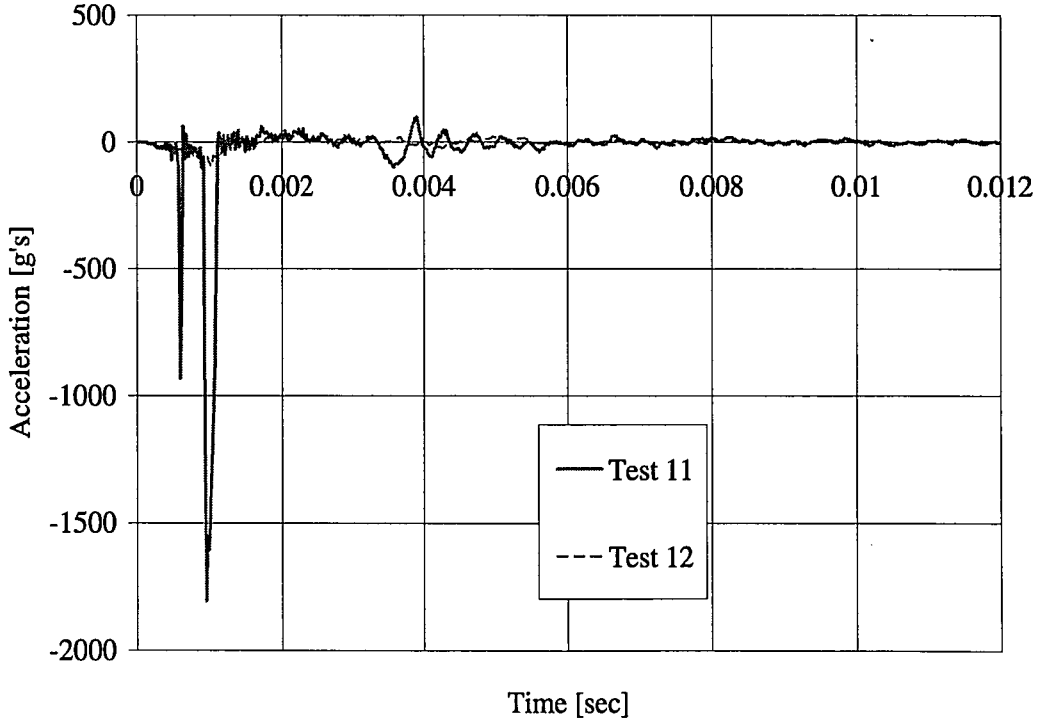


Figure 6-33: Midspan Accelerations for Coated Specimens that Fractured from a 6 inch Drop

Ignoring Test 11, which had a partial tear and saw extremely high accelerations compared to all other results of coated specimens tested at a drop height of six inches and was the only Type 1 concrete coated for this drop height, the average peak tup acceleration values were -187.5 g's and 225 g's. Both of these values are less than the average peak tup accelerations of Type 2 concrete, which were -225 g's and 350 g's. The negative peak tup acceleration for plain specimens is 20% higher than coated specimens and the positive peak tup acceleration for plain specimens is 55.6% greater than the coated specimens. The average midspan accelerations of the coated beams are also less than the uncoated specimens. The negative peak midspan acceleration for uncoated specimens is 33.3% higher than that of the coated specimens. The average positive peak midspan accelerations of uncoated specimens are 8% higher than that of coated specimens. This means that the coated specimens are absorbing more energy without fracture, more than their fractured uncoated counterparts. This can be concluded since all systems have the same drop height and therefore have approximately the same energy going into them, but both the tup and the beam are seeing less acceleration after the hit for the coated specimens, meaning these specimens are absorbing more of the energy.

The drop weight test was performed on three plain specimens using a drop height of 4 inches. Test 21 and Test 23 were both Type 1 concrete and Test 22 was Type 2 concrete. As can be seen in Figure 6-34, there does not seem to be any trend in the tup acceleration data for these tests. The tests with the same concrete type do not have similar peak accelerations and the test with Type 2 concrete does not resemble either of the other two tests. It is expected that the acceleration range for these tests

would be lower than that of the tests performed at six inches, due to the difference in drop height. This is true of Test 21 and 22, which saw a range of -150 g's to 200 g's, but not true for Test 23.

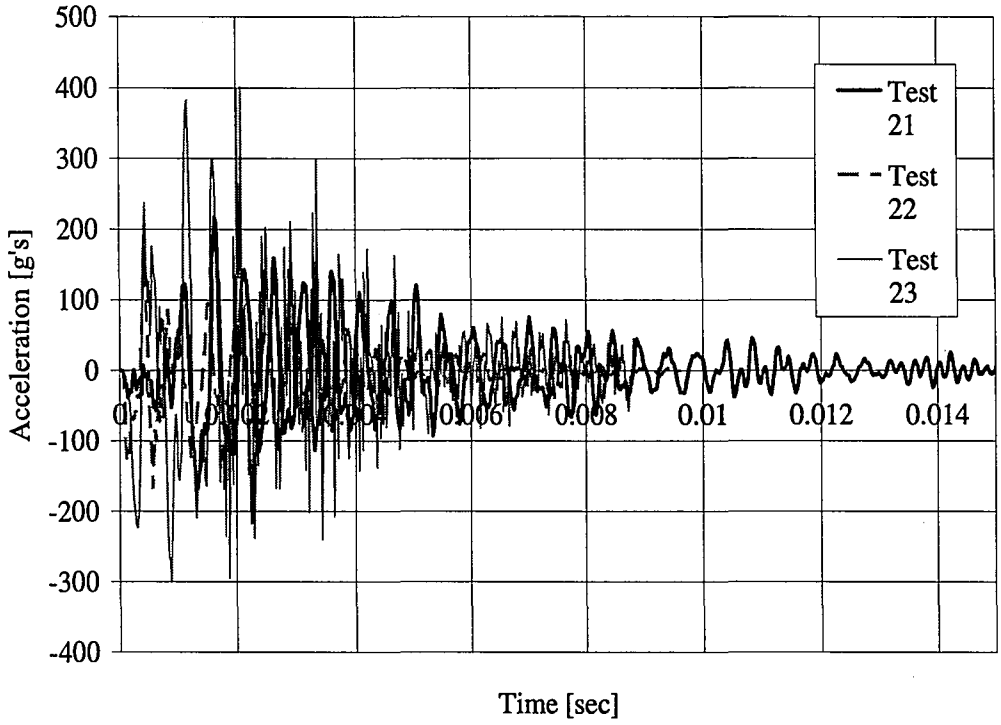


Figure 6-34: Tup Acceleration for Plain Concrete at a Drop Height of 4 inches

Although Figure 6-35, which graphs the beams' midspan accelerations for plain specimens tested at a four inch drop height, shows the expected behavior with the drops and rises. There is still no similarity between the maximum acceleration values for specimens with the same concrete type. Test 22 shows a much larger initial dip in accelerations than has been seen before for plain specimens. The average midspan acceleration is -316 g's compared to the average of -350 g's for a six inch drop height on uncoated specimens. This indicates that it is harder to fracture the concrete at this height.

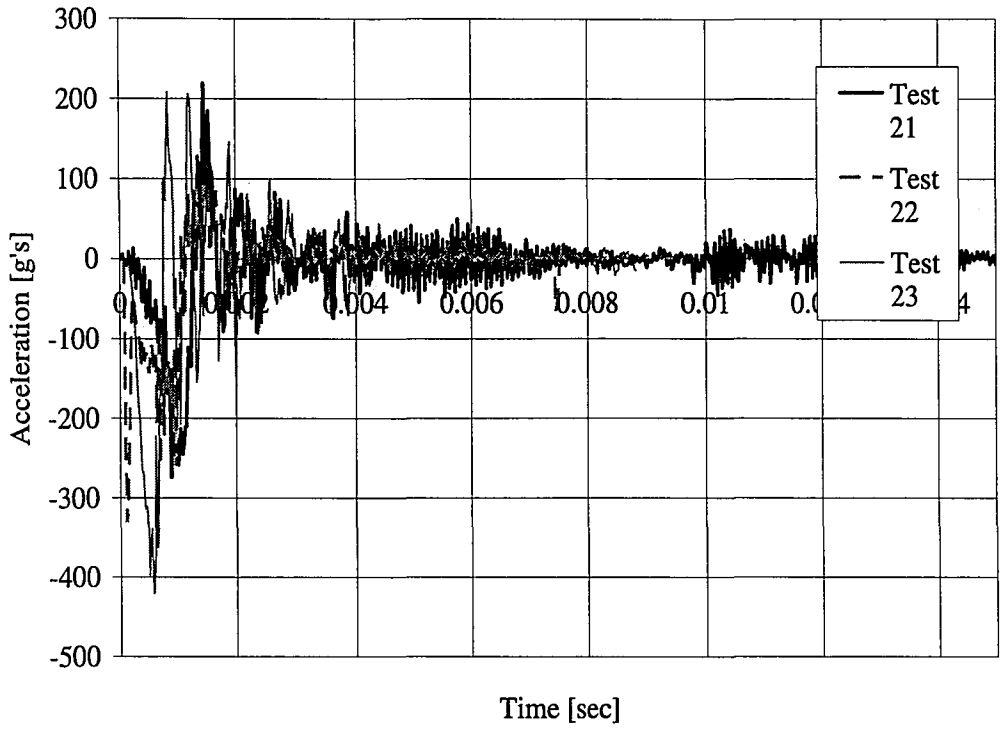


Figure 6-35: Midspan Accelerations for Uncoated Specimens Tested at a 4 inch Drop Height

Looking at the tup acceleration data from tests conducted at a 4 inch drop height with a polyurea coating of Figure 6-36, the acceleration values are similar for the first five peaks, before Test 20 starts to have higher peak acceleration values than Test 20. For these tests, the concrete type is the same, but the beams are coated with different batches of polyurea. Also, Test 19 resulted in a partial fracture of the polyurea similar to that of Test 11. However, the extreme increase in acceleration that was seen in Figure 6-31 for Test 11 is not seen in Figure 6-36 for Test 19. Figure 6-37 also shows that the extreme midspan acceleration that Test 11 produced is not reproduced by the partial fracture of Test 19. It also shows extremely similar midspan acceleration behavior between the two tests. The only difference comes later in time, when the polyurea is more active and the accelerations for Test 19 are

higher due to the partial fracture. The average midspan accelerations for the 4 inch drop height are higher than those of the six inch drop height, but there were fewer specimens. A larger sample is needed to really compare the values.

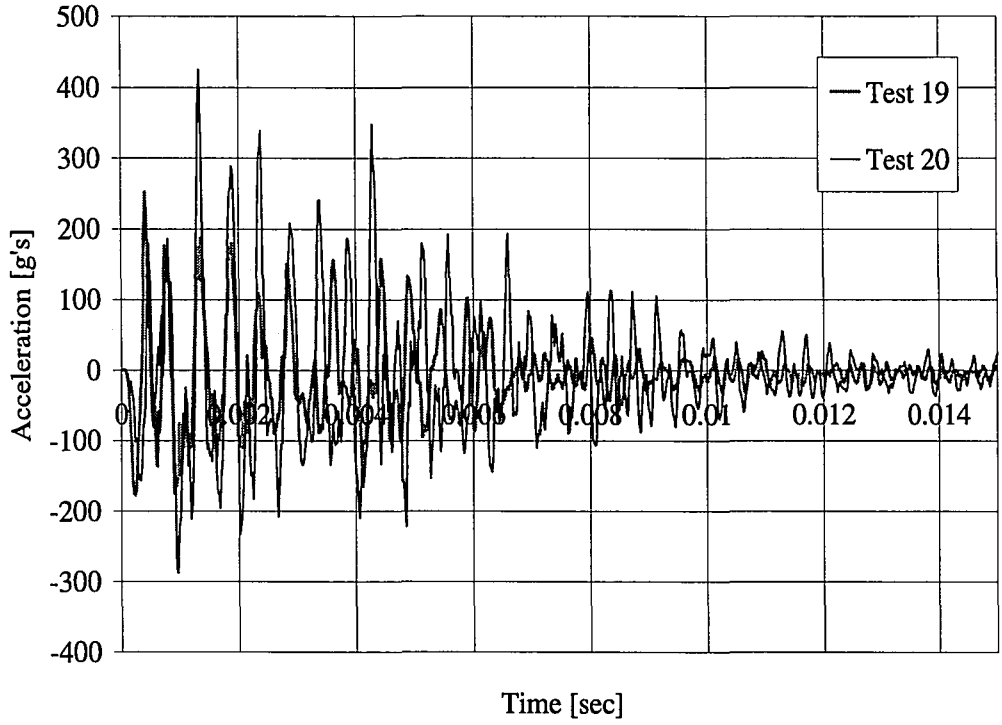


Figure 6-36: Tup Acceleration for Tests with 4 inch Drop Heights and Polyurea Coating

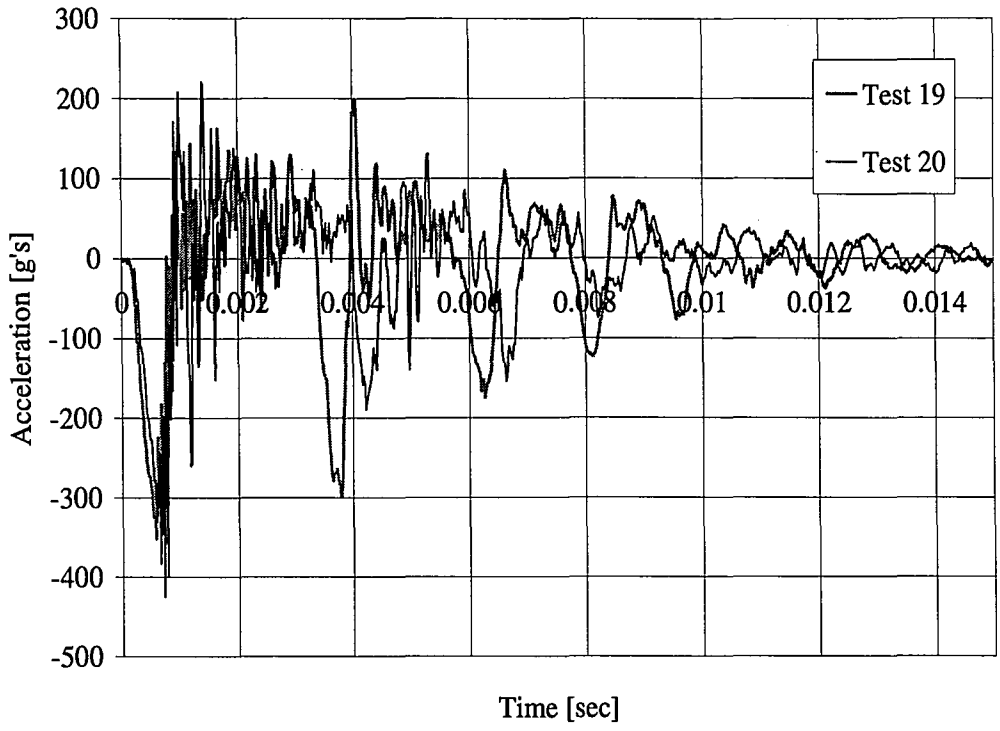


Figure 6-37: Midspan Acceleration for Tests with 4 inch Drop Heights and Polyurea Coating

Comparing the average peak tup accelerations for coated and uncoated beams, there is no difference for Type 1 concrete. The average negative peak midspan acceleration for Type 1 concrete coated with polyurea is 13.3% lower than that of the uncoated specimen's. The average positive peak midspan acceleration for Type 1 concrete coated with polyurea is 14.3% higher than that of the uncoated specimen. This means that the energy coming out of the systems is essentially the same. Therefore, the same amount of energy is absorbed by coated and uncoated systems at a 4 inch drop height; however the coated specimens did not fracture.

Real fracture energies could not be calculated for the dynamic tests due to the fact that the acceleration data both recorded by accelerometers on the tup and on the

beams needs to be calibrated with high rate load cells in order to determine what real acceleration data is and what is not. With this kind of dynamic data, a generalized bending load, which would be a function of time, could be determined and plotted versus displacement. A method for determining the generalized bending load from the real acceleration data is presented in a paper titled "Impact Testing of Concrete Using a Drop-weight Impact Machine". The generalized bending load as a function of time is simply the tup load (which is also a function of time) minus the inertial load of the beam over time. The tup load would simply be the mass of the tup multiplied by its acceleration at a given point in time. The inertial load of the beam is actual a distributed load along the length of the beam, but it can be substituted by a generalized point load in order to calculate the generalized bending load. The inertial load is based on a hinge mode of the beam and the acceleration is assumed to be linear along the length of the beam (Banthia et al., 1987). The generalized inertial load can be calculated using Equation 6-3.

$$P_i(t) = \rho A \ddot{u}_o(t)[\frac{l}{3} + \frac{8}{3}\frac{h^3}{l^2}]$$

*where*:

$P_i(t)$ = Generalized inertial load [lb]

$\rho$ = mass density of beam material [$lb * s^2 / ft^4$]

$A$ = area of crosssection of beam [$in^2$]

$\ddot{u}_o(t)$ = midspan acceleration [$in/s^2$]

$l$ = length between supports [in.]

$h$ = length of hangover [in.]

Equation 6-3: Generalized Inertial Load of the Beam [lb] (Banthia et al., 1987)

### 6.4.2 Strain Data

A change in drop height for the different tests was used to achieve different strain rates within the polyurea. Table 6-3 calculates the actual strain rate in the polyurea by dividing the rate at which the crack opens, from the beginning of the test to just prior to when the maximum crack opening occurs, by the initial debonded length of a ¼ inch. A correlation coefficient corresponding to the calculated strain rate is also provided. The maximum actual strain of each test given is also based on the maximum crack opening divided by the original debonded length.

| Test ID | Drop Height [in] | Polyurea Batch | Thickness [in] | Temp. [°F] | Concrete Type | End of Test | Maximum Strain [in/in] | Strain Rate [1/sec] | Corr. Coeff. |
|---|---|---|---|---|---|---|---|---|---|
| 7 | 30 | 6 | 0.254 | 73.2 | 1 | Fracture | 11.58 | 539 | 0.998 |
| 9 | 18 | 7 | 0.273 | not taken | 2 | Fracture | 7.02 | 426 | 0.997 |
| 10 | 6 | 7 | 0.247 | not taken | 2 | No Fracture | 4.58 | 152 | 0.911 |
| 11 | 6 | 6 | 0.247 | not taken | 1 | Partial Fracture | 4.60 | 191 | 0.992 |
| 12 | 6 | 7 | 0.251 | 76.7 | 2 | Fracture | 6.00 | 164 | 0.989 |
| 13 | 6 | 8 | 0.338 | not taken | 2 | No Fracture | 3.24 | 198 | 0.984 |
| 14 | 6 | 8 | 0.223 | 75.2 | 2 | No Fracture | 4.01 | 206 | 0.988 |
| 19 | 4 | 6 | 0.271 | not taken | 1 | Partial Fracture | 3.08 | 154 | 0.988 |
| 20 | 4 | 5 | 0.255 | 80.4 | 1 | No Fracture | 3.44 | 167 | 0.989 |

Table 6-3: Strain Rates and Maximum Strains of Dynamic Beam Tests

As expected, the averages of strain rates at the different drop heights as well as the maximum strain in the polyurea decreases as the height decreases. The variation in strain rates is due to the different combinations of concrete types and polyurea batches. It should be noted that tests with the same drop height, the same polyurea batch, and the same concrete type (Test 10/Test 12 and Test 13/Test 14) show similar results.

Trends can be seen in the displacement data of the different specimens as well. Figure 6-38 shows displacement versus time for beams that fractured. Tests conducted with a drop rate of 30 inches have the highest displacement rates. The coated specimen displaces at a slower rate than the uncoated specimen at this height. The test conducted with a drop height of 18 inches is seen to have the next highest displacement rate. The six and four inch drop heights give a grouping of displacement rates, but the coated specimen that fractured at six inches displaces at a slower rate than all other 6 inch drop height tests as well as all 4 inch drop height tests.

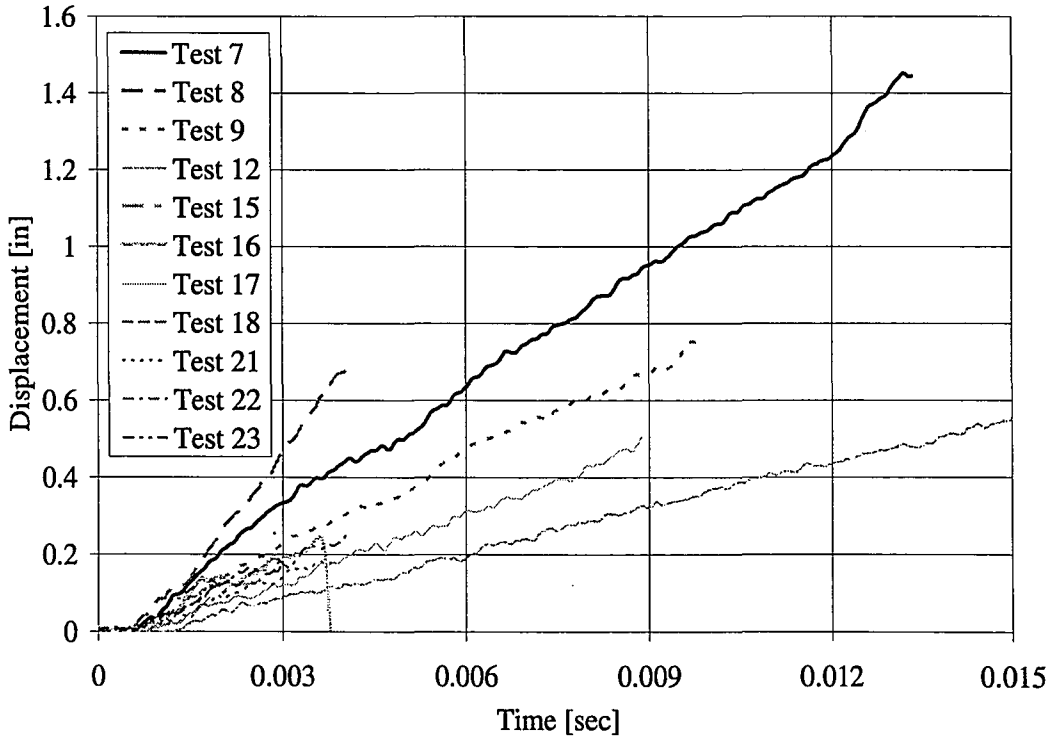


Figure 6-38: Displacements of Specimens that Fractured

The displacements versus time for specimens that did not fracture are presented in Figure 6-39. The initial displacement rates for the two coated specimens tested at a drop height of 4 inches are similar and less than all six inch drop height displacement rates except for Test 13. This is probably due to the fact that Test 13 has a much thicker coating than all test specimens. The variation seen in the displacement of Test 19 and Test 11 is due to the partial tearing. The behavior of Test 10 may be the result of a strain gauge wire interfering with the laser readings. The six inch drop height displacements are also similar to each other.

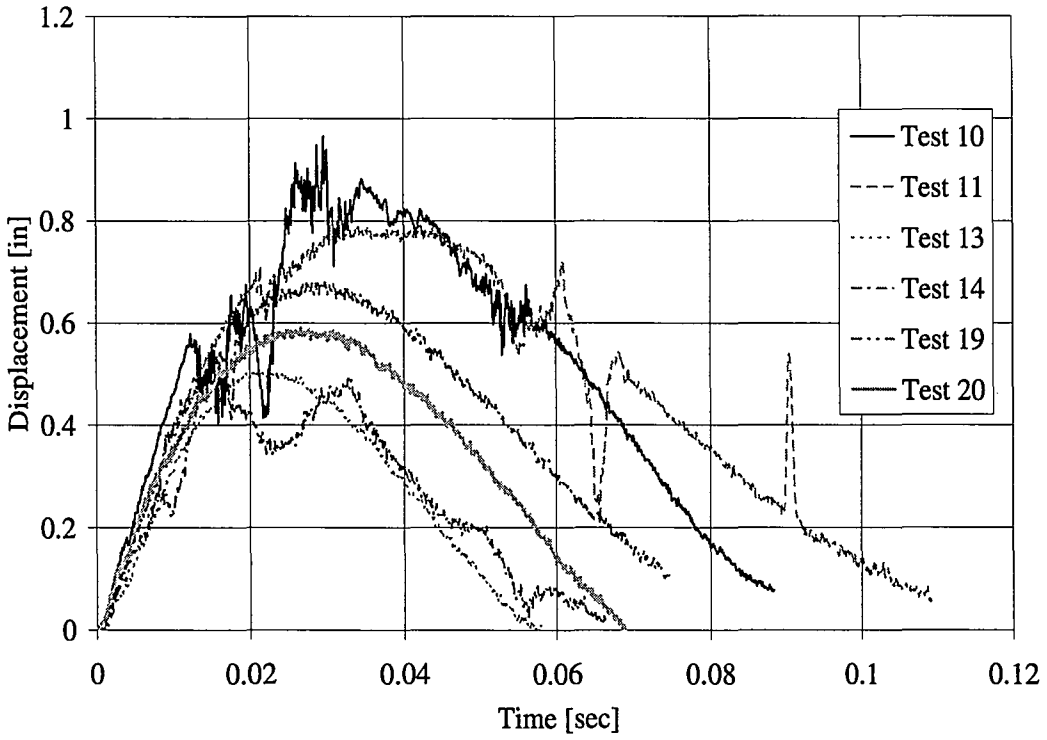


Figure 6-39: Displacements of Specimens that Did not Fracture

Next, the strain along the length of the beam was evaluated at different rotations of interest. Since the rotations were calculated from displacement values read by a laser sensor, the results and rotational behavior is similar to the displacement behavior.

For all polyurea coated beams, the strain along the length of the beam was graphed at the following rotations: 0.25°, 0.5°,1°, 1.5°, 3°, and 1.5° during the rebound phase for beams that did not fracture. More rotations were chose earlier on in the test because there would be more active gauges for these values and a maximum rotation of 3° was chosen because that is a rotation that all specimens achieved. The rotations at which the strains were evaluated for each test are shown in Figure 6-40, Figure 6-41, and Figure 6-42.

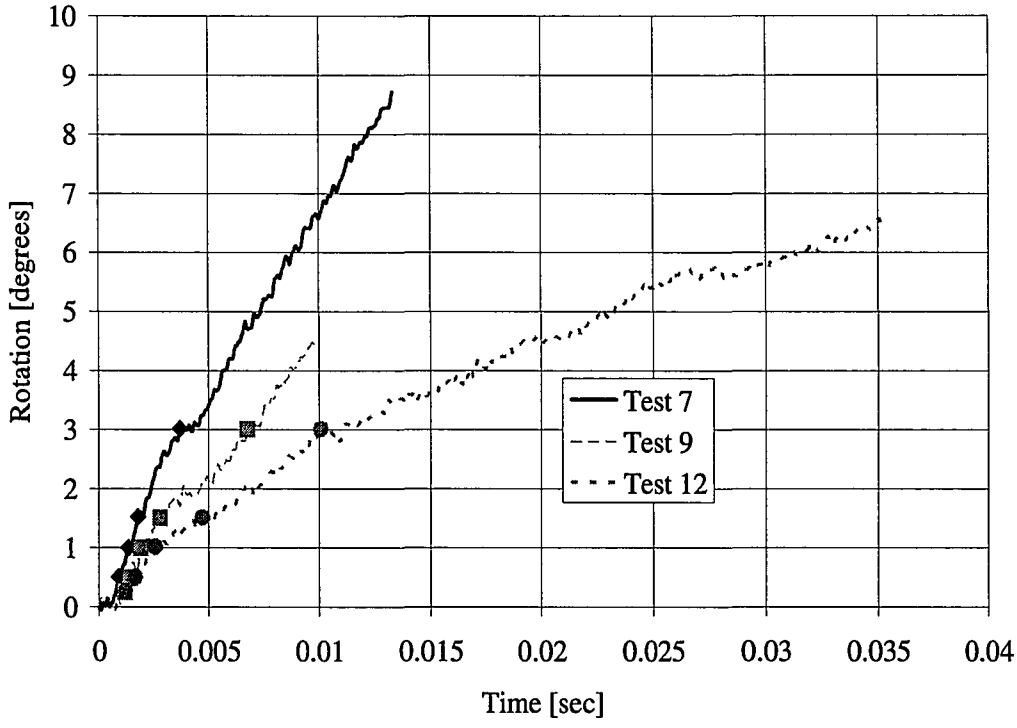


Figure 6-40: Rotations of Interest for Tests that Fractured

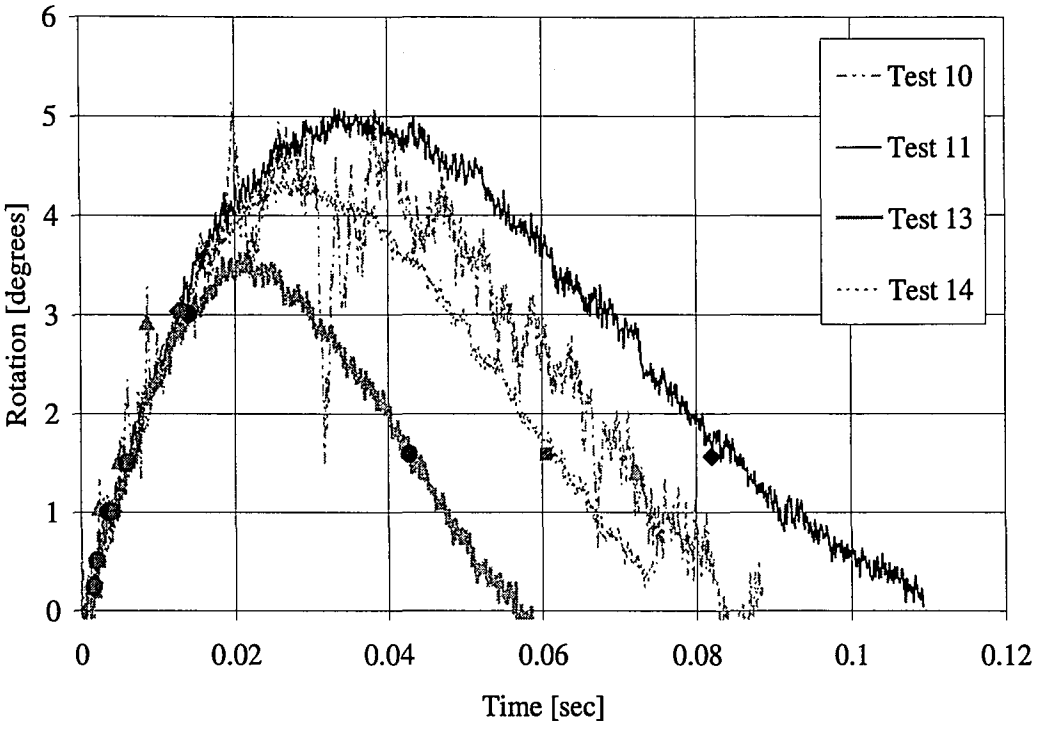


Figure 6-41: Rotations of Interest for 6 inch Drops without Full Fracture

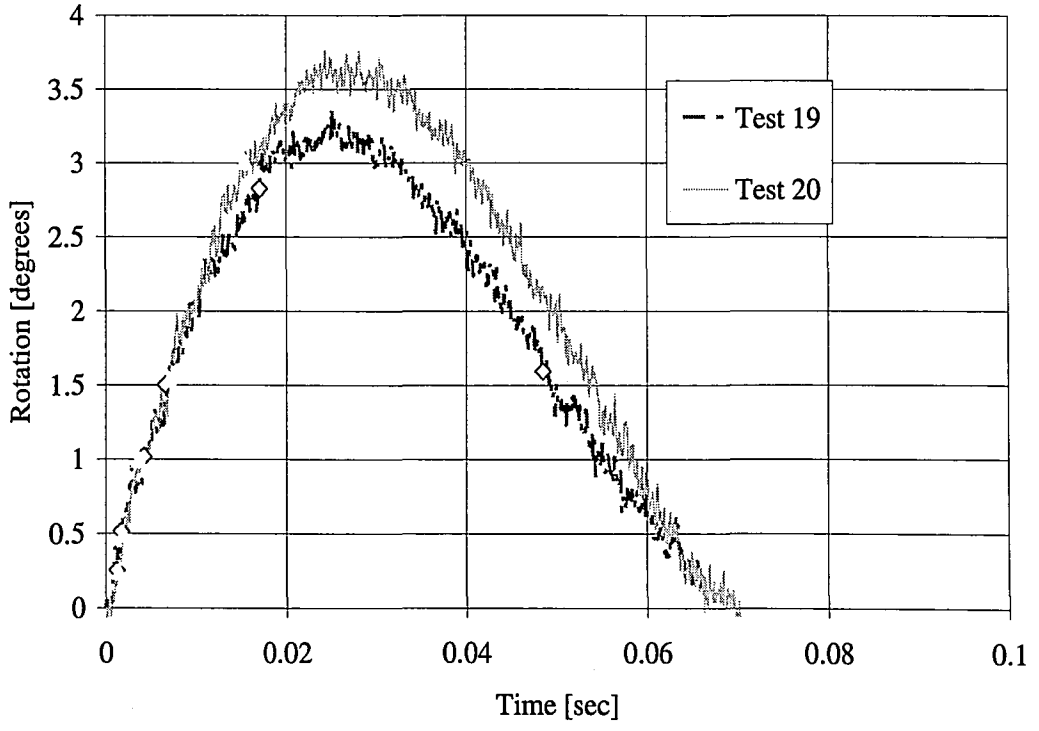


Figure 6-42: Rotations of Interest for 4 inch Drops without Full Fracture

Figure 6-43 shows the strain profile along the length of the beams at a rotation of 0.25° for all tests. This rotation was chosen, because at these rotations, the center gauge, or gauge located closest to the center, was active for most all tests and a full strain profile can be seen. The center gauge had already reached its capacity for Test 10 and Test 20 at this rotation and therefore no real strain profile is seen for these tests. It must be noted again that not all beams have the same strain profile. For instance, Test 14 is the only test to have a gauge located at a ½ inch outside the center and therefore a kink in its profile is seen that is not seen in the rest of the tests. This means that there could be a similar strain behavior for all tests at this distance, but since there was no strain gauge at the location it is not seen in Figure 6-43. As would be expected, the tests with the largest strain value at the center gauge were Test 7 and Test 9, which had drop heights of 30 inches and 18 inches. However, the next highest strain group contains Tests 11 and Test 19, which were tested with a 6 inch drop height and a 4 inch drop height. Both of these specimens are coated with the Batch 6 polyurea and the tests resulted in partial fracture. The remaining tests are all six inch drop height tests and are clustered together.

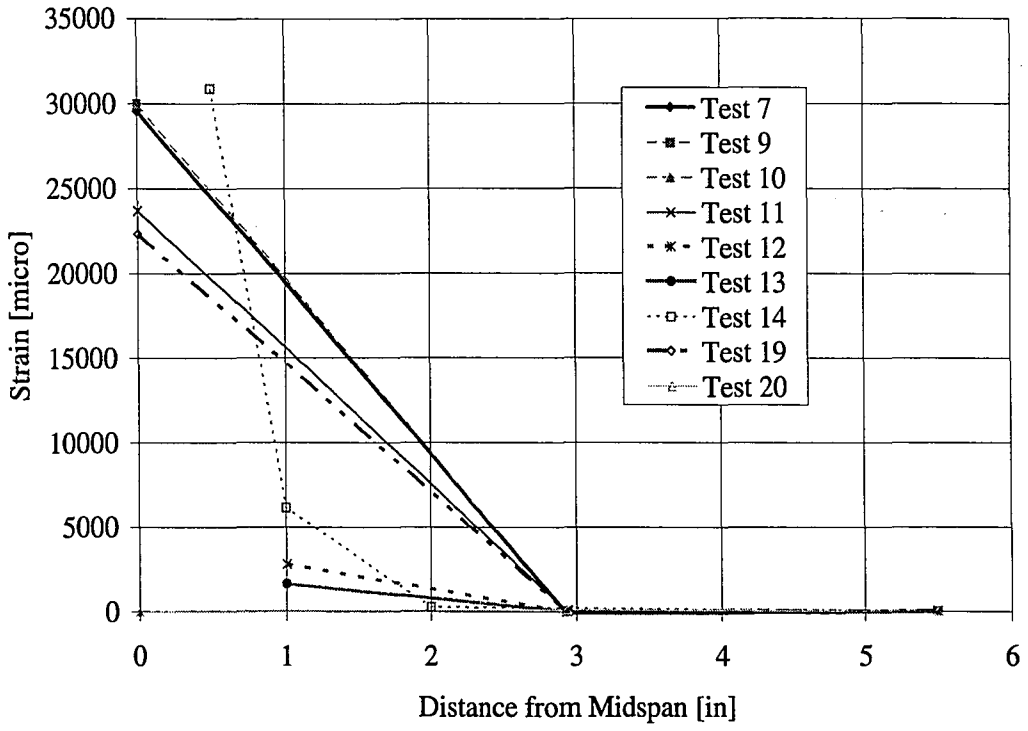


Figure 6-43: Strain along Length of Beam at Rotation of 0.25°

Since Test 14 has a gauge pattern where the gauges are more clustered toward the center of the beam at 0.5 inches from center, 1 inch from center, and 2 inches from center, with one gauge way outside center at a distance of 5.5 inches, the response of this test was studied at the different rotations of interest and a graphical representation of the strain along the length of the beam is shown in Figure 6-44.

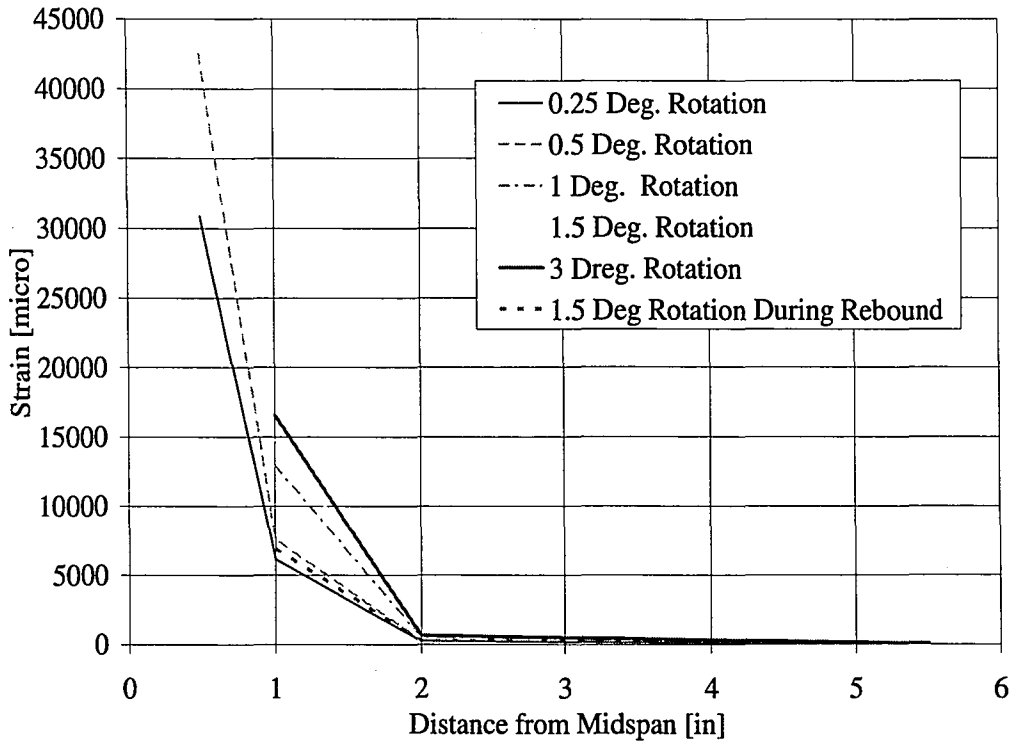


Figure 6-44: Strain along Beam for Test 14 Rotations

After a rotation of 0.5°, the gauge located at 0.5 inches away from the center was lost. The strains at 1 and 2 inches away from center increase with increasing rotation as expected. However, at 2 inches away from midspan, the amount of strain is minimal compared to the strains seen at 1 inch from center, especially after 0.5° of rotation. The rebound strains at a 1.5° rotation are less than those seen at this rotation during the loading phase. The strains are more similar to the rotations of 0.25° and 0.5° during loading. There is no region of constant strain seen at any of the rotations, and the strains at the largest rotation are still less than the gauge closest to the center gauge strain at the smallest rotation meaning that the debonded length did not increase beyond two inches at center.

At a rotation of 0.5° the only tests for which the center gauge is still active are Test 11 and Test 19, as can be seen in Figure 6-45. The tests show very similar strain behavior even though the drop heights vary for the two tests, but both specimens are coated with the same polyurea and both tests resulted in partial fracture of the polyurea. All 6 inch drop height tests that contained a gauge at 1 inch away from center show similar behaviors. The gauge located at 2 inches from the center for Test 14 shows that there may not be any strain experienced at this distance from the center for the six inch drops.

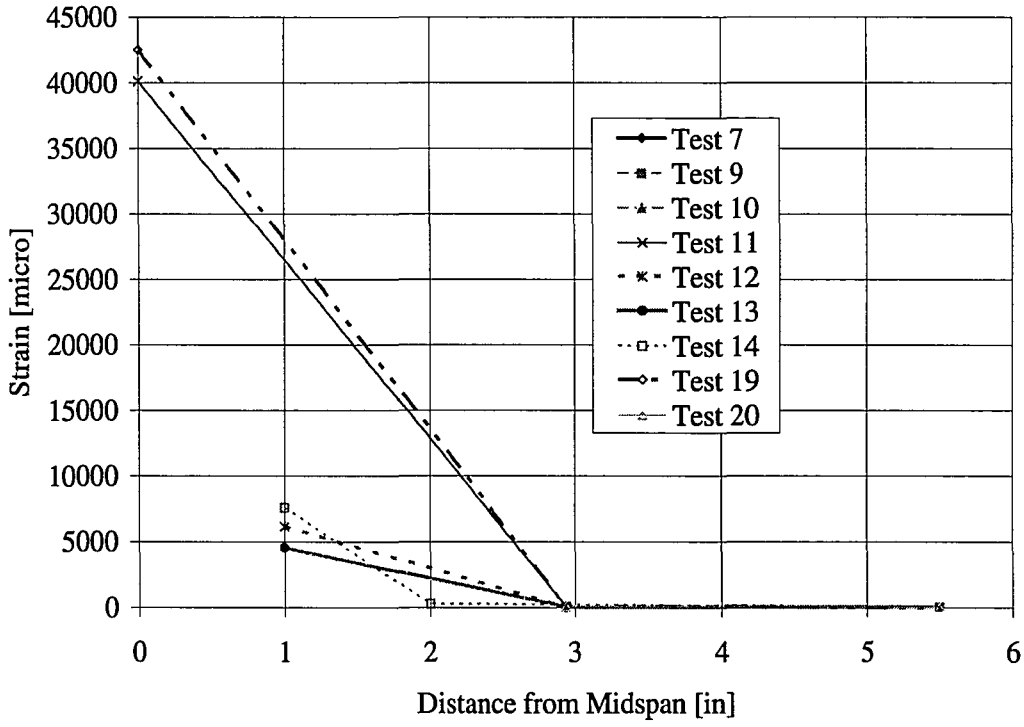


Figure 6-45: Strain along Beam at a Rotation of 0.5°

In Figure 6-46, a new trend arises from the gauges located at 1 inch from the center for three tests conducted from a six inch drop height. Test 13 and Test 14 show similar values of strain whereas Test 12, which previously had been similar, has

lower strain at this rotation. Test 13 and Test 14 are coated with Batch 8 polyurea, where Test 12 is coated with Batch 7 polyurea. The two batches are behaving differently. Again, the Test 14 strain behavior shows that there is minimal strain at 2 inches away from center, but it is rising.

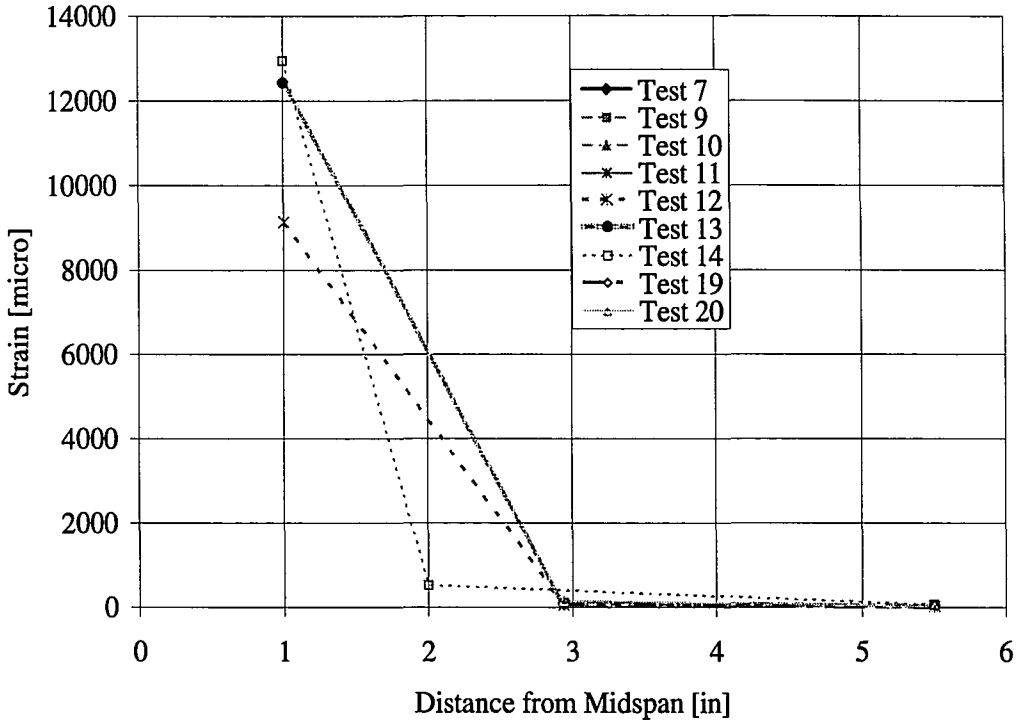


Figure 6-46: Strain along Beam at 1° Rotation

Looking at the strain values along the length of the beam at a rotation of 3° shown in Figure 6-47, some interesting behaviors present themselves. At close to 2.94 inches from the center, the test seeing the most strain is Test 20, which is the result of the lowest drop height of 4 inches. However, the temperature of this polyurea when tested was 5 °F warmer than the other test specimens. This could weaken the polyurea and maybe even the bond strength, therefore allowing it to see much higher strains than other tests at a similar location. Without a gauge at 2.94 inches from the

center, it is unknown whether Test 14 shows a similar value to that of Test 13, which are both coated with Polyurea Batch 8. The tests conducted at 6 inches and coated with Polyurea Batch 7, Test 10 and Test 12, do show similar strain values at this location, which are much lower than those coated with Batch 8 and Batch 6. Test 11, which saw partial tearing of the Batch 6 coat, saw strains similar to values of Test 7 and Test 9, which fractured. It seems that the outcome of the test, the polyurea batch, and the temperature of the polyurea at the time of testing can all affect that strain behavior.

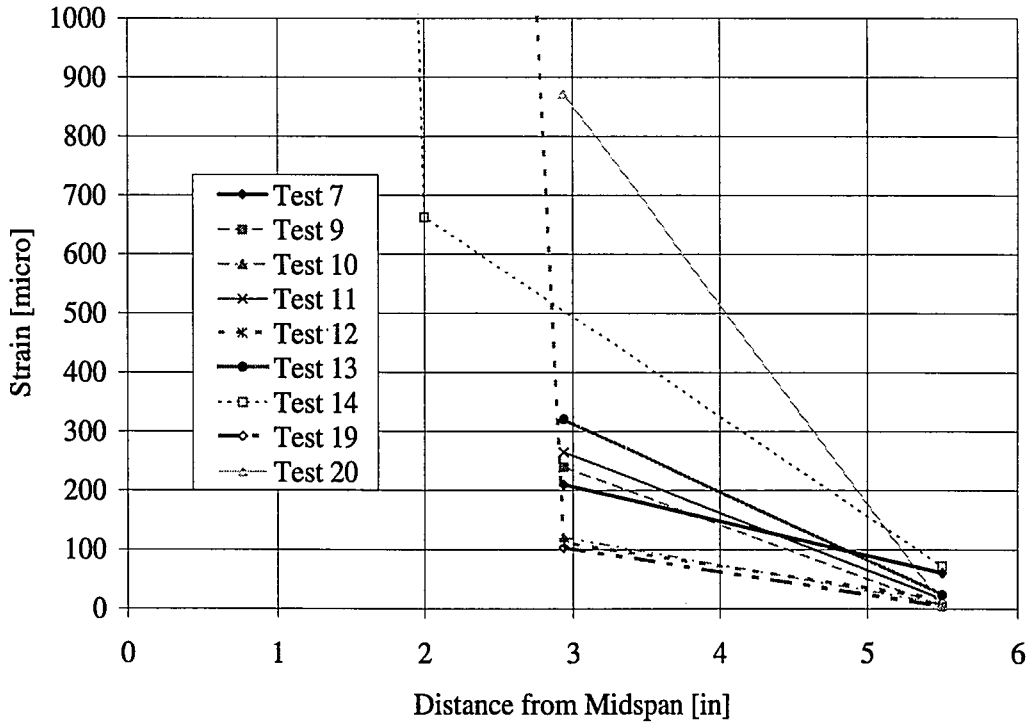


Figure 6-47: Zoomed View of Strain along Beam at Rotation of 3°

When comparing the strain saw during rebound at a rotation of 1.5° to the strain seen during loading at a rotation of 1.5°, the usual trend is that the rebound strain is less than the loading strain (Figure 6-48). However, for Test 11 and Test 20 this is not the

case. Test 20 may have been affected by its high polyurea temperature, which may have made it more viscous and resistant to a change in movement direction. Test 11 resulted in partial fracture of the polyurea, which may have caused a rise in strain at this location not seen in other tests, although this did not occur in Test 19, which also saw partial fracture, but the partial fracture did not extend as far across the width of the beam as it did in Test 11.

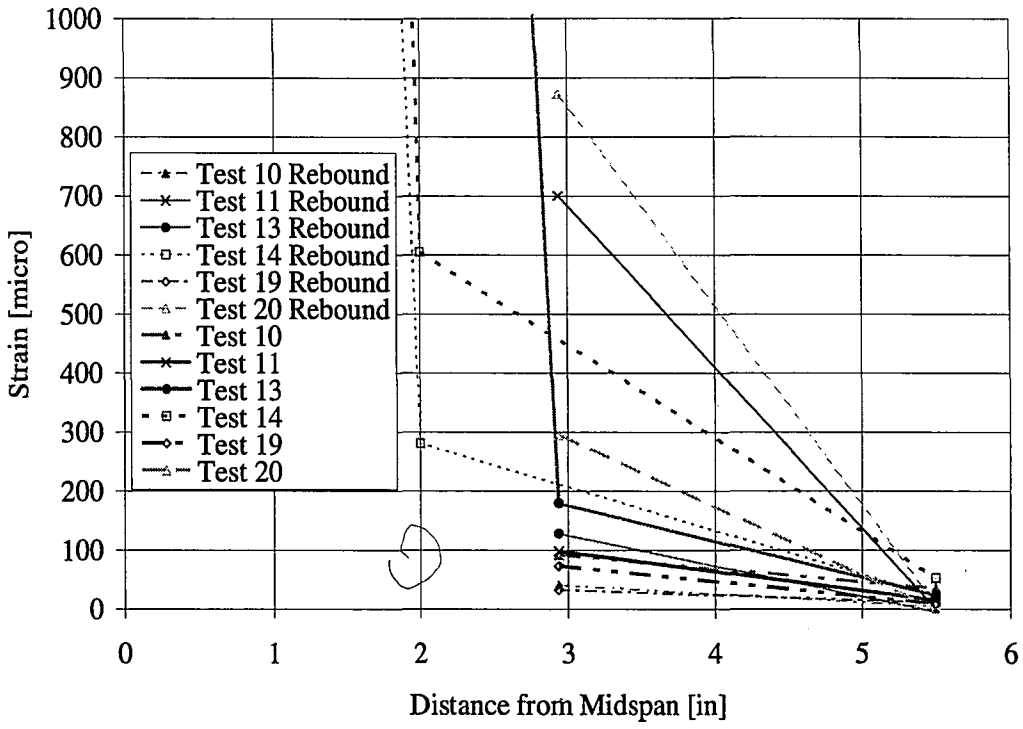


Figure 6-48: Strain along Beam during Loading and Rebound at Rotation of 1.5°

Figure 6-49, which shows the time history of the center strain gauges, also shows that Test 20 saw higher than expected strains, similar to those resulting from an 18 inch drop height (Test 9). Temperature must have been a factor in the performance of polyurea. The jumps in center strain seen in Test 11 and in Test 19 indicate when tearing of the polyurea occurred. For Test 11 it seems that tearing occurred at two

different instances in time. The jump in strain is more severe for this test than Test 19 due to the amount of partial fracture produced in the polyurea.

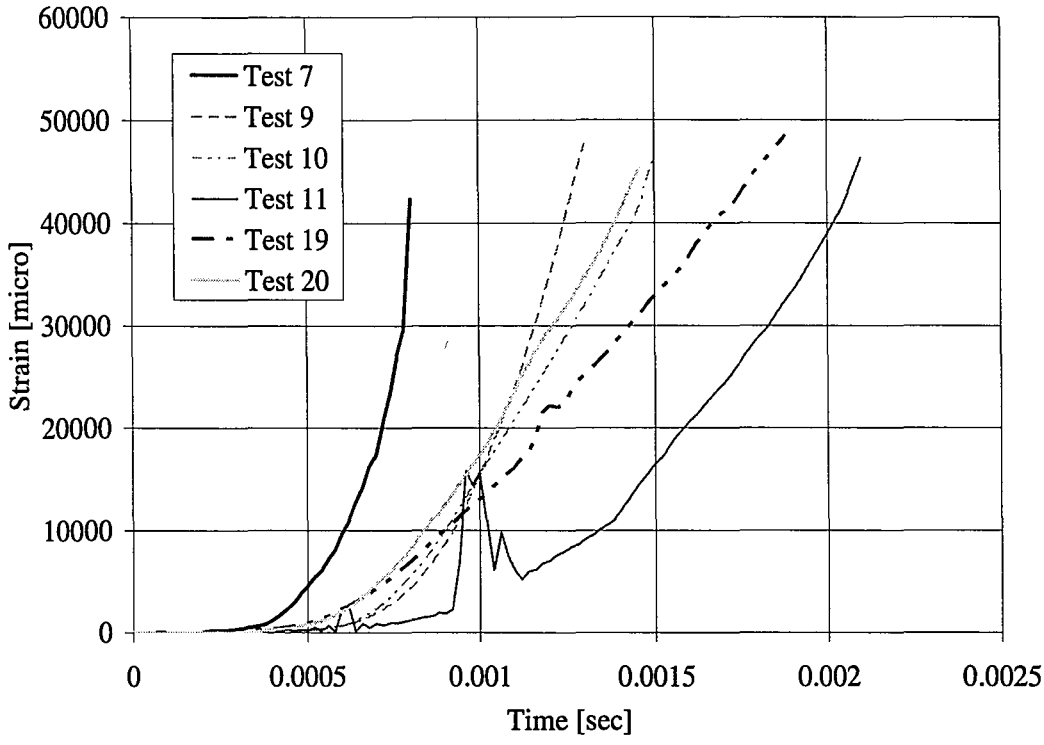


Figure 6-49: Center Strain

Figure 6-50 shows the strain behavior over time of gauges located 1 inch from the center. According to the plot, the gauges start seeing strain at around 0.0008 seconds. Test 12 through Test 14 specimens are all made with Type 2 concrete. According to the midspan acceleration data, the most negative peak , which is after the concrete has fracture and the beam has displaced downward and just prior to the stiffening of the polyurea to decelerate the beam in its downward movement, occurs at an average time of 0.00095 seconds for Type 2 concrete. Therefore it can be assumed that the polyurea 1 inch away from midspan starts seeing strain at the time crack opening begins. The between the strains of Test 13 and Test 14, which are coated with Batch

8 polyurea, is the thickness of the coating. Test 12 is coated with a different batch of polyurea. This may also insinuate that Test 14 has a longer initial debonded length of polyurea than Test 12 and Test 13, which allows the strain to be spread over a larger distance, decreasing the strain at this location.

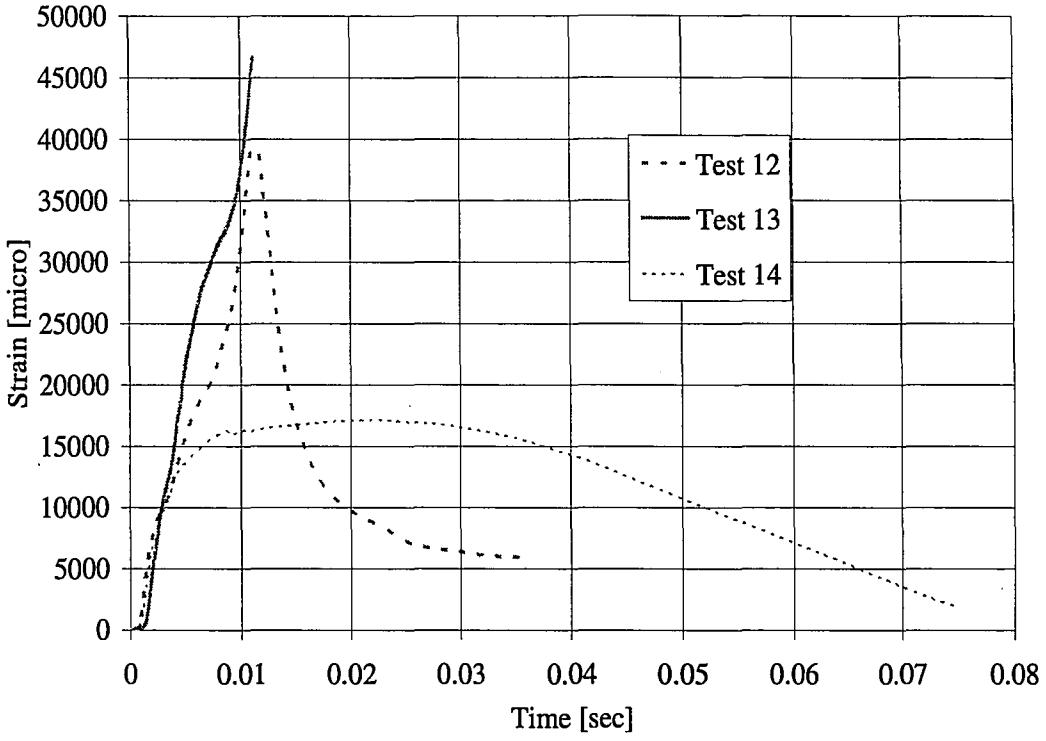


Figure 6-50: Strain 1" From Center

Section 5.4.2.2 describes how to calculate strain using the rotation data by dividing the crack opening (Equation 3-1) with the initial debonded length. From the strain value, a corresponding stress can be calculated using the stress-strain relationship of polyurea at dynamic rates shown in Figure 2-14. The stress multiplied by the cross-sectional area of the polyurea is the tension force in the polyurea. If this is multiplied by the moment arm, the moment in the section is produced. This allows for the moment-rotation diagram of Figure 6-51 for Test 7. A moment can also be calculated

using the center strain gauge data in the same way. As can be seen the strain gauge data does not align with the rotation data. By changing the original debonded length of polyurea, as was done in Chapter 5, to 2 inches, for the calculations, a better correlation between the data is seen (Figure 6-52). This was done for all specimens and it was found that the original debonded length ranged from 1.5 inches to 3 inches, with the most frequent debonded length of polyurea being 2 inches. To show that this change in debonded length of polyurea provides a better correlation for all drop heights, from highest to lowest, data is also presented in Figure 6-53 and Figure 6-54 for Test 20, which was tested at a 4 inch drop height.

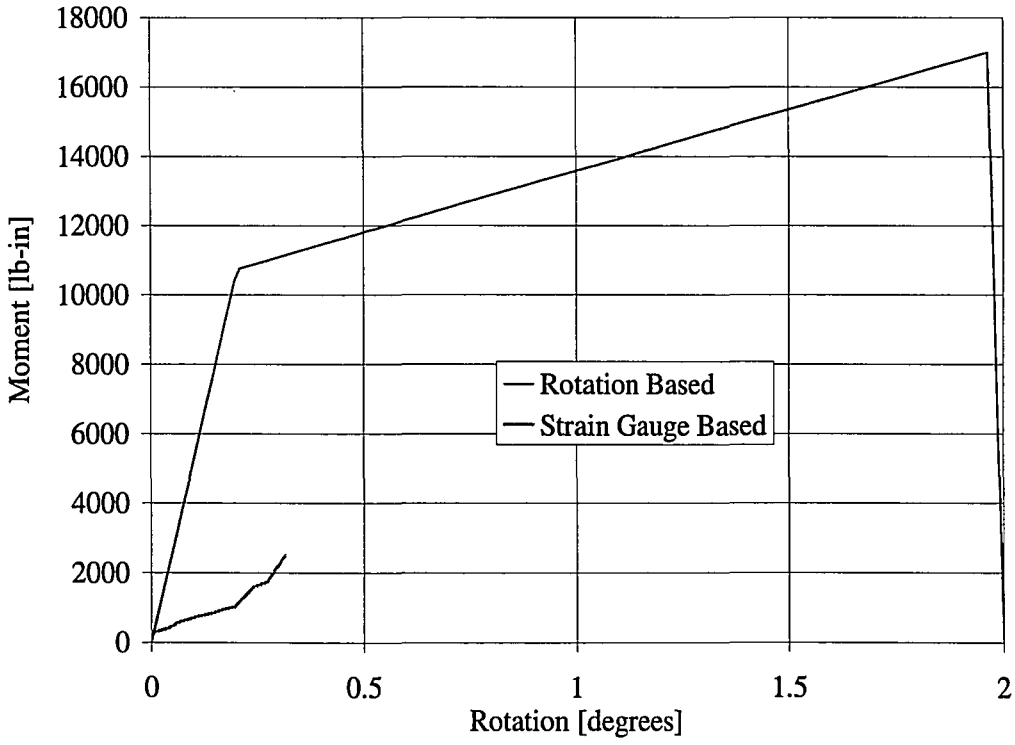


Figure 6-51: Moment versus Rotation using Original Debonded Length for Test 7

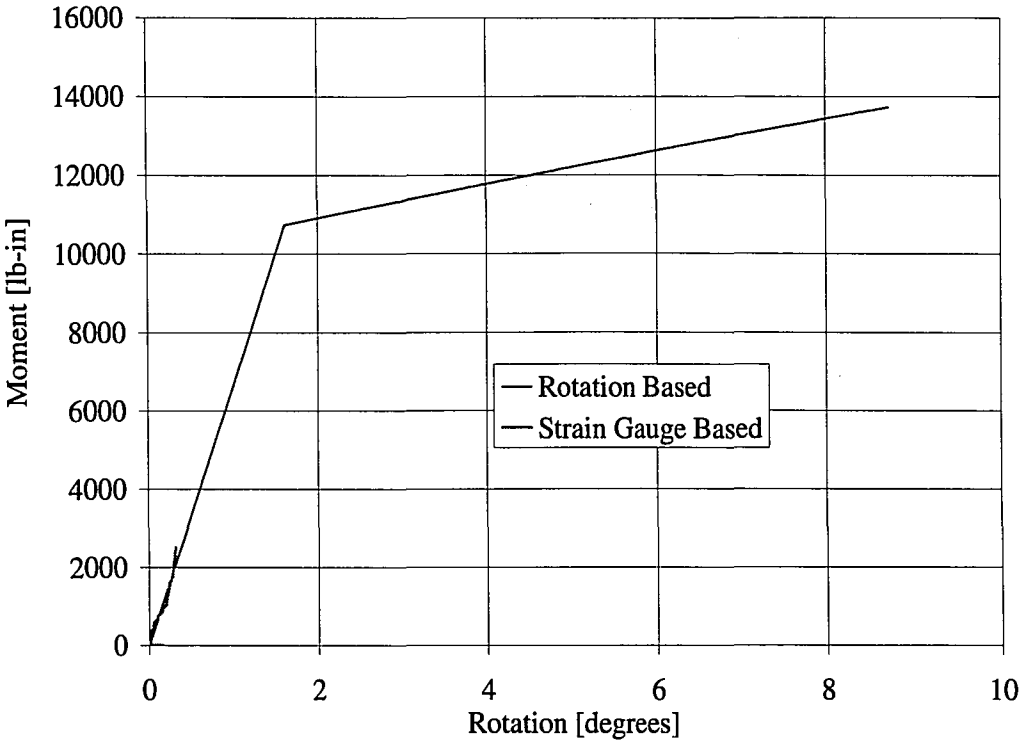


Figure 6-52: Moment versus Rotation with Adjusted Debonded Length for Test 7

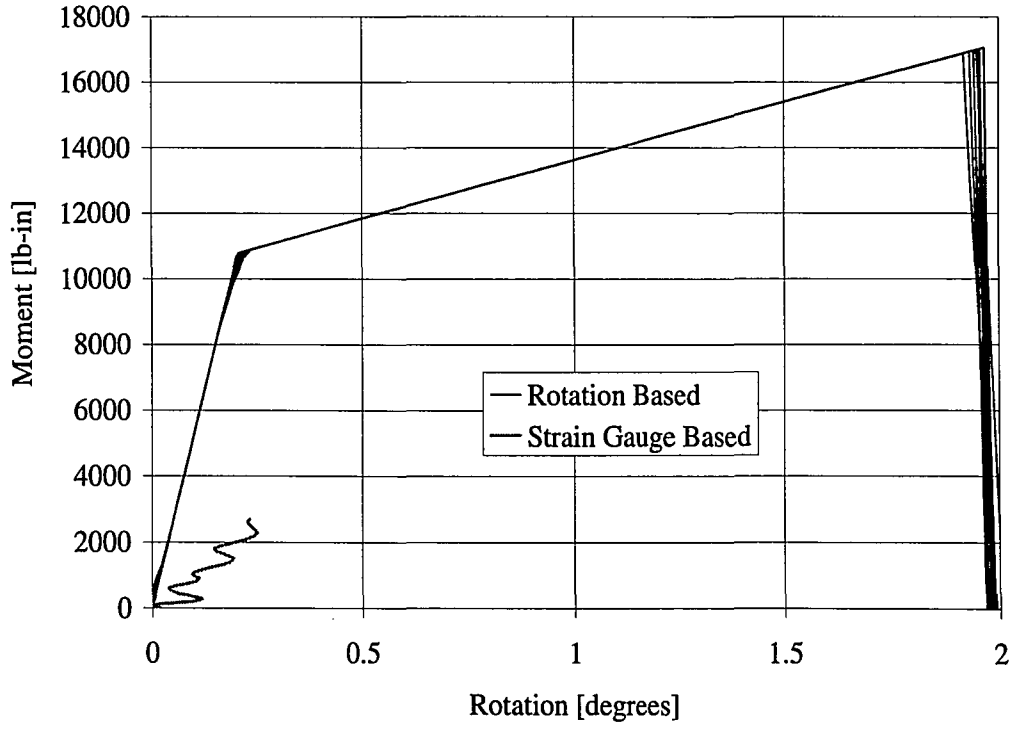


Figure 6-53: Moment versus Rotation with Original Debonded Length for Test 20

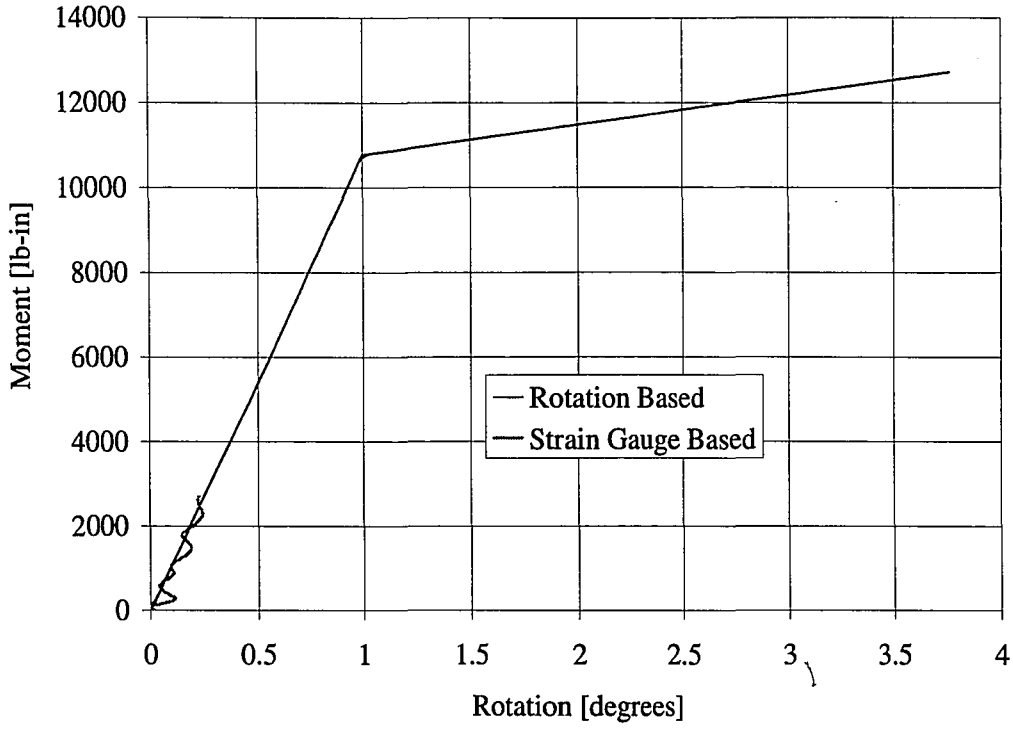


Figure 6-54: Moment versus Rotation with Adjusted Debonded Length for Test 20

## 6.5 Conclusions from Dynamic Testing

Although there was the presence of noise from additional vibration modes of the tup and drop weight set-up seen in the tup acceleration data and beam acceleration, it was still clear that at a drop height of 6 inches, the coated systems were able to absorb more energy than the plain specimens were able to. In addition, the coated specimens did not fail at this height unless there was a defect in the polyurea coating. The defect either allowed the entire system to fail or created a partial failure. Even though it wasn't clear whether the amount of energies absorbed by the coated specimens tested at a 4 inch were greater than or about the same as the plain specimens, the coated specimens did not fail at this drop height. Again, if a defect in the polyurea coating was present, it did result in partial fracture.

For future testing the accelerometers need to be calibrated using a high speed load cell in order for the accelerometer data to be useful and to help determine what is real and what data is noise in their time histories. When this is achieved the data can be used to calculate a generalized bending load, allowing for the fracture energies to be calculated at all strain rates.

For specimens having the same drop height, the same polyurea coating, and the same concrete type, similar strain rates were produced in the polyurea (the calculation being based on the rate of crack opening and the original debonded length). Also, similarities were seen for Test 13 and Test 14 in the profile of strain along the length of the beam for a rotation of 1°. The difference seen at other rotations is due to the difference in thickness of the polyurea coating. Another factor seen to influence the strain behavior was temperature. Test 20 saw much higher strains than the other coated specimen tested at 4 inches due to the fact that the polyurea temperature was 5 °F higher than other tests. Strains produced during the rebound phase saw lower strains than the strains produced at the same rotation during the loading phase except for the test with the high temperature, Test 20, and also for Test 11, which saw partial fracture of the beam.

Partial fractures cause the center strain gauge values to be higher than other tests done at the same drop heights at different rotations. Also, partial fractures cause jumps in the displacement data over time, which could indicate when tearing occurs. In terms of displacement of the systems, all coated specimens are seen to displace at a slower rate than those of uncoated specimens tested at the same drop height.

The strain values along the length of the beams at different rotations indicate that the debonded lengths do not increase beyond 4 inches since gauges located approximately 2 and 3 inches away from the center of the beam do not see significant strains and always remain lower than the center gauge values at the lowest rotations analyzed. However, making a correlation between the moment rotation plot based on the rotation data and the moment rotation plot based on the strain gauge data indicates that the polyurea requires at least 0.875 inches to establish a bond to the concrete.

# 7 Conclusions

The material testing of both polyurea on its own and as part of a retrofitted system with CMU and concrete beams along with the full scale blast test conducted on a CMU Wall have introduced many factors that affect the polyurea's retrofit performance.

The chemical make-up and structure of the polyurea largely determines the material properties. The use of different isocyanates and resin blends define such things as cure rate and chemical bond strengths within the material. The cure rate needs to be sufficient enough to allow a stronger crystalline structure to form before hardening. The crystalline structure is composed of hard segments or cross-links whose strength is defined by the chemical bond strength holding them in position. It is also composed of an amorphous region, or soft segments, where the chains of atoms are askew and the bonds are not as strong. The balance of hard and soft segments and their locations relative to each other determine whether the polyurea will be flexible and or strong when a load is applied.

During batching different factors such as temperature, mixing ratio, and the ability to remove air bubbles can affect the polyurea's behavior as well. This stage is where imperfections can be introduced, which will cause stress concentrations during testing. As was seen by testing different polyureas with either all of the same make-up but with different batching techniques or polyureas with different make-ups and batching techniques using the testing methods of ASTM D-42 shows the variation in properties that can be produced. If a refined process for producing polyurea is used,

it may be possible to define its properties with some degree of certainty at different strain rates, including blast rates by the use of dynamic testing.

Static center-point testing conducted at static rates on specimens that were cut from CMU pieces coated with polyurea retrieved from a full scale blast test gave insight on the outcome of the blast tests themselves. The blast tests saw failure of a CMU wall coated with the stronger of the two polyureas used. The difference in the center-point loading test results, including load versus displacement behavior, fracture energies, and strain in the polyurea of two specimens coated with the same polyurea type points to the fact that the mixture may not be consistent throughout. Fractures may have occurred in the weaker regions, contributing to the walls failure. The successful blast test indicates that when an adequate batch of polyurea is used as a blast retrofit, the retrofit is able to contain dangerous fragmentation and keep interior pressures at an acceptable level from a human safety standpoint.

The CMU test results also indicate that the polyurea coating is able to increase the peak load, modulus of rupture, and the ability of the system to absorb energy before fracture compared to a non retrofitted specimen.

In addition to the conclusions resulting from the CMU tests, further static center-point loading tests were conducted on larger scale concrete beam specimens, which were coated with polyureas batched at Lehigh University. These tests also analyzed the affects of the initial debonded length of polyurea. Again it was seen that the polyurea coating allowed the system to continue displacing after complete cracking of concrete occurred. The specimens were also able to rebound significantly after testing was ended. The amount of rebound decreased with increasing initial debonded length of

polyurea. The peak load and modulus of rupture were again higher than those of non retrofitted specimens. Specifically, the ability to absorb energy was increased, on average, by 275% as compared to non retrofitted specimens at concrete cracking. The average increase of energy absorption was over 1000% at a displacement of 2.11 inches as compared to non retrofitted specimens. If a flaw in the polyurea coating was present, decreases in the benefits of the polyurea were seen and it allowed the retrofitted specimen to fracture at static rates even with the constrictions of the test set-up.

Polyurea coating as well as the initial debonded length of polyurea affected the stiffness of the initial phase. An increase in stiffness was seen for retrofitted specimens after the displacement caused by the compression of the polyurea at the supports was accounted for. A longer debonded region allowed the strains at the center of the specimen to remain lower by having a longer length to spread the strain to. Also correlations of rotation data to strain gauge data indicated that for fully bonded specimens, a length of at least 0.875 inches was needed to ensure a bond was made with the concrete. This data also shows that, for a polyurea coated beam with an initial debonded length of 5.5 inches, the debonded length increased during testing. With less of a debonded length, a good portion of polyurea remains almost entirely ineffective and inactive during the loading process of the retrofitted system and therefore, it is recommended that in order to utilize the full retrofit, that a larger initial debonded length is used, which is capable of maintaining similar increases in peak load, modulus of rupture, and fracture energy.

The need for a length of 0.875 inches in order to ensure bond between polyurea and concrete for a fully bonded specimen was also a conclusion made at all dynamic testing rates that the concrete beams were tested at using a drop weight machine to apply the a center-point load. The dynamic testing also presented the need for the calibration of accelerometers using high speed load cells for future testing. This would allow for the filtering of the accelerometer data to determine what is the real data and what data is noise. When this is achieved, the calculation of absorbed energy or fracture energy will be possible. From examining the acceleration data visually, it seems that that coated specimens can absorb more energy than the uncoated specimens at lower drop heights. Knowing that the coated specimens did not fracture at drop heights of 4 and 6 inches, unless a flaw was present, when all non retrofitted specimens did fracture also supports this conclusion.

The dynamic testing series again indicated the importance of flaws within the polyurea, as these specimens resulted in either full or partial fracture of the polyurea. Strain behaviors also indicated that other factors affecting the performance of the polyurea coating is temperature at testing. Higher temperatures weaken the polyurea, but do not necessarily make it ineffective. Increasing the thickness of the coating also lowers the strain seen in the specimen as compared to specimens with thinner layers.

All of these influencing factors determined through multiple testing methods need to be considered when designing a polyurea retrofit. A polyurea retrofit does have the ability to prevent fragmentation due to a blast from entering a structure as well as well as has the ability to keep interior pressures low enough for human safety and comfort.

# References

50-FMC. (1985), "Determination of the Fracture Energy of Mortar and Concrete by Means of Three-Point Bend Tests on Notched Beams." Rilem Draft Recommendation, *Materials and Strctures*, Committee on the Fracture Mechanics of Concrete, 18(106), pp. 285-290.

Aliphatic compound. (2007), *Encyclopedia Britannica*. Retrieved June 12, 2007, from Encyclopedia Britannica Online: http://www.britannica.com/eb/article-9005736.

Aromatic compound. (2007), *Encyclopedia Britannica*. Retrieved June 12, 2007, from Encyclopedia Britannica Online: http://www.britannica.com/eb/article-9009593.

ASTM C-39. (1996), *Standard Test Method for Compressive Strength of Cylindrical Concrete Specimens*, American Society for Testing Materials, West Conshohocken, PA.

ASTM C-109/C-109M. (2001), *Standard Test Method for Compressive Strength of Hydraulic Cement Mortars (Using 2-in. or 50-mm Cube Specimens)*, American Society for Testing Materials, West Conshohocken, PA.

ASTM C-293. (1994), *Standard Test Method for Flexural Strength of Concrete (Using Simple Beam With Center-Point Loading)*, American Society for Testing Materials, West Conshohocken, PA.

ASTM D-412. (1998), *Standard Test Methods for Vulcanized Rubber and Thermoplastic Elastomers-Tension*, American Society for Testing Materials, West Conshohocken, PA.

ASTM D-575. (2001), *Standard Test Methods for Rubber Properties in Compression*, American Society for Testing Materials, West Conshohocken, PA.

ASTM D-5279. (2001), *Standard Test Method for Plastics: Dynamic Mechanical Properties: In Torsion*, American Society for Testing Materials, West Conshohocken, PA.

Banthia, N., Mindess, S., Bentur, A., and Pigeon, M. (1989), "Impact Testing of Concrete Using a Drop-weight Impact Machine." *Experimental Mechanics*, pp. 63-69.

Broekaert, M. (2003). "Polyurea spray applied systems for concrete protection." *4th European Congress on Construction Chemicals*, Nürnberg, Germany.

Clegg, D.W. and Collyer, A.A. (1993), *The Structure and Properties of Polymeric Materials,* The Institute of Materials, London, pp.1-5.

Davidson, J.S., Fisher, J.W., Hammons, M.I., Porter, J.R., and Dinan, R.J. (2005), "Failure Mechanisms of Polymer-Reinforced Concrete Masonry Walls Subjected to Blast." *Journal of Structural Engineering*, 131(8), 1194-1205.

Davidson, J.S., Porter, J.R., Dinan, R.J., Hammons, M.I., and Connell, J.D. (2004). "Explosive testing of polymer retrofit masonry walls." *Journal of Performance Construction Facility*, 18(2), pp. 100-106.

Explosive Incident Report. (2003), *Statistics*. Bureau of Alcohol, Tobacco, Firearms, and Explosives. Retrieved July 5, 2007 from Explosive Incident Reports Online: http://www.atf.treas.gov/aexis2/statistics.htm

FEMA 453. (2006), *Design Guidance for Shelters and Safe Rooms Providing Protection to People and Buildings Against Terrorist Attacks,* FEMA.

"Introduction to Plastics." (2005), *Hands on Plastics*, American Plastics Council. Retrieved July 7, 2006, from American Plastics Council: http://www.handsonplastics.com/hands_on_plastics/introtoplastics/teachers.html.

"Isonate 143L Modified MDI." (2001), *Product Information*, DOW Plastics.

Kaufman, Morris. (1968), *Giant Molecules the Technology of Plastics, Fibers, and Rubbers*, Doubleday&Company, Inc., New York.

Knox, K.J., Hammons, M.I., Lewis, T.T., and Porter, J.R. (2000), *Polymer Materials for Structural Retrofit*, Report, Force Protection Branch, Air Expeditionary

Forces Technology Division, Air Force Research Laboratory, Tyndall AFB, Florida.

Lane, Richard, Craig, Benjamin, and Babcock, Wade. (2001), *Materials for Blast and Penetration Resistance*, AMPTIAC, Rome, Ney York.

Moore, W.R. (1963), *An Introduction to Polymeric Chemistry*, Adline Publishing Company, Chicago.

Morton-Jones, David H. and Ellis, John W. (1986), *Polymer Products Design Materials and Processing*, Chapman and Hall Ltd., London.

Naito, C., Wheaton, K. (2006), "Blast Assessment of Load Bearing Reinforced Concrete Shear Walls," *ASCE Practice Periodical on Structural Design and Construction*, Vol. 11, No. 2, pp. 112-121.

O'Kelly-Lynch, Ken. (2007), "Development of an Experimental Technique for Tensile Testing of a Material at High Strain Rate with Application to Polyurea." *Master's Thesis*, Lehigh University, Bethlehem, PA.

PDA. (2006), *The Polyurea Development Association.* Retrieved July 7, 2006 from The Polyurea Development Association: http://www.pda-online.org.

"Polyurea Coatings Product Guide." (1997), Resin Technology Company. Retrieved October 2005 from Resin Technology Company: http:www.resintechnology.com/1pg-polyurea.html.

Primeaux II, Dudley J. (2004), *Polyurea Elastomer Technology: History, Chemistry & Basic Formulating Techniques*, Primeaux Associates, LLC, Texas.

Randall, David and Lee, Steve, ed. (2002), *The polyurethanes book*, John Wile & Sons, Ltd.

Rhosdy, G.S. (2005), *Armor Including a Strain Rate Hardening Elastomer*, The Patent Cooperation Treaty, World Intellectual Property Organization.

Rosthauser, J.W., Haider, K.W., Steinlein, C., and Eisenbach, C.D. (2006), "Mechanical and Dynamic Mechanical Properties of Polyurethane and Polyurethane/Polyurea Elastomers Based on 4,4'-Diisocyanatodicyclohexyl Methane." *Journal of Applied Polymer Science*, 64 (5).

U.S. Army Corp of Engineers. (1998), "Protective Structures Automated Design System (PSADS)", Omaha, NE.

"Versalink P-1000 Oligomeric Diamine." Air Products.

Wang, Kuan-Jong. (1989), "Reactive processing of polyureas and polyurethane-polyester hybrids." *Dissertation*, Ohio State University.

# Vita

Lynne E. Starek was born on January 10, 1983 in Natick, MA. She is the daughter of Paul and Anne Starek. Lynne earned her Bachelor of Science degree in Civil and Environmental Engineering at the University of Massachusetts Amherst in May of 2005. At the University of Massachusetts Amherst, Lynne was a member of the Commonwealth College and graduated with Departmental Honors and Summa Cum Laude. In the fall of 2005, she attended Lehigh University to pursue her Masters of Science Degree in Structural Engineering. Lynne will receive her degree in September of 2007, at which point she will work as a structural engineer for CH2M Hill in Atlanta, GA.

# END OF TITLE